NUREG/IA-0133
CAMP004

International Agreement Report

Development, Implementation, and Assessment of Specific Closure Laws for Inverted-Annular Film-Boiling in a Two-Fluid Model

Prepared by
François de Cachard

Thermal-Hydraulics Laboratory
Paul Scherrer Institute
CH-5232 Villigen PSI
Switzerland

Office of Nuclear Regulatory Research
U.S. Nuclear Regulatory Commission
Washington, DC 20555-0001

October 1996

Prepared as part of
The Agreement on Research Participation and Technical Exchange
under the International Thermal-Hydraulic Code Assessment
and Maintenance Program (CAMP)

Published by
U.S. Nuclear Regulatory Commission

AVAILABILITY NOTICE

Availability of Reference Materials Cited in NRC Publications

Most documents cited in NRC publications will be available from one of the following sources:

1. The NRC Public Document Room, 2120 L Street, NW., Lower Level, Washington, DC 20555-0001

2. The Superintendent of Documents, U.S. Government Printing Office, P. O. Box 37082, Washington, DC 20402-9328

3. The National Technical Information Service, Springfield, VA 22161-0002

Although the listing that follows represents the majority of documents cited in NRC publications, it is not intended to be exhaustive.

Referenced documents available for inspection and copying for a fee from the NRC Public Document Room include NRC correspondence and internal NRC memoranda; NRC bulletins, circulars, information notices, inspection and investigation notices; licensee event reports; vendor reports and correspondence; Commission papers; and applicant and licensee documents and correspondence.

The following documents in the NUREG series are available for purchase from the Government Printing Office: formal NRC staff and contractor reports, NRC-sponsored conference proceedings, international agreement reports, grantee reports, and NRC booklets and brochures. Also available are regulatory guides, NRC regulations in the *Code of Federal Regulations*, and *Nuclear Regulatory Commission Issuances*.

Documents available from the National Technical Information Service include NUREG-series reports and technical reports prepared by other Federal agencies and reports prepared by the Atomic Energy Commission, forerunner agency to the Nuclear Regulatory Commission.

Documents available from public and special technical libraries include all open literature items, such as books, journal articles, and transactions. *Federal Register* notices, Federal and State legislation, and congressional reports can usually be obtained from these libraries.

Documents such as theses, dissertations, foreign reports and translations, and non-NRC conference proceedings are available for purchase from the organization sponsoring the publication cited.

Single copies of NRC draft reports are available free, to the extent of supply, upon written request to the Office of Administration, Distribution and Mail Services Section, U.S. Nuclear Regulatory Commission, Washington, DC 20555-0001.

Copies of industry codes and standards used in a substantive manner in the NRC regulatory process are maintained at the NRC Library, Two White Flint North, 11545 Rockville Pike, Rockville, MD 20852-2738, for use by the public. Codes and standards are usually copyrighted and may be purchased from the originating organization or, if they are American National Standards, from the American National Standards Institute, 1430 Broadway, New York, NY 10018-3308.

DISCLAIMER NOTICE

This report was prepared under an international cooperative agreement for the exchange of technical information. Neither the United States Government nor any agency thereof, nor any of their employees, makes any warranty, expressed or implied, or assumes any legal liability or responsibility for any third party's use, or the results of such use, of any information, apparatus, product, or process disclosed in this report, or represents that its use by such third party would not infringe privately owned rights.

NUREG/IA-0133
CAMP004

International Agreement Report

Development, Implementation, and Assessment of Specific Closure Laws for Inverted-Annular Film-Boiling in a Two-Fluid Model

Prepared by
François de Cachard

Thermal-Hydraulics Laboratory
Paul Scherrer Institute
CH-5232 Villigen PSI
Switzerland

Office of Nuclear Regulatory Research
U.S. Nuclear Regulatory Commission
Washington, DC 20555-0001

October 1996

Prepared as part of
The Agreement on Research Participation and Technical Exchange
under the International Thermal-Hydraulic Code Assessment
and Maintenance Program (CAMP)

Published by
U.S. Nuclear Regulatory Commission

Contents

1 Abstract

Inverted-Annular Film-Boiling (IAFB) is one of the post-burnout heat transfer modes taking place, in particular, during the reflooding phase of the loss-of-coolant accident, when the liquid at the quench front is subcooled. Under IAFB conditions, a continuous liquid core is separated from the wall by a superheated vapour film.

The heat transfer rate in IAFB is influenced by the flooding rate, liquid subcooling, pressure, and the wall geometry and temperature. These influences can be accounted by a two-fluid model with physically sound closure laws for mass, momentum and heat transfers between the wall, the vapour film, the vapour-liquid interface, and the liquid core. The applicability of existing IAFB two-fluid models is limited. This is attributed to shortcomings in the description of heat transfer within the liquid core, to the use of certain correlations outside their validity range, and to a limited use of experimental information on IAFB. The usual approach has been to develop models employing generally applicable closure laws including, however, adjustable parameters, and to adjust these using global experimental results. The present approach has been to develop IAFB-specific closure laws in such a form that they could be adjusted separately using detailed, IAFB-relevant, experimental results. Steady-state results, including heat flux, wall temperature and void fraction data have been used for the adjustment.

A key issue in IAFB modeling is to predict how the heat flux reaching the vapour-liquid interface is split into a liquid heating term and a vaporization term. In the model proposed, convective liquid heating is related to the liquid velocity relative to the interface, and not to the absolute liquid velocity, as in previous models. This relative velocity is deduced from the interfacial shear stress, using the liquid-interface friction law. With this modification, the prediction of the experimental trends is greatly improved.

The non-smoothness of the vapour-liquid interface may considerably enhance interfacial transfers. Complex physical processes are involved, such as waves, oscillations of the liquid core, droplet entrainment and redeposition, and turbulence in the vapour film. In the closure laws proposed, these effects are accounted by semi-empirical laws based on simple physical models. The vapour film is divided into a laminar sublayer near the wall which controls heat transfer, and a well-mixed sublayer near the interface. The ratio of the laminar sublayer thickness to the total film thickness has been empirically correlated. Semi-empirical expressions have also been developed for the vapour and liquid friction factors. The main correlating variable used is a non-dimensional film thickness, which is shown to be representative of the degree of irregularity of the interface, and may be easily derived from void fraction measurements. Three possible geometries of the liquid core are considered: flow in a tube, and in square- or triangular-lattice rod bundles. Heat transfer within the liquid core is deduced from momentum transfer using the Chilton-Colburn analogy.

The model is extensively assessed against forced flow, low quality post-dryout data from four independent sources. A total of 52 experiments have been analysed. The quench front velocity, the initial flow parameters just downstream from the quench front, and the wall temperature distribution in the dry region are carefully derived from the measurements and given as inputs to the model. The model then predicts the heat flux and void fraction distributions, which are compared with the experimental values. The overall predictions are good. The model is shown to apply to steady-state as well as to transient (reflooding) conditions, with very different geometries, i.e. tubes and rod bundles with hydraulic diameters ranging from 4 to 14 mm, and for large parameter ranges, i.e. 3 to 50 cm/s in flooding rate, 0 to 30 °C in subcooling, 1 to 4 bar in pressure, and 300 to 1000 °C in wall temperature.

The IAFB-specific closure laws proposed have also intrinsic value, and may be used in other two-fluid models. They should allow to improve the description of post-dryout, low quality heat transfer by the safety codes.

2 Analytical modeling of inverted-annular film-boiling

2.1 Introduction

Inverted-annular film-boiling (IAFB) is one of the modes of post-burnout heat transfer taking place in a number of situations and in particular during the reflooding phase of the Loss-of-Coolant Accident (LOCA).

IAFB takes place when the liquid at the quench front is subcooled. A thin vapour film develops on the wall, starting at the location of the quench front. Heat is transferred from the wall to the vapour and superheats it. The superheated vapour transfers heat to the vapour-liquid interface, where some vaporization takes place. The vapour generated at the interface thickens the vapour film and tends to decrease the rate of heat transfer.

IAFB resembles film boiling in a pool but only superficially. Indeed, the important influences of liquid flow and subcooling are absent in pool boiling of a saturated liquid. Thus, attempts to use classical film boiling correlations for modeling IAFB situations are in general not successful. On the contrary, approaches based on two-fluid modeling have shown promise (e.g. Chan & Yadigaroglu, 1980; Denham, 1983; Kawaji, 1984; Analytis & Yadigaroglu, 1987; Takenaka et al., 1989).

The work described here follows the general lines of the model of Analytis & Yadigaroglu (1987). Its purpose is to generalize it and make it applicable to both tubes and bundles; to remove certain global, purely empirical correction factors that were used previously, as well as correlations that were applied outside their validity range, to further test and verify the model against data from tubes and bundles of different geometries (square and triangular lattices) and hydraulic diameters. Thus, certain closure laws in the model were modified to improve the physical representation of the phenomena. In particular, the formulation of the heat and momentum transfers within the liquid core has been changed, and IAFB specific, physically consistent correlations have been developed, using carefully checked, IAFB relevant, experimental data.

In a reflooding situation, the quench front progresses slowly along the bundle. Seen in a frame of reference moving with the quench front, the phenomena change very slowly. Thus, to easily test the model and to confront it to a large number of experimental data without having to use a large two-fluid code (such as the ones used for system analysis), a quasi-steady state approach and simple, ad-hoc two-fluid code were used: the equations are written, and both the calculations and the data reduction are performed in a frame of reference moving with the quench front. This, however, does not at all preclude a fully dynamic implementation of such a model in a two-fluid code; this indeed has already been done using a previous version of the model (Analytis, 1990). On the contrary, with the quasi-steady-state approach used here, one can investigate in great detail the influence of certain closure laws and assumptions and perform very detailed comparisons to the available experimental data.

2.2 Basic equations

The conservation equations already used by Analytis & Yadigaroglu (1987) are also used here. These are the steady-state equations for mass, momentum and energy conservation for the liquid core and the vapour film, considered in a frame of reference moving with the quench front. The flow is assumed to be vertically upwards. U_l and U_v are the liquid and vapor velocities in the moving frame of reference.

$$\frac{d}{dz}\left[\rho_l \alpha_l U_l\right] = -\frac{M_{vap}}{A} \tag{1}$$

$$\frac{d}{dz}\left[\rho_v (1-\alpha_l) U_v\right] = \frac{M_{vap}}{A} \tag{2}$$

$$-\alpha_l \frac{dp}{dz} - \alpha_l \rho_l U_l \frac{dU_l}{dz} = \alpha_l \rho_l g - \frac{\tau_i P_i}{A} - \frac{M_{vap}(U_l - U_i)}{A} \tag{3}$$

$$-(1-\alpha_l)\frac{dp}{dz} - \rho_v(1-\alpha_l)U_v\frac{dU_v}{dz} = \rho_v(1-\alpha_l)g + \frac{\tau_i P_i}{A} + \frac{\tau_w P_w}{A} + \frac{M_{vap}(U_v - U_i)}{A} \quad (4)$$

$$\alpha_l U_l \frac{dT_l}{dz} = \frac{Q_{lh}}{c_{pl}\rho_l A} - \frac{M_{vap}(h_{ls} - h_l)}{c_{pl}\rho_l A} \quad (5)$$

$$(1-\alpha_l)U_v\frac{dT_v}{dz} = \frac{Q_{vh}}{c_{pv}\rho_v A} + \frac{M_{vap}(h_{vs} - h_v)}{c_{pv}\rho_v A} \quad (6)$$

where M_{vap} denotes the vaporization mass flowrate (per unit height), τ_i and τ_w the interfacial and wall shear stress, respectively, and Q_{lh} and Q_{vh} the liquid and vapour sensible heating rates (per unit height), respectively.

For a cylindrical tube of radius R, the relation between the liquid fraction α_l and the film thickness δ is

$$\alpha_l = [\frac{(R-\delta)}{R}]^2 \quad (7)$$

while, for a square lattice rod bundle,

$$\alpha_l = \frac{p^2 - \pi(R+\delta)^2}{p^2 - \pi R^2} \quad (8)$$

and for a triangular lattice rod bundle,

$$\alpha_l = \frac{(\sqrt{3}/2)p^2 - \pi(R+\delta)^2}{(\sqrt{3}/2)p^2 - \pi R^2} \quad (9)$$

R is the rod diameter and p is the bundle pitch.

The interfacial perimeter P_i and the flow area A are given for a tube by

$$P_i = 2\pi(R-\delta) \quad (10)$$

$$A = \pi R^2 \quad (11)$$

and for a bundle by

$$P_i = 2\pi(R+\delta) \quad (12)$$

$$A = p^2 - \pi R^2 \quad \text{(square lattice)} \quad (13)$$

$$A = (\sqrt{3}/2)p^2 - \pi R^2 \quad \text{(triangular lattice)} \quad (14)$$

The wall perimeter is

$$P_w = 2\pi R \quad (15)$$

in both cases.

The remaining quantities, namely M_{vap}, U_i, τ_i, τ_w, Q_{lh} and Q_{vh} are expressed by the closure relationships given below.

2.3 Closure relationships

The various components of the heat and momentum transfers are represented in figure 1, together with the velocity profile.

The interfacial velocity U_i is implicity obtained by writing the interface equilibrium condition:

$$\tau_{vi} = \tau_{il} \quad (16)$$

where τ_{vi} and τ_{il} are the interfacial shear stress expressions on the vapour side and on the liquid side, respectively.

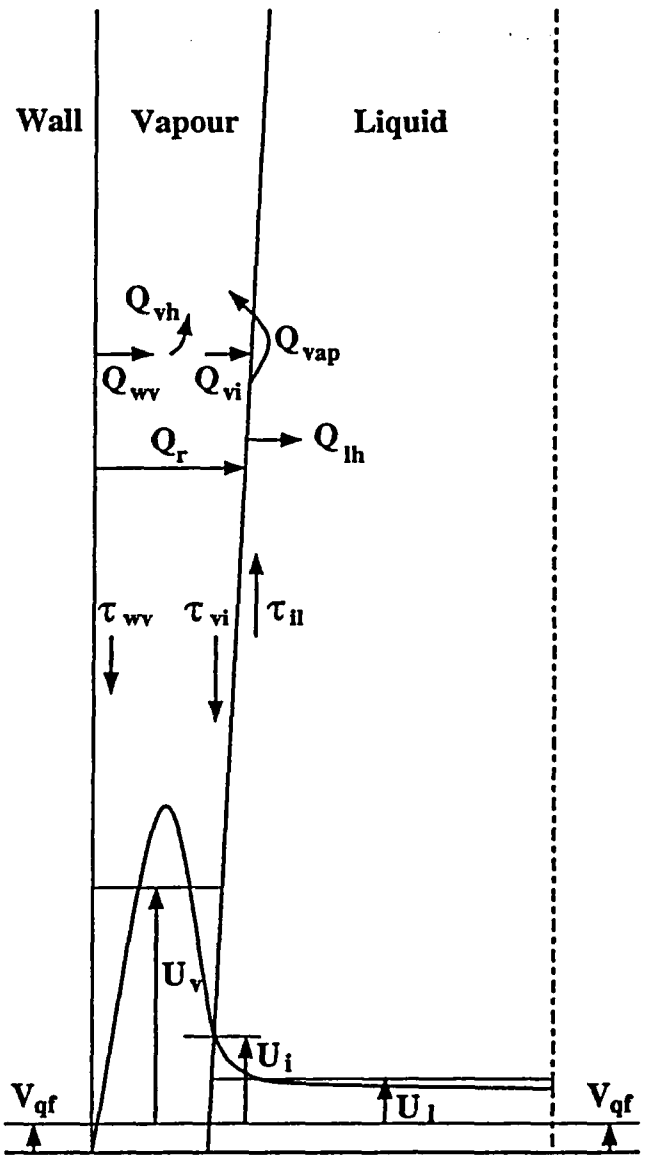

Figure 1: **Velocity profile in "ideal" IAFB; momentum and heat transfers.**
In fact, the velocity profile is often strongly disturbed by some fluctuations of the vapour-liquid interface.

The vapour interfacial mass flowrate is given by

$$M_{vap} = \frac{Q_{vap}}{h_{vap}} \tag{17}$$

where the vaporization heat rate Q_{vap} is obtained from a heat balance for the interface, expressing the fact that the fraction of the heat rate from the wall and the vapour to the interface, that is not used to heat up the liquid, goes into vapor generation:

$$Q_{vap} = Q_{vi} + Q_r - Q_{lh} \tag{18}$$

where Q_{vi} and Q_r are the heat transfer rates from the vapour to the interface and the radiation heat transfer rate (per unit height), respectively.

The vapour sensible heating rate is given by the following balance

$$Q_{vh} = Q_{wv} - Q_{vi} \tag{19}$$

where Q_{wv} is the heat transfer rate from the wall to the vapour (per unit height).

Expressions for Q_{wv}, Q_{vi}, Q_r, Q_{lh}, τ_w, τ_{vi} and τ_{il} are provided by an analysis of the heat and momentum transfers in the vapour film and in the liquid core.

2.3.1 Vapour film

The vapour field is treated as a flow between two parallel plates, i.e., the wall and the liquid interface. The **wall shear stress** is expressed by

$$\tau_w = f_w \rho_v |U_v + V_{qf}| \frac{(U_v + V_{qf})}{2} \tag{20}$$

where V_{qf} is the quench front velocity. Indeed, the wall velocity relative to the moving frame is $-V_{qf}$.

The following expressions are used for the friction factor

$$f_w = \frac{24}{\mathrm{Re}_w} \quad \text{for } \mathrm{Re}_w < 2000 \tag{21}$$

and

$$f_w = \frac{0.085}{\mathrm{Re}_w^{0.25}} \quad \text{for } \mathrm{Re}_w > 2000 \tag{22}$$

The Reynolds number is defined by

$$\mathrm{Re}_w = \rho_v |U_v + V_{qf}| \frac{2\delta}{\mu_v} \tag{23}$$

Although it is often acknowledged that the flow regime in the vapour film is turbulent even for low Reynolds numbers (Kao et al., 1972; Suryanarayana & Merte, 1972; Kawaji, 1984; Takenaka et al., 1989), the use of the usual turbulent flow correlations at low Reynolds numbers (often below 100) is questionable, since these correlations lead to unreasonably low values when extrapolated outside their intended range. Therefore, the turbulent flow friction law in the original model has been replaced by relations 21 and 22.

Similarly, the **interfacial shear stress** is expressed by

$$\tau_{vi} = f_{vi} \rho_v |U_v - U_i| \frac{(U_v - U_i)}{2} \tag{24}$$

where U_i is the interface velocity in the moving frame of reference,

with

$$f_{vi} = \lambda_{fv} \frac{24}{\mathrm{Re}_{vi}} \tag{25}$$

and

$$\mathrm{Re}_{vi} = \rho_v |U_v - U_i| \frac{2\delta}{\mu_v} \tag{26}$$

λ_{fv} is a factor accounting for the enhancement of the momentum transfer from the vapour to the interface, due to interfacial disturbances and turbulence. The derivation of λ_{fv}, as well as of the similar

quantities λ_{hv} (equation 36) and λ_l (equation 51) introduced later is a key point of the present study. It is described in details in section 2.5. The expression proposed for λ_{fv} is

$$\lambda_{fv} = c_1(\delta^*)^{c_2} \tag{27}$$
$$c_1 = 0.0362 \tag{28}$$
$$c_2 = 1.96 \tag{29}$$

where δ^* is a non-dimensional film thickness defined by

$$\delta^* \triangleq \delta \left(\frac{\rho_v (\rho_l - \rho_v) g}{\mu_v^2}\right)^{\frac{1}{3}} \tag{30}$$

whose introduction is also justified in section 2.5.

When δ^* is small, a minimal value $\lambda_{fv} = 1$ is used.

As turbulence effects on the interfacial shear stress are included in the factor λ_{fv}, equation 25 is used whithout restriction on the Reynolds number range.

The error made by not accounting for the cylindrical geometry (parallel plates) may be estimated, for laminar flow, from Shigechi & Lee (1991). In cylindrical geometry, the inner and the outer shear stress differ by 1.8 % for a surface area ratio (void fraction) of 10 %, and by 12% for a surface area ratio of 50%. The assumption of parallel plates is thus acceptable.

As in Kawaji (1984), Kays' (1980) formalism is applied to the **heat transfer in the vapour film.** Again, the approximation of parallel plates is made. The exchange perimeter is considered to be $(P_w + P_i)/2$ (mean perimeter). The resulting expressions of the heat transfer rates (per unit height) Q_{wv} and Q_{vi} from the wall to the vapour and from the vapour to the interface are

$$Q_{wv} = \frac{k_v \,\mathrm{Nu}_v}{2\delta} \frac{P_w + P_i}{2} \frac{(T_w - T_v)}{1 + (\frac{Q_{vi}}{Q_{wv}})\Theta} \tag{31}$$

$$Q_{vi} = \frac{k_v \,\mathrm{Nu}_v}{2\delta} \frac{P_w + P_i}{2} \frac{(T_v - T_s)}{1 + (\frac{Q_{wv}}{Q_{vi}})\Theta} \tag{32}$$

where Nu_v is the vapour Nusselt number, Θ the influence coefficient and T_s the vapour-liquid interface temperature, assumed to be the saturation temperature. This formulation has been modified to account for the heat transfer enhancement, due to interfacial disturbances and turbulence. The following expressions are proposed:

$$Q_{wv} = \lambda_{hv} \frac{k_v \,\mathrm{Nu}_v}{2\delta} \frac{P_w + P_i}{2} \frac{(T_w - T'_v)}{1 + (\frac{Q_{vi}}{Q_{wv}})\Theta} \tag{33}$$

$$Q_{vi} = \lambda_{hv} \frac{k_v \,\mathrm{Nu}_v}{2\delta} \frac{P_w + P_i}{2} \frac{(T'_v - T_s)}{1 + (\frac{Q_{wv}}{Q_{vi}})\Theta} \tag{34}$$

$$\tag{35}$$

where λ_{hv} is a factor given by

$$\lambda_{hv} = c_3(\delta^*)^{c_4} \tag{36}$$
$$c_3 = 0.679 \tag{37}$$
$$c_4 = 0.509 \tag{38}$$

(when δ^* is small, a minimal value $\lambda_{hv} = 1$ is used) and T'_v is the mean vapour temperature in a postulated wall sublayer (cf. section 2.5), and is given by

$$T'_v = T_v + (\lambda_{hv} - 1)(T_v - T_s) \tag{39}$$

The vapour thermal conductivity k_v is evaluated at T'_v (the other physical properties are taken at T_v).

Equations 33 and 34 are solved for Q_{wv} and Q_{vi}, giving

$$Q_{wv} = \lambda_{hv} \frac{k_v \, \mathrm{Nu}_v}{2\delta(1-\Theta^2)} \frac{P_w + P_i}{2} [(T_w - T'_v) - \Theta(T'_v - T_s)] \tag{40}$$

$$Q_{vi} = \lambda_{hv} \frac{k_v \, \mathrm{Nu}_v}{2\delta(1-\Theta^2)} \frac{P_w + P_i}{2} [(T'_v - T_s) - \Theta(T_w - T'_v)] \tag{41}$$

For laminar flow and constant heat rate, Nu and Θ are given by (Kays, 1980)

$$\mathrm{Nu}_v = 5.385 \tag{42}$$

$$\Theta = 0.346 \tag{43}$$

which we use without restriction on the Reynolds number range, turbulence effects being included in the factor λ_{hv}.

The error made by not accounting for the cylindrical geometry (parallel plates) may be estimated from a pure conduction calculation. For a film thickness-to-radius ratio of 1/3, i.e. a void fraction of 56 %, the relative error on the heat transfer rate is only 1 %.

For a tube, the radiation heat transfer rate is given by

$$Q_r = \frac{\sigma P_i (T_w^4 - T_s^4)}{\frac{1}{\varepsilon_l} + \frac{P_i}{P_w}(\frac{1}{\varepsilon_w} - 1)} \tag{44}$$

and for a bundle by

$$Q_r = \frac{\sigma P_w (T_w^4 - T_s^4)}{\frac{1}{\varepsilon_w} + \frac{P_w}{P_i}(\frac{1}{\varepsilon_l} - 1)} \tag{45}$$

The radiation absorption in the vapour film is neglected. A value $\varepsilon_l = 0.96$ is used for the water emittance (assumed to be equal to the absorbance), according to Eckert's recommendation for 0.1 mm or more thick water (in Rohsenow & Hartnett, 1973, pp. 15-23). For the wall emittance, the values recommended in the experimental data sources analysed are used. For Inconel 600, by default, the following relation is used:

$$\varepsilon_w = 1.979\,10^{-4} T_w + 0.5735 \tag{46}$$

where T_w is expressed in Kelvin.

It is a linear approximation, between 580 K and 1260 K, of the values recommended by Kawaji (1984, pp. 31), based on a report from *The International Nickel Company, Inc.*

2.3.2 Liquid core

Proper modeling of the heat and momentum transfers from the vapour-liquid interface to the bulk of the liquid is of primary importance, as it describes how the wall heat flux is separated into a liquid heating term and a vaporization term. The approach here differs from the original model formulation, in that we consider, as the reference velocity for the transfers, the liquid velocity relative to the interface $U_l - U_i$, instead of U_l (figure 1). This requires use of one more closure equation, which is the liquid-interface friction law. Notice that $U_l - U_i$ is negative, as the vapour velocity is greater than the liquid velocity.

The liquid Reynolds number relative to the interface is defined as

$$\mathrm{Re}_{li} = \rho_l |U_l - U_i| \frac{D_{hl}}{\mu_l} \tag{47}$$

where D_{hl} denotes the hydraulic diameter of the liquid column.

Specific friction and heat transfer laws are used depending on the liquid core geometry. For inverted annular flow in a tube, the liquid flow relative to the interface is assumed to be equivalent to flow in a tube (radius $R - \delta$). For inverted annular flow in a rod bundle, the liquid flow is assumed to be equivalent to flow in a rod bundle (pitch p, rod radius $R + \delta$).

The **interfacial shear stress** is given by

$$\tau_{il} = -f_l \rho_l |U_l - U_i| \frac{U_l - U_i}{2} \tag{48}$$

with different expressions for the friction factor f_l, depending on the geometry and on the flow regime.

For laminar flow in a tube, we use

$$f_l = \lambda_l \frac{16}{\mathrm{Re}_{li}} \tag{49}$$

while for turbulent flow,

$$f_l = \lambda_l \frac{0.079}{\mathrm{Re}_{li}^{0.25}} \tag{50}$$

where λ_l is a factor given by

$$\lambda_l = c_5(1 + c_6 \frac{D_h}{z}) \tag{51}$$

$$c_5 = 4.18 \tag{52}$$

$$c_6 = 0.7 \tag{53}$$

and accounting for the enhancement of the transfers from the interface to the liquid, in particular due to interfacial disturbances, and for entrance length effects (section 2.5). When z is small, a maximal value $\lambda_l = 10$ is used.

For a rod bundle, we use the results of Cheng and Todreas (in Todreas & Kazimi, 1989), which depend on the flow regime and the bundle geometry. The friction factor is given by

$$f_l = \lambda_l \frac{c_l}{\mathrm{Re}_{li}^n} \tag{54}$$

with

$$4\, c_l = a + b(\frac{p}{D'} - 1) + c(\frac{p}{D'} - 1)^2 \tag{55}$$

and

$$D' = 2(R + \delta) \tag{56}$$

Values of the coefficients n, a, b and c, valid for pitch-to-diameter ratios between 1.1 and 1.5, are presented in table 1. λ_l is the IAFB-specific factor given by equations 51 to 53.

Flow regime	laminar		turbulent	
Lattice	square	triangular	square	triangular
n	1		0.18	
a	35.55	62.97	0.1339	0.1458
b	263.7	216.9	0.09059	0.03632
c	-190.2	-190.2	-0.09926	-0.03333

Table 1: **Coefficients in equations 54 and 55.**

The liquid-to-interface friction factor is corrected for the influence of temperature dependent properties; this correction may be significant for high liquid subcooling. Denoting by f_l the value given by the above equations and f_{lc} the corrected value, the following relations are used (Kays, 1980).

For laminar flow:

$$f_{lc} = f_l \left(\frac{\mu_s}{\mu_l}\right)^{0.58} \tag{57}$$

and for turbulent flow:

$$f_{lc} = f_l \left(\frac{\mu_s}{\mu_l}\right)^{0.25} \tag{58}$$

where μ_s is the liquid viscosity at the saturation temperature T_s and μ_l the liquid viscosity at the mean liquid temperature T_l.

The largest of the laminar or turbulent values of the friction coefficient is used. In practice, laminar flow is only predicted over very short lengths near the quench front: from some fractions of a millimeter for the largest hydraulic diameters in our data bank (about 14 mm), to some millimeters for the smallest (4 mm).

The **heat transfer from the interface** at T_s to the bulk of the liquid is expressed by

$$Q_{lh} = h_l P_i (T_s - T_l) \tag{59}$$

where T_l is the bulk liquid temperature and h_l the liquid-interface heat transfer coefficient.

For laminar flow, the liquid-interface Nusselt number

$$\mathrm{Nu}_l \triangleq \frac{h_l D_{hl}}{k_l} \tag{60}$$

for a tube at constant surface temperature is given by

$$\mathrm{Nu}_l = 3.66 \tag{61}$$

In a rod bundle, the results of Sparrow & Loeffler (in Todreas & Kazimi, 1989), based on constant axial heat flux, are used. For uniform circumferential temperature and a pitch-to-diameter ratio of 1.13,

$$\mathrm{Nu}_l = 6.0 \tag{62}$$

For a pitch-to-diameter ratio of 1.33,

$$\mathrm{Nu}_l = 9.4 \tag{63}$$

As these values correspond to a constant axial heat flux boundary condition and the modeled situation is for a constant (saturation) axial temperature, in an attempt to correct them, they are multiplied by the ratio

$$\frac{\mathrm{Nu}_t}{\mathrm{Nu}_f} \tag{64}$$

where Nu_t and Nu_f are the constant temperature and constant heat flux Nusselt numbers in a tube:

$$\mathrm{Nu}_t = 3.66 \tag{65}$$

$$\mathrm{Nu}_f = 4.364 \tag{66}$$

The laminar heat transfer coefficient is also corrected for the influence of temperature dependent properties according to Kays (1980). The corrected value is

$$h_{lc} = h_l \left(\frac{\mu_s}{\mu_l}\right)^{-0.14} \tag{67}$$

Finally, to account for interfacial disturbance effects, the same factor λ_l as for the friction coefficient is applied to h_{lc}.

For turbulent flow, the liquid-interface heat transfer coefficient is deduced from the interfacial shear stress through the Chilton-Colburn analogy:

$$h_l = \frac{|\tau_i| \, c_{pl}}{|U_l - U_i| \, \mathrm{Pr}_l^{2/3}} \tag{68}$$

The enhancement factor λ_l is implicitely applied to h_l through τ_i. Again, the largest of the two values of the heat transfer coefficient for laminar or turbulent flow is used.

2.4 Implementation

The initial values of the variables p, U_v, U_l, α_l, T_v and T_l at the quench front, the quench front velocity, and the wall temperature distribution in the dry region are given as input to the calculations. Equations 1 to 6, together with the closure laws 7 to 68 are solved by a standard Runge-Kutta method. As the computed variables may vary strongly near the quench front, a very small initial step (10^{-10} m) is used. This step is then exponentially increased.

The results allow us to derive the distribution of the wall heat flux, given by

$$q_w = \frac{Q_w}{P_w} = \frac{Q_{wv} + Q_r}{P_w} \tag{69}$$

and of a heat transfer coefficient defined by

$$h \triangleq \frac{q_w}{T_w - T_s} \tag{70}$$

where T_s is the saturation temperature.

2.5 Semi-empirical description of interfacial disturbance effects

2.5.1 Needs

Numerous reported observations of IAFB (De Jarlais & Ishii, 1985; Kawaji et al., 1985; Costigan & Wade, 1984; Edelman et al., 1983) indicate that the vapour-liquid interface is irregular. In addition, liquid droplets may be entrained in the vapour film, as well as vapour bubbles in the liquid core. It is generally agreed that the interfacial disturbances should increase the wall heat flux by locally thinning the vapour film and lowering the vapour temperature. The vapour-liquid momentum and heat transfer should also be enhanced, due to the hydrodynamic drag of interfacial waves, to the enlargement of the transfer area, and to the transfers between the vapour and liquid droplets. The interfacial disturbances also promote the appearance of turbulence in the vapour film, which further enhances heat and mass transfer. Finally, the interface-liquid bulk heat and momentum transfers should also be increased, due to roughness effects. The true boundary condition, i.e. a fluid-fluid instead of fluid-wall interface, should also play a role in that it affects the turbulence structure near the interface (e.g., Rashidi & al., 1991).

The way interfacial disturbance effects were accounted for in the original model is shown below to present some shortcomings. A new formulation of the momentum and heat transfer enhancements due to interfacial disturbances has since been developed and included in the IAFB model.

2.5.2 Physical background

The physical processes involved in heat and momentum transfer enhancement, i.e. waves, oscillations of the whole liquid core, droplet entrainment and redeposition, and turbulence, are very complex. As their modeling only represents one part of the IAFB model, which is in other respects already complex,

any attempt of a fully analytical description of these effects seems hopeless. Therefore, these effects are accounted for in a global, semi-empirical manner. Four physical processes are specifically adressed, i.e. the momentum and heat transfers in the vapour and the liquid.

On the vapour side, a first enhancement factor λ_{fv} is applied to the **vapour-interface momentum transfer** (equation 25). It accounts for the hydrodynamic drag of interfacial waves, the equivalent roughness effect of ripples, and the momentum transfer between the vapour and liquid droplets. This factor will be correlated empirically.

The **vapour film heat transfer** description is modified, based on the following simple considerations and assumptions. The effective thermal conductivity in the vapour film may be much higher near the vapour-liquid interface than near the wall, due to interfacial waves, entrained droplets and turbulence. The temperature profile is then almost flat near the interface, and steep near the wall. The film is arbitrarily split into two sublayers (figure 2).

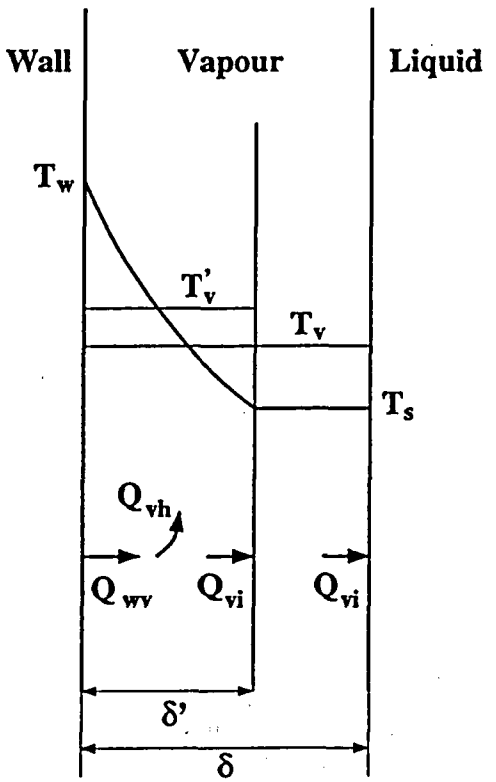

Figure 2: **Film heat transfer model.**

Near the interface, the vapour temperature is assumed to be uniform and equal to the saturation temperature. Near the wall, a laminar sublayer of thickness δ' is assumed to control heat transfer. The heat rates entering and leaving this sublayer are then given by (section 2.2, equations 31 and 32)

$$Q_{wv} = \frac{k_v \, \mathrm{Nu}_v}{2\delta'} \frac{P_w + P_i}{2} \frac{(T_w - T'_v)}{1 + (\frac{Q_{vi}}{Q_{wv}})\Theta} \tag{71}$$

$$Q_{vi} = \frac{k_v \, \mathrm{Nu}_v}{2\delta'} \frac{P_w + P_i}{2} \frac{(T'_v - T_s)}{1 + (\frac{Q_{wv}}{Q_{vi}})\Theta} \tag{72}$$

where T'_v denotes the mean vapour temperature in the wall sublayer.

Introducing the factor λ_{hv} defined as

$$\lambda_{hv} \triangleq \frac{\delta}{\delta'} \tag{73}$$

where δ is the total film thickness, equations 71 and 72 become

$$Q_{wv} = \lambda_{hv} \frac{k_v \, \mathrm{Nu}_v}{2\delta} \frac{P_w + P_i}{2} \frac{(T_w - T'_v)}{1 + (\frac{Q_{vi}}{Q_{wv}})\Theta} \tag{74}$$

$$Q_{vi} = \lambda_{hv} \frac{k_v \, \mathrm{Nu}_v}{2\delta} \frac{P_w + P_i}{2} \frac{(T'_v - T_s)}{1 + (\frac{Q_{wv}}{Q_{vi}})\Theta} \tag{75}$$

Neglecting the vapour film curvature and the velocity profile effects, T_v (the mean bulk vapour temperature used in the 6 equation model), T'_v, T_s (the saturation temperature), δ and δ' are related by

$$T_v = \frac{\delta'}{\delta} T'_v + \frac{(\delta - \delta')}{\delta} T_s \tag{76}$$

or

$$T'_v = T_v + (\lambda_{hv} - 1)(T_v - T_s) \tag{77}$$

The factor λ_{hv} will be correlated empirically.

The simple model proposed does not attempt a rigorous description of the heat transfer in the vapour film. It only provides a basis for a correlation.

It should be pointed out that, for realistic values of the variables involved, the predicted wall and interfacial heat transfer rates Q_{wv} and Q_{vi} are very close, and about equal to the pure conduction heat transfer rate through a vapour film of thickness δ, enhanced by a factor λ_{hv}. This is due to the low thermal capacity of the vapour film. Nevertheless, the use of equations 74, 75 and 77, rather than of a single conduction equation presents a major advantage. It allows to keep the frame of a full 6-equation model, whereas a single conduction equation would have fixed the vapour temperature at the average value between wall and saturation temperatures, making the vapour energy conservation equation obsolete. Moreover, the proposed model may predict a much lower value of the vapour temperature than the average between wall and saturation, which is realistic and significant, in that it influences the values of the steam physical properties.

As, according to the present model, the heat transfer is controlled by the wall sublayer, the vapour thermal conductivity k_v is evaluated at the temperature T'_v, whereas the vapour physical properties which are involved in the hydrodynamic equations, i.e. density and viscosity, are evaluated at the mean bulk temperature T_v.

The expressions for the λ_{fv} and λ_{hv} factors, which characterize the momentum and heat transfer enhancement in the vapour film, have to rely on experimental data. Correlations have to be developed, which should, to the extent possible, involve the determining physical variables.

In the original model, the following enhancement factor,

$$\lambda = 1 + 150\,(\delta/R) \tag{78}$$

where δ denotes the film thickness and R the tube diameter, was applied to both the vapour-interface heat and momentum transfers. This correlation due to Wallis (1970) has also been applied to IAFB by Fung & Groeneveld (1981). However, it has originally been developed for the friction coefficient between the gas core and the gas-liquid interface in annular flow, which is quite a different situation. The correlating variable δ/R itself seems inadequate for IAFB in general. For example, this variable looses its significance in the ideal, limiting case of film boiling along a vertical flat plate, whereas the transfer enhancement mechanisms are still present in this case.

Another shortcoming of the original model is that the enhancement factor λ was only applied to the vapour-interface heat flux, and not to the wall-vapour heat flux. The wall heat flux was only indirectly modified, through the decrease in vapour temperature; as a consequence, for a given film thickness,

it could not be increased by a factor greater than two (a factor two would correspond to an infinite value of the enhancement factor, and to a vapour temperature equal to the saturation temperature). This is clearly shown by experimental values of the wall heat flux enhancement factor (figure 4) to be insufficient.

The enhancement of the vapour-interface transfers may be attributed to two basic mechanisms, i.e. turbulence and continuity waves. These two mechanisms, which are mutually dependent, appear to be strongly related to the vapour Reynolds number. Evidence of the Reynolds number influence on the development of continuity waves may be found in linear stability analyses as the one by Kao et al. (1972). Shortly, inverted-annular flow (IAF) is always unstable with respect to long wavelengths (for short wavelengths, surface tension acts as a restoring force), and the rate of growth of instabilities strongly increases with the vapour Reynolds number.

The hydrodynamic stability of IAF is influenced by several other parameters than the vapour Reynolds number. However, it seems reasonable to leave these effects aside in this study, which mostly concerns the reflooding of nuclear reactor cores with water. The following qualitative justification may be given. As long as the liquid is water in a relatively narrow temperature range (i.e. with relatively constant physical properties), with a much larger hydraulic diameter than that of the vapour film and a much lower velocity, the hydrodynamic boundary conditions for the vapour film remain more or less the same. The vapour and interface hydrodynamics are thus largely specified by the vapour Reynolds number.

Thus, the vapour film Reynolds number appears to be a convenient correlating variable for λ_{fv} and λ_{hv}. Unfortunately, no vapour velocity measurements are available. A correlation based on the vapour Reynolds number would then have to rely on a computed vapour velocity, which seems precarious for further applications. Thus, use was made of a dimensionless film thickness, defined as follows:

$$\delta^* = \delta \left[\frac{\rho_v(\rho_l - \rho_v)\, g}{\mu_v^2}\right]^{\frac{1}{3}} \tag{79}$$

The link between the vapour Reynolds number and the non-dimensional film thickness δ^* appears by considering the momentum conservation equations in the IAFB two-fluid model (equations 3 and 4). A linear combination of these equations, with the factors $(1-\alpha_l)$ and $(-\alpha_l)$ respectively, neglecting the convective terms (which, according to the numerical results, is realistic, even with significant vaporization), gives

$$\frac{\tau_i P_i}{A} + \alpha_l \frac{\tau_w P_w}{A} = \alpha_l(1-\alpha_l)(\rho_l - \rho_v)g \tag{80}$$

Physically, relation 80 expresses that the vapour film buoyancy is entirely compensated by the wall and interfacial friction forces.

Assuming laminar vapour flow, a liquid fraction close to 1, and a liquid velocity much lower than the vapour velocity, and assimilating the vapour-liquid interface to a smooth wall, gives

$$P_i \simeq P_w \tag{81}$$

$$1-\alpha_l \simeq \frac{P_i\,\delta}{A} \tag{82}$$

$$\tau_i \simeq \tau_w \simeq \frac{24}{\mathrm{Re}_v}\rho_v \frac{U_v^2}{2} \tag{83}$$

where the vapour Reynolds number Re_v is given by

$$\mathrm{Re}_v \triangleq \frac{\rho_v U_v\, 2\delta}{\mu_v} \tag{84}$$

Substituting U_v (equation 84) in equation 83 yields

$$\tau_i = \frac{3\,\mu_v^2}{\rho_v\,\delta^2}\,\mathrm{Re}_v \tag{85}$$

Whith the above simplifications, equation 80 becomes

$$\tau_i = \frac{(\rho_l - \rho_v)g\,\delta}{2} \tag{86}$$

Combining equations 85 and 86 produces

$$\mathrm{Re}_v = \frac{(\delta^*)^3}{6} \tag{87}$$

which means that, under the assumptions made, δ^* may replace Re as the correlating variable. Real IAF approaches the "ideal" situation pictured by these assumptions near the quench front, and further up if the liquid subcooling remains high (in this case, the wall heat flux is high and goes almost entirely into the liquid core, the vapour film remaining thin). Indeed, very thin vapour films should remain laminar, and, according to the reported observations, relatively smooth. Relation 87 is no longer valid for very high flooding rates (of the order of 1 m/s or greater), where the liquid velocity may no longer be neglected.

A similar analysis with a turbulent friction law (constant friction coefficient) leads to a vapour Reynolds number proportional to $(\delta^*)^{3/2}$. Thus, the physical effects attributed to the Reynolds number may also be correlated with δ^* if some turbulence is present. Finally, it has been checked that the relation between Re_v and δ^* does not depend on the flow geometry (tube or rod bundle).

In summary, the quantity δ^* appears as a physically suited correlating parameter for the vapour-interface transfer enhancement during IAFB in reflooding situations.

A third enhancement factor, λ_l, is applied to the **interface-liquid momentum transfer** (equations 49 to 54). As the **heat transfer** is deduced from the momentum transfer using the Chilton-Colburn analogy (equation 68), it is also affected by this third coefficient.

The choice of correlating parameters for this factor is difficult. Indeed, the enhancement of the transfers within the liquid core may be attributed to several distinct effects. There is an increase of the transfers near the quench front due to the violent changes in the flow that take place there and cause a strong mixing. This effect should decrease downstream due do the development of a velocity profile in the liquid core. There is also a "roughness" effect due to the interfacial disturbances. This should increase along the flow, as the film Reynolds number and the wave amplitudes increase.

In the original model, the entrance-length effect was approximately accounted by applying the following enhancement factor,

$$F = 1 + 1.4\,(R/z) \tag{88}$$

to the interface-liquid heat transfer, where R denotes the tube diameter and z the distance from the quench front. This factor approximatively fits the thermal-entrance-length effect for turbulent flow in a circular tube, for constant heat rate and a Prandtl number of the order of 0.7 (the Reynolds number has little influence) (e.g., Kays, 1980, figs. 13-8 and 13-9, pp. 264 and 265).

Still in the original model, another enhancement factor was required (a constant value of 2.5 was used), in some cases, in order to reach good agreement between the experimental and computed results. This was attributed to the "roughness" effect.

R/z or, rather, D_h/z (D_h: hydraulic diameter of the flow) seems a convenient correlating parameter with regards to the entrance-length effect, whereas the "roughness" effect could be accounted by using δ/D_h.

2.5.3 IAFB-specific correlations

The enhancement factors λ_{fv}, λ_{hv} and λ_l have been correlated using Fung's (University of Ottawa, 1981) experimental results. Fung obtained steady-state, post-dryout heat transfer data for vertical flow of water inside electrically heated inconel tubes of about 12 mm inside diameter and 800 mm length. The data were obtained using the "hot patch" technique in which an indirectly heated copper block brazed onto the inlet of the test section supplies the critical heat flux. This hot patch stabilizes the quench front upstream of the tube, which may then be operated in post-dryout, down to relatively low heat fluxes and steam qualities. The wall temperature was measured at ten locations, and the heat

transfer rates were derived from these measurements, taking into account axial conduction and heat losses. The void fraction was measured at five locations using γ-densitometry. The way input data for the present IAFB model are obtained from Fung's data, is described in section 3, together with the processing of data from other sources.

Fung's results constitute a particularly well suited data base for IAFB-specific correlations since many of his experiments were performed in the IAFB-relevant parameter range (34 have been used for the new correlations) and they also include void fraction measurements. In addition to specifying a meaningful variable all along the flow, these measurements give access to the film thickness and thus to the correlating variable δ^* (equation 79).

Values of the three enhancement factors along the flow have been obtained, for each experiment, in the following way: All along the length of the flow, two experimental results are available, i.e. the wall heat flux and the void fraction. Near the quench front, the first enhancement factor (vapour friction) has little influence on the numerical results. The underlying physical reason is that, the liquid subcooling being high, most of the wall heat flux goes into the liquid core, and vapour generation is low. On the contrary, far away from the quench front, the third enhancement factor (transfers inside the liquid) becomes ineffective. The reason is that the liquid is close to saturation, and only absorbs a small part of the wall heat flux. Each experimental (heat flux and void fraction vs. distance from the quench front) curve was divided into two sections. In the first section, near the quench front, the second enhancement factor (vapour heat transfer) and the third one (transfers inside the liquid) were considered as dominant and stepwise computed, at each elevation, from the experimental results. In the second section, further downstream, the first enhancement factor(vapour friction) and the second one (vapour heat transfer) were computed. In each section, an extrapolation was used for the remaining enhancement factor. The results from each section depend to some extent on the results from the other. An iterative procedure was thus used until convergence was reached. The process was complex and partly interactive.

The results obtained for λ_{fv} (vapour-interface friction) differ to some extent from one experiment to another. Nevertheless, a common trend may clearly be detected, as may be seen in figure 3. The results obtained for λ_{hv} (heat transfer in the vapour film) correlate fairly well with δ^*, as shown in figure 4. It may be noted that no clear transition to turbulence (change in slope) appears in this curve.

The following laws are retained for the relations between the first two enhancement factors and δ^*:

$$\lambda_{fv} = c_1(\delta^*)^{c_2} \tag{89}$$

$$c_1 = 0.0362 \tag{90}$$

$$c_2 = 1.96 \tag{91}$$

$$\lambda_{hv} = c_3(\delta^*)^{c_4} \tag{92}$$

$$c_3 = 0.679 \tag{93}$$

$$c_4 = 0.509 \tag{94}$$

(When δ^* becomes small, λ_{fv} and λ_{hv} are not allowed to drop below 1, which would be physically meaningless).

The results obtained for λ_l (interface-liquid transfers, figure 5) are quite scattered, especially in the region downstream from the hot patches where, for some experiments, λ_l takes very large values. This might be due to a shortcoming of the present IAFB model, due e.g. to a physical phenomenon not being accounted for in this zone. However, it is believed that the hot patch technique is, at least partially, responsible for the effect observed. Indeed, the same trend (enhanced heat flux, in some cases, in the

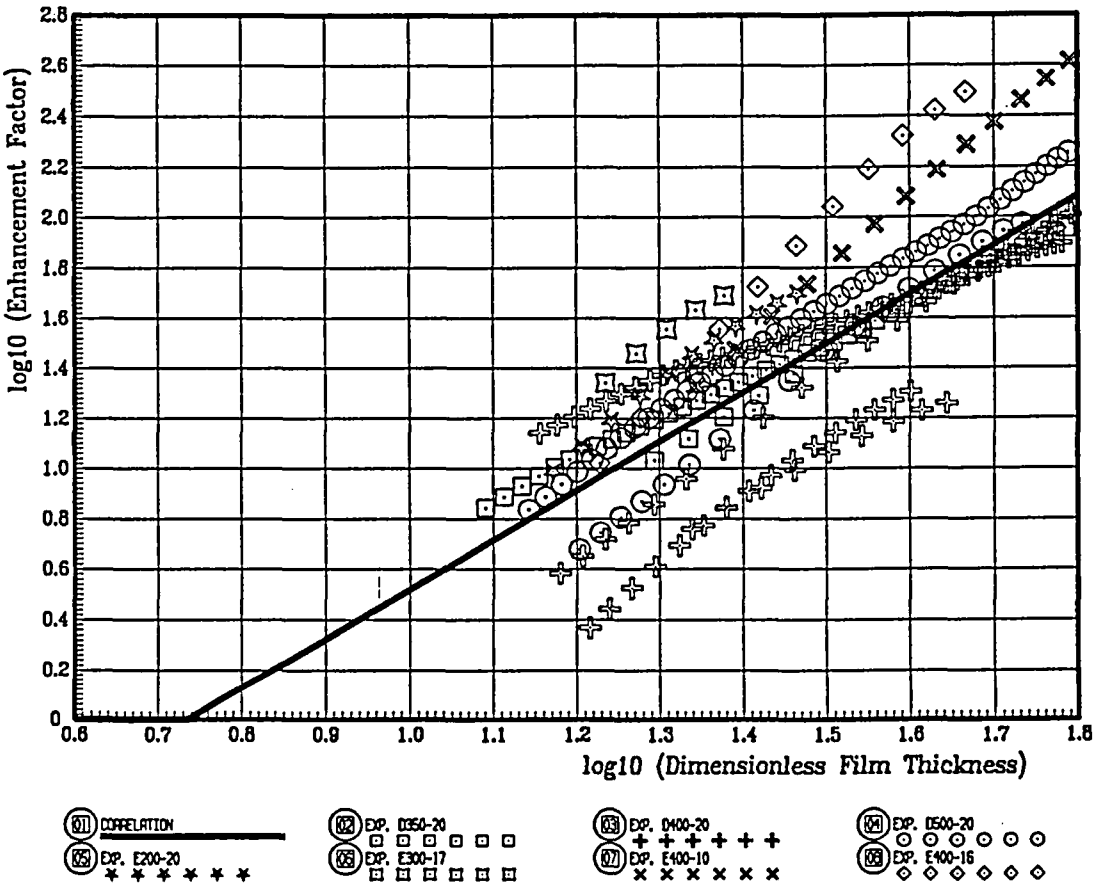

Figure 3: **Vapour-interface friction.**
Correlation of the vapour-interface friction enhancement factor λ_{fv} using Fung's (1981) experimental data.
The absence of experimental points in the left part of the graph is due to the low influence of the vapour-interface friction in this region (see text).
In the experiment designation, the first letter refers to the test section. The first three numbers represent the inlet velocity (in mm/s) and the last two represent the inlet subcooling (in °C).

region downstream from the hot patch) may be directly observed in the wall heat flux profiles (curves in Annex). The hot patches being relatively long, i.e., 5.3 times the tube diameter in most cases and 2.1 in the remaining ones, and the quench front being most likely situated near the hot patch inlet, the zone concerned is already quite far from the quench front. Extrapolation of the measured heat flux up to the quench front region yields, in the cases concerned, to very high values, several times larger than for comparable reflooding experiments without hot patch. The high values of the wall heat flux downstream from the hot patch are encountered when the wall temperature is relatively low in this region (roughly, below 600 °C). The heat transfer enhancement might be due to partial and/or intermittent rewetting of the inconel tube downstream from the hot patch. Anyway, this effect, which seems to be hot-patch-related, is left aside in this study, which mostly concerns reflooding. However, this means that the values of λ_i obtained may only be used rather far from the hot patch.

For all experiments, at some point, λ_i reaches an approximatively constant value (figure 5). The average of the quasi-constant values obtained for the 14 experiments analysed is 4.18, with a standard deviation

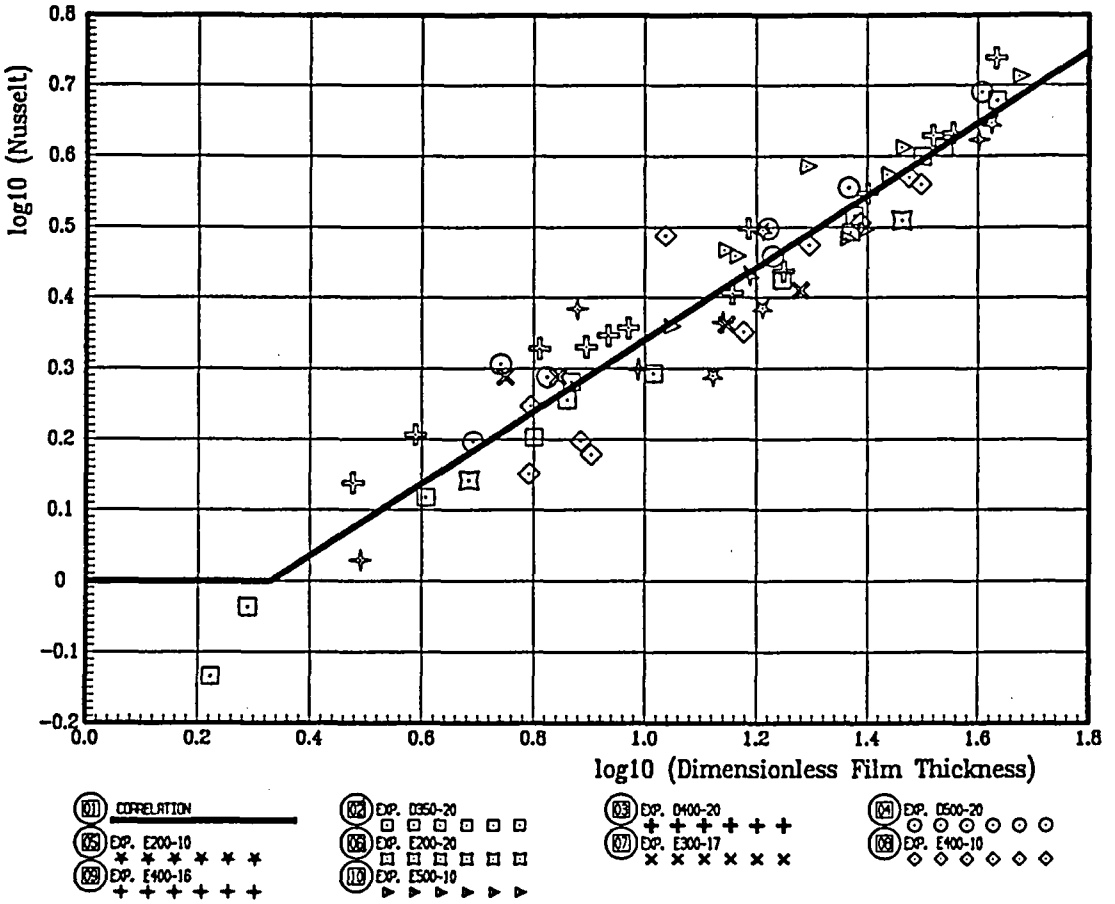

Figure 4: **Vapour film heat transfer.**
Correlation of the vapour film heat transfer enhancement factor λ_{hv} using Fung's (1981) experimental data.
The basic model is very close to pure conduction; the enhancement factor may be interpreted as a Nusselt number.
Experiment designation as in figure 3.

of 0.61, which gives, with a 95% probability threshold:

$$\lambda_l = 4.18 \pm 0.35 \tag{95}$$

The obtention of a constant value may be interpreted as follows: in a tube, according to Norris (Kays, 1980, pp. 271), the heat transfer increases with the wall roughness up to a certain point only, and then remains unchanged. For the liquid core in IAFB, far from the quench front, the vapour-liquid interface would thus be equivalent to a very rough wall.

The constant value $\lambda_l = 4.18$ far from the quench front is retained in the present IAFB model. Entrance-length effects should also be accounted for in the quench front region. As the results derived from Fung's data may not be used in this region, the relation used in the original model (equation 88) is combined

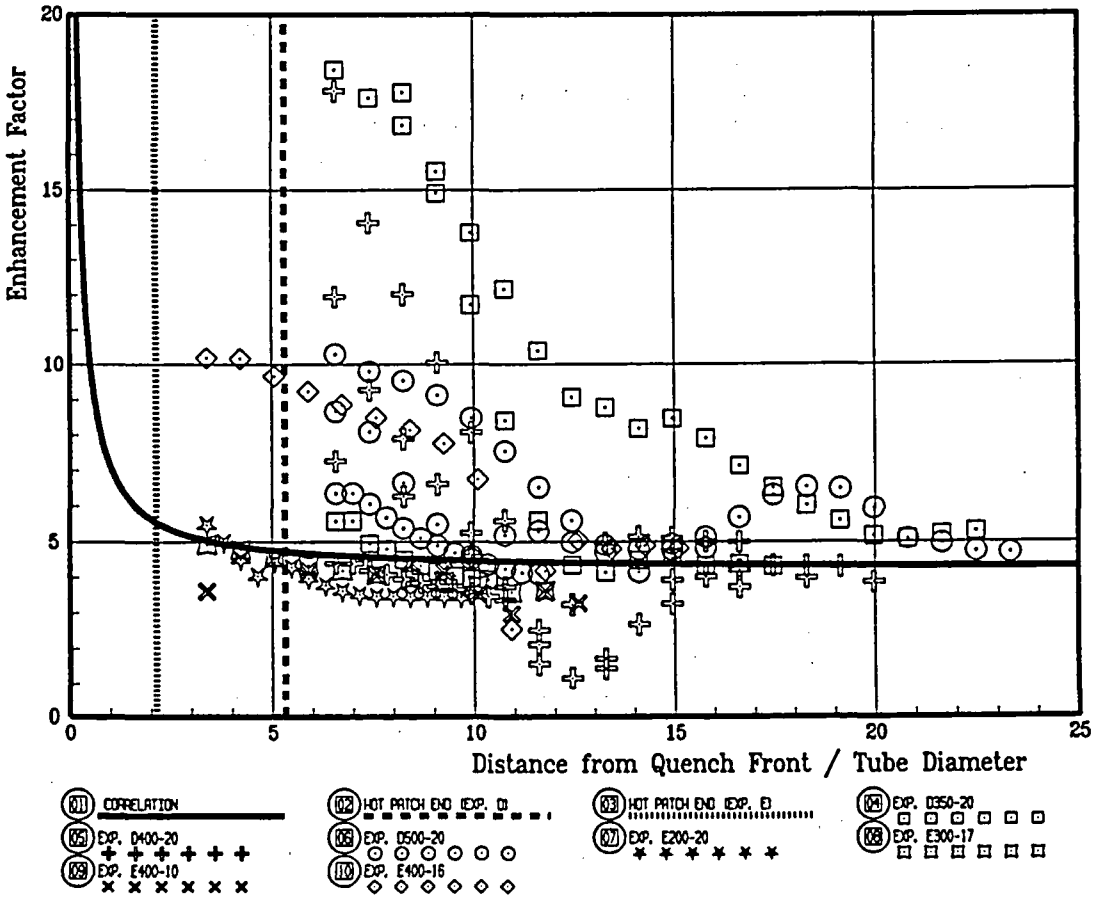

Figure 5: **Interface-liquid transfers.**
Correlation of the interface-liquid transfer enhancement factor λ_l using Fung's (1981) experimental data. The quench front is assumed to be located at the hot patch inlet. The vertical lines represent the hot patch end, for each test section.
The large values of λ_l, in the left part of some curves, are attributed to a hot-patch-specific effect, and not accounted for in the correlation (see text).
Experiment designation as in figure 3.

with the result obtained here in the following way:

$$\lambda_l = c_5(1 + c_6 \frac{D_h}{z}) \quad (96)$$

$$c_5 = 4.18 \quad (97)$$

$$c_6 = 0.7 \quad (98)$$

where D_h denotes the hydraulic diameter of the flow and z the distance from the quench front. When z is small, a maximal value $\lambda_l = 10$ is used.

As explained above, the empirical parameters appearing in the new correlations have been derived from Fung's results (1981) only, whereas experimental data from other sources have been processed and analysed (sections 3 and 4). A statistical analysis has been conducted (Schraeder, 1992) to try to optimize these parameters with respect to the entire data bank. Slightly better parameter sets could thus be obtained for each individual series of experiments (for example, for the NEPTUN tight lattice

experiments), but the overall prediction could not be significantly improved. As Fung's experiments provide more experimental information than the others (i.e. void fraction measurements), it has been decided to keep the empirical coefficients unchanged.

Finally, it should be pointed out that the model results are very sensitive to the value of λ_{hv} (film heat transfer enhancement), the two other factors representing smaller corrections. The derivation of this factor from the experimental results is rather straightforward, and can be achieved independently from the IAFB model. Indeed, as mentioned above, λ_{hv} is very close to the ratio between the convection wall heat flux and the pure conduction heat flux (the small difference corresponding to the vapour sensible heating rate):

$$\lambda_{hv} \simeq \frac{q_{wv}}{q_{cond}} \tag{99}$$

with

$$q_{wv} = q_w - q_r \tag{100}$$

(q_r is the radiation heat flux) and

$$q_{cond} = k_v \frac{T_w - T_s}{\delta} \tag{101}$$

The variables involved in equations 99 and 101, as well as in the correlating variable δ^* (equation 79), are directly derived from experimental results (provided void fraction or film thickness measurements are available). The correlation proposed for λ_{hv} (equation 92) has thus an intrinsic value and is very reliable, provided the experimental results used are precise.

Another advantage of this correlation (and also of the correlation proposed for λ_{fv}, equation 89) is that it is, to a large extent, independent of the flow channel geometry and of the parameter ranges. The reason for this is that the vapour film geometry remains the same, i.e. an annular geometry, in both a tube and a rod bundle. The tube or rod diameter should not much influence the results since the most determining parameter is the film thickness, which keeps the same order of magnitude in all cases. The only significant limitation of the correlation is at high liquid velocities (several m/s), where the interface velocity is no longer small in comparison with the vapour velocity; in this case, as mentioned above, δ^* is no more suited as a correlating variable. Experimental results corresponding to this situation are presented in section 3. However, this situation is not likely to occur during reflooding.

3 Processing of experimental data

The model presented above has been assessed against experimental data from four independant sources. The first one is the NEPTUN rod bundle reflooding experiment at the Paul-Scherrer Institute (Dreier et al., 1990; Grütter et al., 1980). The second one is the University of California-Berkeley single tube, internally reflooded tube experiment (Seban, 1983; Seban et al., 1978). The third and the fourth ones are the University of Ottawa (Fung, 1981) and UKAEA-Winfrith (Savage et al., 1989, 1991) steady-state tube experiments using the hot patch technique. Among the available data, the most relevant to the IAFB regime have been selected, i.e. the experiments where the equilibrium quality above the quench front is still negative and the quench front velocity is much lower than the flooding rate. In fact, among the NEPTUN and UC-Berkeley data, these IAFB-relevant experiments constitute a minority. For the University of Ottawa and UKAEA-Winfrith data, the availability of void fraction measurements has also been a choice criterion.

3.1 NEPTUN data

3.1.1 Experimental conditions

The data analysed were obtained by forced-feed bottom reflooding of a simulated standard pressurized water reactor (PWR) bundle (Frei & Stierli, 1984; Stierli & Yanar, 1985) and a simulated light water

high conversion reactor (LWHCR) bundle (Rouge, Dreier & al., 1992). The heated length was 1.68 m. A continuously variable cosine profile with a peaking factor of 1.58 was used. The PWR bundle consisted of 33 electrically heated rods and 4 guide tubes, with a square lattice and a pitch-to-diameter ratio of 1.33 (13.6 mm hydraulic diameter), placed in an octagonal housing. The LWHCR bundle consisted of 37 heated rods, with a triangular lattice and a pitch-to diameter ratio of 1.13 (4.4 mm hydraulic diameter), placed in a hexagonal housing.

The test bundle was instrumented at 8 equally spaced levels. At these levels, the cladding temperature was measured, and the wall heat flux was derived by means of an inverse one-dimensional heat conduction computation (Güntay, 1980; Aksan et al., 1979).

The quench time of each measurement level is derived from the temperature vs. time traces. An interpolation gives the time trace of the quench front position, and the quench front velocity is derived (Dreier, 1985).

The liquid flow rate and temperature at the inlet of the bundle are measured, as well as the absolute pressure at the outlet of the bundle and the differential pressures between the successive levels and for the whole test section.

The measurement results obtained for the various rod bundles tested, as well as the secondary variables, have been put together, in a standardized form, in the *NEPTUN Working Data Bank* (Taube, 1985; Richner & Dreier, 1986; Rouge, 1990; Rouge et al., in progress). Documented software (Richner, 1987; Rouge, 1989) allow easy access, visualization and processing of the data.

3.1.2 Interpolation method

For implementation and assessment of the model, the wall temperature and heat flux are needed as functions of the distance from the quench front, $\zeta = z - z_{qf}$, for a given position of this quench front. What is, however, available are only several temperature and heat flux histories at discrete elevations. Thus, a specific interpolation method was devised to obtain the temperature and heat flux profiles, minimizing the error introduced by this procedure.

The temperature, for example, is only known as a function of time at the eight measurement levels. The measured values are transposed from the (t, z) coordinates into the (t, ζ) coordinates. In this frame, the temperature is known on eight curves $\zeta(t)$ corresponding to the eight thermocouples. The value of the temperature at a given time and a given ζ is interpolated vs. time between the values given by two successive thermocouples for the same ζ (but at different times). This is coherent with the assumption of a quasi-steady process propagating with the quench front velocity.

3.1.3 Conditions at the quench front

The values of the flow variables immediately above the quench front are needed as initial conditions for the model. In practice, it is assumed that the whole heat release at the quench front serves to reduce the liquid subcooling (no vapour generation). The validity of this assumption is discussed below. The liquid velocity and temperature, and the pressure, have to be specified.

The liquid velocity is deduced from the inlet flow-rate. The pressure at the quench front p_{qf} is deduced from the measured values of the pressure at the outlet of the bundle p_{out} and the test section pressure drop $[\Delta p]_{in}^{out}$, assuming a zero void fraction below the quench front and neglecting the frictional and accelerational terms in this region:

$$p_{qf} = p_{out} + [\Delta p]_{in}^{out} - \bar{\rho}_l g z_{qf} \tag{102}$$

where z_{qf} denotes the quench front elevation and $\bar{\rho}_l$ the average liquid density (averaged between the

inlet and saturation conditions).

The liquid temperature is derived from a heat balance following a fluid particle:

$$\rho_l A c_{pl} \frac{DT_l}{Dt} = q_w P_w \tag{103}$$

where $\frac{D}{Dt}$ denotes the substantial derivative; q_w is the wall heat flux and P_w the wall perimeter.

Relation 103 is integrated numerically between the bundle inlet and the quench front, which requires knowledge of the wall heat flux at any axial position and at any time. This heat flux is evaluated using the interpolation method described above.

3.2 UC-Berkeley data

These data were obtained by forced reflooding of single electrically heated vertical tubes, about 14.3 mm in inside diameter and 3.7 m high. The wall temperature was measured at several points along the tube. The wall heat flux was then estimated from a lumped-parameter heat balance for the heated wall, the heat losses being accounted for.

The software developed for the NEPTUN data require, as input, detailed computer files of numerous experimental variables. For lack of such files, these software could not be applied to the UC-B results. More approximative procedures had to be used for the derivation of the wall temperature and heat flux distributions, and of the liquid temperature just above the quench front. The measurements from a single thermocouple were used to obtain the entire temperature and heat flux distributions, as a function of the distance from the quench front approaching that particular thermocouple; a space-time transformation (without interpolation of data from adjoining thermocouples) was used.

For the liquid temperature just above the quench front, the following model is used. The basic assumption is that the liquid enthalpy rise between the test section inlet and a cross section situated just above the quench front results from the superposition of two contributions: the release of the heat (electrically) generated in the wall, and the heat release associated with the quench phenomenon:

$$\Delta h_l = (c_p T)_l^+ - (c_p T)_l^{in} = (\Delta h_l)_{el} + (\Delta h_l)_q \tag{104}$$

where the superscripts *in* and + refer to the test section inlet and the quench front, respectively.

The first contribution (electrical heating) is evaluated using the energy balance for the fluid and the solid wall (tube) in the fixed control volume limited by the test section inlet and the quench front position at the time considered. As in Lee et al. (1983), the release of the electrically generated heat is assumed to be a steady process. The energy balance reads

$$\rho_l A V_l^{in} (\Delta h_l)_{el} = \dot{Q}_{el} - \dot{Q}_l \tag{105}$$

where $\dot{Q}_{el}$ and $\dot{Q}_l$ denote the electrical power and the heat losses (for the region concerned), respectively.

The heat release associated with the quench is assumed to be a quasi-steady process, i.e., invariant in a frame of reference moving with the quench front. Therefore, for the evaluation of the resulting liquid enthalpy rise, the control volume (between inlet and quench front) is assumed to move with the quench front velocity V_{qf}. The energy balance for the fluid and the solid wall reads

$$\rho_l A (V_l^{in} - V_{qf})(\Delta h_l)_q = [(CT)_w^+ - (CT)_w^{in}] V_{qf} \tag{106}$$

where C_w denotes the wall heat capacity per unit length.

Equations 104 to 106 give

$$T_l^+ = T_l^{in} + \frac{1}{c_{pl}\rho_l A}\left[\frac{\dot{Q}_{el} - \dot{Q}_l}{V_l^{in}} + \frac{[(CT)_w^+ - (CT)_w^{in}]V_{qf}}{V_l^{in} - V_{qf}}\right] \quad (107)$$

The approximative relation proposed (equation 107) has been assessed against the (presumably) more accurate computational procedure developed for the NEPTUN data (integration of equation 103), using the NEPTUN data bank. The results are remarkably coherent (less than 2 °C difference for T_l^+ for the NEPTUN runs presented in this study).

3.3 University of Ottawa data

These data, which have served as a basis for the three new correlations, have already been discussed in section 2.5.3.

The estimation of the liquid temperature just downstream of the quench front poses a particular problem when the "hot patch" technique is used. Indeed, the hot patch, being a few centimeter long, cannot be considered as punctual, and large axial heat fluxes take place within it. The hot-patch-fluid heat transfer is only known as a whole and some assumptions have to be used to discriminate between the amount of heat that is released at (or upstream of) the quench front, and the heat released downstream.

A specific model has been developed for the estimation of the liquid temperature just downstream of the quench front, in hot-patch experiments, using the IAFB model itself, and based on the following considerations. The quench front is supposed to stay at the hot patch inlet, and no vapour generation is assumed at this quench front, the whole quench front heat release being used to reduce the liquid subcooling; this last assumption was already used in reflooding situations. An arbitrary value of the quench front heat release is first chosen, which allows to run the IAFB model over the hot patch length. This gives an estimation of the wall heat transfer rate between the quench front and the outlet. The sum of this heat rate and of the assumed quench front heat release is then compared to the total hot patch heat rate, which was measured. An iterative process enables the right value of the quench front heat release to be calculated.

3.4 UKAEA-Winfrith data

These data are steady-state, post-dryout heat transfer data for vertical flow of water inside an electrically heated Nimonic tube of 9.75 mm inside diameter and 920 mm length. As for the University of Ottawa experiments, the "hot patch" technique was used. The wall temperature was measured at 15 axial locations, and the heat transfer rates were derived from these measurements. The void fraction was measured at three locations using γ-densitometry. The hot patch model described above has also been used for these data.

4 Model assessment and conclusions

The model is implemented in the way described in section 2.4. The computational results are displayed as values of the heat transfer coefficient plotted against the distance from the quench front. In the cases where void fraction measurements are available, the predicted axial void fraction profiles are also plotted.

4.1 Importance of the initial conditions

Lacking any experimental information, no vapour flow rate at the quench front is assumed as an initial condition. Anyway, the model is, to a certain extent, insensitive to the initial vapour flow rate: this was shown by computational tests performed assuming that half the heat release at the quench front served to vaporize some liquid. For these tests, an initial vapour temperature had to be specified for the model. Any realistic value (between the saturation temperature and the wall temperature) could in fact be used, without significantly affecting the results. An initial film thickness (or an initial vapour velocity) had also to be specified; this influence was also investigated using plausible values of the film thickness. In any case, beyond 1 mm from the quench front, the results were not significantly different from those obtained without initial vapour flow.

4.2 Results

The cases analysed, together with the main experimental parameters, are listed in tables 2 to 7. The computational results are exhaustively displayed (Annex) in the form of comparison with the experimental results and the predictions of the original model. The calculations are arbitrarily stopped when a void fraction of 60 % is reached. Indeed, it is unlikely that IAFB could persist beyond this value. The irregularities in the left parts of certain curves obtained for the "hot patch" experiments are attributed to the transition between the hot patch and the test section itself (section 2.5.3; the quench front, taken as the abscissa origin, is assumed to be located at the hot patch inlet).

Run number	5025		5150		5249		6027		6044	
Geometry	PWR bundle						LWHCR bundle			
Experiment	bottom reflooding									
Hydraulic diameter (mm)	13.6		13.6		13.6		4.4		4.4	
Quench front elevation (cm)	71	94	71	94	48	71	48	71	48	71
Pressure at quench front (bar)	4.4	4.3	4.3	4.2	1.0	1.0	4.4	4.3	1.1	1.0
Flooding rate (cm/s)	10.3	10.2	15.3		2.7		15.9		10.1	
Quench front velocity (cm/s)	1.4	1.5	1.9	1.9	0.3	0.2	1.3	1.2	0.8	0.5
Inlet subcooling (°C) (nominal value)	80									
Subcooling just above quench front (°C)	21	12	27	25	23	0	12	6	13	16
Wall temperature just above quench front (°C)	496	487	544	484	412	403	438	465	374	414
Wall temperature 30 cm above quench front (°C)	614	472	661	516	762	736	637	601	585	593

Table 2: **Main parameters of NEPTUN experiments (Paul Scherrer Institute, Switzerland) used for IAFB model assessment.**

Run number	124	193	129	192	3066	3067	3060
Geometry	tube						
Hydraulic diameter (mm)	14.4				14.25		
Experiment	bottom reflooding						
Quench front elevation (cm)	183				122		
Pressure at quench front (bar)	1.1	1.1	1.2	1.2	1.1	2.1	3.1
Flooding rate (cm/s)	7.5	12.1	16.9	17.3	12.7	12.7	12.7
Quench front velocity (cm/s)	1.4	2.0	5.3	4.6	3.0	3.0	3.0
Inlet subcooling (°C) (nominal value)	79						
Subcooling just above quench front (°C)	7	17	9	21	10	11	11
Wall temperature just above quench front (°C)	315	379	401	406	424	417	411
Wall temperature 30 cm above quench front (°C)	445	528	478	543	576	538	516

Table 3: **Main parameters of UC-Berkeley experiments used for IAFB model assessment.**

Run number	D350						D400					
	-201	-202	-203	-204	-205	-206	-201	-202	-203	-204	-205	-206
Geometry	tube											
Hydraulic diameter (mm)	11.9											
Experiment	steady state (hot patch), upflow											
Hot patch length (cm)	6.3											
Pressure at quench front (bar)	1.1	1.2	1.2	1.2	1.1	1.1	1.2	1.2	1.2	1.1	1.1	1.0
Flooding rate (cm/s)	37.8	37.8	37.8	37.8	37.7	37.7	40.9	40.9	41.0	40.9	40.9	40.9
Inlet subcooling (°C) (nominal value)	20											
Subcooling just above quench front (°C)	14	15	16	14	13	13	15	16	17	14	14	12
Wall temperature just above quench front (°C)	517	522	503	511	515	518	522	513	511	514	502	501
Wall temperature 30 cm above quench front (°C)	914	977	1031	906	835	770	916	989	1042	844	779	700

Table 4: **Main parameters of University of Ottawa experiments used for correlation of heat and momentum transfer enhancement in IAFB (Group I).**

Run number	D500				E200					E300	
	-201	-202	-203	-204	-101	-102	-103	-104	-201	-171	-172
Geometry	tube										
Hydraulic diameter (mm)	11.9										
Experiment	steady state (hot patch), upflow										
Hot patch length (cm)	6.3				2.5						
Pressure at quench front (bar)	1.2	1.2	1.1	1.0	1.1	1.2	1.1	1.1	1.2	1.2	1.2
Flooding rate (cm/s)	51.1	51.1	51.1	51.0	21.2	21.2	21.2	21.2	21.1	31.0	30.9
Inlet subcooling (°C) (nominal value)	20				10				20	17	
Subcooling just above quench front (°C)	16	17	15	13	9	10	9	9	17	16	16
Wall temperature just above quench front (°C)	508	502	493	515	571	576	563	559	561	590	557
Wall temperature 30 cm above quench front (°C)	910	977	831	772	922	982	873	810	1007	967	900

Table 5: **Main parameters of University of Ottawa experiments used for correlation of heat and momentum transfer enhancement in IAFB (Group II).**

Run number	E400							E500			
	-101	-102	-103	-104	-105	-161	-162	-101	-102	-103	-104
Geometry	tube										
Hydraulic diameter (mm)	11.9										
Experiment	steady state (hot patch), upflow										
Hot patch length (cm)	2.5										
Pressure at quench front (bar)	1.3	1.2	1.2	1.2	1.1	1.2	1.2	1.3	1.3	1.2	1.2
Flooding rate (cm/s)	41.1	41.1	41.1	41.0	41.0	41.0	41.0	51.3	51.3	51.2	51.2
Inlet subcooling (°C) (nominal value)	10					16		10			
Subcooling just above quench front (°C)	13	13	13	12	10	16	17	13	14	12	11
Wall temperature just above quench front (°C)	579	583	574	574	518	525	570	547	544	535	535
Wall temperature 30 cm above quench front (°C)	988	937	889	810	757	867	943	926	984	850	812

Table 6: **Main parameters of University of Ottawa experiments used for correlation of heat and momentum transfer enhancement in IAFB (Group III).**

Run number	399	400	401	402	403	404	405	412	413	414
Geometry	tube									
Hydraulic diameter (mm)	9.75									
Experiment	steady state (hot patch), upflow									
Hot patch length (cm)	3.6									
Pressure at quench front (bar)	2.6	2.5	2.5	2.3	2.3	2.3	2.2	5.1	5.1	5.0
Flooding rate (cm/s)	211	211	210	211	208	210	209	215	214	213
Inlet subcooling (°C)	15	14	12	11	10	9	9	6	5	5
Subcooling just above quench front (°C)	13	12	10	9	8	7	7	4	3	3
Wall temperature just above quench front (°C)	590	590	590	590	590	591	591	589	589	589
Wall temperature 30 cm above quench front (°C)	757	696	597	512	455	426	370	422	400	373

Table 7: **Main parameters of UKAEA-Winfrith experiments used for IAFB model assessment.**

The original model predictions are inadequate in many cases. The new IAFB model gives a good overall prediction of Fung's (University of Ottawa) experimental results. This is not surprising since the new closure laws are based on these results. Of more interest, is the assessment of the model against the rest of the data bank, i.e., ten NEPTUN files (standard pressurized water reactor and light water high converter reactor rod bundle reflooding), seven University of California-Berkeley files (tube reflooding) and ten UKAEA-Winfrith files (tube, steady state). For the first two series of data, the overall predictions of the model are also good, with a relative standard deviation lower than 15%.

For the Winfrith experiments, the heat transfer coefficients are fairly well predicted, but the void fraction is underpredicted, as illustrated in figure 6. The reason for this is well understood and has been discussed in section 2 together with the choice of the non-dimensional film thickness δ^* (equation 79) as a correlating parameter. It is related to the high liquid velocities (about 2 m/s, i.e. one order of magnitude larger than in expected reflooding situations) involved in these experiments. If the liquid velocity is no longer small in comparison to the vapour velocity, then, for a given δ^*, the vapour absolute velocity is higher. In this case, the vapour flow becomes turbulent and the heat transfer mechanisms are modified. The model, being based on δ^*, does not account for this effect. As the present work is concerned mostly with reactor core reflooding, no attempt was made to account for this particular effect.

The main experimental trends, i.e. the favourable effects of system pressure, flooding rate and water subcooling just downstream from the quench front on heat transfer, are well described by the model. These main trends are illustrated by figures 7 to 10.

For standard PWR bundle reflooding, the effect of the flooding rate and of the water subcooling at the quench front may be seen in figure 7. The combined increases of water subcooling and flooding rate for Run 5150 in comparison to run 5025 result in increased heat transfer, in agreement with the experimental observations. The combined effects of flooding rate and system pressure are shown for the LWHCR bundle data in figure 8. Again the calculated trends agree with the experimental ones. The effect of system pressure alone is shown in figure 9 for tube reflooding data. The heat transfer coefficient increases with pressure; again the model predicts the experimental trend well.

The model also satisfactorily predicts some less obvious trends of the experimental data. For example, figure 10 illustrates the influence of the local wall temperature on the void fraction. A higher wall temperature leads to a significantly higher void fraction. The following section will ease the physical understanding of such effects.

4.3 Prominent effects and physical variables in IAFB

The following considerations are mainly based on the analysis of the detailed numerical results of the model, physical justifications being rather given *a posteriori*. With certain approximations, an approximative explicit solution may be found to the equations presented in section 2, which allows to point out the prominent mechanisms in IAFB heat transfer. The basic assumption is that both the vapour heating rate Q_{vh} and the vaporization heat rate Q_{vap} are much lower than the wall heat rate Q_w, so that the whole wall heat rate is transferred to the liquid core. That is, neglecting the radiation term:

$$Q_w \simeq Q_{wv} \simeq Q_{vi} \simeq Q_{lh} \tag{108}$$

The validity of this basic assumption, which may be seen in the numerical results to apply for "ideal" IAFB, i.e. when the liquid subcooling is high enough (typically, more than 10 °C) and the void fraction

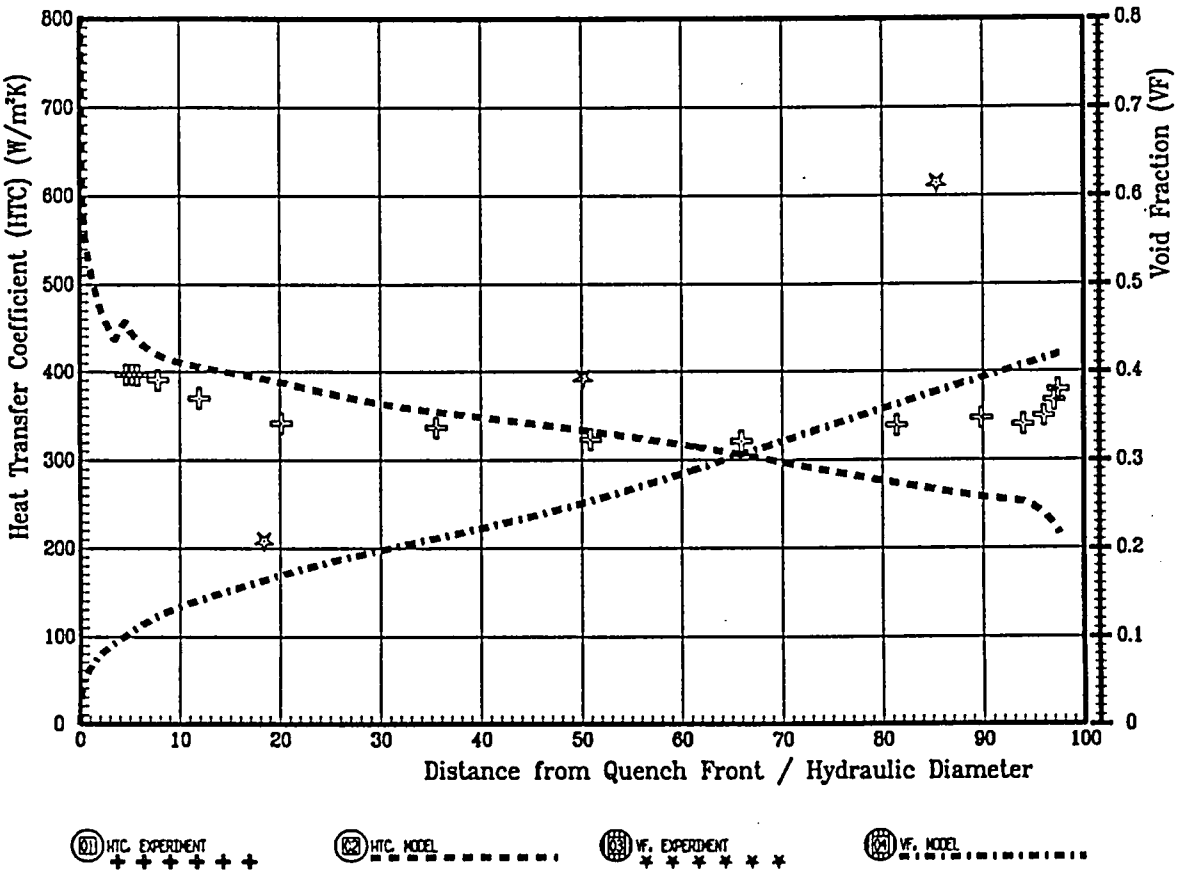

Figure 6: **IAFB heat transfer and void fraction in a tube at high flooding rate.**
Comparison of experimental and predicted heat transfer coefficient and void fraction distributions downstream from the quench front for UKAEA-Winfrith steady-state experiment 399: 211 cm/s flooding rate (2.6 bar pressure and 13 °C subcooling just downstream from the quench front).
Note. The values near the right end of the figure are influenced by the presence of a second hot patch at the test section outlet.

small enough (less than 10 %), will be discussed below.

Furthermore, the film thickness is assumed to be much lower than the hydraulic diameter (this assumption is not required to obtain an explicit solution, but the resulting expressions are simpler). The wall and interfacial perimeters beeing thus close together, equation 108 may be simply rewritten in terms of heat fluxes (instead of heat transfer rates per unit height):

$$q_w \simeq q_{wv} \simeq q_{vi} \simeq q_{lh} \tag{109}$$

As already mentioned in section 2.5.3, the vapour film heat transfer model (equations 33 to 43) is almost equivalent to a pure conduction model where the vapour thermal conductivity is enhanced by a factor λ_{hv}:

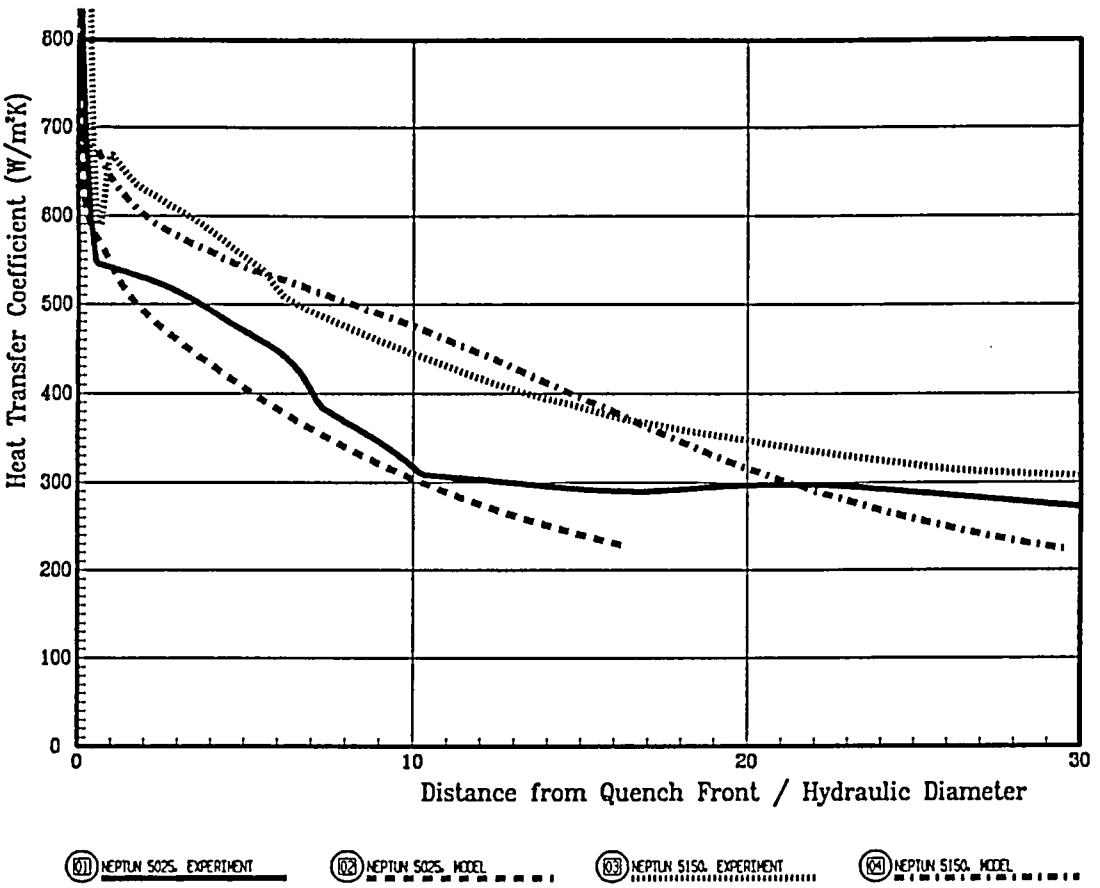

Figure 7: **Effect of subcooling at the quench front and flooding rate on IAFB heat transfer in a standard PWR bundle.**
Comparison of experimental and predicted heat transfer coefficient distributions downstream from the quench front for:
- NEPTUN 5025 reflooding experiment: 12 °C subcooling, 10 cm/s flooding rate
- NEPTUN 5150 reflooding experiment: 25 °C subcooling, 15 cm/s flooding rate
(4 bar pressure in both cases) and 95 cm quench front elevation.
Note. Calculations stopped at 60 % void fraction.

$$q_w \simeq \frac{\lambda_{hv} k_v}{\delta} (T_w - T_s) \tag{110}$$

where the enhancement factor is given by equations 36, 37, 38 and 30.

Substituting equations 36 and 30 in equation 110, with the approximation $c_4 \simeq 1/2$ gives the following expression for the wall heat flux

$$q_w = c_3 \, k_v [\frac{\rho_v (\rho_l - \rho_v) g}{\mu_v^2}]^{\frac{1}{6}} \delta^{-\frac{1}{3}} (T_w - T_s) \tag{111}$$

On the other hand, the liquid heating flux is given by

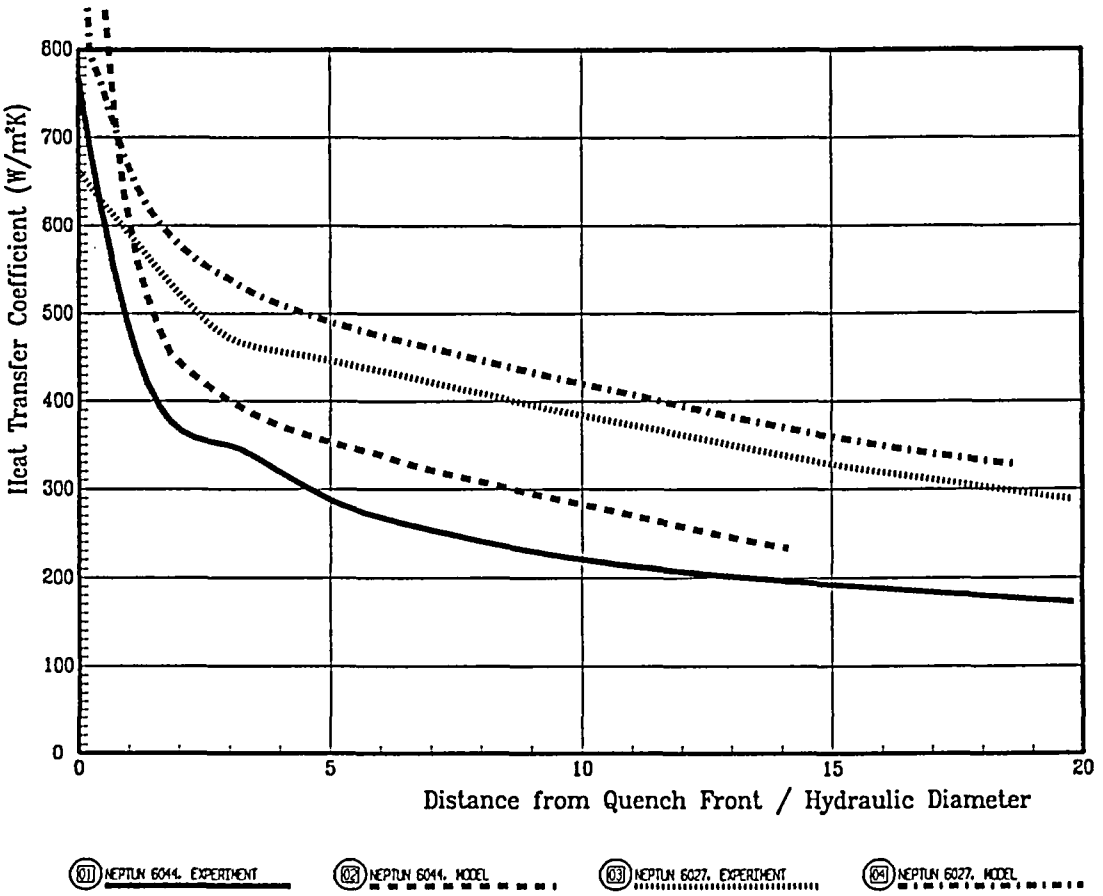

Figure 8: **Effect of flooding rate and pressure on IAFB heat transfer in a LWHCR bundle.** Comparison of experimental and predicted heat transfer coefficient distributions downstream from the quench front for:
- NEPTUN 6044 reflooding experiment: 10 cm/s flooding rate, 1 bar pressure
- NEPTUN 6027 reflooding experiment: 16 cm/s flooding rate, 4 bar pressure
(about 12 °C subcooling at the quench front in both cases) and 48 cm quench front elevation.
Note. Calculations stopped at 60 % void fraction.

$$q_{lh} = h_l(T_s - T_l) \tag{112}$$

with, assuming turbulent flow, a heat transfer coefficient deduced from the interfacial shear stress using the Chilton-Colburn analogy (equations 48 and 68).

The elimination of $U_l - U_i$ between equations 48 and 68, with the approximation of a constant friction coefficient f_l, gives

$$h_l = \frac{c_{pl}}{\mathrm{Pr}_l^{2/3}} \left(\frac{f_l \rho_l}{2}\right)^{\frac{1}{2}} \tau_i^{\frac{1}{3}} \tag{113}$$

The interfacial shear stress is related to the vapour film buoyancy, and then to the void fraction or the

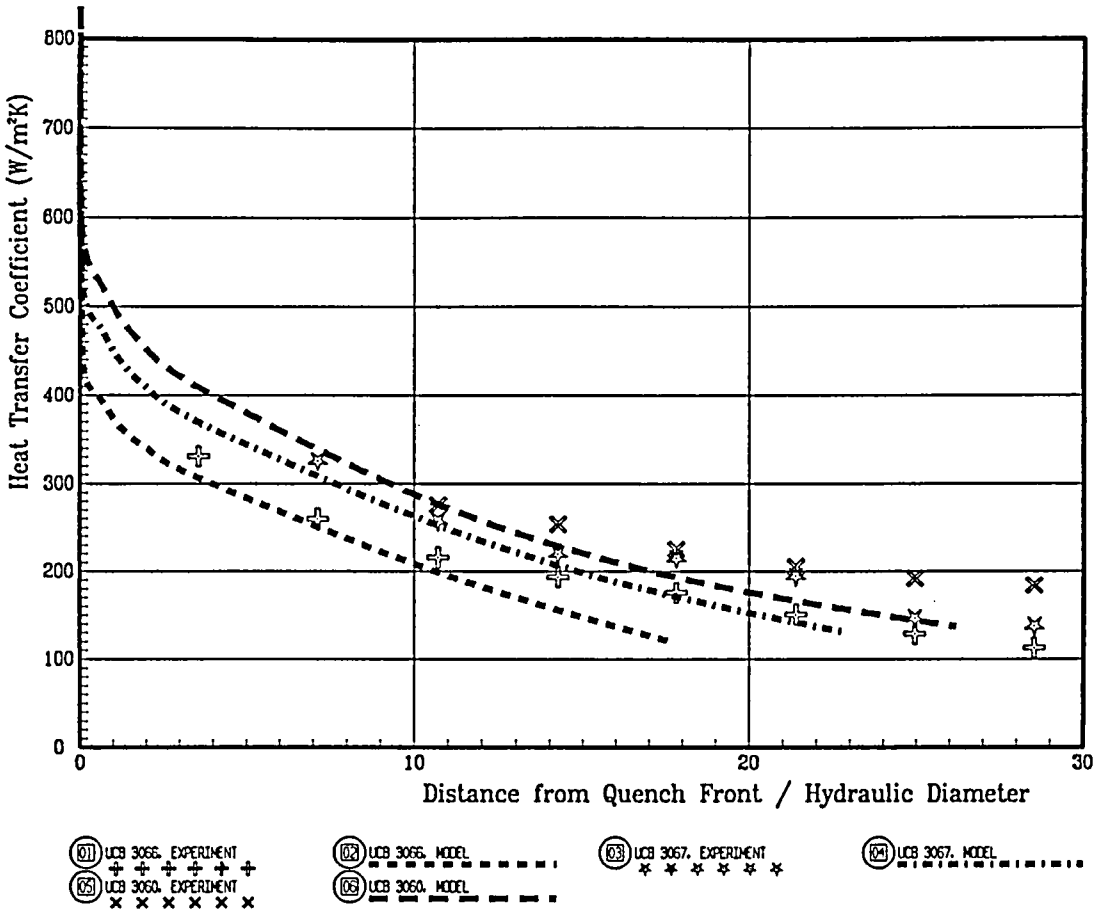

Figure 9: **Effect of pressure on IAFB heat transfer in a tube.**
Comparison of experimental and predicted heat transfer coefficient distributions downstream from the quench front for:
- UC-Berkeley 3066 reflooding experiment: 1 bar pressure
- UC-Berkeley 3067 reflooding experiment: 2 bar pressure
- UC-Berkeley 3060 reflooding experiment: 3 bar pressure
(13 cm/s flooding rate and about 11 °C subcooling at the quench front in all cases) and 122 cm quench front elevation.
Note. Calculations stopped at 60 % void fraction.

vapour film thickness. This relation is obtained by eliminating the pressure gradient between the vapour and liquid momentum conservation equations. Neglecting the convective terms leads to equation 80, which is rearranged using the assumptions $\delta \ll R$ and $\tau_i \simeq \tau_w$, giving

$$\tau_i = (\rho_l - \rho_v) g \, \delta / 2 \tag{114}$$

The last assumption, as it appears in equations 20 to 26, amounts to saying that the vapour-interface momentum transfer enhancement factor λ_{fv} is close to one. This is true for low void fractions: typically, for vapour at 5 bar and 300 °C, in a 14 mm diameter tube, λ_{fv} (equations 27 to 29) is close to one until a void fraction of about 5 % is reached ($\lambda_{fv} = 1.27$ for $\alpha_v = 5$ %). Beyond this value, λ_{fv} strongly increases ($\lambda_{fv} = 5$ for $\alpha_v = 10$ %). Anyway, the error on τ_i is limited to a factor two (corresponding to

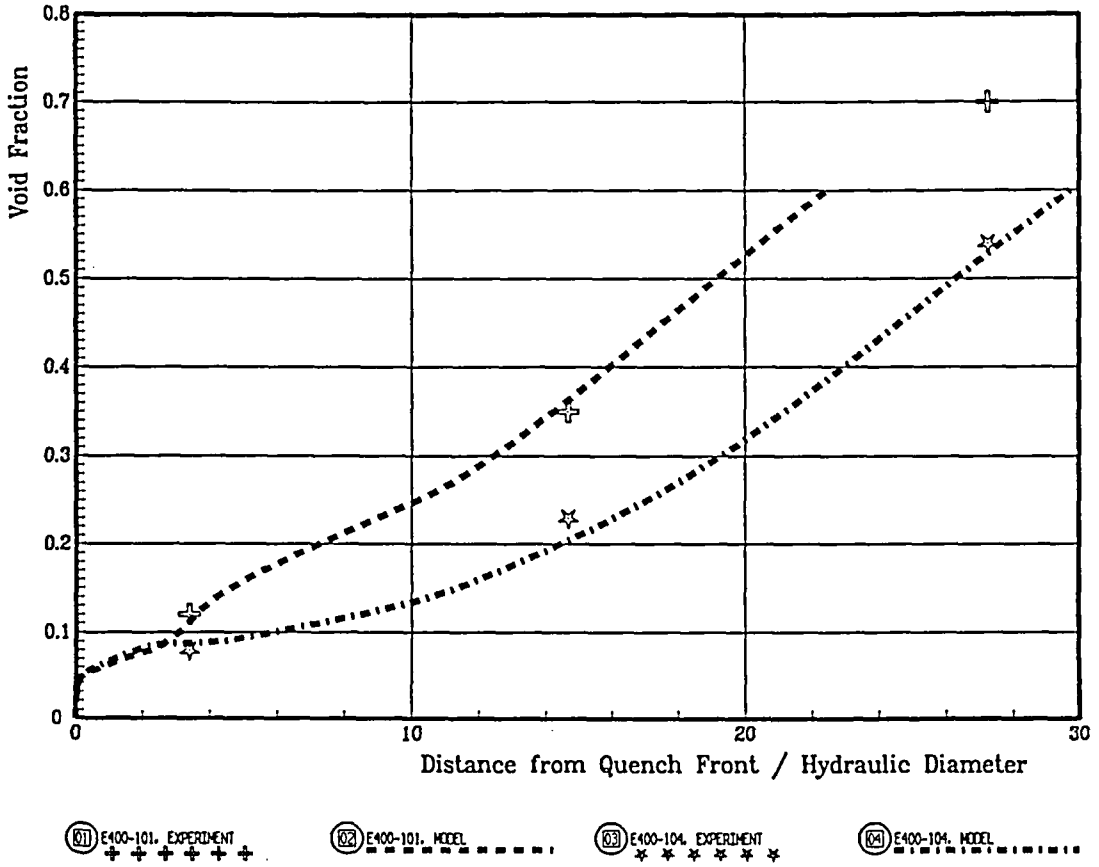

Figure 10: **Effect of wall temperature on IAFB void fraction in a tube.**
Comparison of experimental and predicted void fraction distributions downstream from the quench front for:
- University of Ottawa E400-101 steady-state experiment: 579 °C to 988 °C wall temperature
- University of Ottawa E400-104 steady-state experiment: 574 °C to 810 °C wall temperature
(1 bar pressure, 41 cm/s flooding rate and about 13 °C subcooling just downstream from the quench front in both cases).
Note. Calculations stopped at 60 % void fraction.

$\lambda_{fv} \gg 1$ and thus $\tau_w \ll \tau_i$ in equation 80), which, according to what follows, gives a factor $2^{1/4}$ on the heat transfer, i.e. an error lower than 20 %.

Subsituting τ_i in equation 113, and then h_l in equation 112 gives the following expression for the liquid heating flux

$$q_{lh} = \frac{c_{pl}}{\mathrm{Pr}_l^{2/3}} \left(\frac{f_l \rho_l}{4}\right)^{\frac{1}{2}} [(\rho_l - \rho_v) g]^{\frac{1}{2}} \delta^{\frac{1}{2}} (T_s - T_l) \tag{115}$$

Finally, equating q_w and q_{lh} (equations 111 and 115), and eliminating δ between the two expressions gives

$$\delta = c_3\, k_v \left(\frac{4}{f_l \rho_l}\right)^{\frac{1}{2}} \frac{\mathrm{Pr}_l^{2/3}}{c_{pl}} \left[\frac{\rho_v\,(\rho_l - \rho_v)\,g}{\mu_v^2}\right]^{\frac{1}{6}} \left[(\rho_l - \rho_v)g\right]^{-\frac{1}{2}} \frac{T_w - T_s}{T_s - T_l} \tag{116}$$

and

$$h \triangleq \frac{q_w}{T_w - T_s} = (c_3\, k_v)^{\frac{1}{2}} \left(\frac{f_l \rho_l}{4}\right)^{\frac{1}{4}} \frac{c_{pl}^{1/2}}{\mathrm{Pr}_l^{1/3}} \left[\frac{\rho_v\,(\rho_l - \rho_v)\,g}{\mu_v^2}\right]^{\frac{1}{12}} \left[(\rho_l - \rho_v)g\right]^{\frac{1}{4}} \left[\frac{T_s - T_l}{T_w - T_s}\right]^{\frac{1}{2}} \tag{117}$$

Qualitatively, an interpretation may be given for the heat transfer mechanism in "ideal" (high liquid subcooling, low void fraction) IAFB, based on the following observations. When the film thickness increases, on one hand, the wall-interface heat flux tends to decrease. On the other hand, the buoyancy force, and thus the interfacial force and the heat transfer between the interface and the bulk liquid, tend to increase. Immediately downstream from the quench front, the wall heat flux is very high. Rapid vapour generation takes place, increasing the film thickness and thus the interfacial momentum and heat transfers, and decreasing the wall heat flux. Over a very short distance, a quasi-equilibrium between the wall heat flux and the liquid heating flux is reached. Further downstream, this quasi-equilibrium evolves according to the locally prevailing conditions of liquid subcooling and wall temperature. In fact, the film thickness increases, mainly due to the decrease of the liquid sucooling: the combined effects of the vapour heat transfer reduction and liquid-interface heat coefficient augmentation compensate the reduction of the liquid-interface temperature difference. The validity of the basic assumption made (equation 108) relates to the fact that the proportion of the wall heat flux needed to generate some vapour and restore the quasi-equilibrium remains low. This situation lasts until the liquid subcooling becomes too low and the liquid core is no more able to absorb the near totality of the wall heat flux.

An interesting feature of the approximative solution (equation 117) is that it does not involve any vapour film friction factor. Some numerical tests have shown that the exact model itself is relatively insensitive to the expression for the vapour film friction factor. Reciprocally, this explains the dispersion of the values obtained when the friction factor is back-computed from void fraction and heat transfer results (figure 3).

The liquid velocity U_l does not appear explicitely in the approximative solution. As the closure laws of the complete model involve only the liquid velocity relative to the interface, they are also little sensitive to U_l, provided it remains much lower than the vapour velocity. However, the liquid velocity, or flow rate, has a strong "integral" effect on the results through the energy conservation equation: the rate of decrease of the liquid subcooling along the flow is inversely proportional to the liquid flow rate.

Equation 117 clearly shows that the liquid subcooling is an influential variable for IAFB heat transfer.

An unfavourable effect of the wall temperature T_w on the heat transfer coefficient also appears in equation 117. However, this effect is also linked to the temperature dependence of the vapour physical properties. In order to understand how the various effects compete, the following approximation is made:

$$T_v \simeq (T_w + T_s)/2 \tag{118}$$

The influence of T_w on the heat transfer coefficient may then be obtained from equation 117:

$$\frac{1}{h}\frac{\partial h}{\partial T_w} \simeq \frac{1}{4k_v}\frac{\partial k_v}{\partial T_v} + \frac{1}{24\rho_v}\frac{\partial \rho_v}{\partial T_v} - \frac{1}{12\mu_v}\frac{\partial \mu_v}{\partial T_v} - \frac{1}{2(T_w - T_s)} \tag{119}$$

For some typical conditions ($p = 1\ bar$, $T_w = 700$ °C), the following numerical values are obtained:

$$\frac{1}{4k_v}\frac{\partial k_v}{\partial T_v} = 5.2\,10^{-4}\ °\mathrm{C}^{-1} \tag{120}$$

$$\frac{1}{24\rho_v}\frac{\partial \rho_v}{\partial T_v} = -0.6\,10^{-4}\ ^\circ C^{-1} \quad (121)$$

$$-\frac{1}{12\mu_v}\frac{\partial \mu_v}{\partial T_v} = -1.4\,10^{-4}\ ^\circ C^{-1} \quad (122)$$

$$-\frac{1}{2(T_w - T_s)} = -8.3\,10^{-4}\ ^\circ C^{-1} \quad (123)$$

There is thus a resulting, unfavourable effect, of the wall temperature on the heat transfer coefficient:

$$\frac{1}{h}\frac{\partial h}{\partial T_w} \simeq -5.1\,10^{-4}\ ^\circ C^{-1} \quad (124)$$

However, this effect (5% heat transfer reduction for 100 °C temperature increase) is still of secondary order.

Concerning the void fraction (or film thickness), the conclusion is quite different. In equation 116, it may be seen that, this time, the favourable effect of the wall temperature on the void fraction is no more attenuated, but amplified by the temperature dependence of the vapour thermal conductivity. This is the trend shown in figure 10.

The favourable effect of the pressure (shown in figure 9) also appears in equation 117, through ρ_v, although this effect is rather weak (exponent 1/12). From figure 9, one would expect a stronger dependence. However, a deeper analysis of the test parameters (table 3) shows that the differences between the three curves in figure 9 are due to some small differences in the subcooling and in $T_w - T_s$ as much as to the pressure influence.

4.4 Conclusions

A six equation model was supplemented with closure laws specific to the IAFB regime. Closure laws applicable to tube and various bundle geometries were proposed; thus, all cases can be calculated with the same basic model.

The key point of the model proposed is the formulation of the heat and momentum transfers between the vapour-liquid interface and the liquid bulk, based on the liquid velocity relative to the interface. Indeed, the heat transfer rate in IAFB is strongly influenced by the heat transfer within the liquid core, which in turn is strongly coupled with the vapour film hydrodynamics. The formulation proposed in section 2.3.2 appears to be the only way to account for this coupling. Such a formulation does not seem to have been previously applied to IAFB.

The classical single-phase fluid dynamics and heat transfer laws have proven to be insufficient for describing IAFB. The interactions between the two phases, and, in particular, the irregular nature of the interface, have to be accounted for. As attempting a fully analytical description would have led to very complex developments, the use of, at least partially, empirical closure laws was required. In the previous models, some correlations were used that had been derived for other situations than IAFB, and whose applicability to IAFB was questionable. In the model proposed, some new correlations have been developed, based this time on measurements performed in IAFB. These new closure laws may be used outside the frame of the present model and thus have an intrinsic value.

Such specific closure laws are essential for accurate predictions of the heat fluxes or wall temperatures during IAFB. Indeed, the models actually implemented in the computer codes used for safety analysis can be shown to produce inadequate predictions (Analytis, 1990).

Forced flow, subcooled film boiling experimental results from four different sources have been processed and analysed. The IAFB model has been successfully assessed against 57 experiments corresponding to very different geometries and parameter ranges in the Annex to this report. Although further assessment

would be useful, particularly against void fraction data, this model seems now to represent an efficient analysis tool.

It seems useful to try and apply the results of the IAFB analysis to the safety codes in order to improve their description of post dryout, low-quality heat transfer .

A Nomenclature

A	cross sectional flow area $[m^2]$
$c_1 ... c_6$	constants (eqs. 27, 36, 51) [–]
c_p	specific heat at constant pressure $[J/(kg\,K)]$
D_h	hydraulic diameter $[m]$
f	friction factor [–]
g	gravitational constant $[m/(s^2)]$
h	specific enhalpy, heat transfer coefficient $[J/kg]$, $[W/m^2\,K]$
h_l	liquid-interface heat transfer coefficient (eq. 59) $[W/m^2\,K]$
h_{vap}	latent heat of vaporization $[J/kg]$
k	thermal conductivity $[W/(m\,K)]$
M	mass flowrate per unit height $[kg/(s\,m)]$
Nu_l	liquid core Nusselt number (eq. 60) [–]
Nu_v	vapour film Nusselt number (eq. 31, 32) [–]
P	perimeter $[m]$
p	pressure, rod bundle pitch $[Pa]$, $[m]$
Pr	Prandtl number [–]
Q	heat transfer rate per unit height $[W/m]$
q	heat flux $[W/m^2]$
Q_h	sensible heating rate (per unit height) (eqs. 5, 6) $[W/m]$
Q_r	radiation heat transfer rate (per unit height) $[W/m]$
Q_{vap}	vaporization heat rate (per unit height, eq. 17) $[W/m]$
R	tube (internal), rod (external) radius $[m]$
Re	Reynolds number [–]
T	temperature $[K]$
T_v'	vapour temperature in the wall sublayer (eqs. 33, 34) $[K]$
U	velocity in a frame of reference moving with the quench front $[m/s]$
V	velocity in a fixed frame $[m/s]$
z	height $[m]$

Greek letters

α	area fraction [–]
δ	vapour film thickness [m]
δ^*	non-dimensional film thickness (eq. 30) [–]
δ'	wall sublayer thickness (eqs. 71, 72) [m]
ϵ	emissivity [–]
Θ	influence coefficient (eqs. 31, 32) [–]
λ_{fv}	enhancement factor (vapour-interface momentum transfer, eq. 25) [–]
λ_{hv}	enhancement factor (vapour film heat transfer, eqs. 33, 34) [–]
λ_l	enhancement factor (interface-liquid transfers, eqs. 49, 50) [–]
μ	viscosity [$Pa\,s$]
ρ	density [kg/m^3]
σ	Stefan-Boltzman constant [$W/(m^2\,K^4)$]
τ	shear stress [Pa]

Subscripts

i	interface
l	liquid
qf	quench front
s	saturation
v	vapour
w	wall

Additional nomenclature is defined locally in the text.

B Acknowledgments

This work was supported by the *Bundesamt für Energiewirtschaft (BEW), Bern*, represented by the *Hauptabteilung für Sicherheit der Kernanlagen (HSK).*

Many thanks are adressed to:

Prof. G. Yadigaroglu, who initiated, stimulated and reviewed this work, allowing the author to benefit from his vast knowledge of reflooding heat transfer and inverted-annular film-boiling (IAFB);

Dr. J. Dreier, who led this project at the *Paul-Scherrer Institute*, and acquainted the author with the *NEPTUN* experiments;

Dr. G. Analytis, whose research on IAFB has been taken as basis for this study;

Mr. L. Voser, for his contribution to the *NEPTUN* experiments;

Mr. N. Rouge, for his contribution to the *NEPTUN* data processing, for the maintenance and extension of our software, and for the solution of all computer-related problems encountered in this work;

Mr. C. Schraeder, *Technische Universität Braunschweig*, for his contribution to the model assessment.

Dr. K. Fung, whose experimental results obtained at the *University of Ottawa* have been extensively used in this study; Dr. S. Cheng, for providing us with these results.

AEA Technology, Dr. D. Swinnerton, who communicated us some valuable data obtained on the *Winfrith Post-Dryout Heat Transfer Rig*; *Nuclear Electric*, Mr. P. Lightfoot, and *HSE*, Dr. G. Artingstall, who allowed us to access their proprietary data.

C References

Aksan, S.N., Varadi, G. & Güntay, S., 1979, Properties of some materials for use in the analysis of light water reactor fuel rods and their simulators (e.g. LOFT, NEPTUN), *Swiss Federal Institute for Reactor Research (EIR) Report* TM-IN-816.

Analytis, G. Th., 1990, Implementation and assessment of an inverted annular flow model in RELAP5/MOD2, *ICAP Meeting, Madrid, Spain.*

Analytis, G. Th. & Yadigaroglu, G., 1987, Analytical modeling of inverted-annular film-boiling, *Nucl. Eng. Des.* 99, 201-212.

Arrieta, L. & Yadigaroglu, G., 1978, Analytical model for bottom reflooding heat transfer in light water reactors (the UCFLOOD code), *EPRI* NP-756.

de Cachard, F. & Yadigaroglu, G., 1991, Analytical modeling of inverted-annular film-boiling: improvement and assessment, *European Two-Phase Flow Group Meeting, Rome*, C1.

Chan, K.C. & Yadigaroglu, G., 1980, Calculations of film boiling heat transfer above the quench front during reflooding, Exp. and anal. modeling of LWR safety experiments, *Proc. 19 th Nat. Heat Transfer Conf., Orlando, Florida* 7, 65-72.

Costigan, G. & Wade, C. D., 1984, Visualisation of the reflooding of a vertical tube by dynamic neutron radiography, *Proc. Int. Workshop on Post-Dryout Heat Transfer, Salt Lake City, Utah.*

De Jarlais, G. & Ishii, M., 1985, Inverted annular flow experimental study, *Technical Report NUREG/CR-4277.*

Denham, M. K., 1983, Inverted annular film boiling and the Bromley model, *Report AEE-Winfrith* 1590.

Dreier, J., 1990, Auswertung und Modellierung von NEPTUN- Wiederbenetzungsdaten, *Jahresbericht, Bundesamt für Energiewirtschaft, Bern.*

Dreier, J., 1985, NEPTUN-Auswertungen: Quenchfrontinterpolation und Quenchfrontgeschwindigkeitberechnungen während dem Flutungsvorgang, *Eidg. Institut für Reaktorforschung interner Bericht* TM-32-85-15.

Dreier, J., Chawla, R., Rouge, N. & Yanar, S., 1990, The NEPTUN experiments on LOCA thermal-hydraulics for tight-lattice PWRs, *Proc. IAEA Technical Committee on Technical and Economic Aspects*

of High Converters, Nürnberg.

Edelman, Z., Elias, E. & Naot, D., 1983, Optical illustration of liquid penetration to the vapour film in inverted annular film boiling, *Int. J. Heat Mass Transfer* 26-11, 1715-1717.

Frei, E. & Stierli, F., 1984, NEPTUN: Information about the reflood-experiments 5012-5056, *Swiss Federal Institute for Reactor Research (EIR)* TM 32-83-6.

Fung, K. K., 1981, Subcooled and low quality film boiling of water in vertical flow at atmospheric pressure, *Ph. D. Thesis, University of Ottawa.*

Fung, K. K. & Groeneveld, D.C., 1981, A physical model of subcooled and low quality film boiling of water in vertical flow at atmospheric pressure, *Proc. 7 $\frac{th}{}$ Int. Heat Transfer Conference.*

Grütter, H., Stierli, F., Aksan, S.N. & Varadi, G., 1980, NEPTUN bundle reflooding experiments: test facility description, *Swiss Federal Institute for Reactor Research (EIR) Report* 386.

Güntay, S., 1980, INCON, a computer program for the calculation of non-linear inverse heat conduction problem in cylindrical geometry using integral heat flux method, *Swiss Federal Institute for Reactor Research (EIR) Report* TM 32-80-8.

Kao, H. S., Morgan, C. D., Crawford, M. & Jones, J.B., 1972, Stability analysis of film boiling on vertical surfaces as a two-phase flow problem, *AIChE* **118**, 147-155.

Kawaji, M., 1984, Transient non-equilibrium two-phase flow: Reflooding of a vertical flow channel, *Ph.D. Thesis, UC-Berkeley.*

Kawaji, M., Ng, Y.S., Banerjee, S. & Yadigaroglu, G., 1985, Reflooding with steady and oscillatory injection: Part1-Flow regimes, void fraction, and heat transfer, *Trans. ASME* 670-107.

Kays, W. M., 1980, *Convective heat and mass transfer*, McGraw-Hill Book Company.

Lee., N., Wong, S. & Hochreiter, L.E., 1983, Heat transfer mechanism during rod bundle reflooding in transient two-phase flow, *Proceedings of the third CSNI Specialist Meeting*, Hemisphere Publishing Corporation, 243-260.

Rashidi, M., Hetsroni, G. & Banerjee, S., 1991, Mechanisms of heat and mass transport at gas-liquid interfaces, *Int. J. Heat Mass Transfer* **34**, 7, 1799-1810.

Richner, M., 1987, Die Programme der NEPTUN Working Databank und das Programm INCON unter dem Betriebssystem NOS, *Eidg. Institut für Reaktorforschung interner Bericht* AN-32-87-04.

Richner, M. & Dreier. J., 1986, Inhalt der NEPTUN2-Working-Databank, *Eidg. Institut für Reaktorforschung interner Bericht* TM-32-86-15.

Rohsenow, W.M. & Hartnett, J.P., 1973, *Handbook of Heat Transfer*, McGraw-Hill Book Company.

Rouge, N., 1989, NEWS Programm für das Erstellen von graphischen Darstellungen von experimentellen NEPTUN-Daten, *Paul Scherrer Institut* TM 42-89-12.

Rouge, N., 1990, NEPTUN Working Databank: Modifikationen und Anpassungen der Programmen und Daten unter dem Betriebssystem NOS/VE, *Paul Scherrer Institut* TM 42-90-02.

Rouge, N., Dreier, J., Yanar, S. & Chawla, R., 1992, Experimental comparisons for bottom reflooding in tight LWHCR and standard LWR geometries, *Nucl. Eng. Des.* **137**, 35-47.

Rouge, N., Yanar, S., de Cachard, F. and Dreier, J, in progress, Verarbeitung und Auswertung von experimentellen Daten des HP 1000-realtime-Datenerfassungssystems, *Paul-Scherrer Institut Technische Mitteilung.*

Savage, R.A., Swinnerton, D. & Pearson, K.G., 1989, Heat transfer and voidage data in steady-state post-dryout at low quality and medium pressure, *Safety and Engineering Science Division, Atomic Energy Establishment Winfrith, Data Report AEEW* - R 2486.

Savage, R. A., Archer, D. Swinnerton, D., 1991, Post-dryout data from test sections featuring a cold patch and a hot notch, *Physics and Thermal Hydraulics Division, AEA Reactor Services Winfrith, Report AEA-RS*-1095.

Schraeder, C., 1992, Optimization of closure laws for the modeling of inverted-annular film-boiling, *Diplomarbeit, Institut für Raumflug- und Reaktortechnik, Technische Universität Braunschweig.*

Seban, R. A., 1983, Reflooding of a vertical tube at 1, 2 and 3 atmospheres, *EPRI Report* NP-3191.

Seban, R., Grief, R., Yadigaroglu, G., Elias, E., Yu, K., Abdollahian, D. & Peake, W., 1978, UC-B reflood program: Experimental data report, *EPRI Report* NP-743.

Shigechi, T. & Lee, Y., 1991, An analysis on fully developed laminar fluid flow and heat transfer in

concentric annuli with moving cores, *Int. J. Heat Mass Transfer* **34-10**, 2593-2601.

Stierli, F. & Yanar, S., 1985, Flutversuche NEPTUN 2: Übersicht, Unterlagen, *Eidg. Institut für Reaktorforschung interner Bericht* TM-32-85-30.

Suryanarayana, N. V. & Merte, H., 1972, Film boiling on vertical surfaces, *Trans. ASME* 377-384.

Takenaka, N., Fujii, T., Akagawa, K. & Nishida, K., 1989, Flow pattern transition and heat transfer of inverted annular flow, *Int. J. Multiphase Flow* **15**, 767-785.

Taube, P., 1985, NEPTUN Data Bank, *Swiss Federal Institute for Reactor Research (EIR) Report* TM 32-85-20.

Todreas, N. E. & Kazimi, M. S., 1989, *Nuclear Systems*, Hemisphere Publishing Corporation.

Wallis, G. B., 1970, Annular two-phase flow, Part 1: A simple theory, Part 2: Additional effects, *J. of Basic Eng.* 59, 59-72.

Wallis, G. B., 1970, Annular two-phase flow, *Trans. ASME* **92**, D1.

Yu, K.P., 1987, An experimental investigation of the reflooding of a bare tubular test section, *Ph.D. Thesis, UC-Berkeley.*

D Annex

Detailed results of the IAFB model assessment:

- NEPTUN experiments: heat transfer coefficient (graphs 1 to 10)
- UC-Berkeley experiments: heat transfer coefficient (graphs 11 to 17)
- University of Ottawa experiments: heat transfer coefficient and void fraction (graphs 18 to 85)
- UKAEA-Winfrith experiments: heat transfer coefficient and void fraction (graphs 86 to 105)

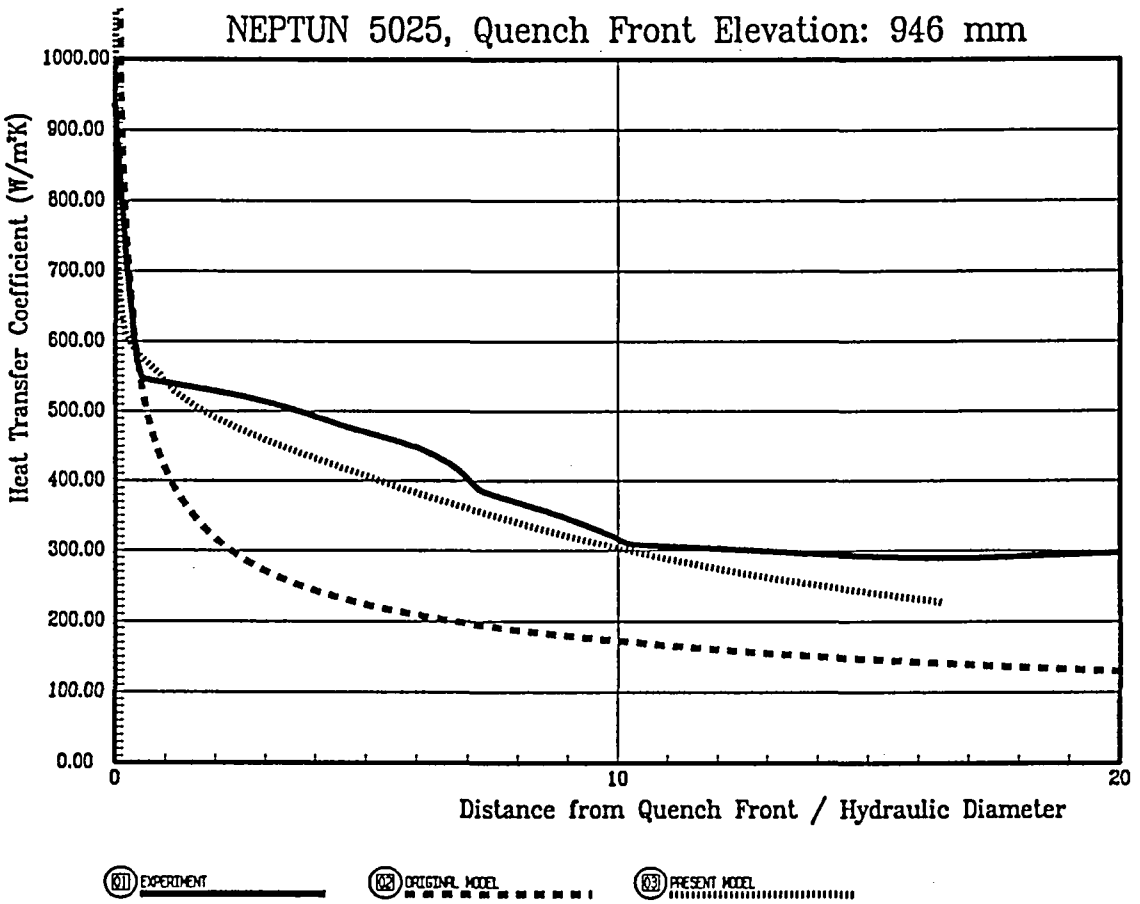
NEPTUN 5025, Quench Front Elevation: 946 mm
Heat Transfer Coefficient (W/m²K)
1000.00
900.00
800.00
700.00
600.00
500.00
400.00
300.00
200.00
100.00
0.00
0
10
20
Distance from Quench Front / Hydraulic Diameter
01 EXPERIMENT
02 ORIGINAL MODEL
03 PRESENT MODEL

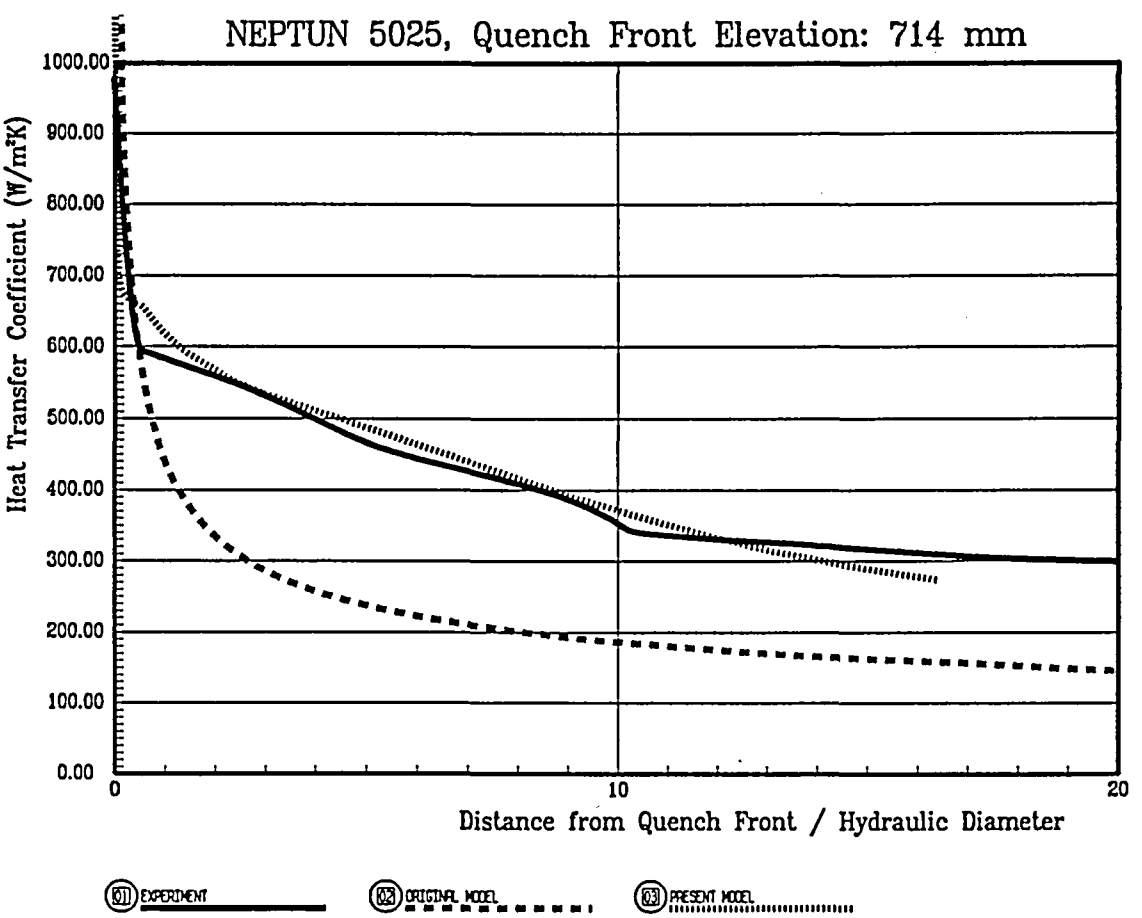
NEPTUN 5025, Quench Front Elevation: 714 mm
Heat Transfer Coefficient (W/m²K)
1000.00
900.00
800.00
700.00
600.00
500.00
400.00
300.00
200.00
100.00
0.00
0
10
20
Distance from Quench Front / Hydraulic Diameter
01 EXPERIMENT
02 ORIGINAL MODEL
03 PRESENT MODEL

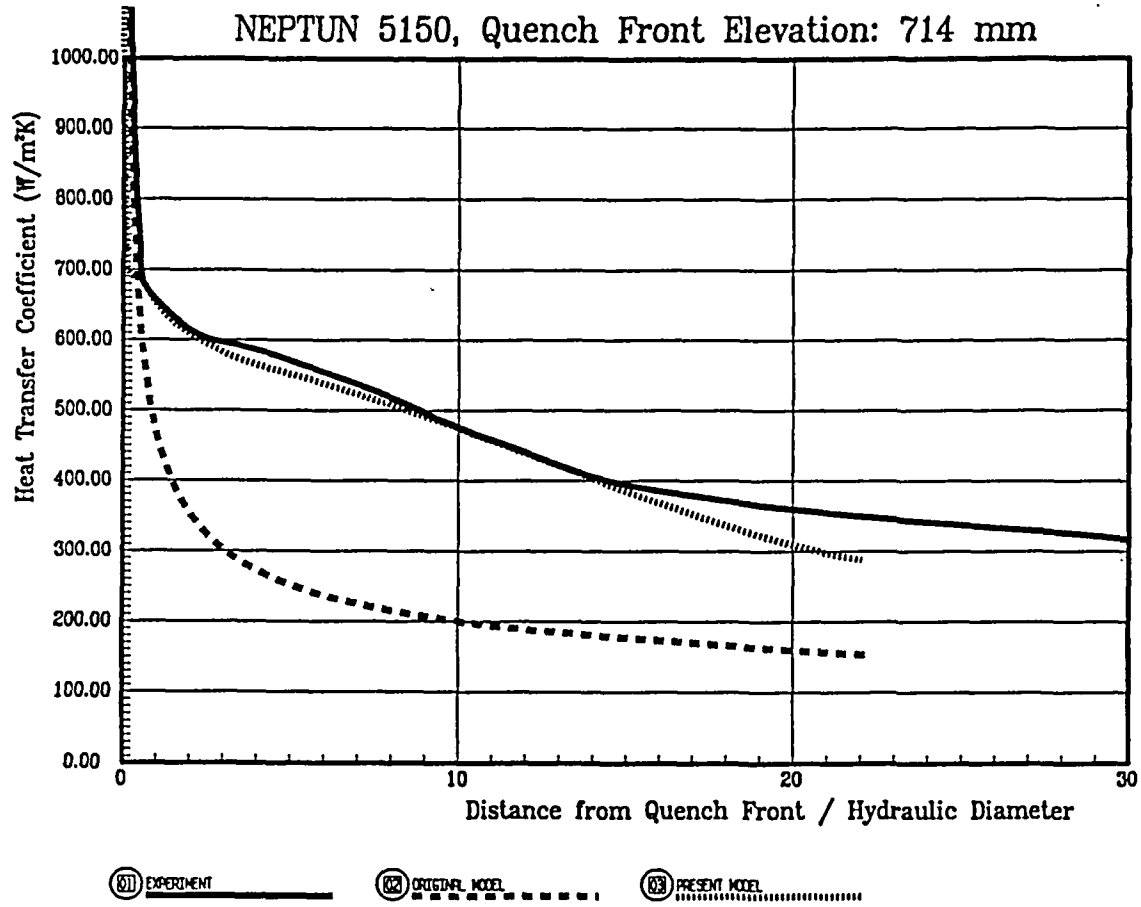
NEPTUN 5150, Quench Front Elevation: 714 mm
Heat Transfer Coefficient (W/m²K)
1000.00
900.00
800.00
700.00
600.00
500.00
400.00
300.00
200.00
100.00
0.00
0
10
20
30
Distance from Quench Front / Hydraulic Diameter
01 EXPERIMENT
02 ORIGINAL MODEL
03 PRESENT MODEL

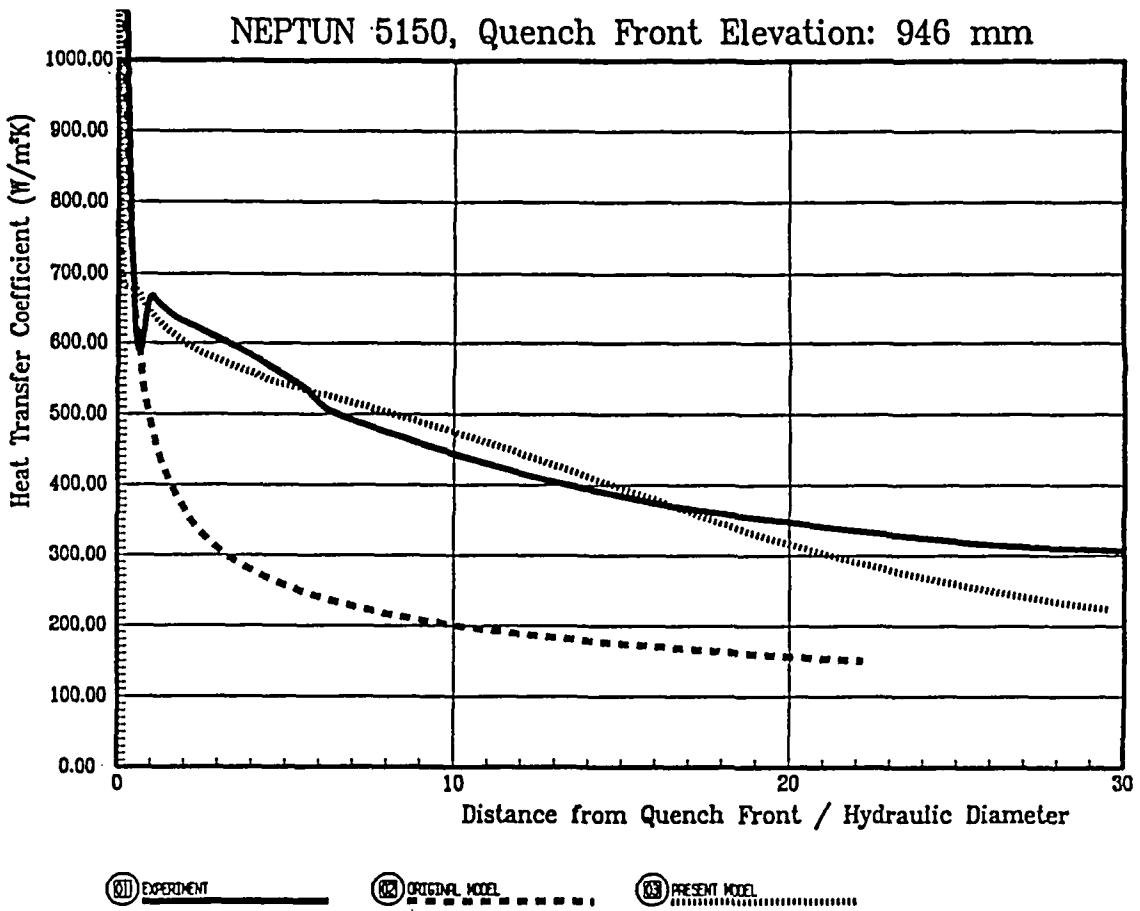
NEPTUN 5150, Quench Front Elevation: 946 mm
Heat Transfer Coefficient (W/m²K)
1000.00
900.00
800.00
700.00
600.00
500.00
400.00
300.00
200.00
100.00
0.00
0
10
20
30
Distance from Quench Front / Hydraulic Diameter
01 EXPERIMENT
02 ORIGINAL MODEL
03 PRESENT MODEL

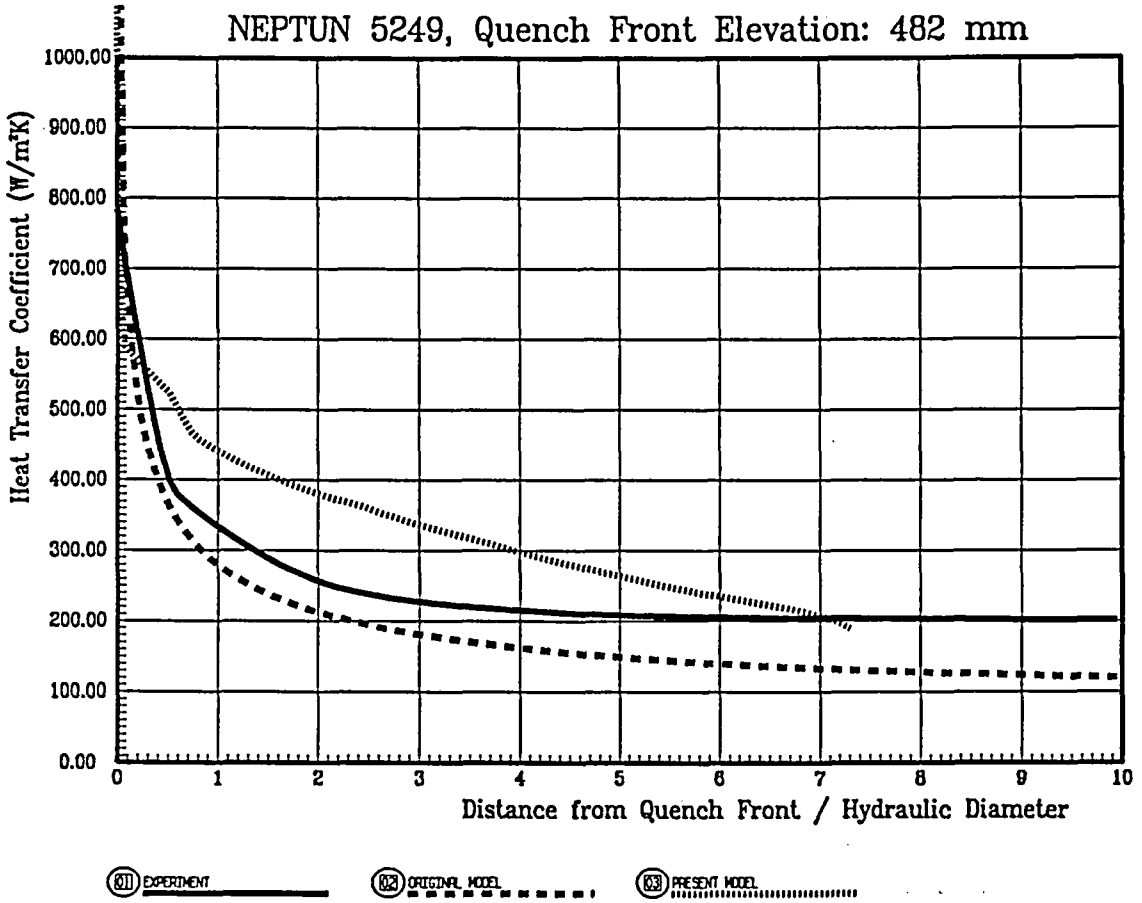
NEPTUN 5249, Quench Front Elevation: 482 mm
Heat Transfer Coefficient (W/m²K)
1000.00
900.00
800.00
700.00
600.00
500.00
400.00
300.00
200.00
100.00
0.00
0
1
2
3
4
5
6
7
8
9
10
Distance from Quench Front / Hydraulic Diameter
01 EXPERIMENT
02 ORIGINAL MODEL
03 PRESENT MODEL

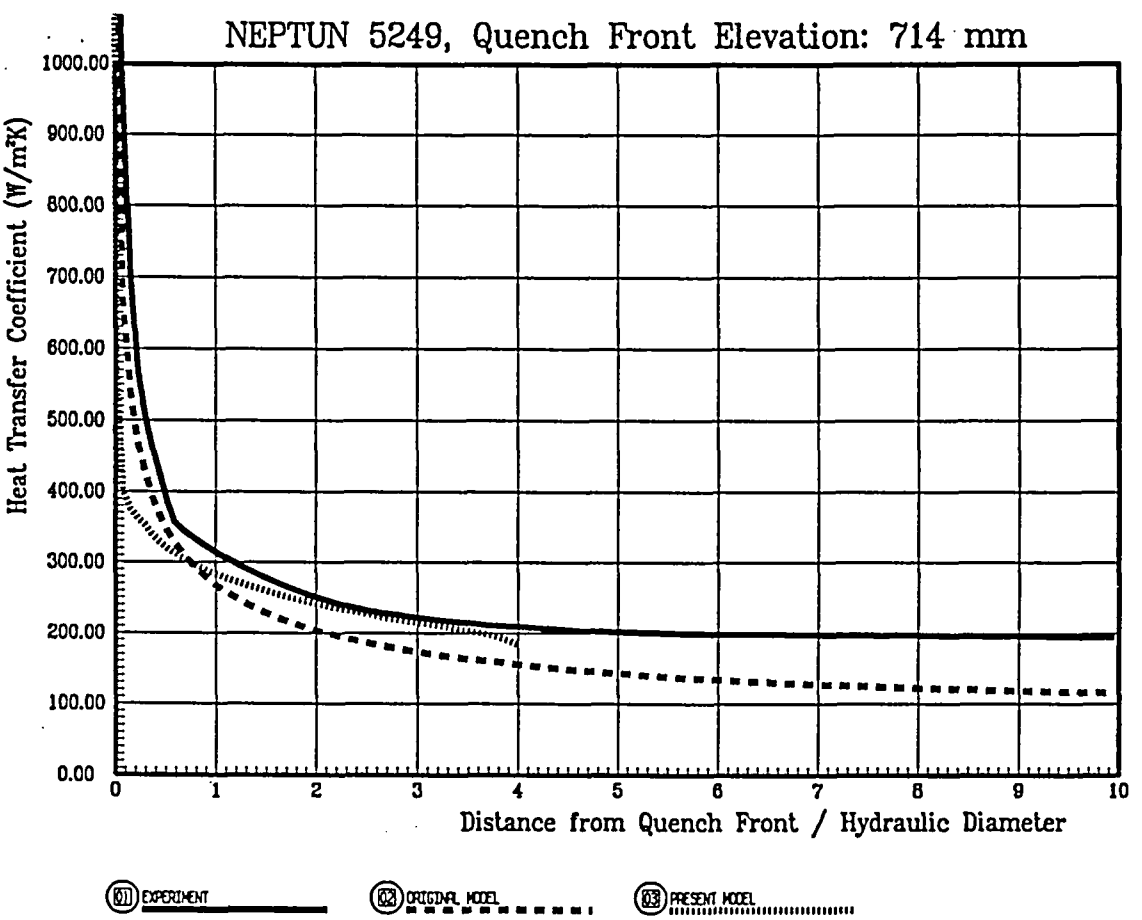
NEPTUN 5249, Quench Front Elevation: 714 mm
Heat Transfer Coefficient (W/m²K)
1000.00
900.00
800.00
700.00
600.00
500.00
400.00
300.00
200.00
100.00
0.00
0
1
2
3
4
5
6
7
8
9
10
Distance from Quench Front / Hydraulic Diameter
01 EXPERIMENT
02 ORIGINAL MODEL
03 PRESENT MODEL

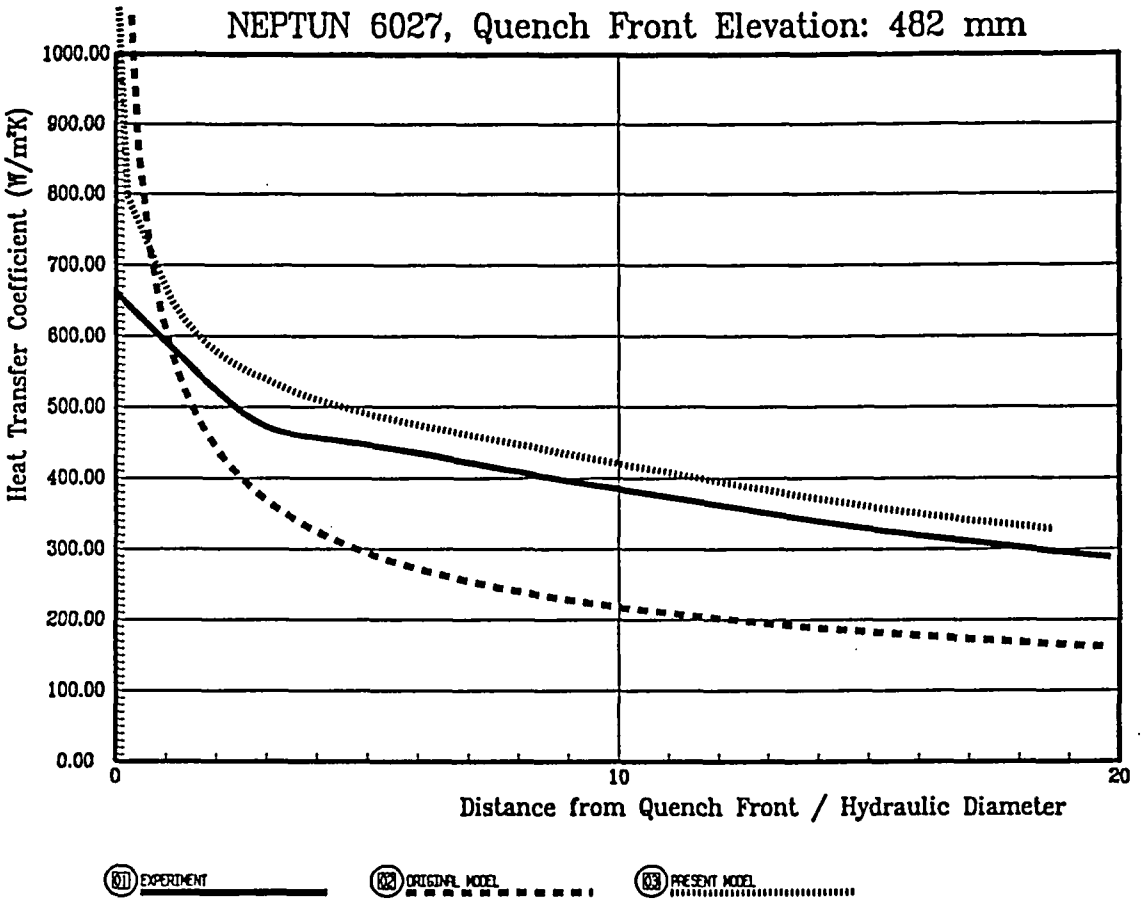
NEPTUN 6027, Quench Front Elevation: 482 mm
Heat Transfer Coefficient (W/m²K)
1000.00
900.00
800.00
700.00
600.00
500.00
400.00
300.00
200.00
100.00
0.00
0
10
20
Distance from Quench Front / Hydraulic Diameter
01 EXPERIMENT
02 ORIGINAL MODEL
03 PRESENT MODEL

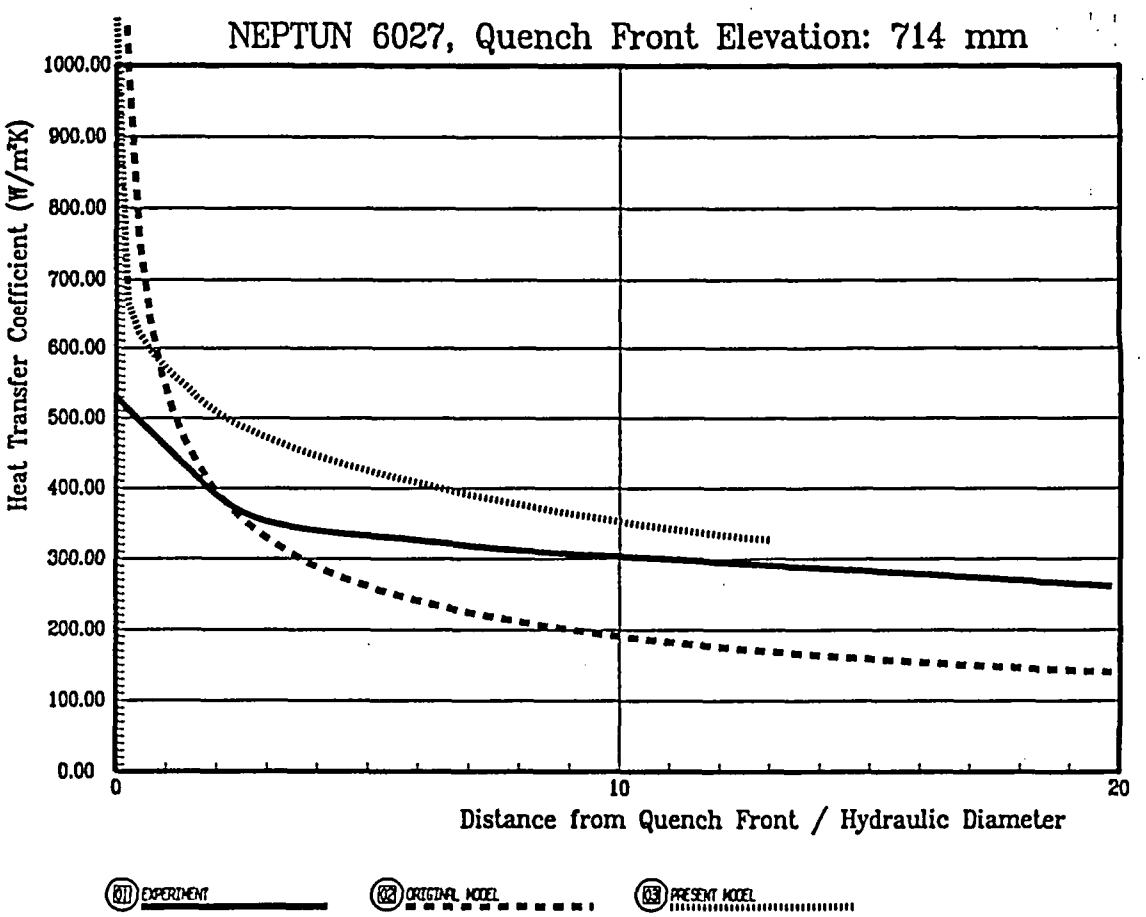
NEPTUN 6027, Quench Front Elevation: 714 mm
Heat Transfer Coefficient (W/m²K)
1000.00
900.00
800.00
700.00
600.00
500.00
400.00
300.00
200.00
100.00
0.00
0
10
20
Distance from Quench Front / Hydraulic Diameter
01 EXPERIMENT
02 ORIGINAL MODEL
03 PRESENT MODEL

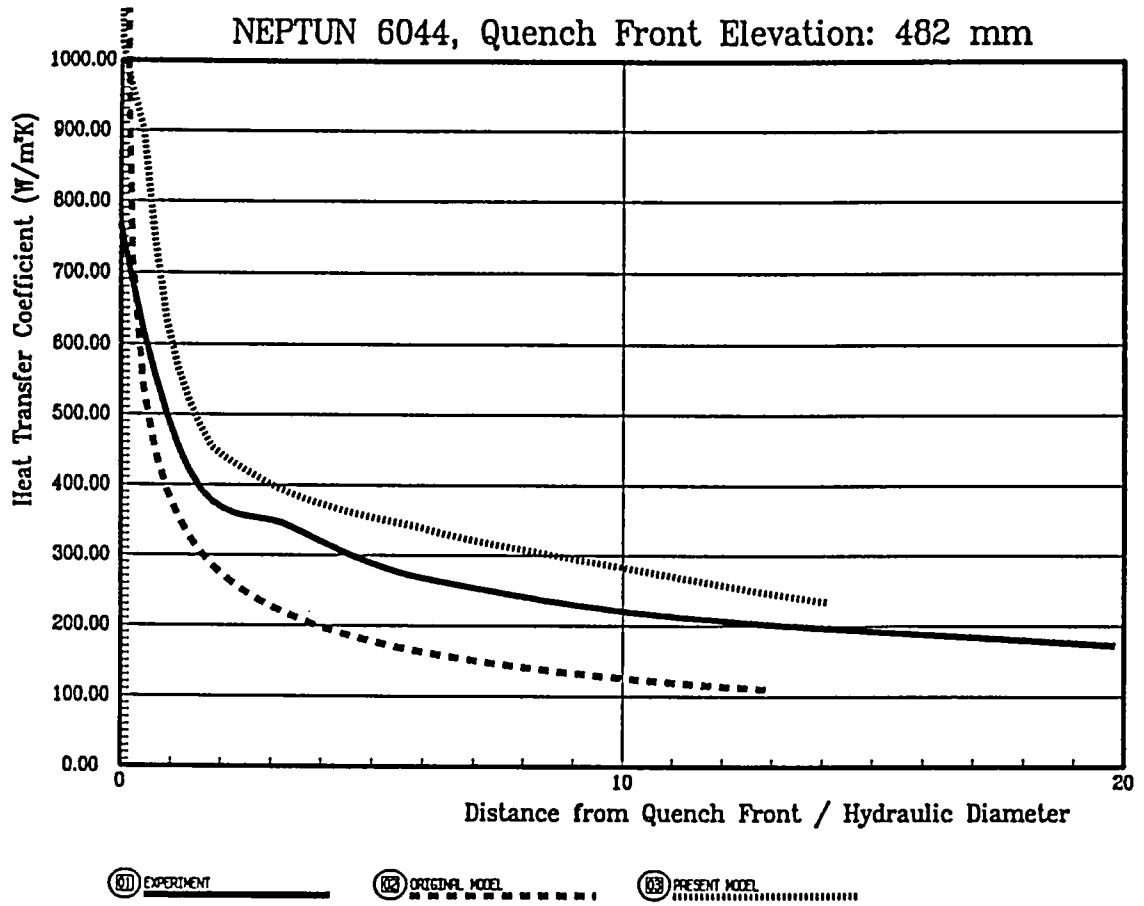
NEPTUN 6044, Quench Front Elevation: 482 mm
Heat Transfer Coefficient (W/m²K)
1000.00
900.00
800.00
700.00
600.00
500.00
400.00
300.00
200.00
100.00
0.00
0
10
20
Distance from Quench Front / Hydraulic Diameter
01 EXPERIMENT
02 ORIGINAL MODEL
03 PRESENT MODEL

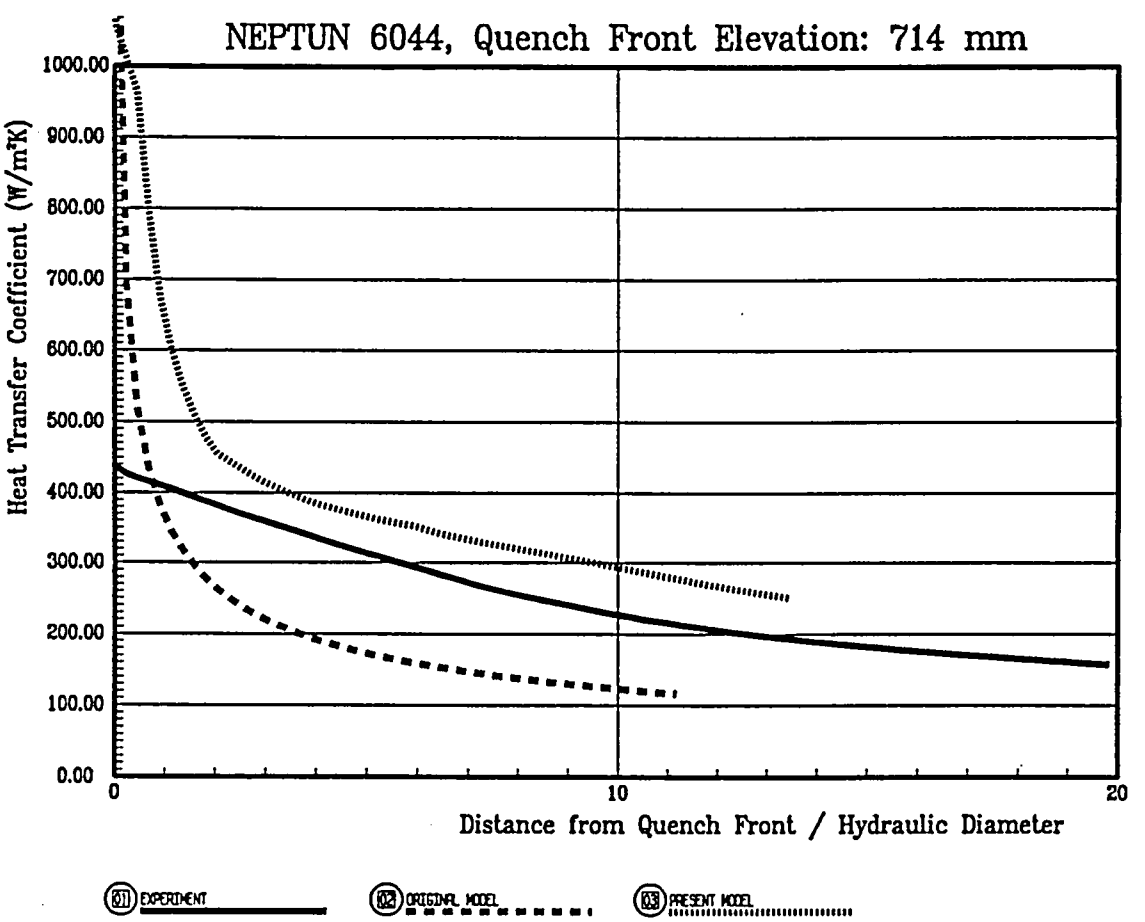
NEPTUN 6044, Quench Front Elevation: 714 mm
Heat Transfer Coefficient (W/m²K)
1000.00
900.00
800.00
700.00
600.00
500.00
400.00
300.00
200.00
100.00
0.00
0
10
20
Distance from Quench Front / Hydraulic Diameter
01 EXPERIMENT
02 ORIGINAL MODEL
03 PRESENT MODEL

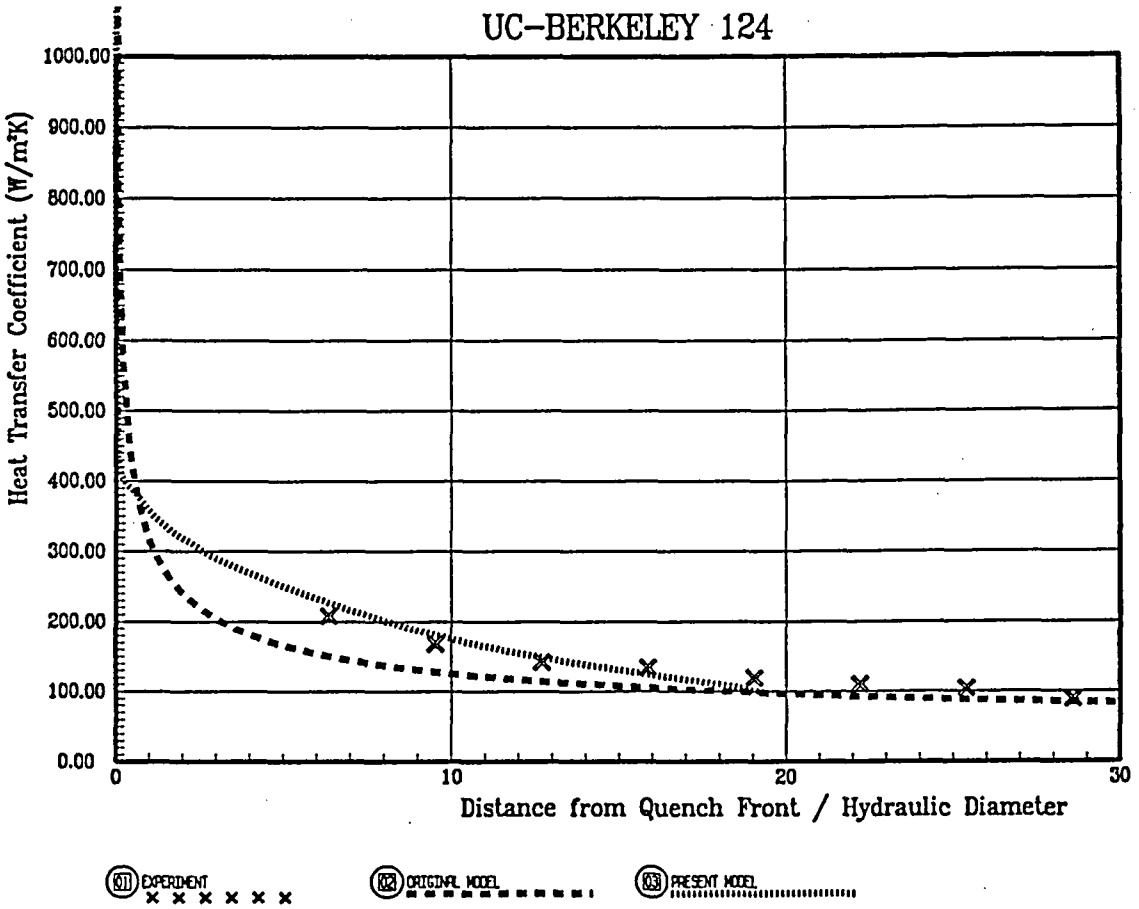
UC-BERKELEY 124
Heat Transfer Coefficient (W/m²K)
1000.00
900.00
800.00
700.00
600.00
500.00
400.00
300.00
200.00
100.00
0.00
0
10
20
30
Distance from Quench Front / Hydraulic Diameter
01 EXPERIMENT
02 ORIGINAL MODEL
03 PRESENT MODEL

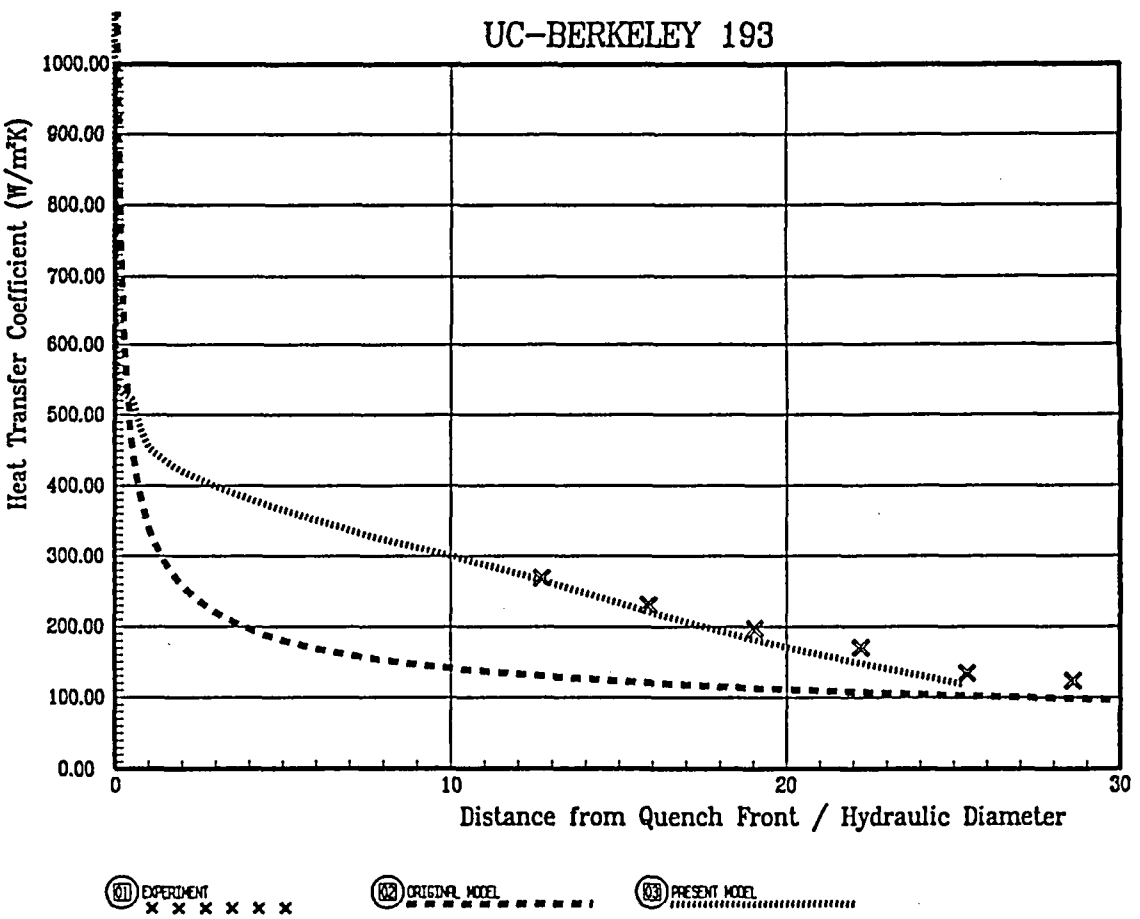
UC-BERKELEY 193
Heat Transfer Coefficient (W/m²K)
1000.00
900.00
800.00
700.00
600.00
500.00
400.00
300.00
200.00
100.00
0.00
0
10
20
30
Distance from Quench Front / Hydraulic Diameter
01 EXPERIMENT
02 ORIGINAL MODEL
03 PRESENT MODEL

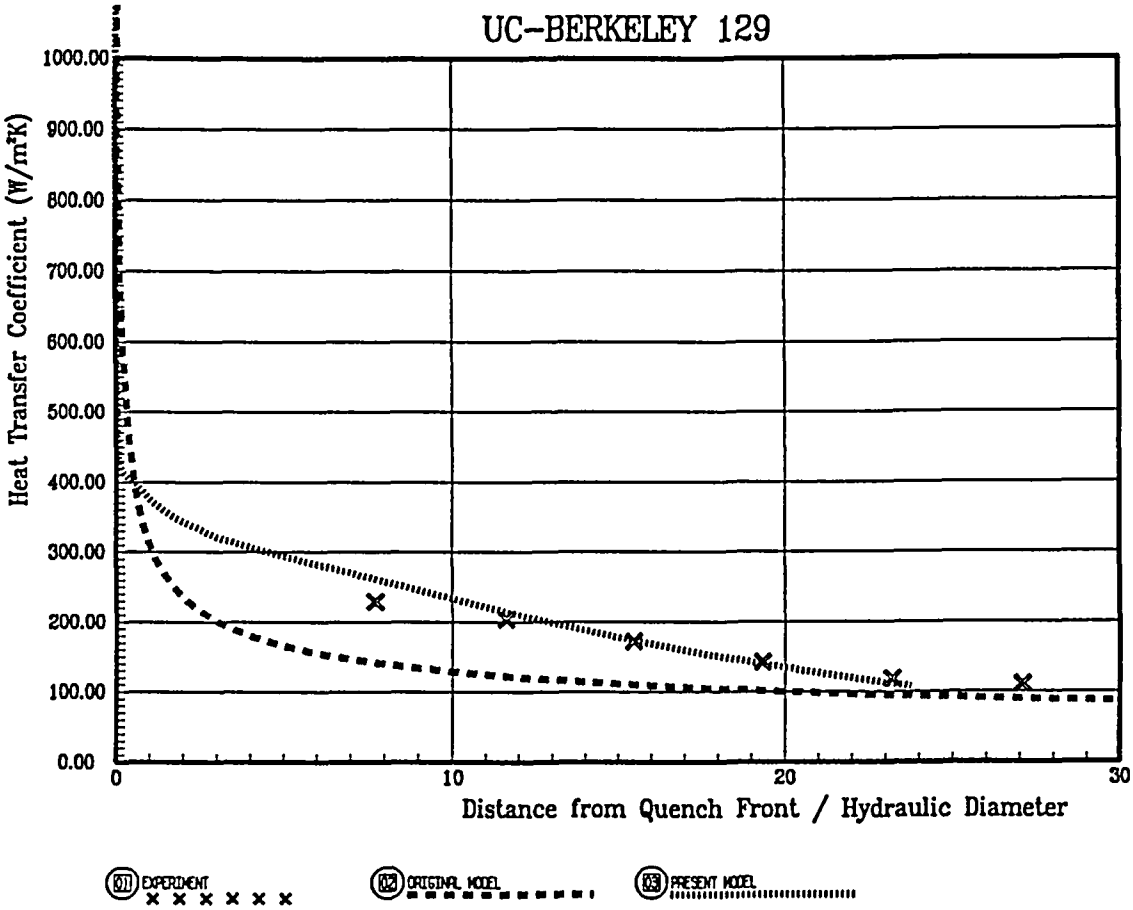
UC-BERKELEY 129
Heat Transfer Coefficient (W/m²K)
1000.00
900.00
800.00
700.00
600.00
500.00
400.00
300.00
200.00
100.00
0.00
0
10
20
30
Distance from Quench Front / Hydraulic Diameter
001 EXPERIMENT
002 ORIGINAL MODEL
003 PRESENT MODEL

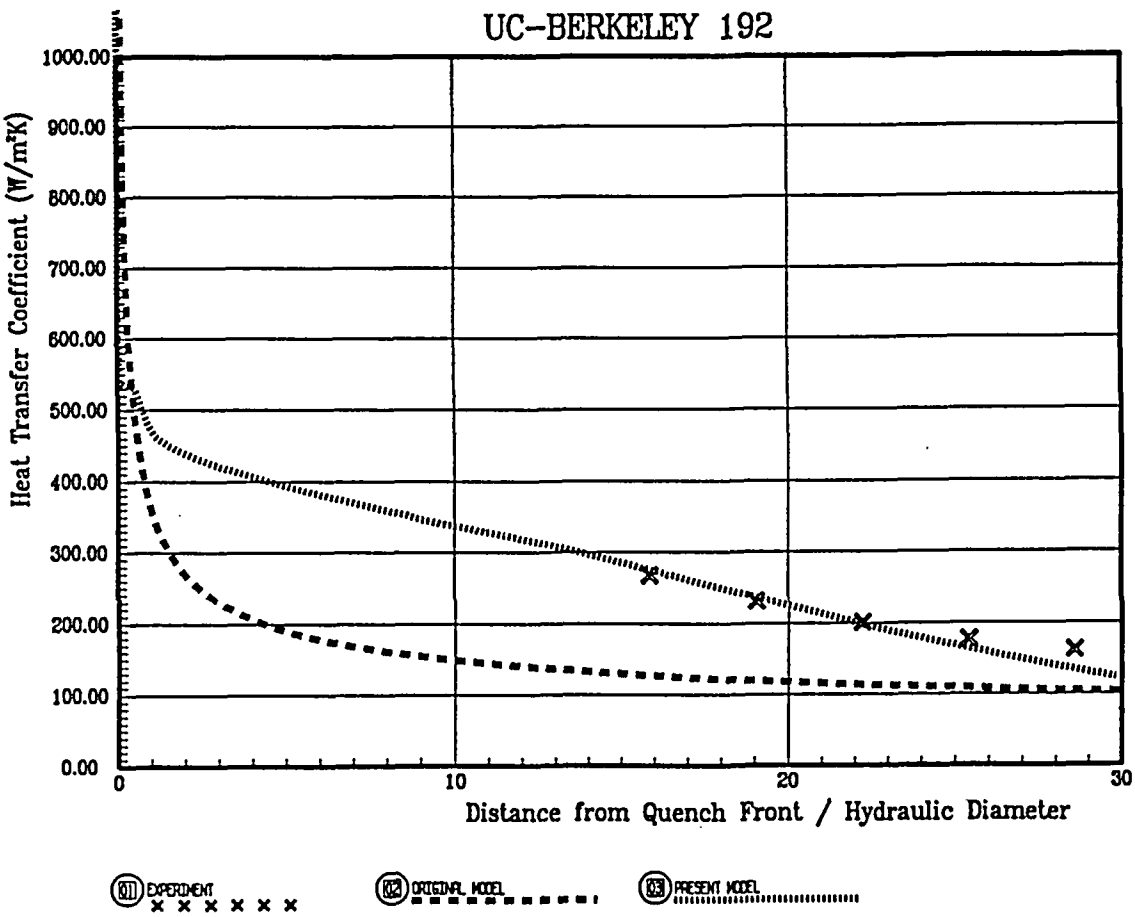
UC-BERKELEY 192
Heat Transfer Coefficient (W/m²K)
1000.00
900.00
800.00
700.00
600.00
500.00
400.00
300.00
200.00
100.00
0.00
0
10
20
30
Distance from Quench Front / Hydraulic Diameter
001 EXPERIMENT
002 ORIGINAL MODEL
003 PRESENT MODEL

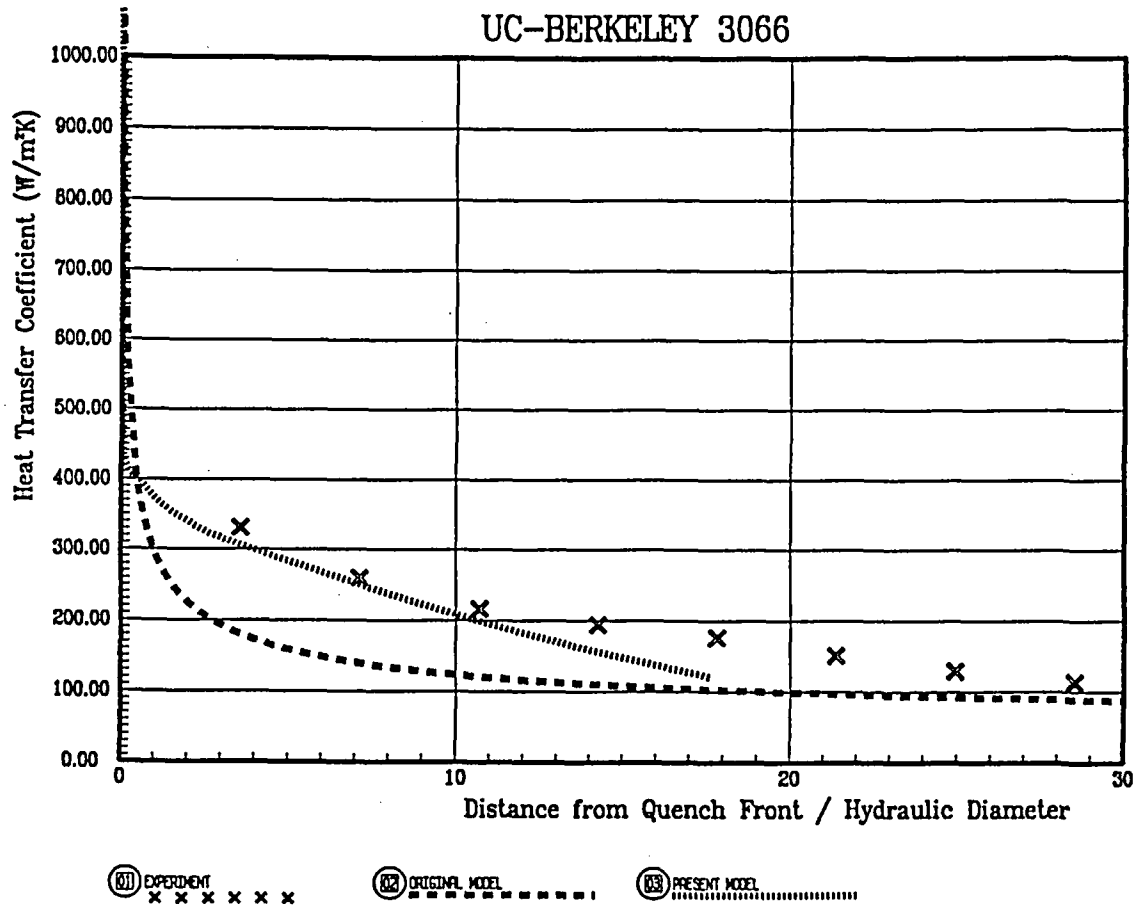
UC-BERKELEY 3066
Heat Transfer Coefficient (W/m²K)
1000.00
900.00
800.00
700.00
600.00
500.00
400.00
300.00
200.00
100.00
0.00
0
10
20
30
Distance from Quench Front / Hydraulic Diameter
01 EXPERIMENT
02 ORIGINAL MODEL
03 PRESENT MODEL

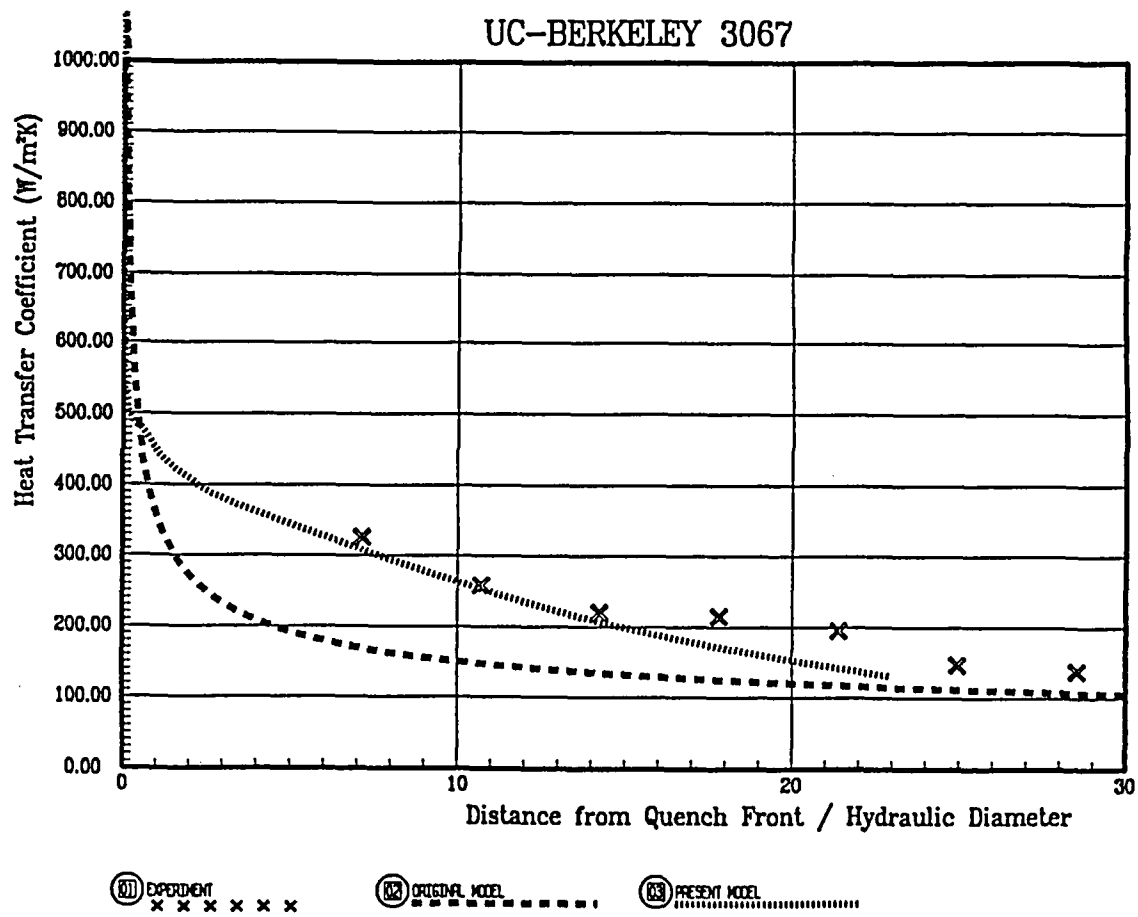
UC-BERKELEY 3067
Heat Transfer Coefficient (W/m²K)
1000.00
900.00
800.00
700.00
600.00
500.00
400.00
300.00
200.00
100.00
0.00
0
10
20
30
Distance from Quench Front / Hydraulic Diameter
01 EXPERIMENT
02 ORIGINAL MODEL
03 PRESENT MODEL

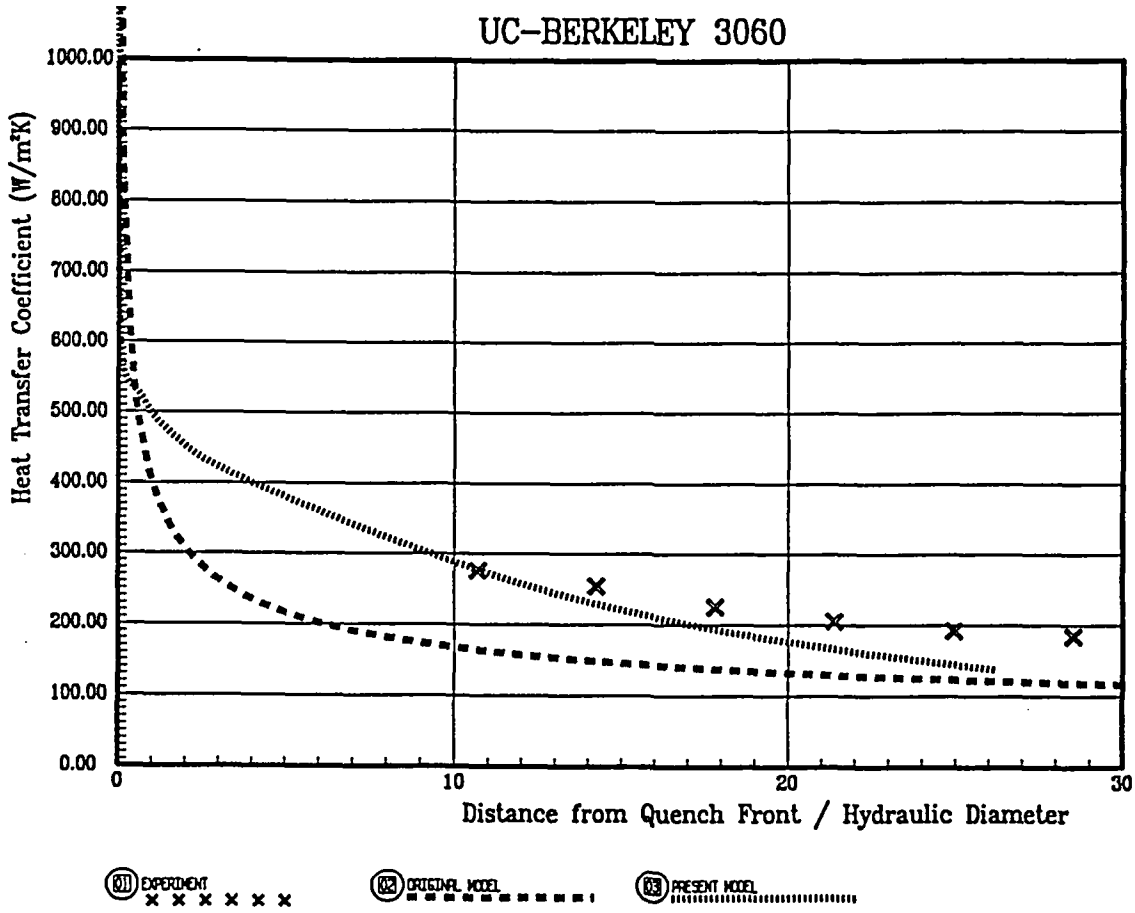
UC-BERKELEY 3060
Heat Transfer Coefficient (W/m²K)
1000.00
900.00
800.00
700.00
600.00
500.00
400.00
300.00
200.00
100.00
0.00
0
10
20
30
Distance from Quench Front / Hydraulic Diameter
01 EXPERIMENT
02 ORIGINAL MODEL
03 PRESENT MODEL

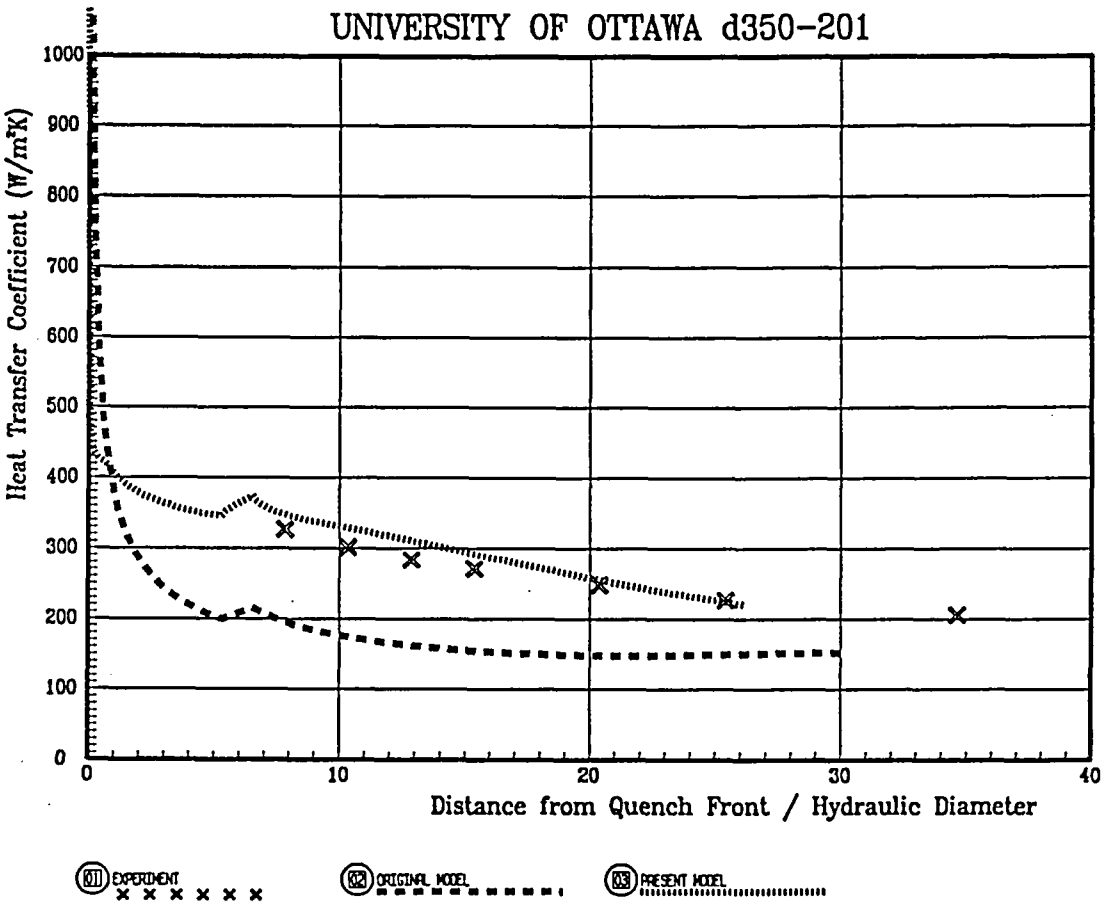
UNIVERSITY OF OTTAWA d350-201
Heat Transfer Coefficient (W/m²K)
1000
900
800
700
600
500
400
300
200
100
0
0
10
20
30
40
Distance from Quench Front / Hydraulic Diameter
01 EXPERIMENT
02 ORIGINAL MODEL
03 PRESENT MODEL

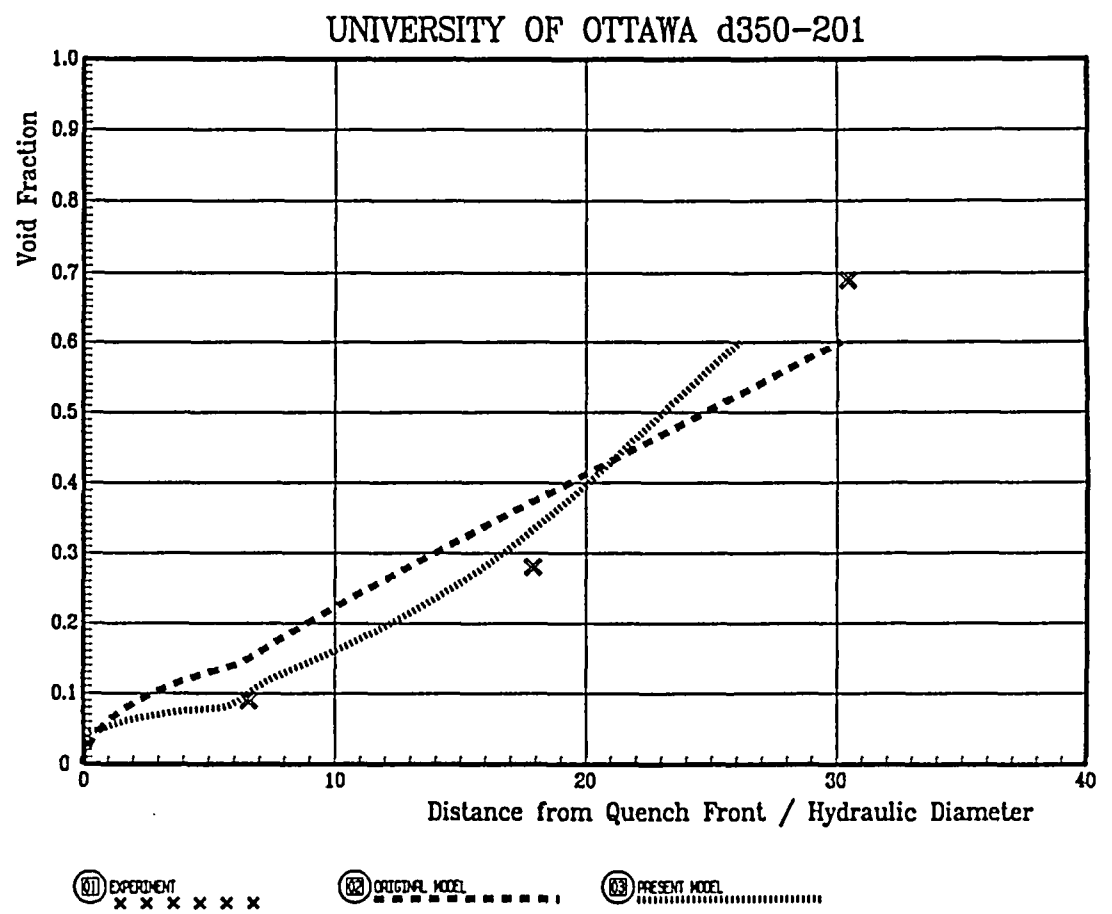
UNIVERSITY OF OTTAWA d350-201
Void Fraction
1.0
0.9
0.8
0.7
0.6
0.5
0.4
0.3
0.2
0.1
0
0
10
20
30
40
Distance from Quench Front / Hydraulic Diameter
01 EXPERIMENT
02 ORIGINAL MODEL
03 PRESENT MODEL

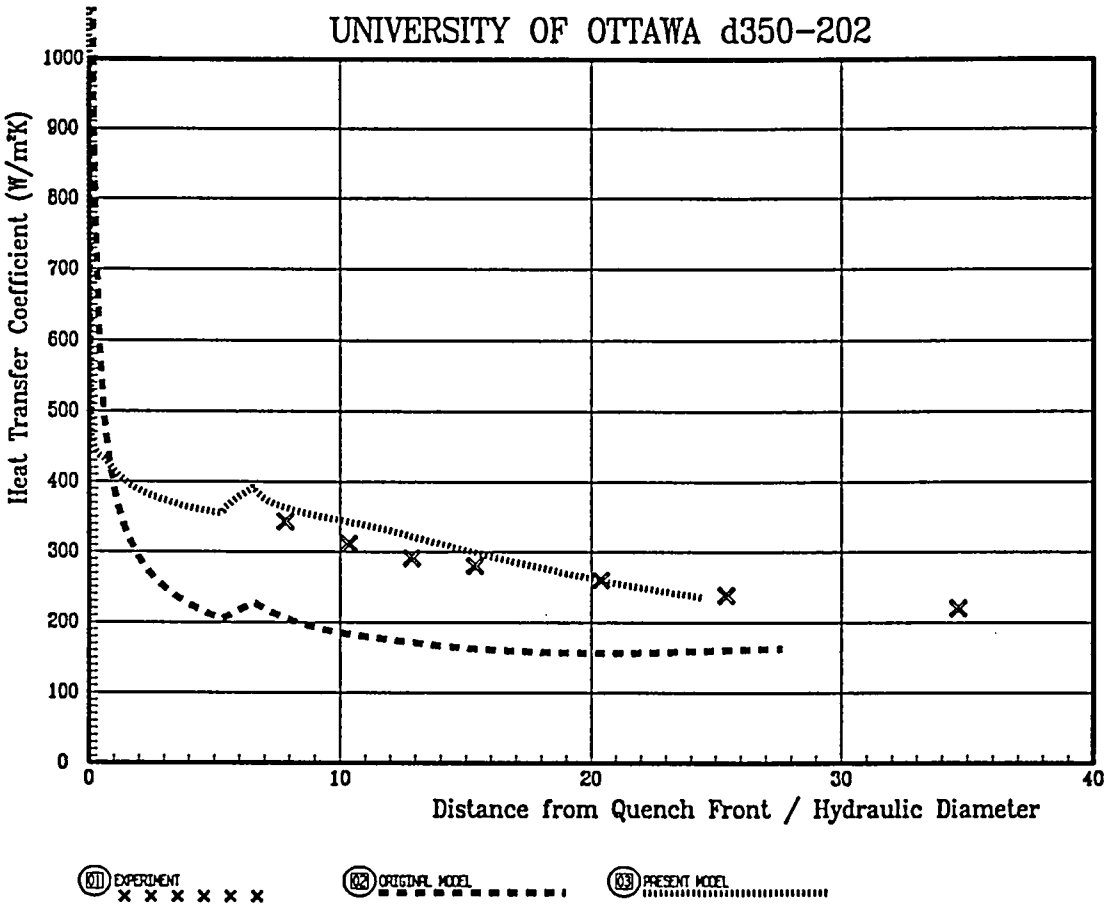
UNIVERSITY OF OTTAWA d350-202
Heat Transfer Coefficient (W/m²K)
1000
900
800
700
600
500
400
300
200
100
0
0
10
20
30
40
Distance from Quench Front / Hydraulic Diameter
01 EXPERIMENT
02 ORIGINAL MODEL
03 PRESENT MODEL

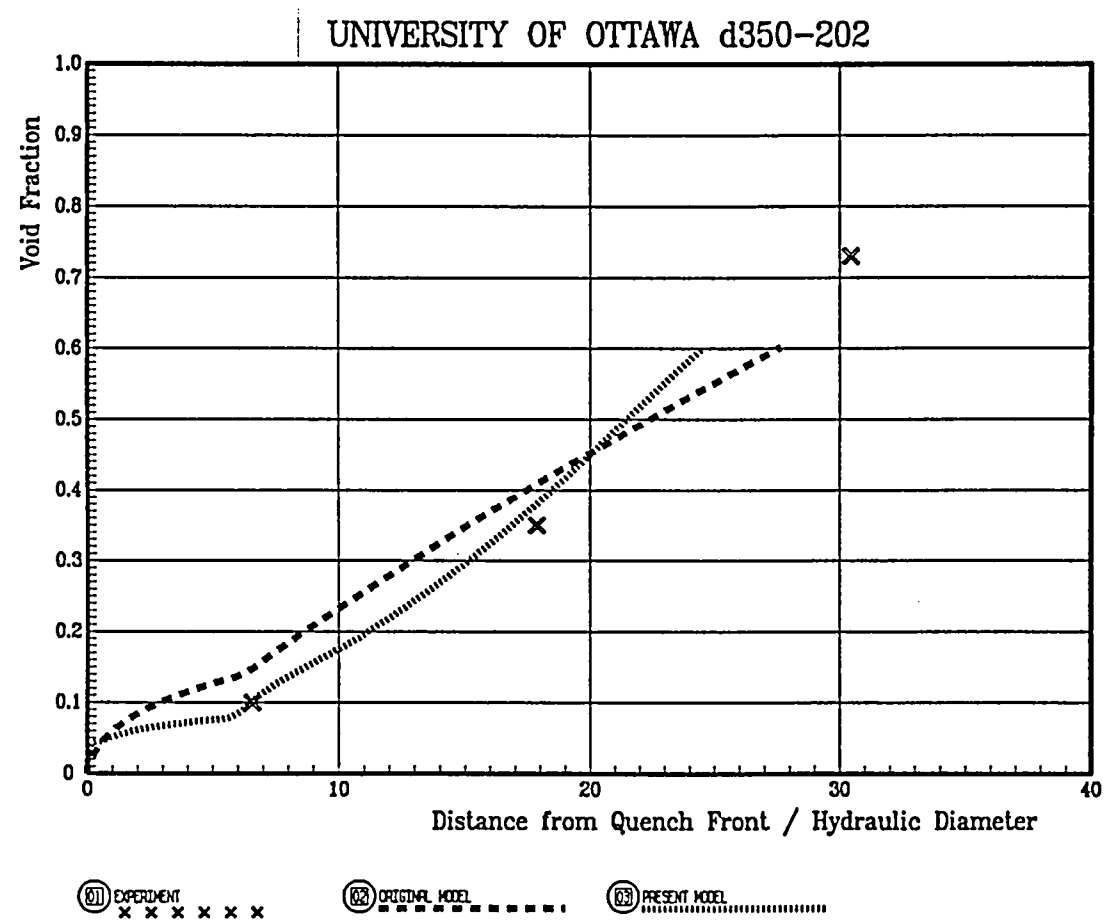
UNIVERSITY OF OTTAWA d350-202
Void Fraction
1.0
0.9
0.8
0.7
0.6
0.5
0.4
0.3
0.2
0.1
0
0
10
20
30
40
Distance from Quench Front / Hydraulic Diameter
01 EXPERIMENT
02 ORIGINAL MODEL
03 PRESENT MODEL

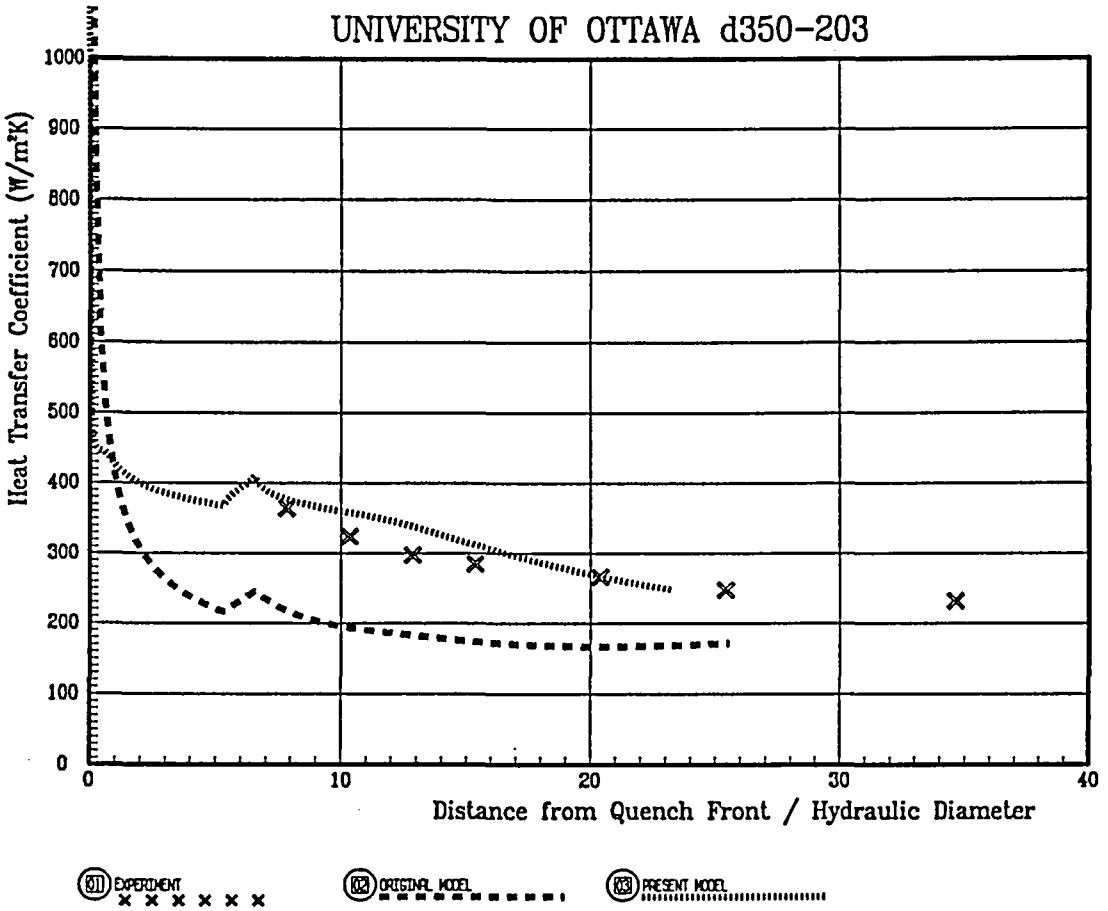
UNIVERSITY OF OTTAWA d350-203
Heat Transfer Coefficient (W/m²K)
1000
900
800
700
600
500
400
300
200
100
0
0
10
20
30
40
Distance from Quench Front / Hydraulic Diameter
01 EXPERIMENT
02 ORIGINAL MODEL
03 PRESENT MODEL

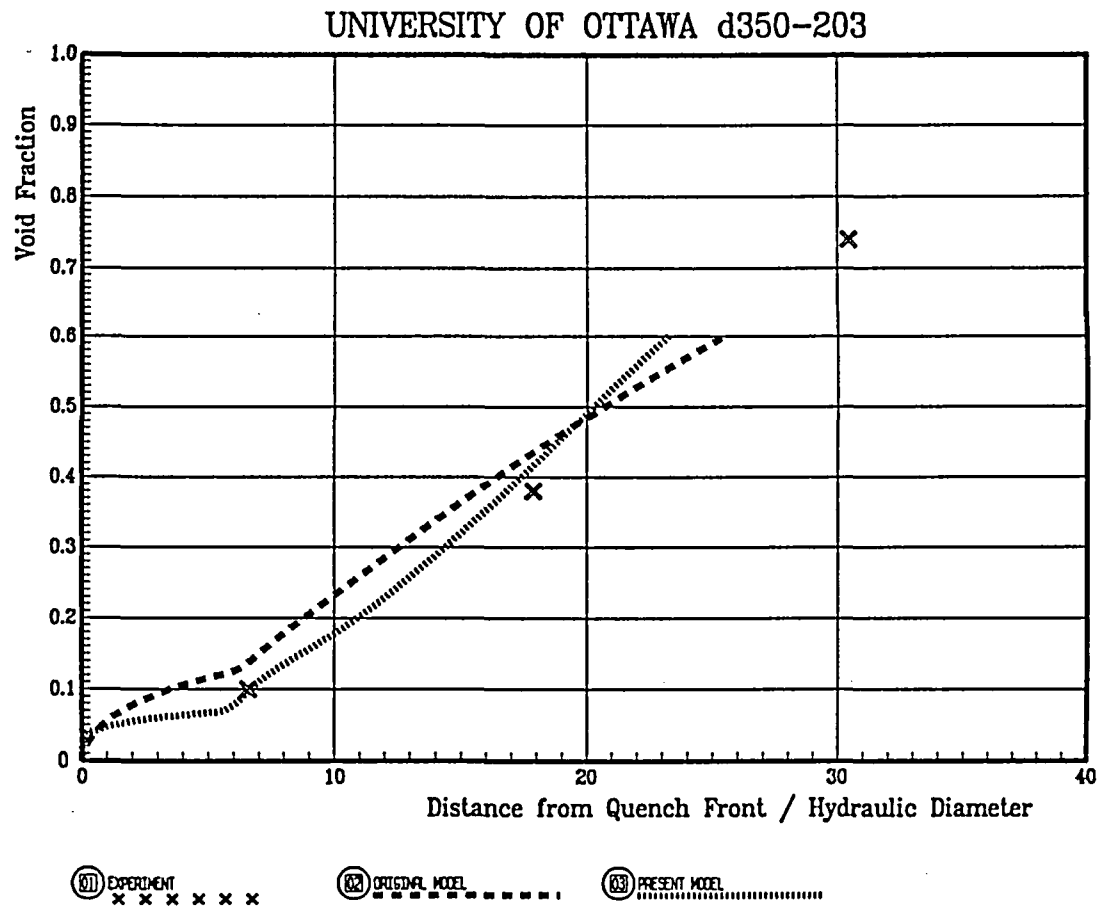
UNIVERSITY OF OTTAWA d350-203
Void Fraction
1.0
0.9
0.8
0.7
0.6
0.5
0.4
0.3
0.2
0.1
0
0
10
20
30
40
Distance from Quench Front / Hydraulic Diameter
01 EXPERIMENT
02 ORIGINAL MODEL
03 PRESENT MODEL

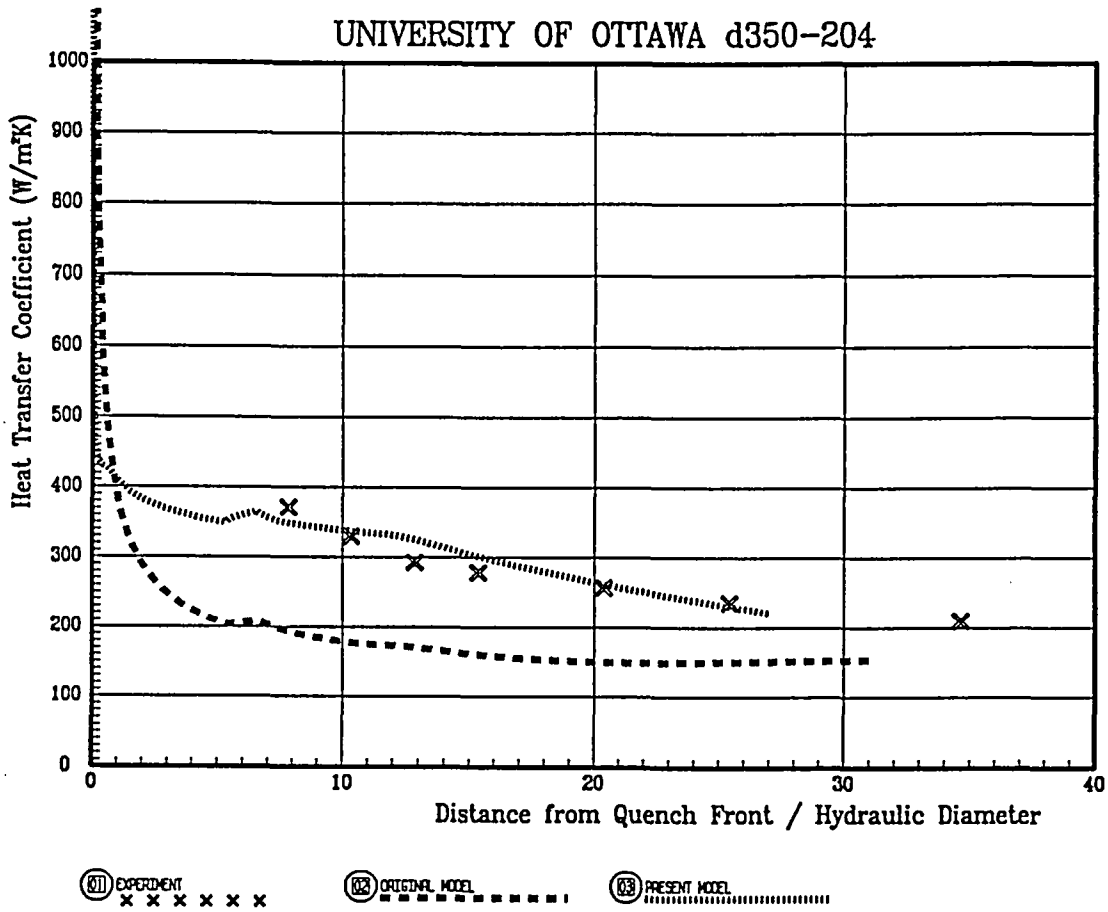
UNIVERSITY OF OTTAWA d350-204
Heat Transfer Coefficient (W/m²K)
1000
900
800
700
600
500
400
300
200
100
0
0
10
20
30
40
Distance from Quench Front / Hydraulic Diameter
01 EXPERIMENT
02 ORIGINAL MODEL
03 PRESENT MODEL

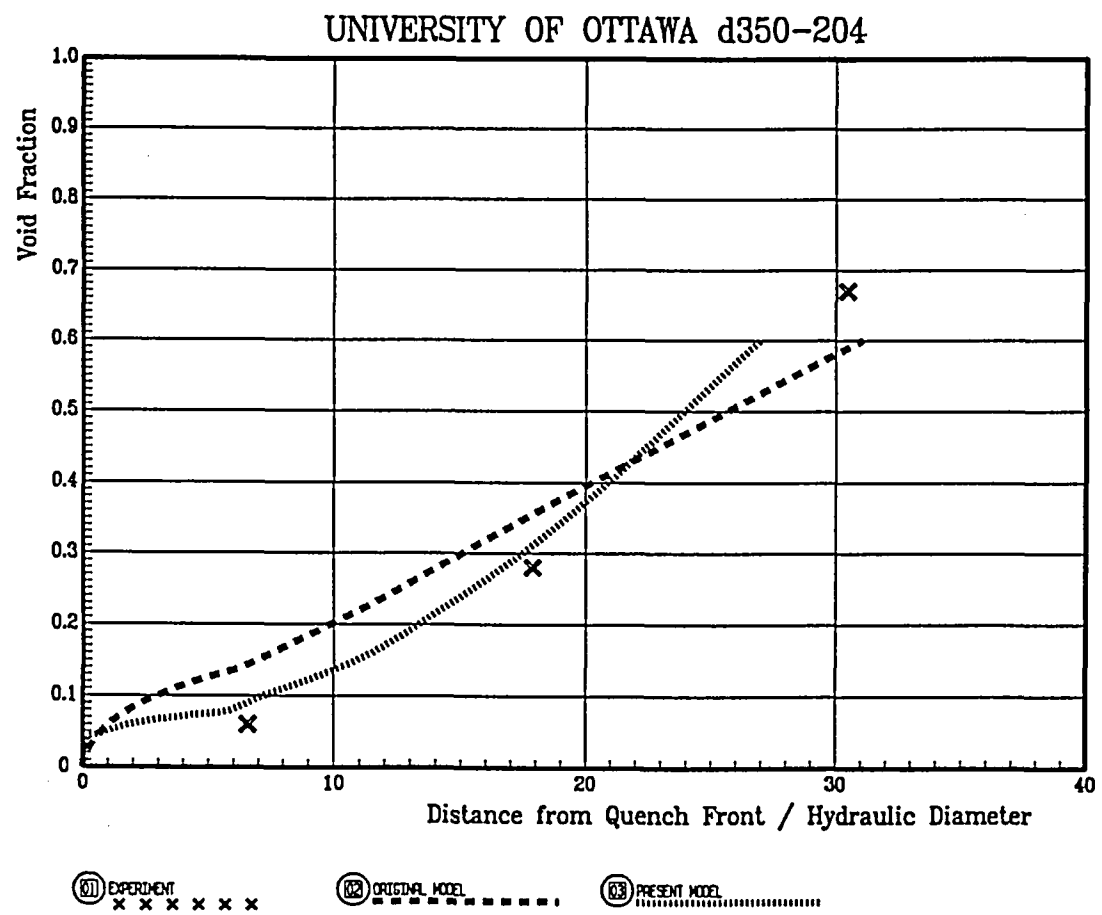
UNIVERSITY OF OTTAWA d350-204
Void Fraction
1.0
0.9
0.8
0.7
0.6
0.5
0.4
0.3
0.2
0.1
0
0
10
20
30
40
Distance from Quench Front / Hydraulic Diameter
01 EXPERIMENT
02 ORIGINAL MODEL
03 PRESENT MODEL

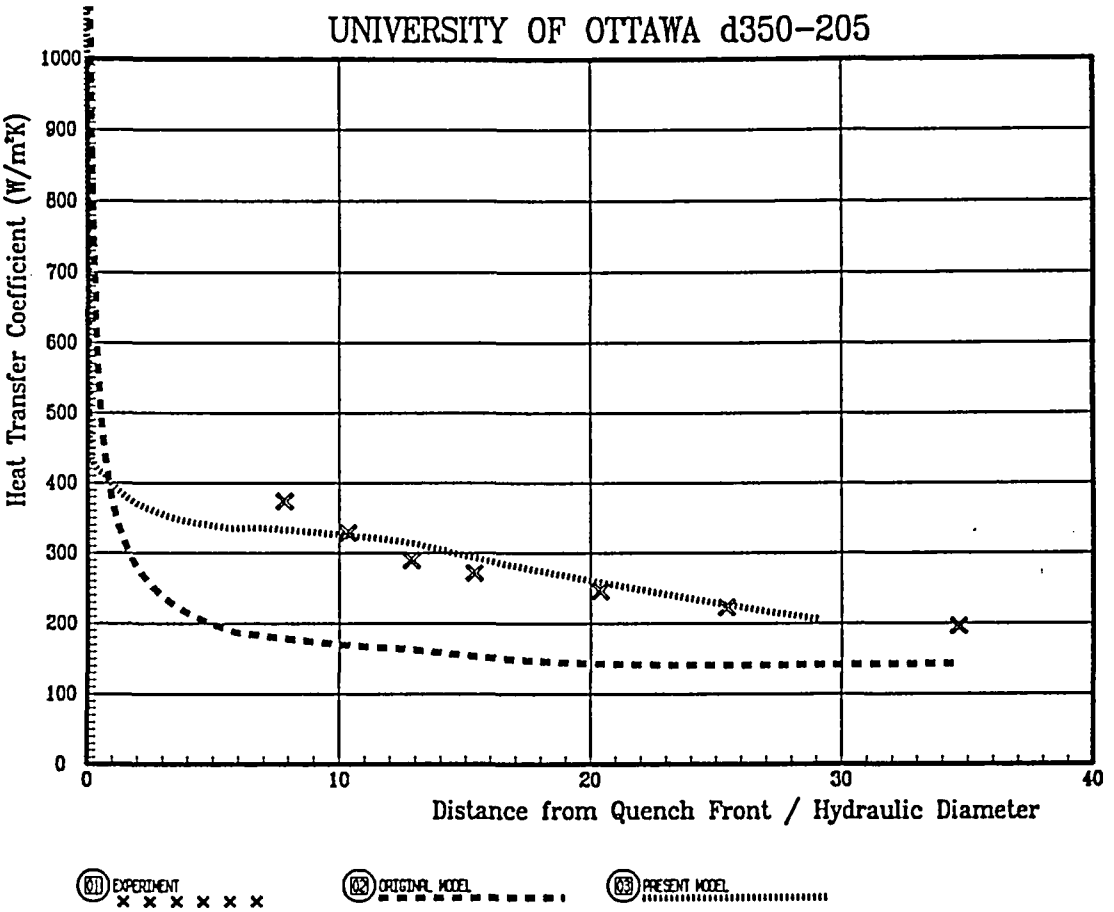
UNIVERSITY OF OTTAWA d350-205
Heat Transfer Coefficient (W/m²K)
1000
900
800
700
600
500
400
300
200
100
0
0
10
20
30
40
Distance from Quench Front / Hydraulic Diameter
01 EXPERIMENT
02 ORIGINAL MODEL
03 PRESENT MODEL

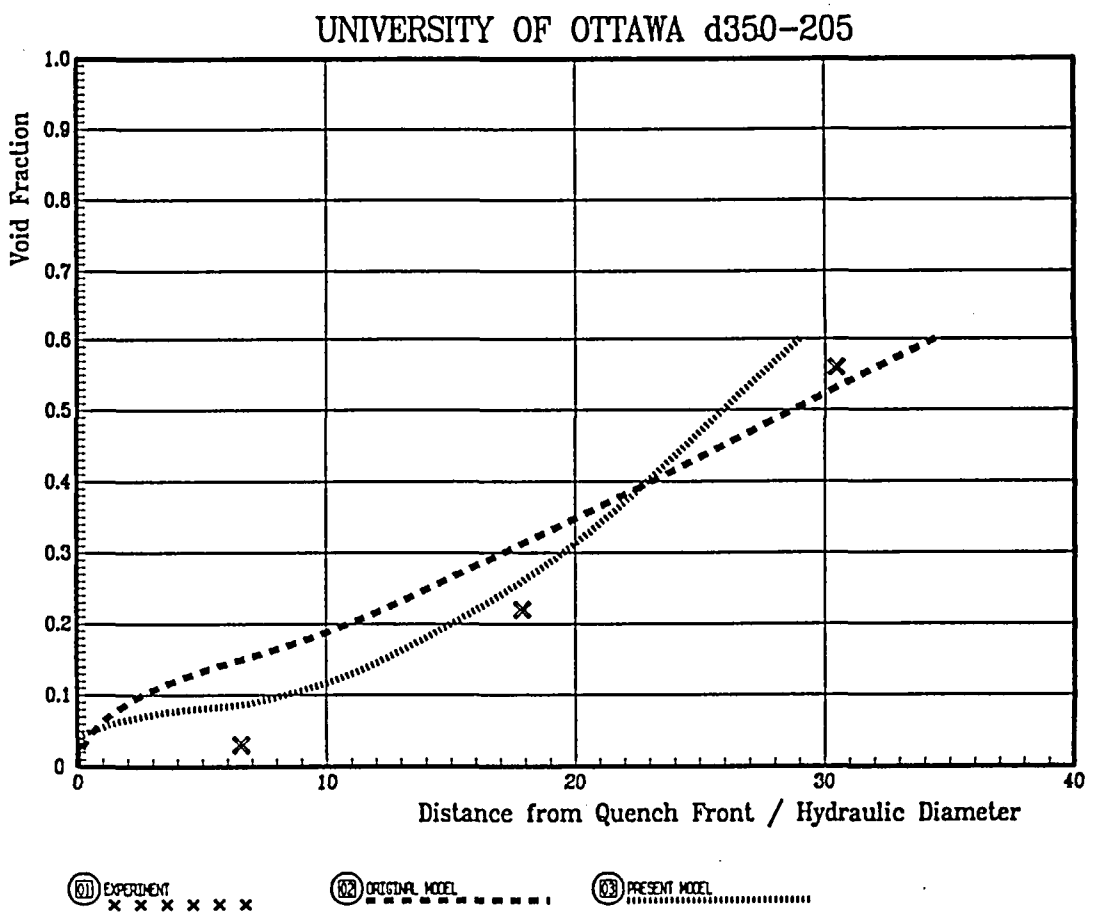
UNIVERSITY OF OTTAWA d350-205
Void Fraction
1.0
0.9
0.8
0.7
0.6
0.5
0.4
0.3
0.2
0.1
0
0
10
20
30
40
Distance from Quench Front / Hydraulic Diameter
01 EXPERIMENT
02 ORIGINAL MODEL
03 PRESENT MODEL

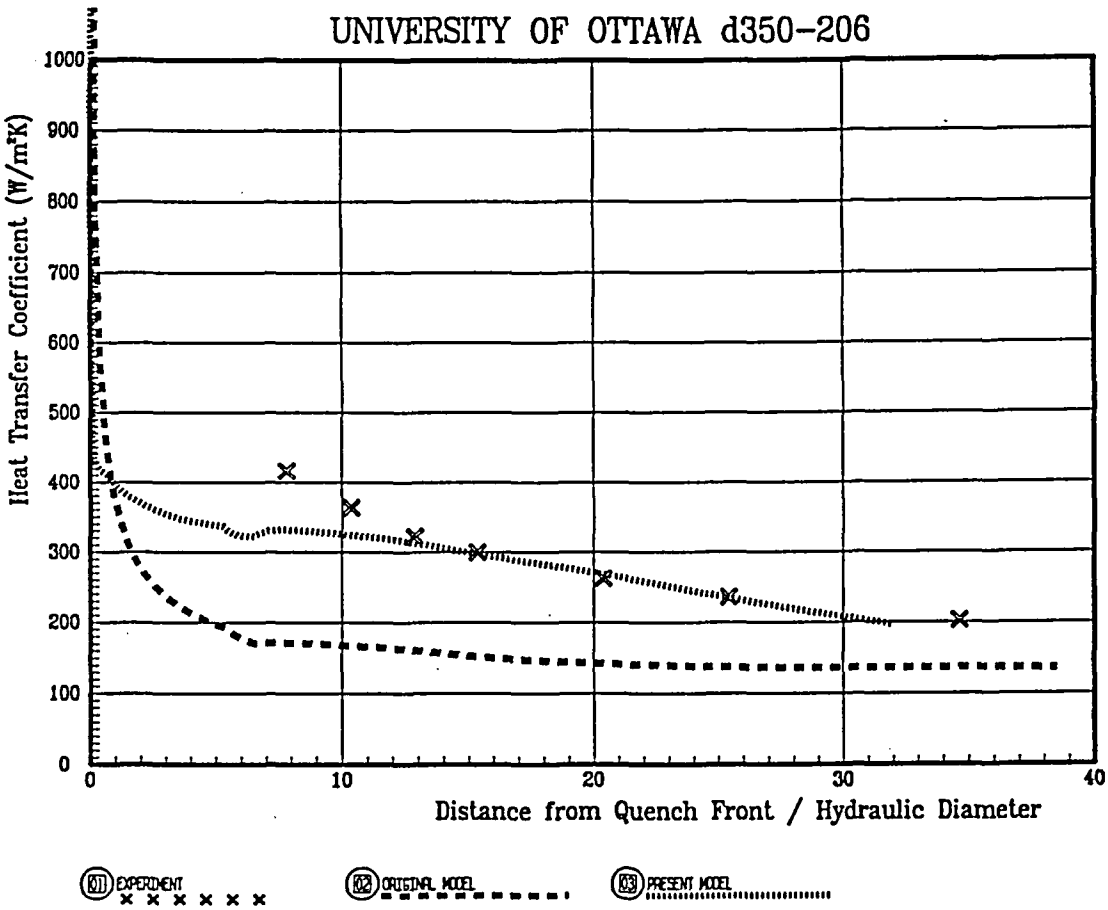
UNIVERSITY OF OTTAWA d350-206
Heat Transfer Coefficient (W/m²K)
1000
900
800
700
600
500
400
300
200
100
0
0
10
20
30
40
Distance from Quench Front / Hydraulic Diameter
01 EXPERIMENT
02 ORIGINAL MODEL
03 PRESENT MODEL

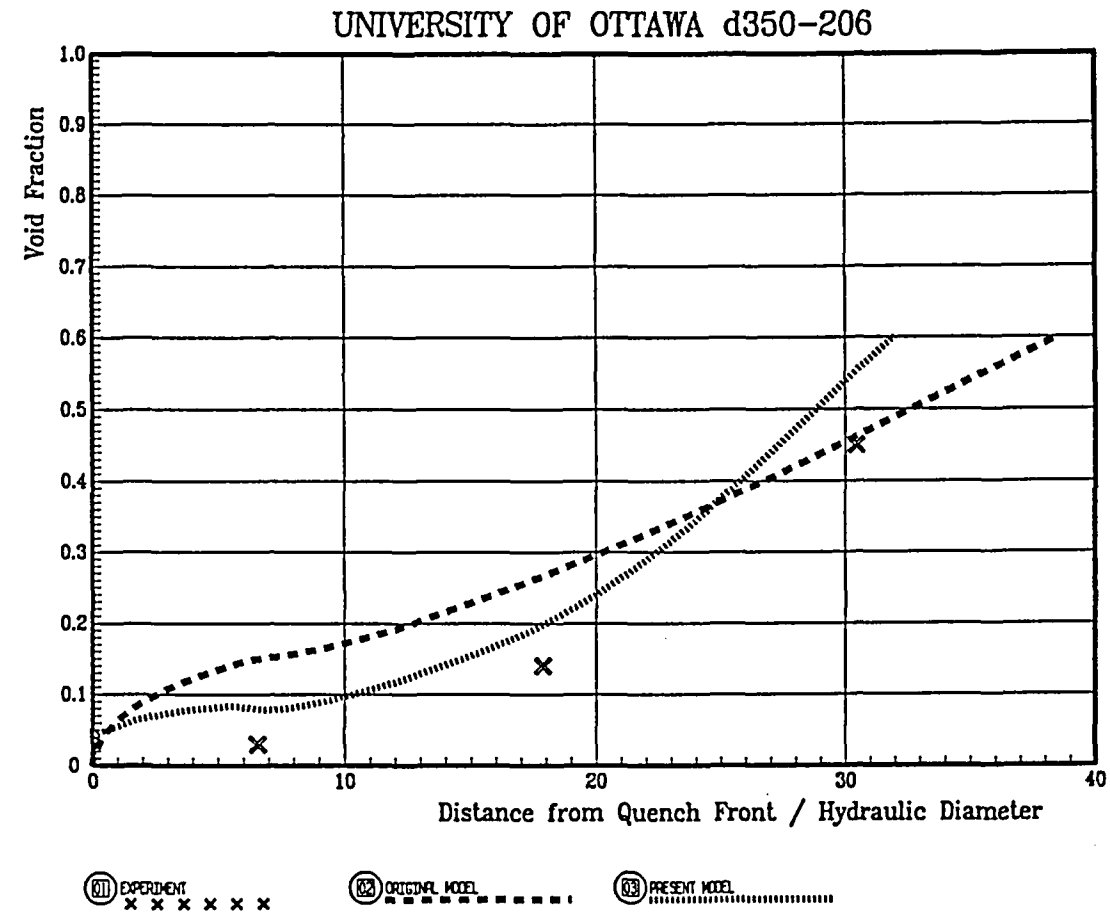
UNIVERSITY OF OTTAWA d350-206
Void Fraction
1.0
0.9
0.8
0.7
0.6
0.5
0.4
0.3
0.2
0.1
0
0
10
20
30
40
Distance from Quench Front / Hydraulic Diameter
01 EXPERIMENT
02 ORIGINAL MODEL
03 PRESENT MODEL

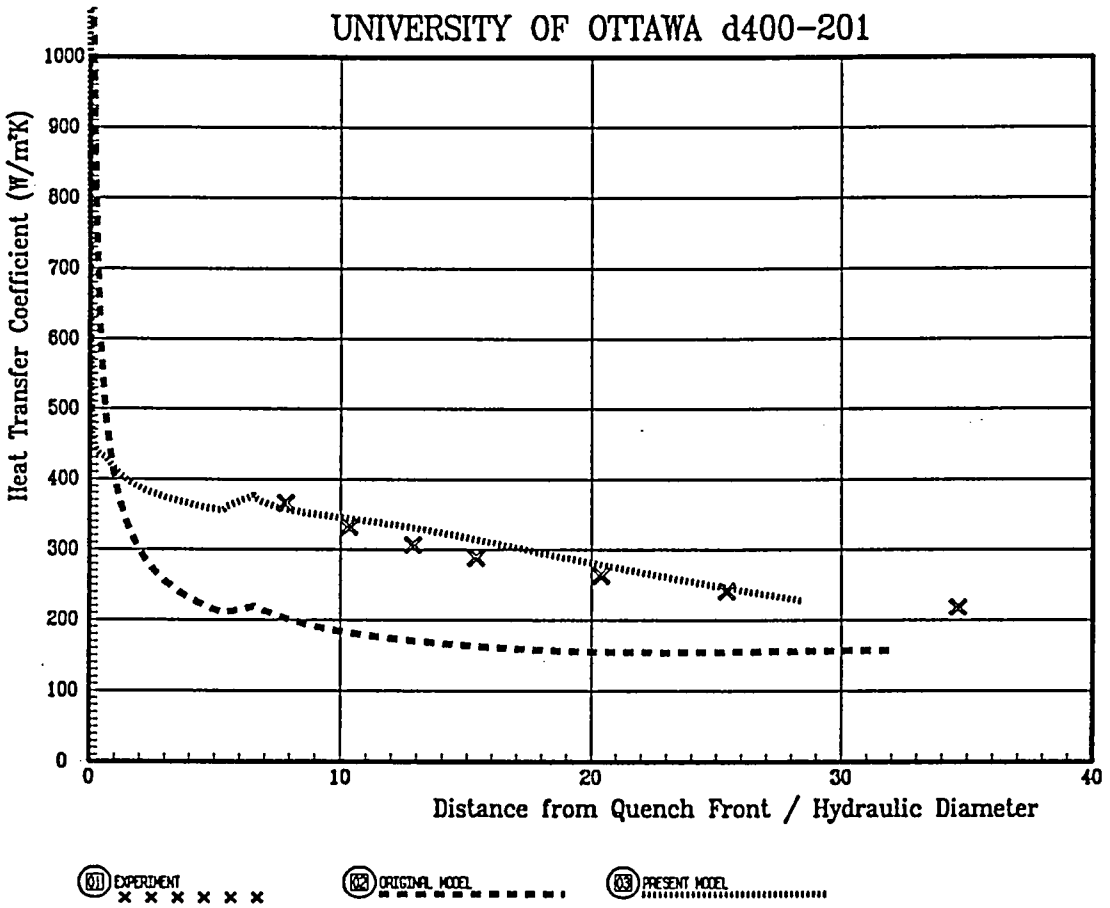
UNIVERSITY OF OTTAWA d400-201
Heat Transfer Coefficient (W/m²K)
1000
900
800
700
600
500
400
300
200
100
0
0
10
20
30
40
Distance from Quench Front / Hydraulic Diameter
01 EXPERIMENT
02 ORIGINAL MODEL
03 PRESENT MODEL

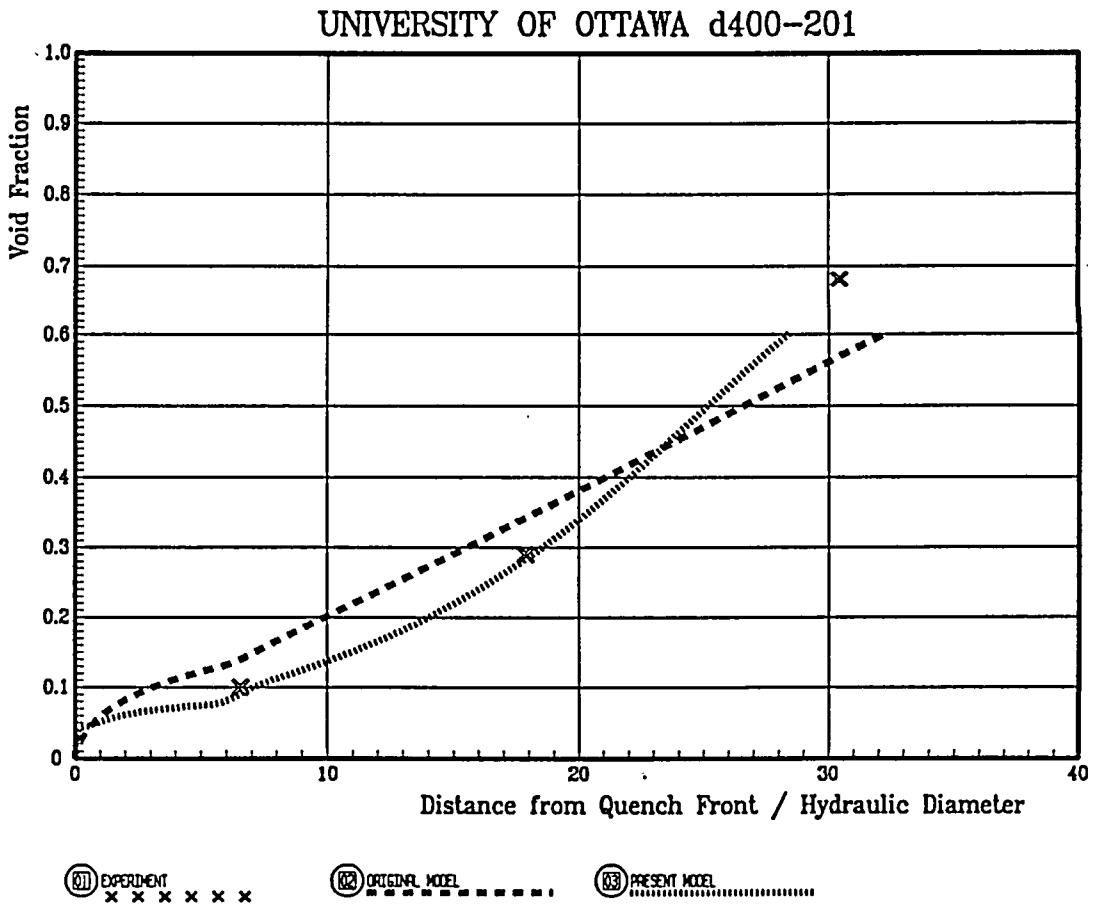
UNIVERSITY OF OTTAWA d400-201
Void Fraction
1.0
0.9
0.8
0.7
0.6
0.5
0.4
0.3
0.2
0.1
0
0
10
20
30
40
Distance from Quench Front / Hydraulic Diameter
01 EXPERIMENT
02 ORIGINAL MODEL
03 PRESENT MODEL

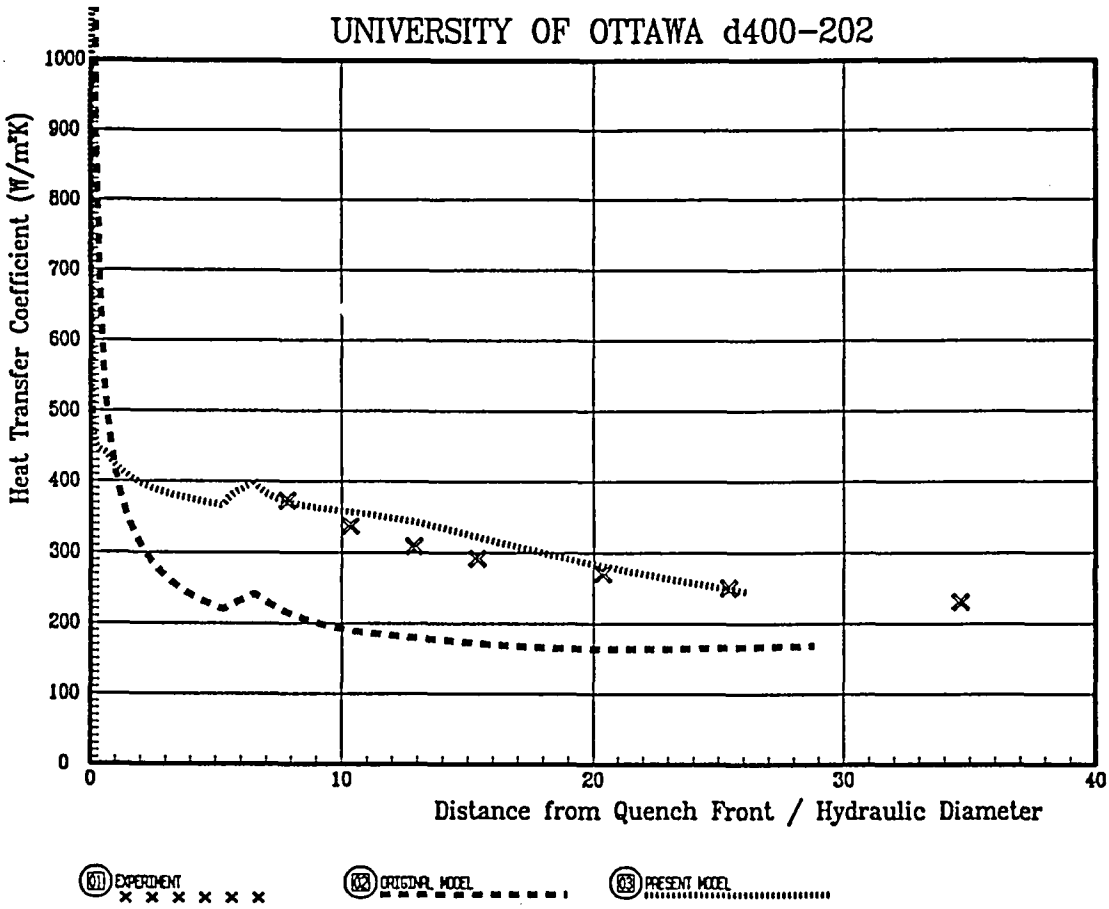
UNIVERSITY OF OTTAWA d400-202
Heat Transfer Coefficient (W/m²K)
1000
900
800
700
600
500
400
300
200
100
0
0
10
20
30
40
Distance from Quench Front / Hydraulic Diameter
01 EXPERIMENT
02 ORIGINAL MODEL
03 PRESENT MODEL

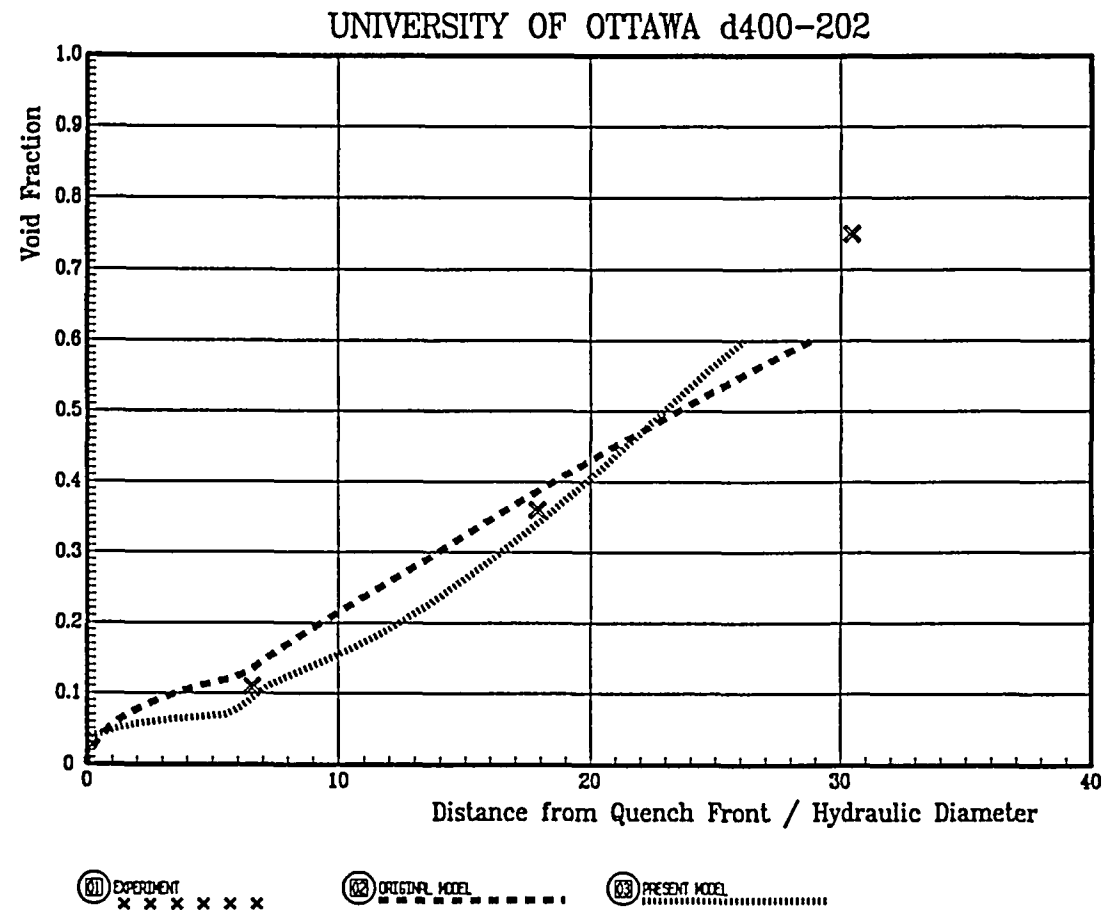
UNIVERSITY OF OTTAWA d400-202
Void Fraction
1.0
0.9
0.8
0.7
0.6
0.5
0.4
0.3
0.2
0.1
0
0
10
20
30
40
Distance from Quench Front / Hydraulic Diameter
01 EXPERIMENT
02 ORIGINAL MODEL
03 PRESENT MODEL

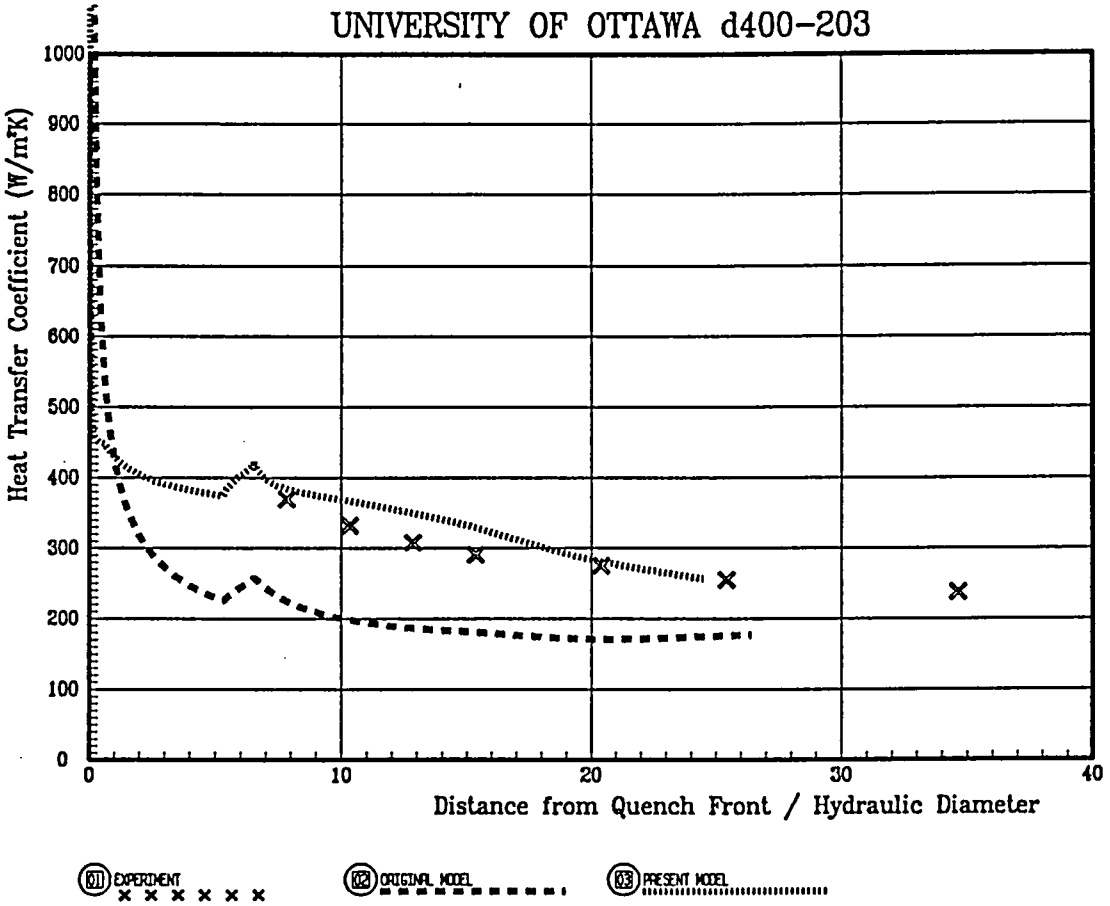
UNIVERSITY OF OTTAWA d400-203
Heat Transfer Coefficient (W/m²K)
1000
900
800
700
600
500
400
300
200
100
0
0
10
20
30
40
Distance from Quench Front / Hydraulic Diameter
01 EXPERIMENT
02 ORIGINAL MODEL
03 PRESENT MODEL

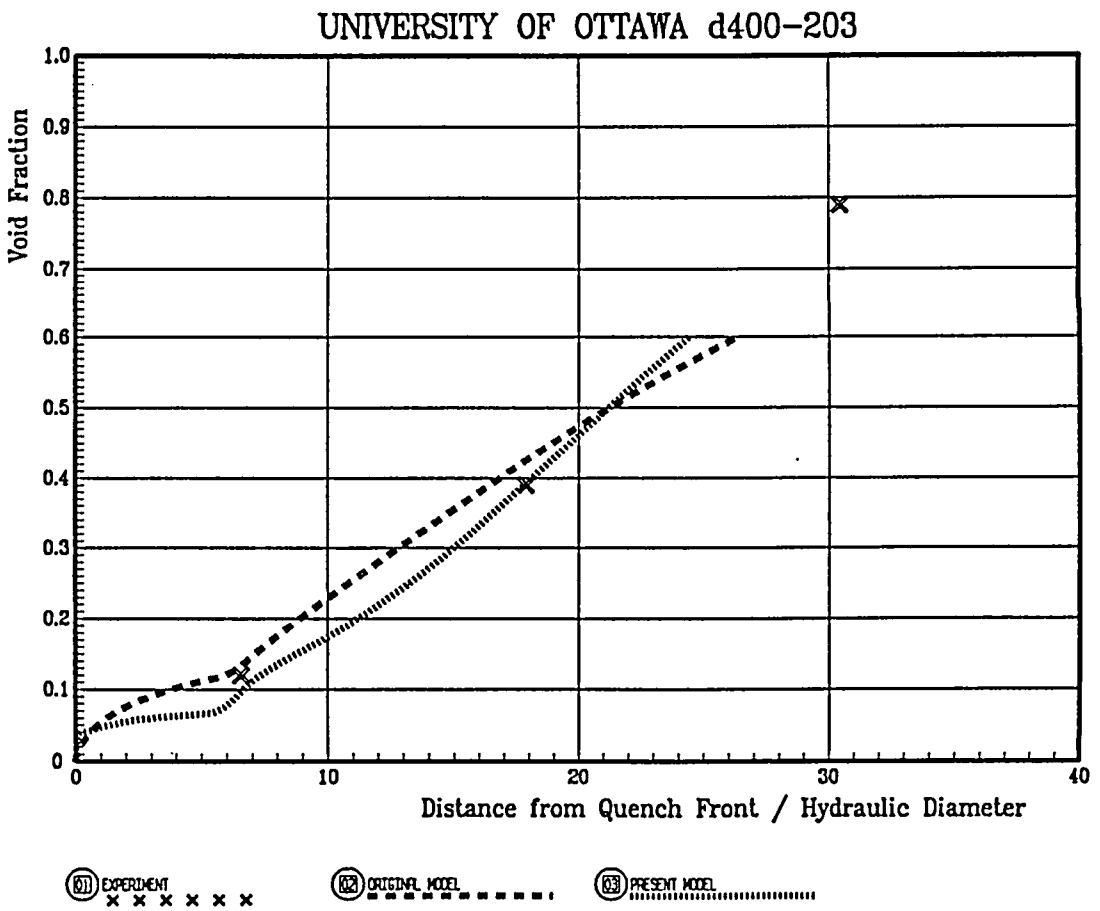
UNIVERSITY OF OTTAWA d400-203
Void Fraction
1.0
0.9
0.8
0.7
0.6
0.5
0.4
0.3
0.2
0.1
0
0
10
20
30
40
Distance from Quench Front / Hydraulic Diameter
01 EXPERIMENT
02 ORIGINAL MODEL
03 PRESENT MODEL

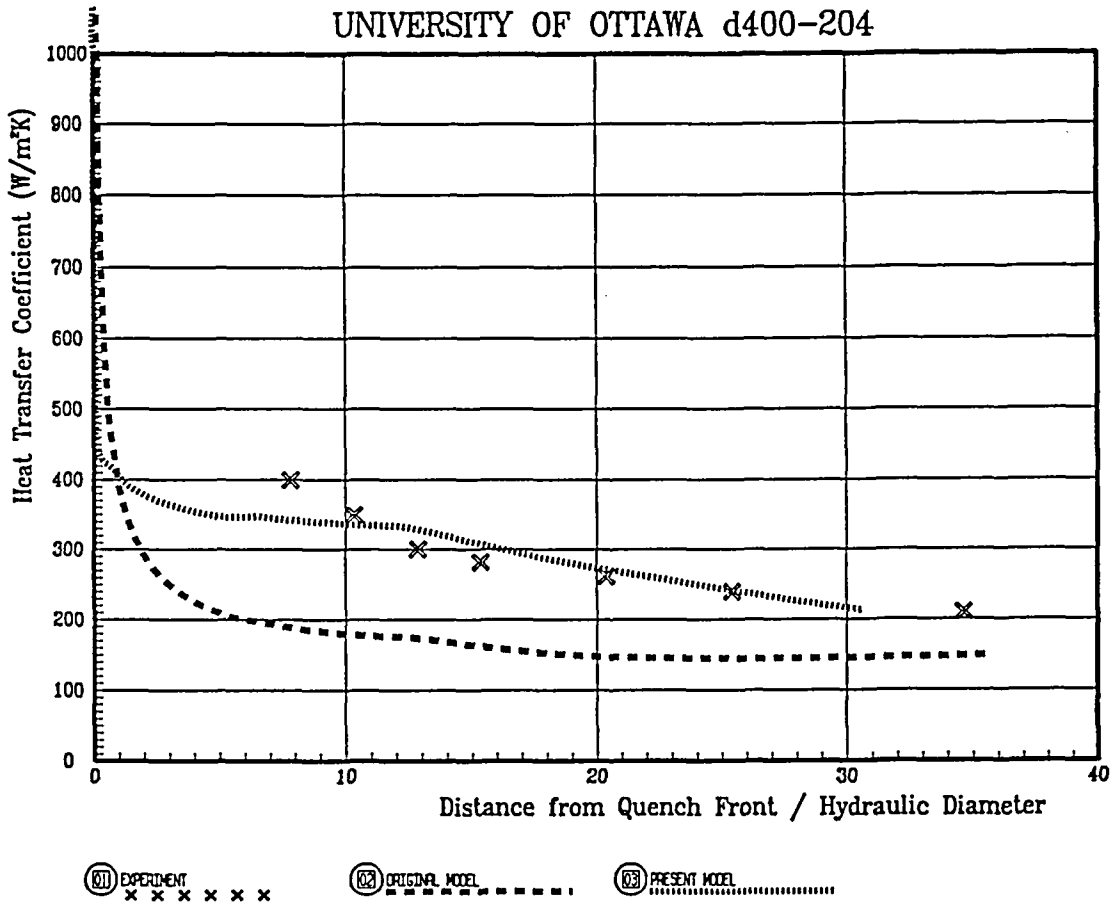
UNIVERSITY OF OTTAWA d400-204
Heat Transfer Coefficient (W/m²K)
1000
900
800
700
600
500
400
300
200
100
0
0
10
20
30
40
Distance from Quench Front / Hydraulic Diameter
01 EXPERIMENT
02 ORIGINAL MODEL
03 PRESENT MODEL

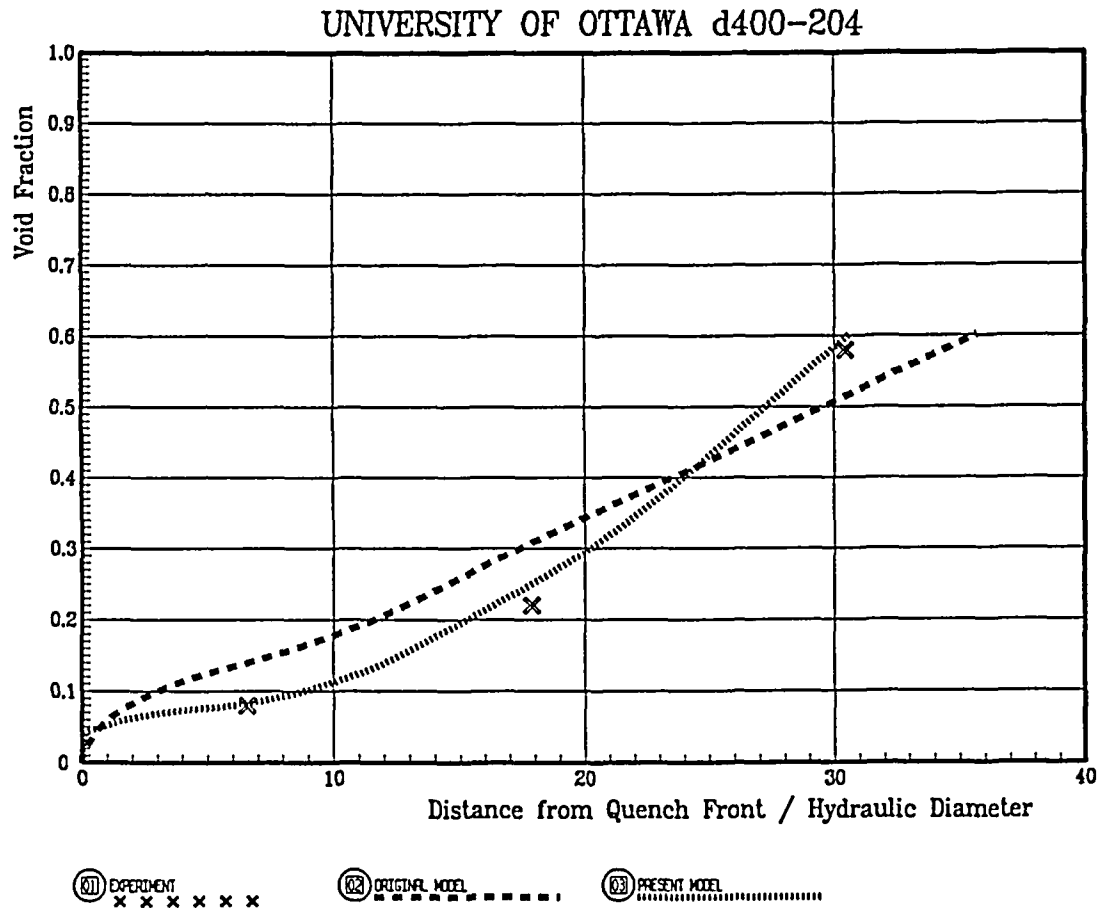
UNIVERSITY OF OTTAWA d400-204
Void Fraction
1.0
0.9
0.8
0.7
0.6
0.5
0.4
0.3
0.2
0.1
0
0
10
20
30
40
Distance from Quench Front / Hydraulic Diameter
01 EXPERIMENT
02 ORIGINAL MODEL
03 PRESENT MODEL

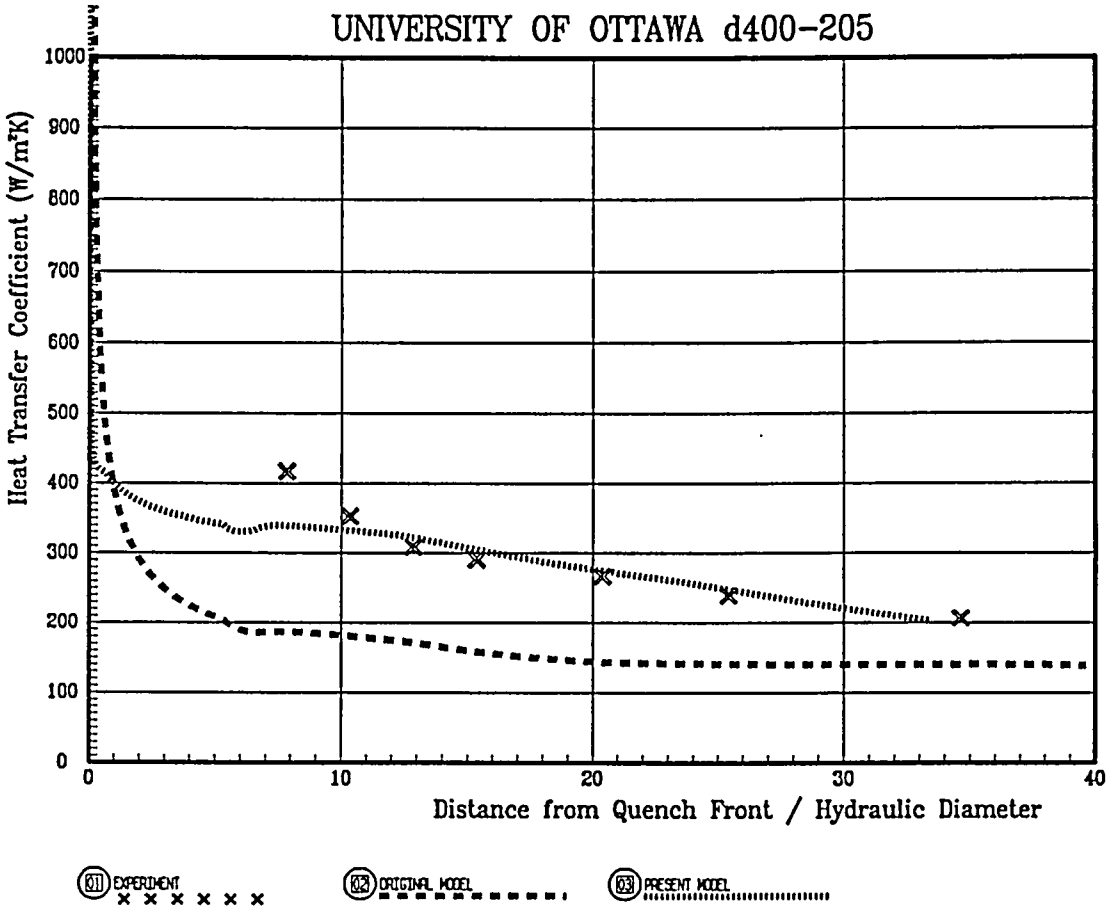
UNIVERSITY OF OTTAWA d400-205
Heat Transfer Coefficient (W/m²K)
1000
900
800
700
600
500
400
300
200
100
0
0
10
20
30
40
Distance from Quench Front / Hydraulic Diameter
01 EXPERIMENT
02 ORIGINAL MODEL
03 PRESENT MODEL

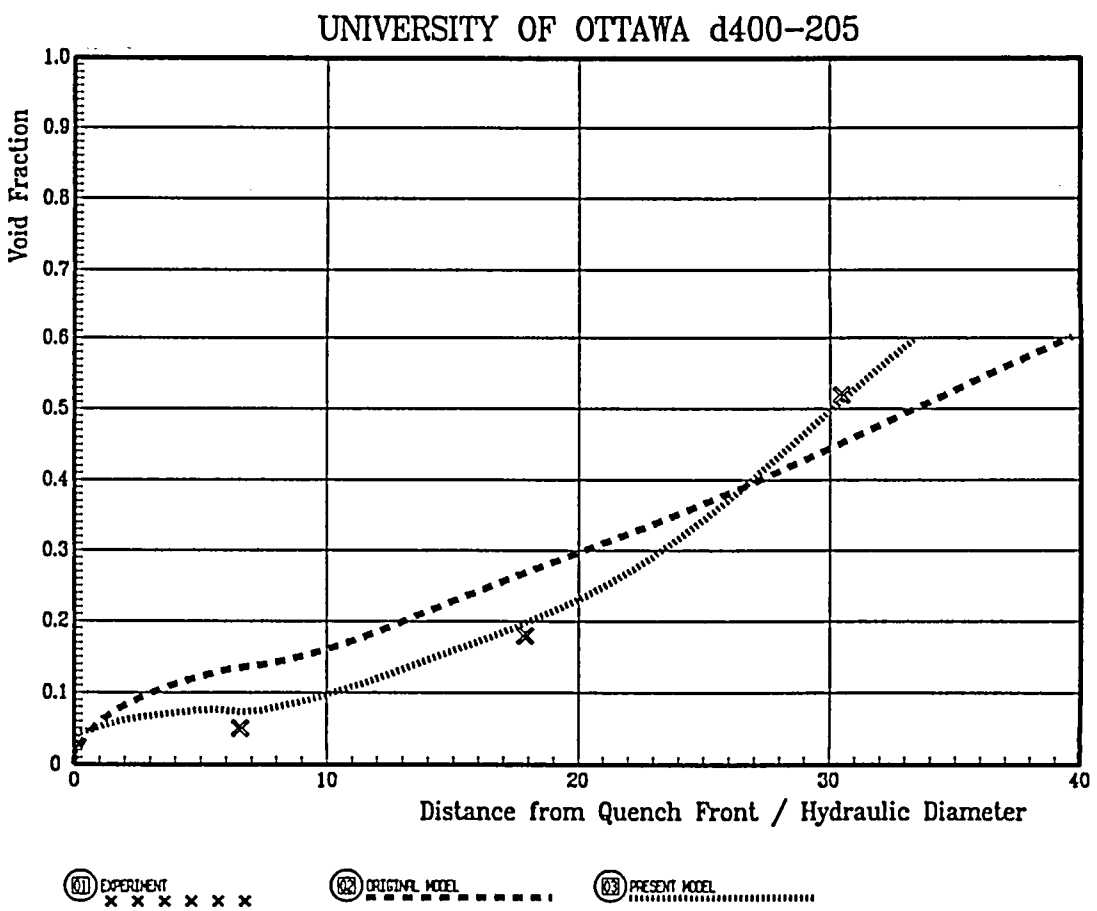
UNIVERSITY OF OTTAWA d400-205
Void Fraction
1.0
0.9
0.8
0.7
0.6
0.5
0.4
0.3
0.2
0.1
0
0
10
20
30
40
Distance from Quench Front / Hydraulic Diameter
01 EXPERIMENT
02 ORIGINAL MODEL
03 PRESENT MODEL

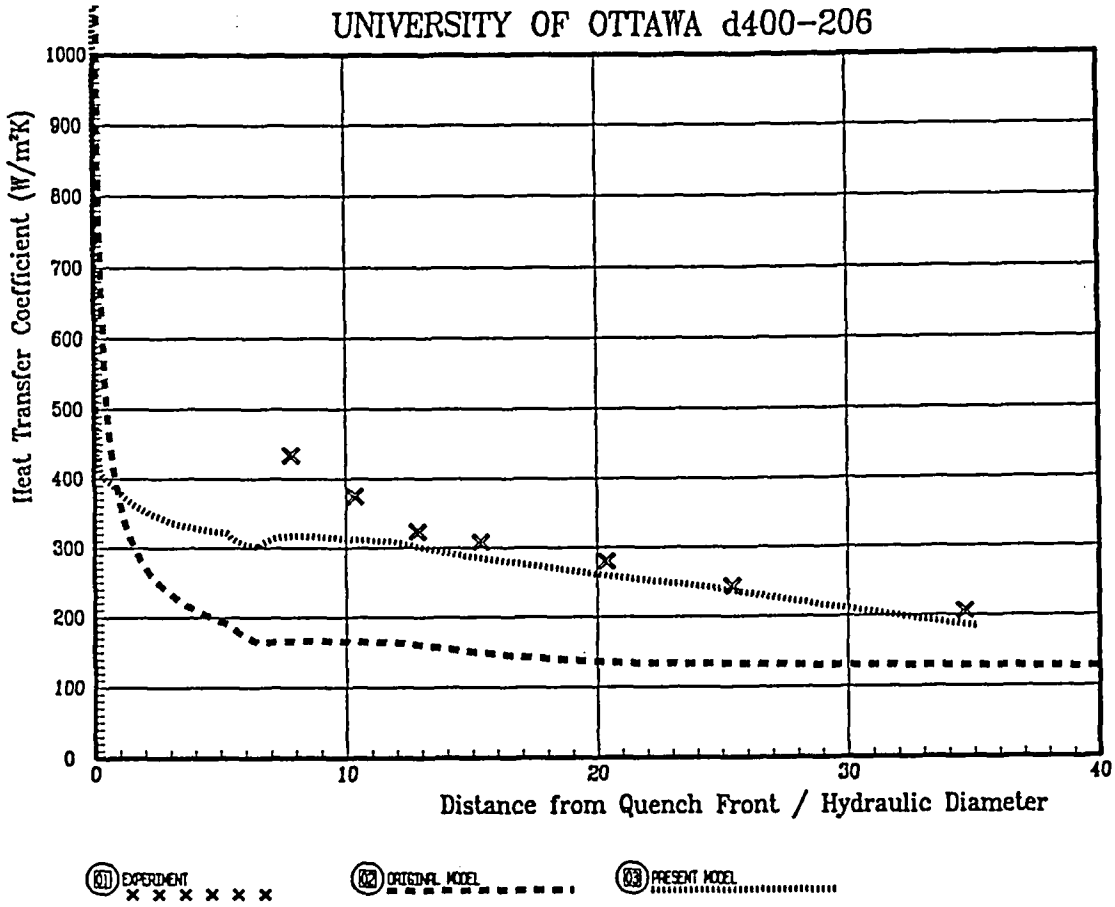
UNIVERSITY OF OTTAWA d400-206
Heat Transfer Coefficient (W/m²K)
1000
900
800
700
600
500
400
300
200
100
0
0
10
20
30
40
Distance from Quench Front / Hydraulic Diameter
(01) EXPERIMENT
(02) ORIGINAL MODEL
(03) PRESENT MODEL

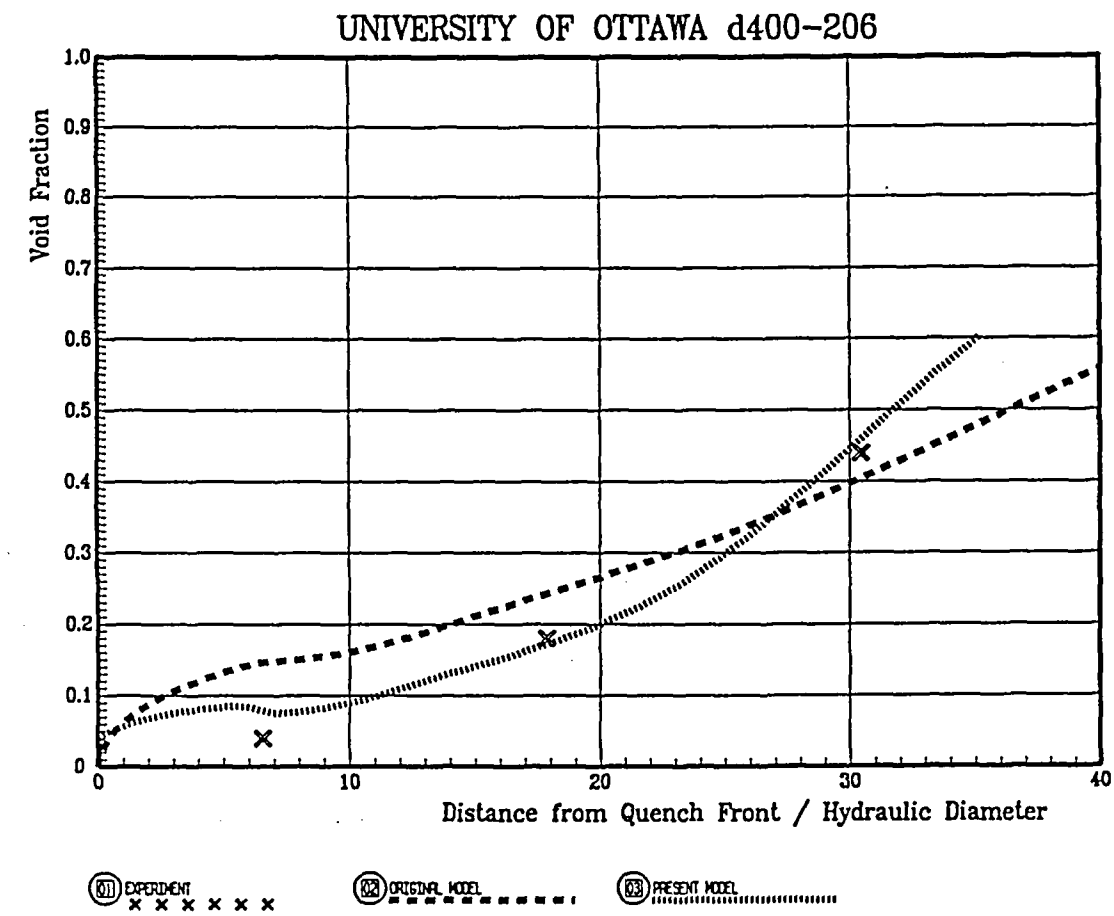
UNIVERSITY OF OTTAWA d400-206
Void Fraction
1.0
0.9
0.8
0.7
0.6
0.5
0.4
0.3
0.2
0.1
0
0
10
20
30
40
Distance from Quench Front / Hydraulic Diameter
(01) EXPERIMENT
(02) ORIGINAL MODEL
(03) PRESENT MODEL

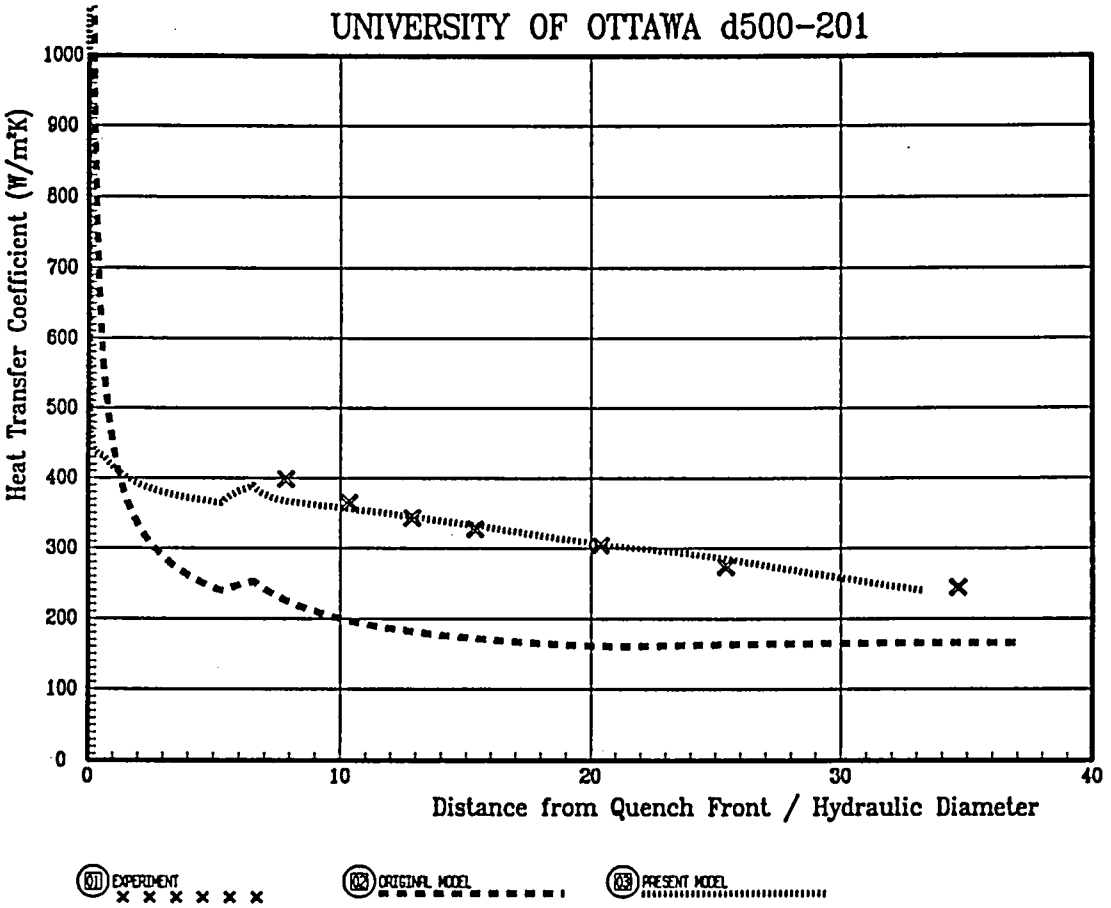
UNIVERSITY OF OTTAWA d500-201
Heat Transfer Coefficient (W/m²K)
1000
900
800
700
600
500
400
300
200
100
0
0
10
20
30
40
Distance from Quench Front / Hydraulic Diameter
01 EXPERIMENT
02 ORIGINAL MODEL
03 PRESENT MODEL

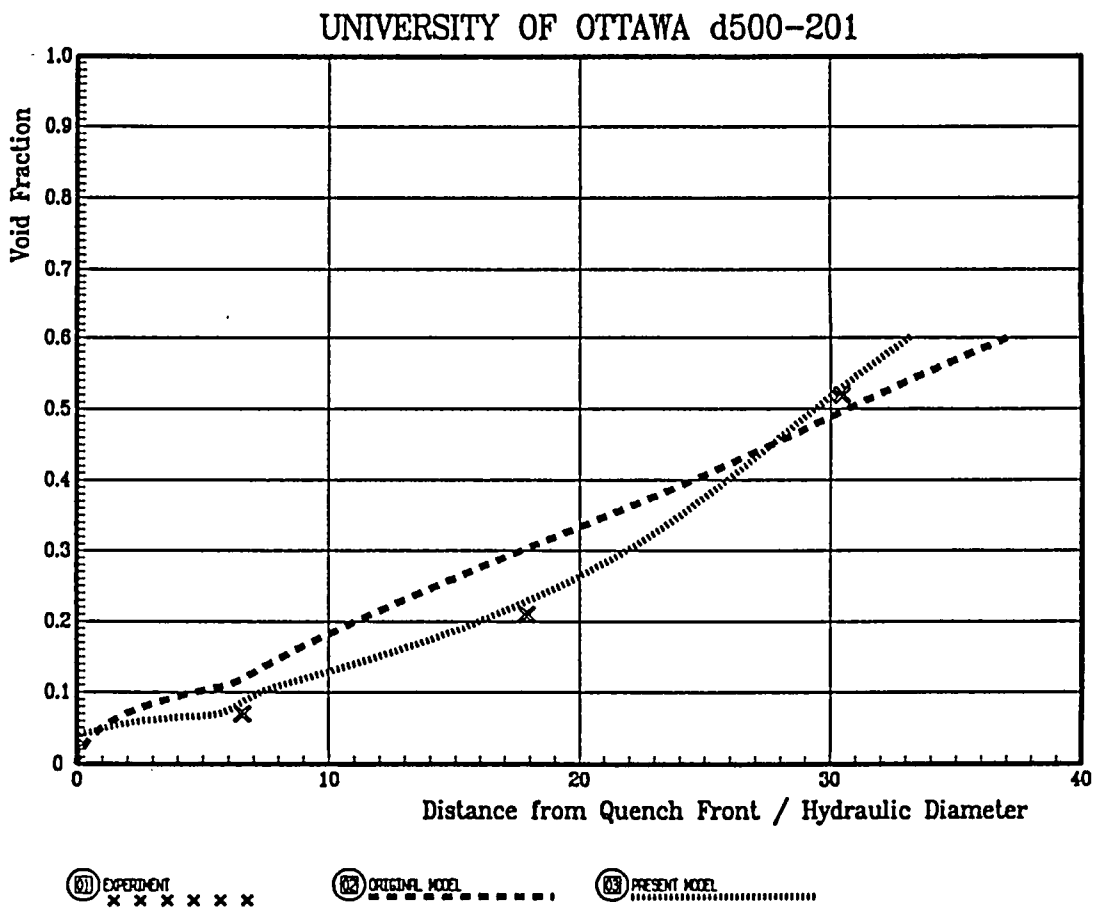
UNIVERSITY OF OTTAWA d500-201
Void Fraction
1.0
0.9
0.8
0.7
0.6
0.5
0.4
0.3
0.2
0.1
0
0
10
20
30
40
Distance from Quench Front / Hydraulic Diameter
01 EXPERIMENT
02 ORIGINAL MODEL
03 PRESENT MODEL

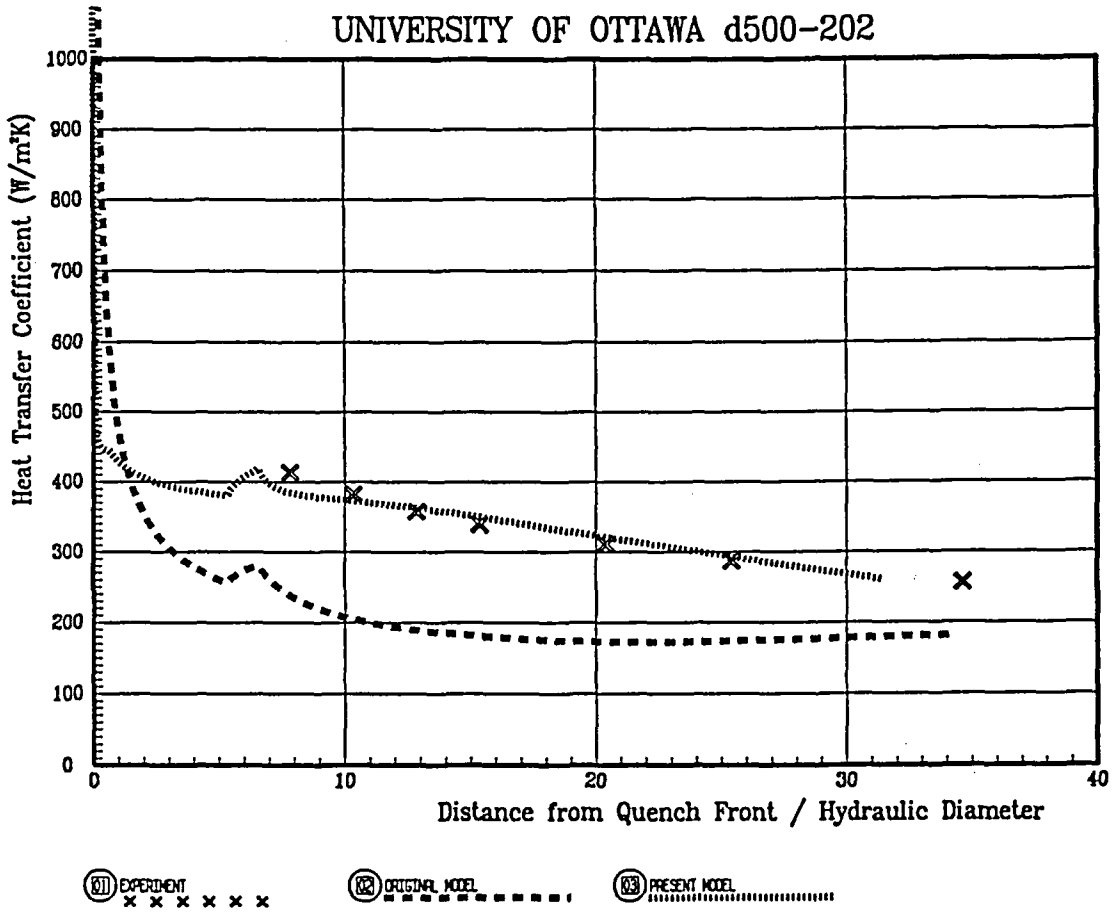
UNIVERSITY OF OTTAWA d500-202
Heat Transfer Coefficient (W/m²K)
1000
900
800
700
600
500
400
300
200
100
0
0
10
20
30
40
Distance from Quench Front / Hydraulic Diameter
01 EXPERIMENT
02 ORIGINAL MODEL
03 PRESENT MODEL

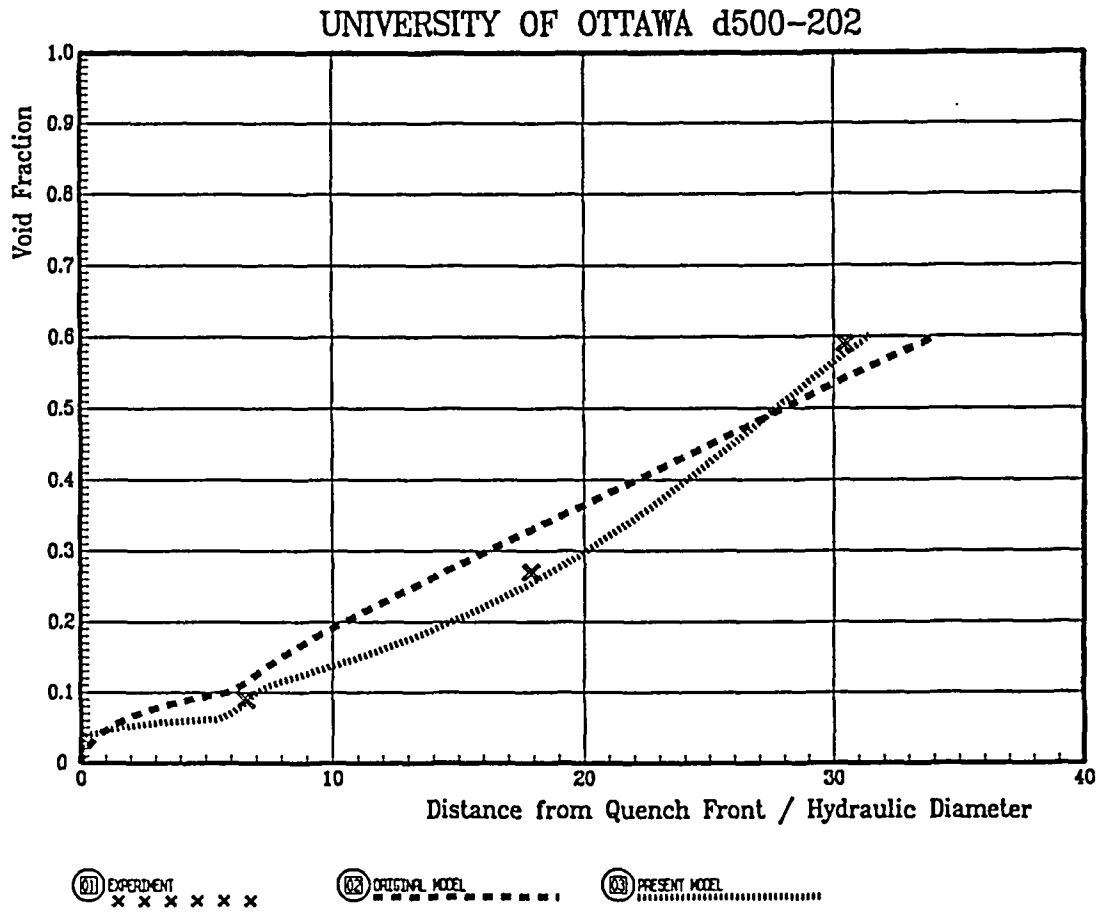
UNIVERSITY OF OTTAWA d500-202
Void Fraction
1.0
0.9
0.8
0.7
0.6
0.5
0.4
0.3
0.2
0.1
0
0
10
20
30
40
Distance from Quench Front / Hydraulic Diameter
01 EXPERIMENT
02 ORIGINAL MODEL
03 PRESENT MODEL

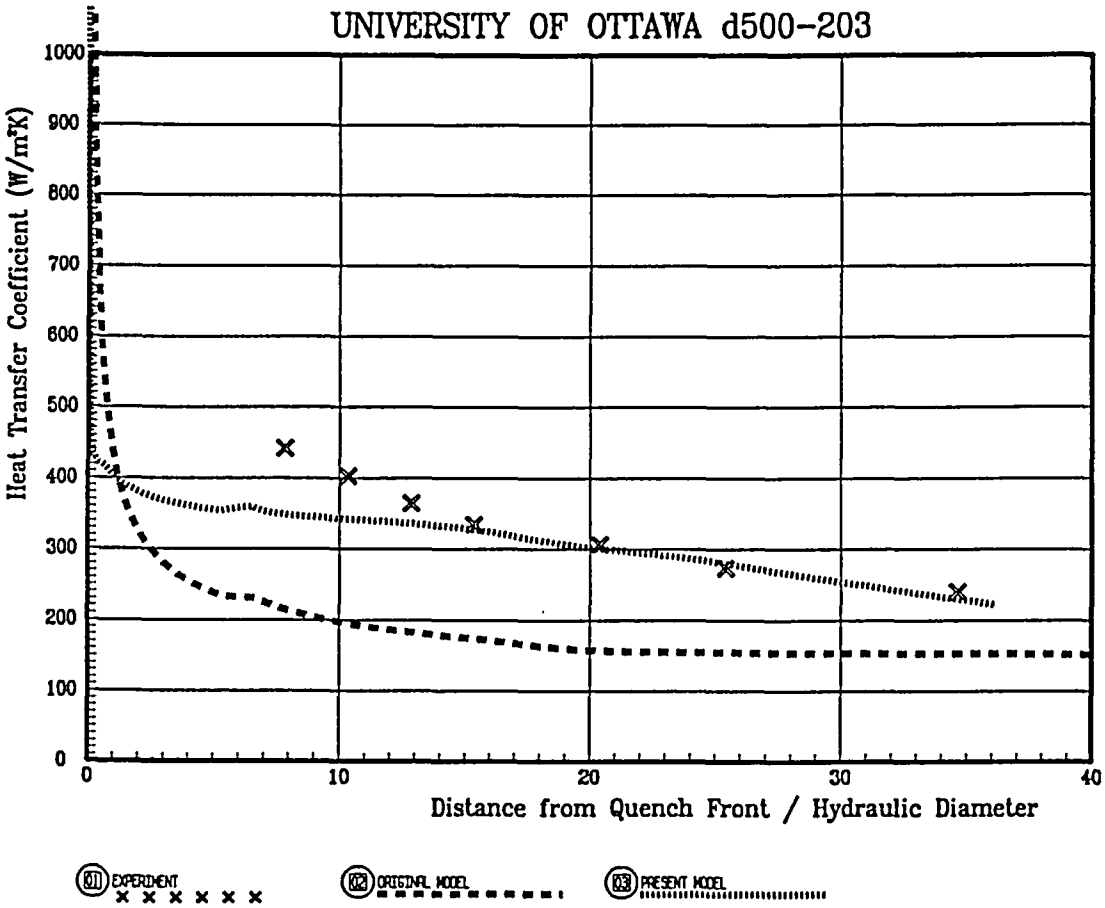
UNIVERSITY OF OTTAWA d500-203
Heat Transfer Coefficient (W/m²K)
1000
900
800
700
600
500
400
300
200
100
0
0
10
20
30
40
Distance from Quench Front / Hydraulic Diameter
01 EXPERIMENT
02 ORIGINAL MODEL
03 PRESENT MODEL

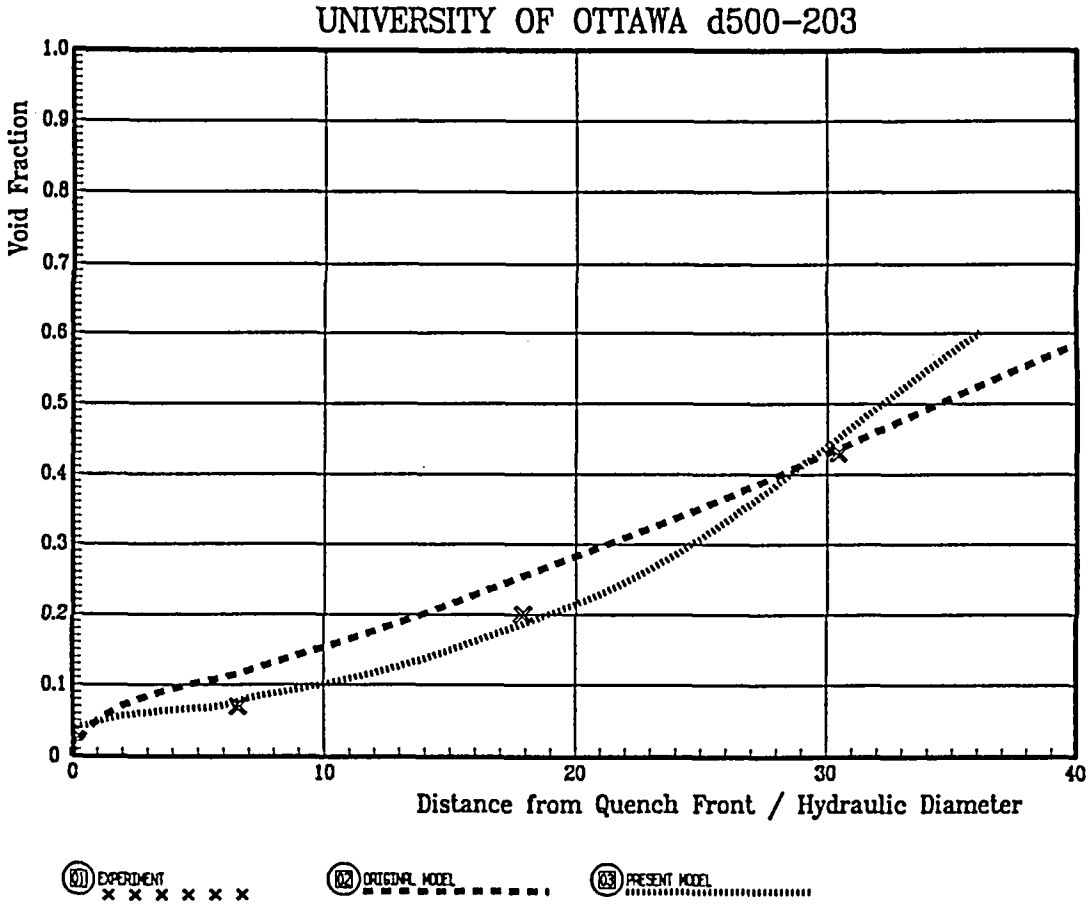
UNIVERSITY OF OTTAWA d500-203
Void Fraction
1.0
0.9
0.8
0.7
0.6
0.5
0.4
0.3
0.2
0.1
0
0
10
20
30
40
Distance from Quench Front / Hydraulic Diameter
01 EXPERIMENT
02 ORIGINAL MODEL
03 PRESENT MODEL

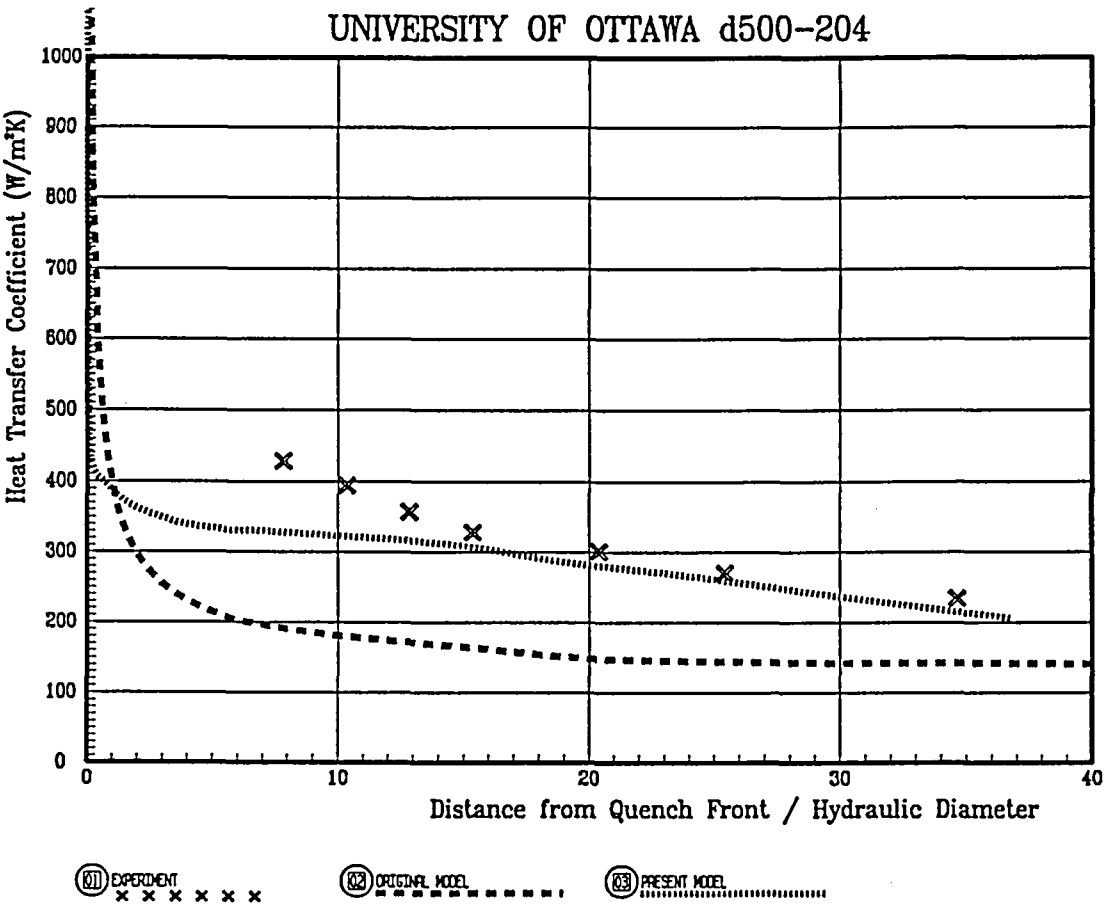
UNIVERSITY OF OTTAWA d500-204
Heat Transfer Coefficient (W/m²K)
1000
900
800
700
600
500
400
300
200
100
0
0
10
20
30
40
Distance from Quench Front / Hydraulic Diameter
01 EXPERIMENT
02 ORIGINAL MODEL
03 PRESENT MODEL

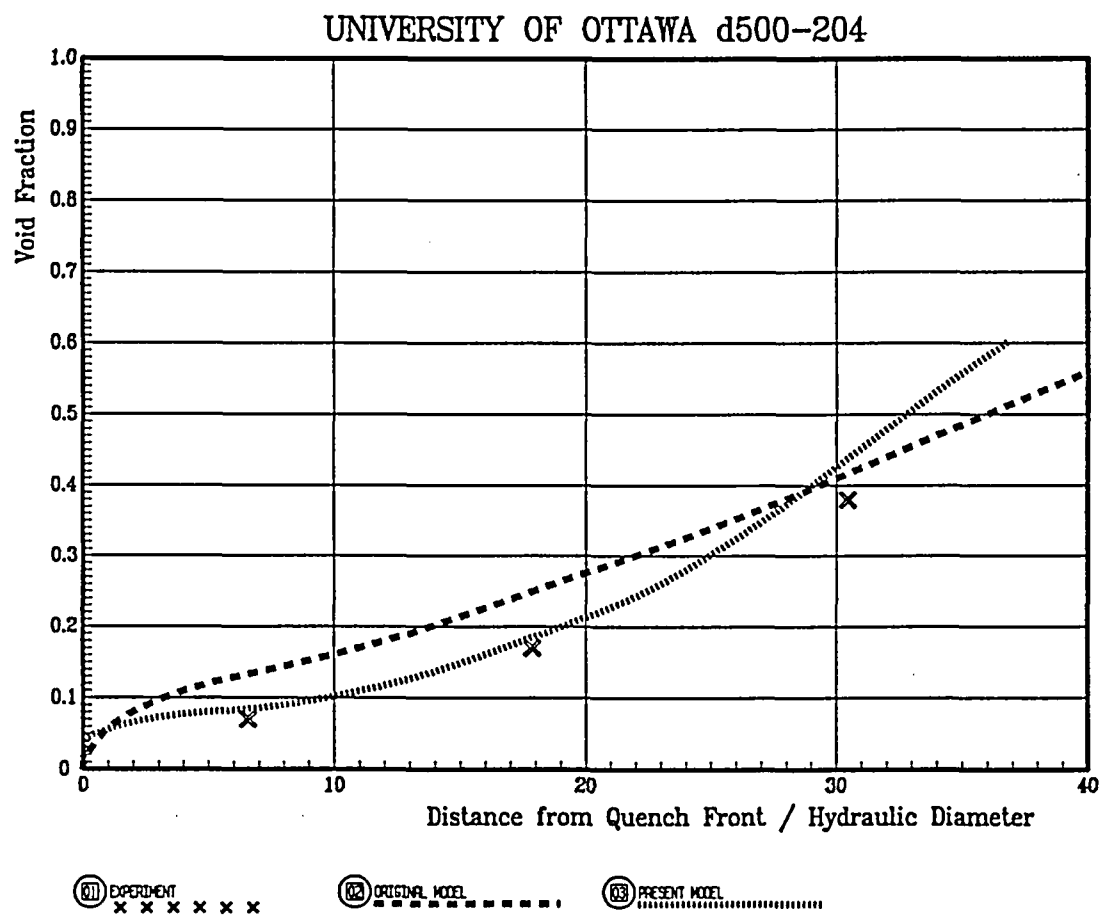
UNIVERSITY OF OTTAWA d500-204
Void Fraction
1.0
0.9
0.8
0.7
0.6
0.5
0.4
0.3
0.2
0.1
0
0
10
20
30
40
Distance from Quench Front / Hydraulic Diameter
01 EXPERIMENT
02 ORIGINAL MODEL
03 PRESENT MODEL

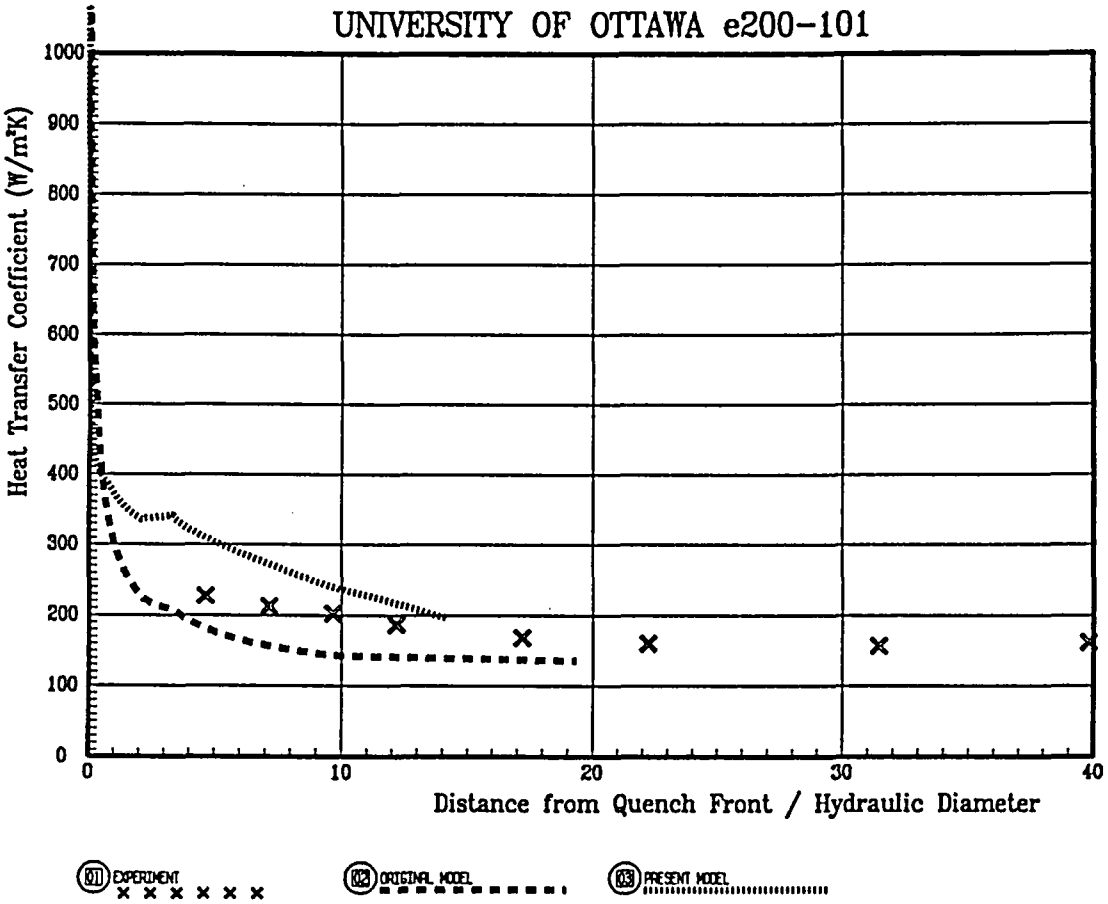
UNIVERSITY OF OTTAWA e200-101
Heat Transfer Coefficient (W/m²K)
1000
900
800
700
600
500
400
300
200
100
0
0
10
20
30
40
Distance from Quench Front / Hydraulic Diameter
01 EXPERIMENT
02 ORIGINAL MODEL
03 PRESENT MODEL

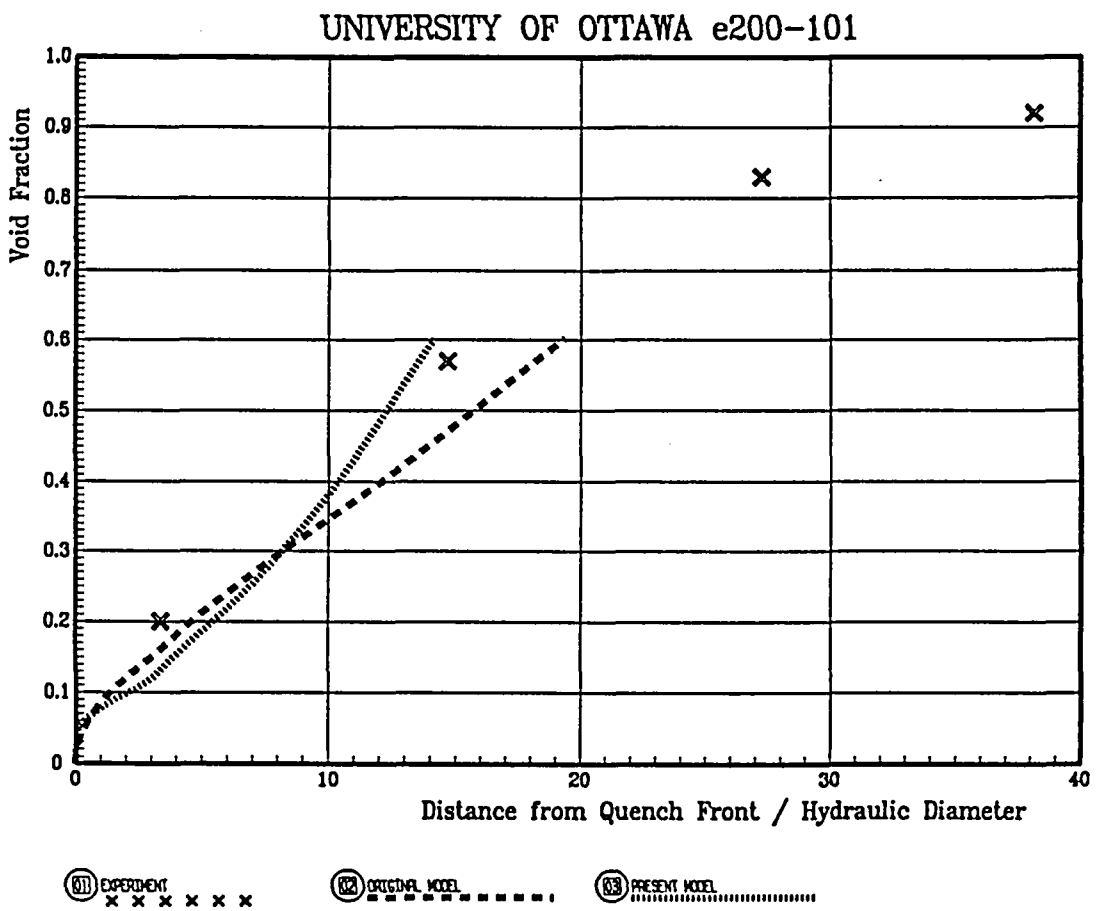
UNIVERSITY OF OTTAWA e200-101
Void Fraction
1.0
0.9
0.8
0.7
0.6
0.5
0.4
0.3
0.2
0.1
0
0
10
20
30
40
Distance from Quench Front / Hydraulic Diameter
01 EXPERIMENT
02 ORIGINAL MODEL
03 PRESENT MODEL

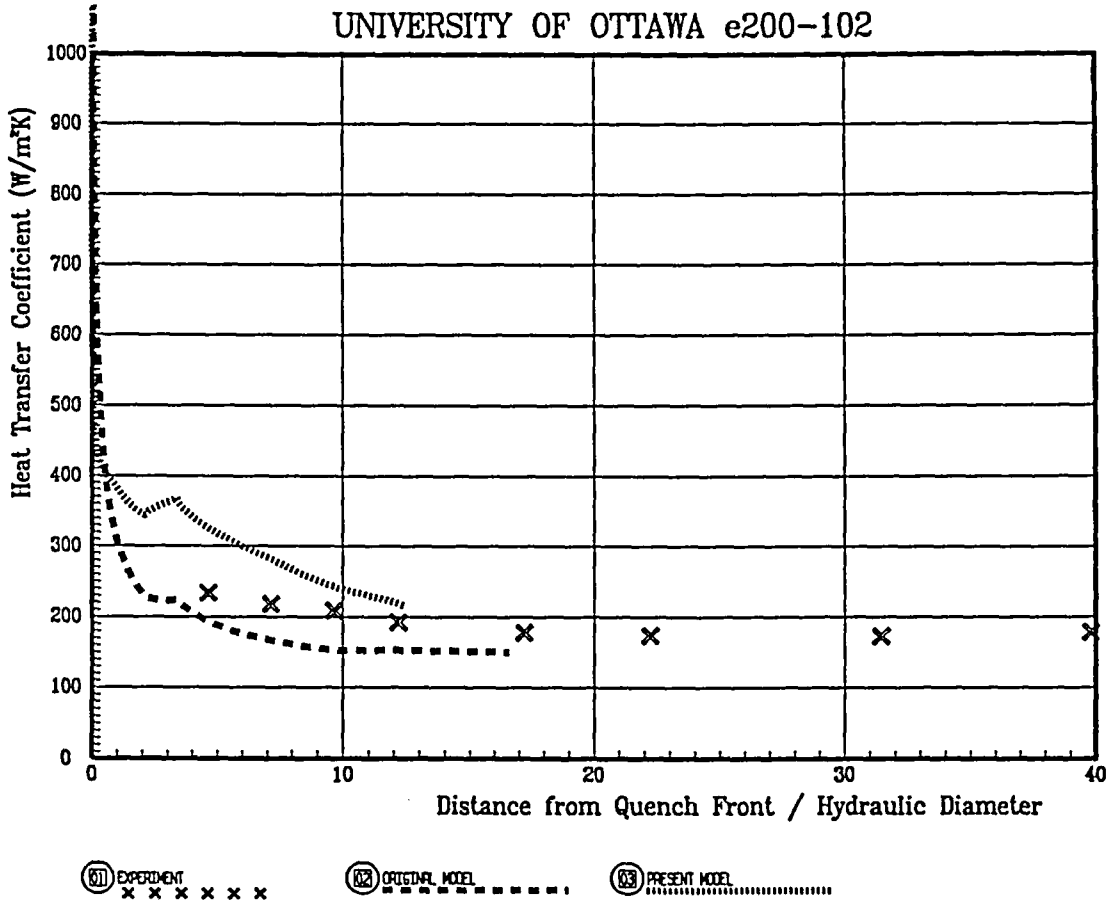
UNIVERSITY OF OTTAWA e200-102
Heat Transfer Coefficient (W/m²K)
1000
900
800
700
600
500
400
300
200
100
0
0
10
20
30
40
Distance from Quench Front / Hydraulic Diameter
01 EXPERIMENT
02 ORIGINAL MODEL
03 PRESENT MODEL

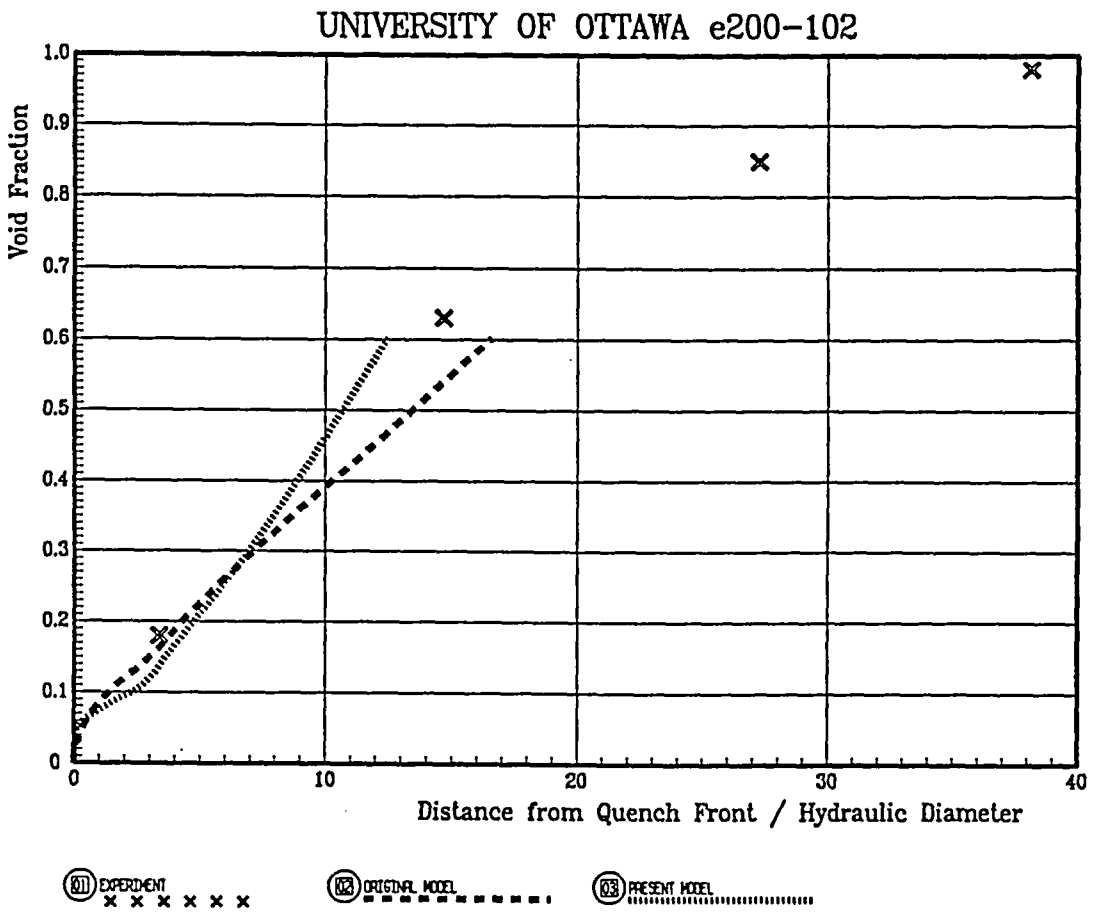
UNIVERSITY OF OTTAWA e200-102
Void Fraction
1.0
0.9
0.8
0.7
0.6
0.5
0.4
0.3
0.2
0.1
0
0
10
20
30
40
Distance from Quench Front / Hydraulic Diameter
01 EXPERIMENT
02 ORIGINAL MODEL
03 PRESENT MODEL

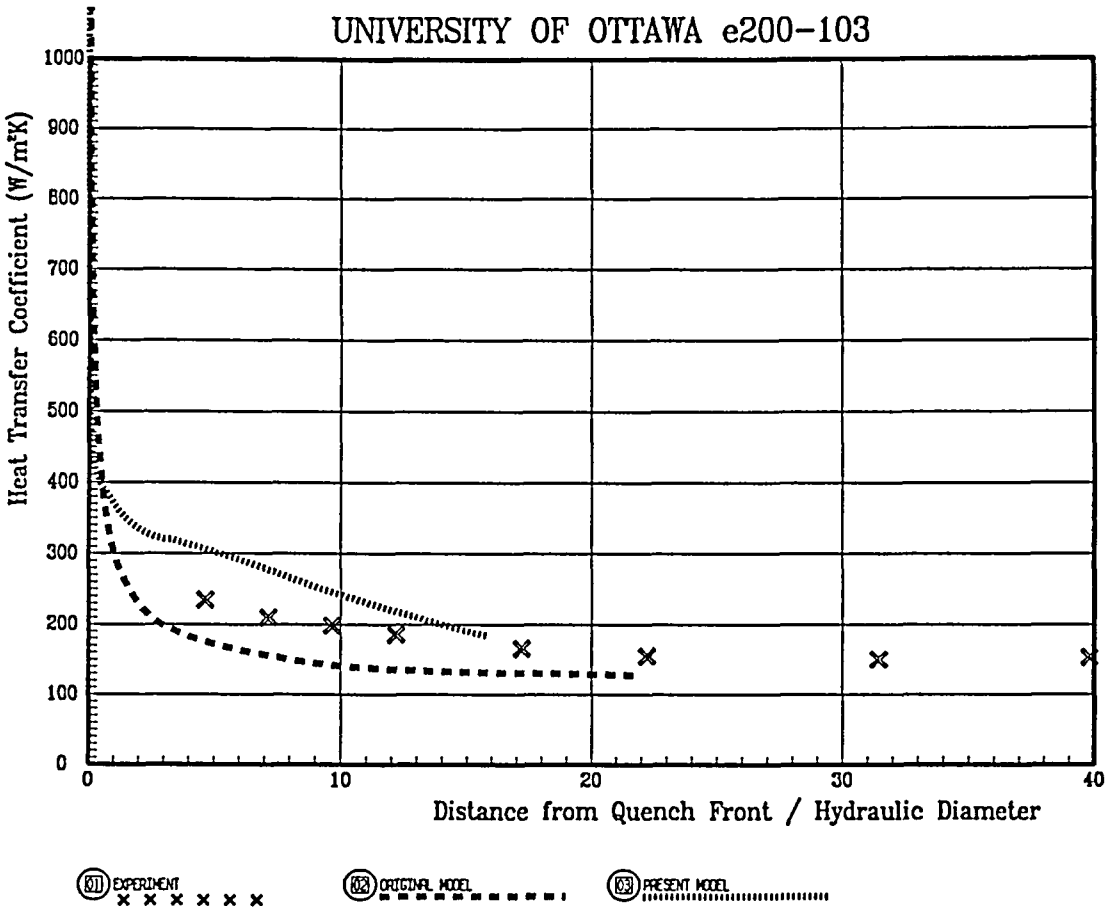
UNIVERSITY OF OTTAWA e200-103
Heat Transfer Coefficient (W/m²K)
1000
900
800
700
600
500
400
300
200
100
0
0
10
20
30
40
Distance from Quench Front / Hydraulic Diameter
01 EXPERIMENT
02 ORIGINAL MODEL
03 PRESENT MODEL

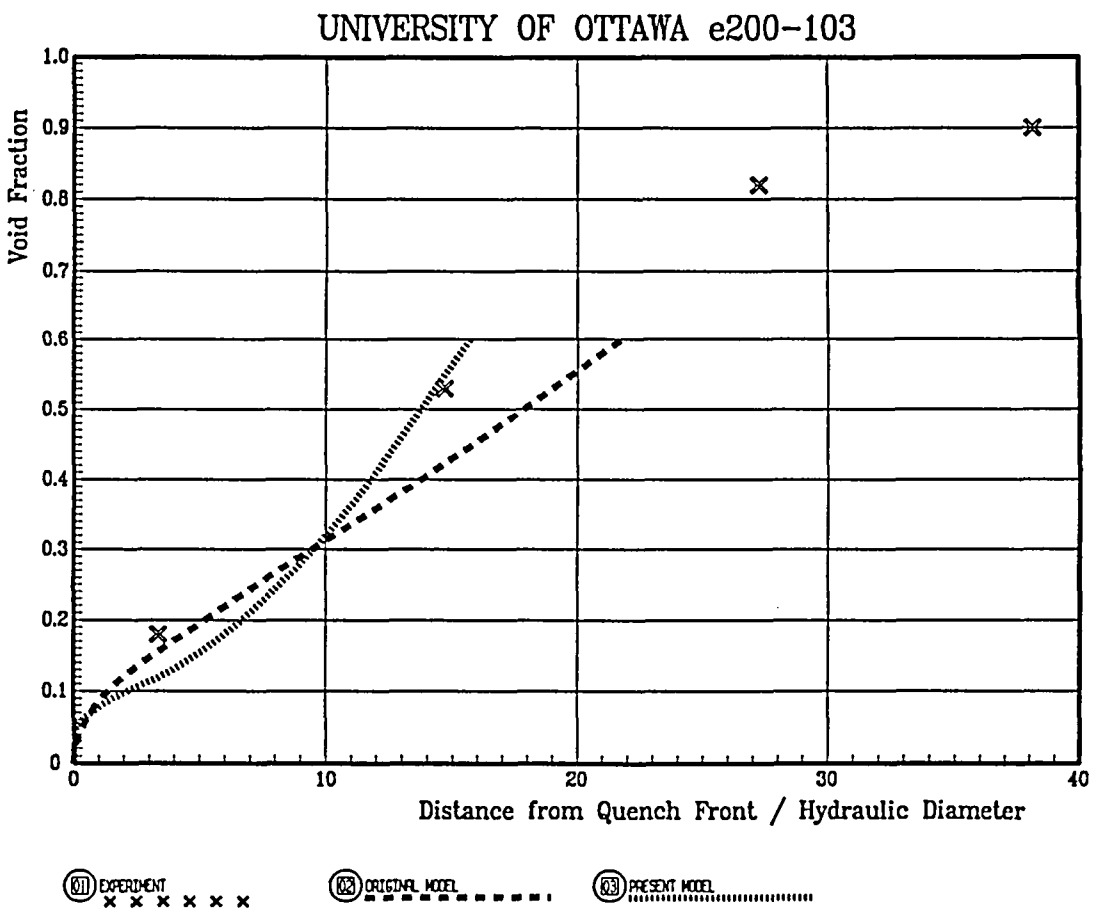
UNIVERSITY OF OTTAWA e200-103
Void Fraction
1.0
0.9
0.8
0.7
0.6
0.5
0.4
0.3
0.2
0.1
0
0
10
20
30
40
Distance from Quench Front / Hydraulic Diameter
01 EXPERIMENT
02 ORIGINAL MODEL
03 PRESENT MODEL

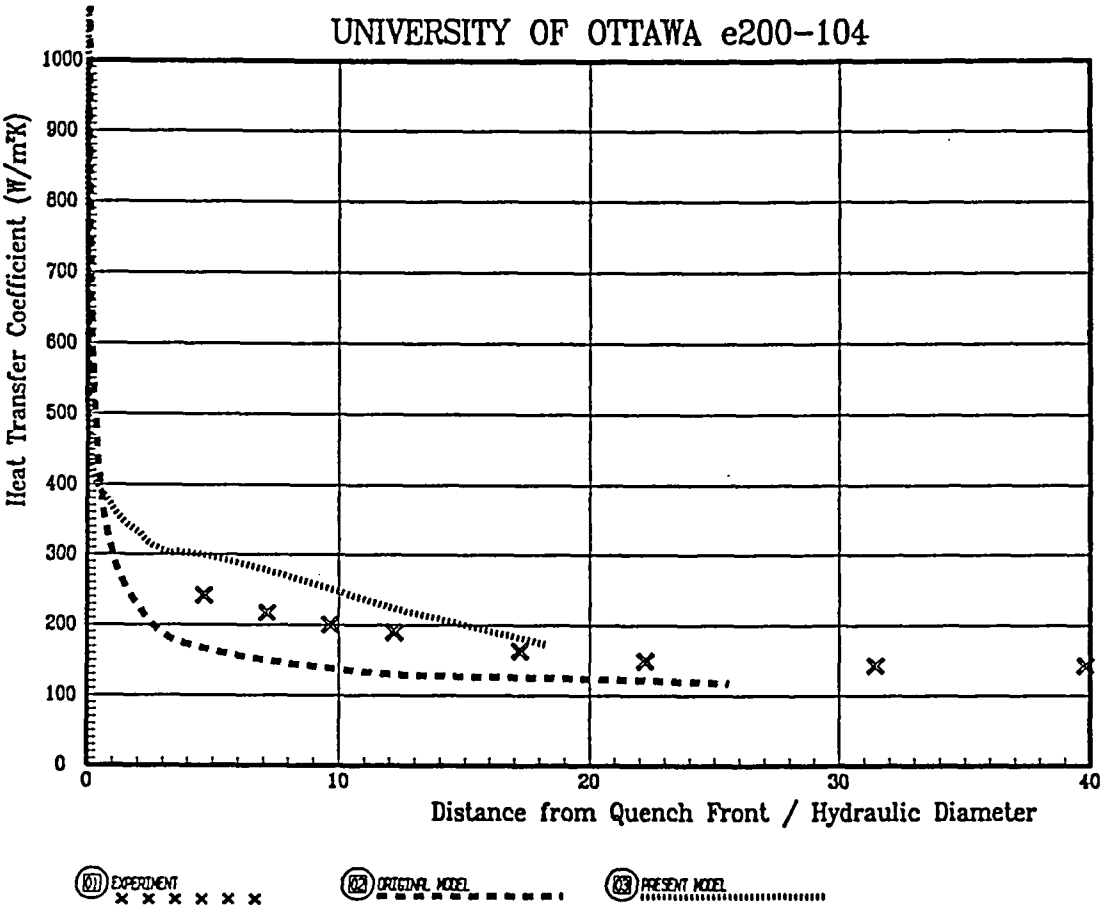
UNIVERSITY OF OTTAWA e200-104
Heat Transfer Coefficient (W/m²K)
1000
900
800
700
600
500
400
300
200
100
0
0
10
20
30
40
Distance from Quench Front / Hydraulic Diameter
001 EXPERIMENT
002 ORIGINAL MODEL
003 PRESENT MODEL

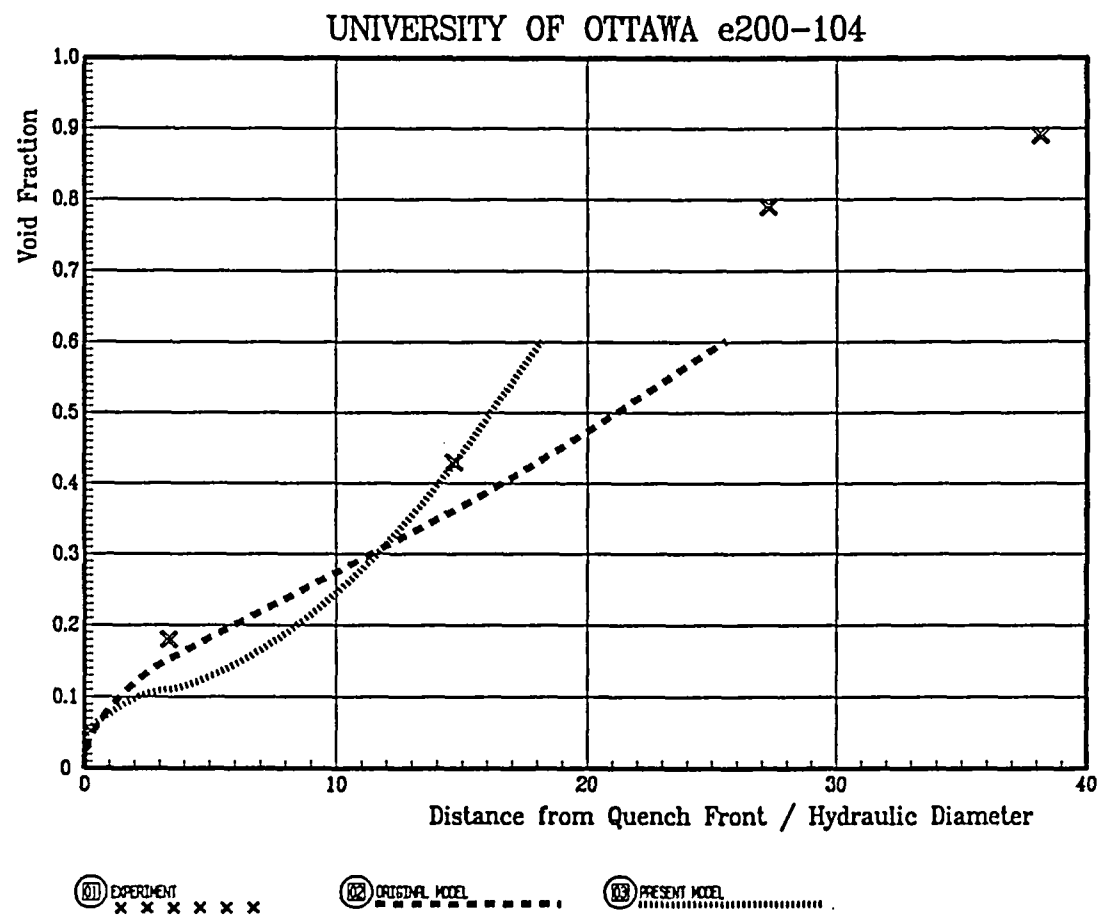
UNIVERSITY OF OTTAWA e200-104
Void Fraction
1.0
0.9
0.8
0.7
0.6
0.5
0.4
0.3
0.2
0.1
0
0
10
20
30
40
Distance from Quench Front / Hydraulic Diameter
001 EXPERIMENT
002 ORIGINAL MODEL
003 PRESENT MODEL

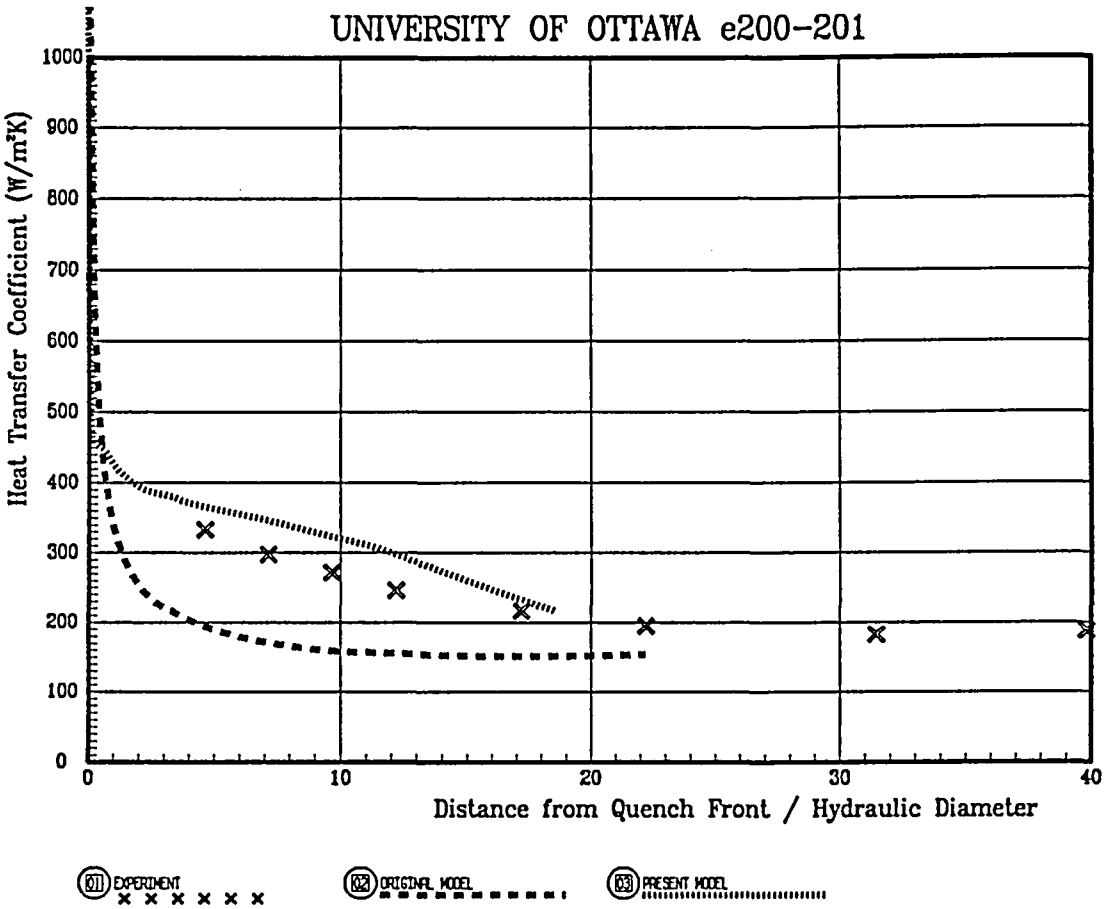
UNIVERSITY OF OTTAWA e200-201
Heat Transfer Coefficient (W/m²K)
1000
900
800
700
600
500
400
300
200
100
0
0
10
20
30
40
Distance from Quench Front / Hydraulic Diameter
01 EXPERIMENT
02 ORIGINAL MODEL
03 PRESENT MODEL

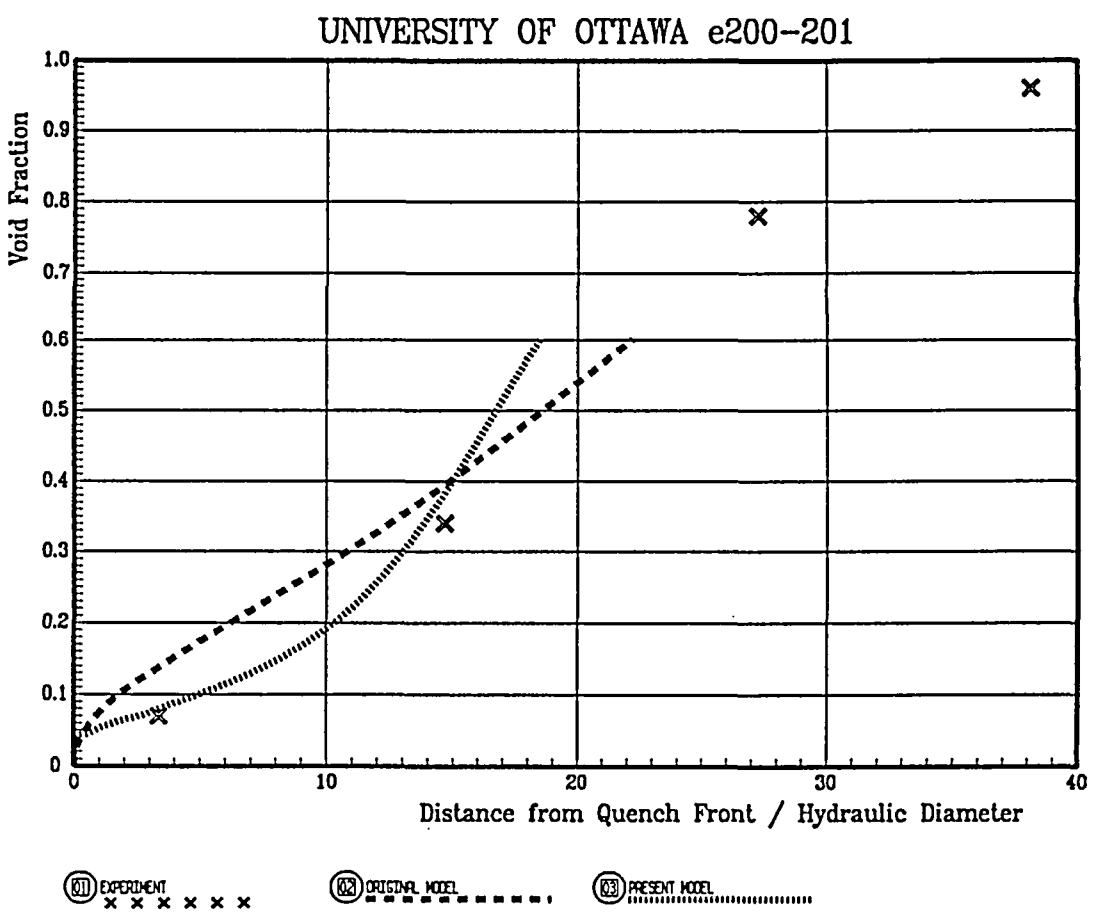
UNIVERSITY OF OTTAWA e200-201
Void Fraction
1.0
0.9
0.8
0.7
0.6
0.5
0.4
0.3
0.2
0.1
0
0
10
20
30
40
Distance from Quench Front / Hydraulic Diameter
01 EXPERIMENT
02 ORIGINAL MODEL
03 PRESENT MODEL

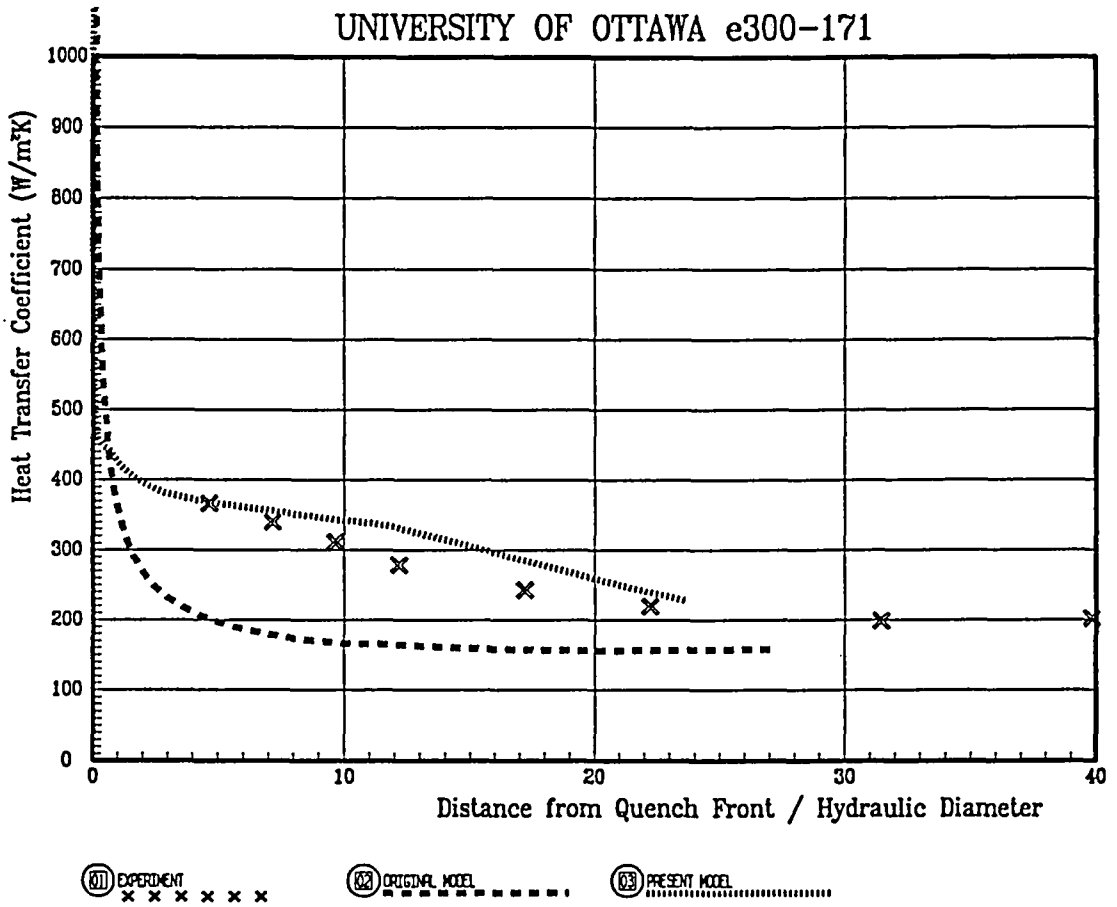
UNIVERSITY OF OTTAWA e300-171
Heat Transfer Coefficient (W/m²K)
1000
900
800
700
600
500
400
300
200
100
0
0
10
20
30
40
Distance from Quench Front / Hydraulic Diameter
(01) EXPERIMENT
(02) ORIGINAL MODEL
(03) PRESENT MODEL

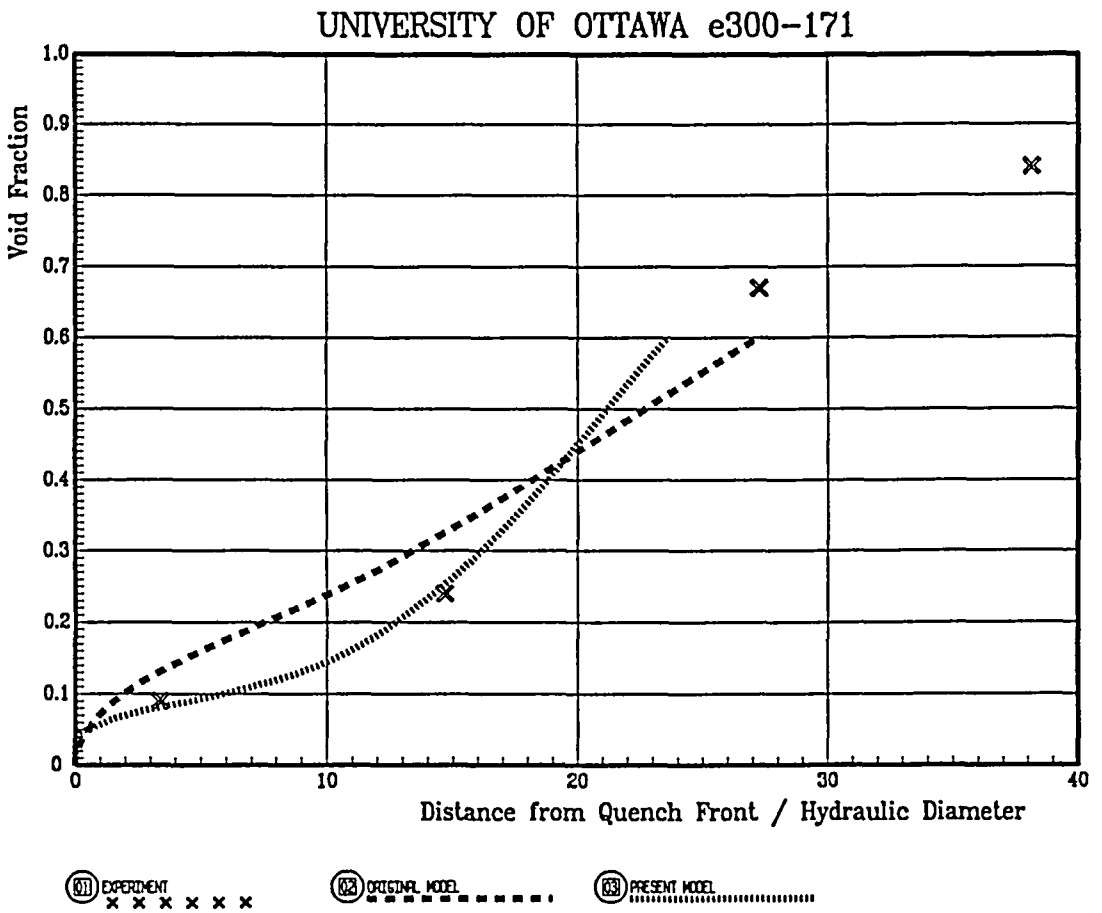
UNIVERSITY OF OTTAWA e300-171
Void Fraction
1.0
0.9
0.8
0.7
0.6
0.5
0.4
0.3
0.2
0.1
0
0
10
20
30
40
Distance from Quench Front / Hydraulic Diameter
(01) EXPERIMENT
(02) ORIGINAL MODEL
(03) PRESENT MODEL

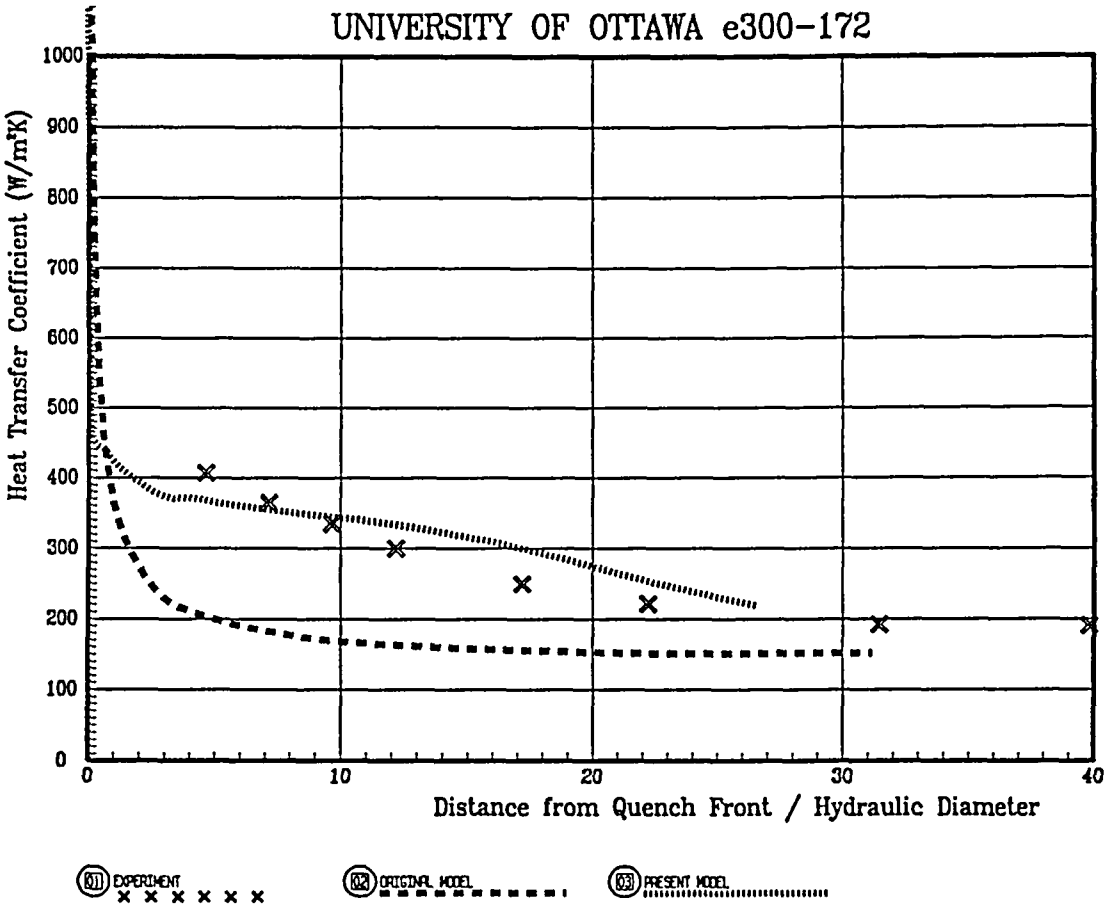
UNIVERSITY OF OTTAWA e300-172
Heat Transfer Coefficient (W/m²K)
1000
900
800
700
600
500
400
300
200
100
0
0
10
20
30
40
Distance from Quench Front / Hydraulic Diameter
01 EXPERIMENT
02 ORIGINAL MODEL
03 PRESENT MODEL

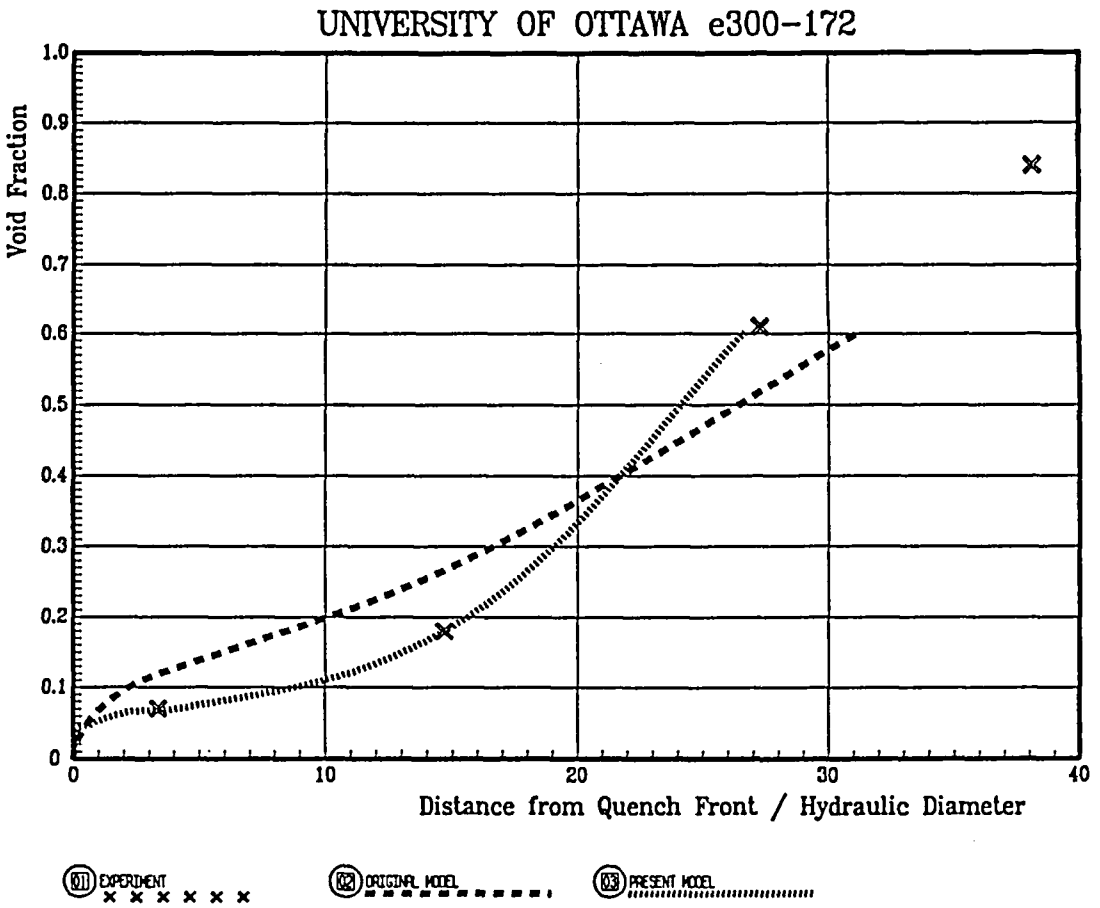
UNIVERSITY OF OTTAWA e300-172
Void Fraction
1.0
0.9
0.8
0.7
0.6
0.5
0.4
0.3
0.2
0.1
0
0
10
20
30
40
Distance from Quench Front / Hydraulic Diameter
01 EXPERIMENT
02 ORIGINAL MODEL
03 PRESENT MODEL

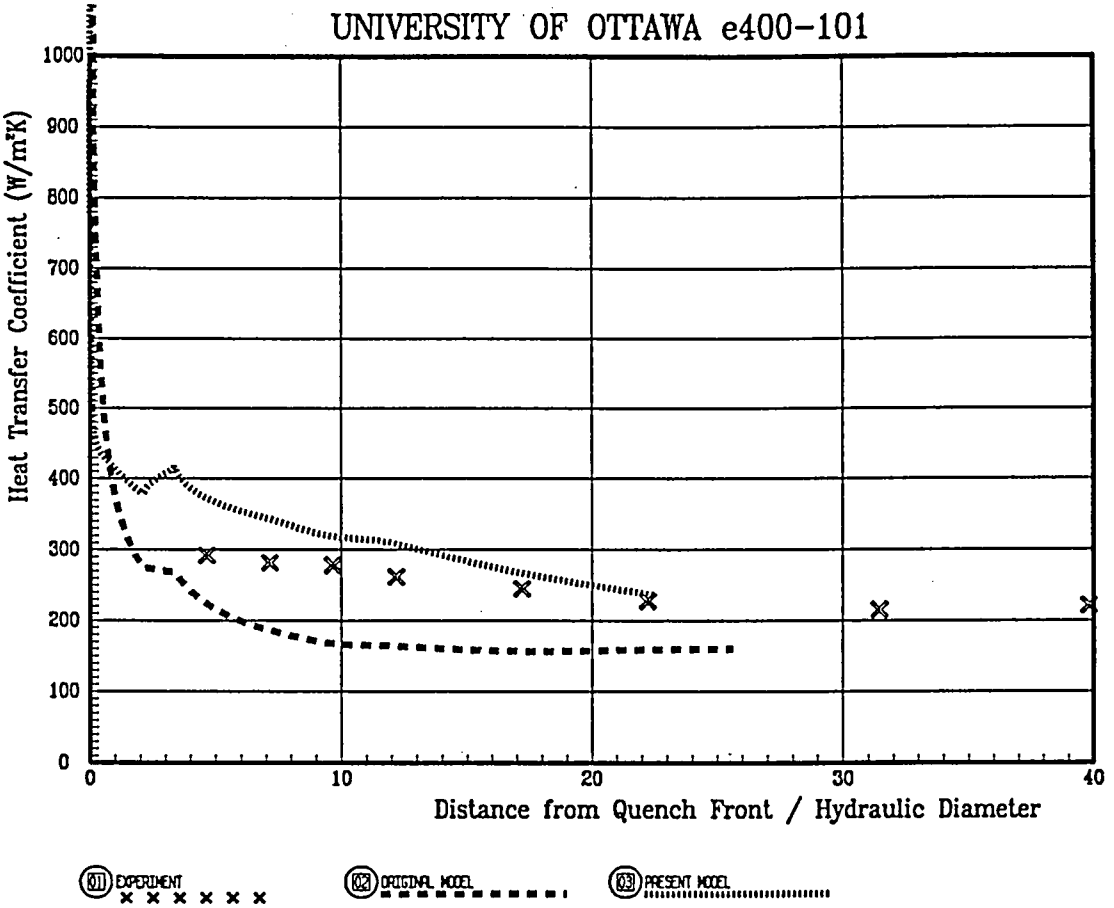
UNIVERSITY OF OTTAWA e400-101
Heat Transfer Coefficient (W/m²K)
1000
900
800
700
600
500
400
300
200
100
0
0
10
20
30
40
Distance from Quench Front / Hydraulic Diameter
01 EXPERIMENT
02 ORIGINAL MODEL
03 PRESENT MODEL

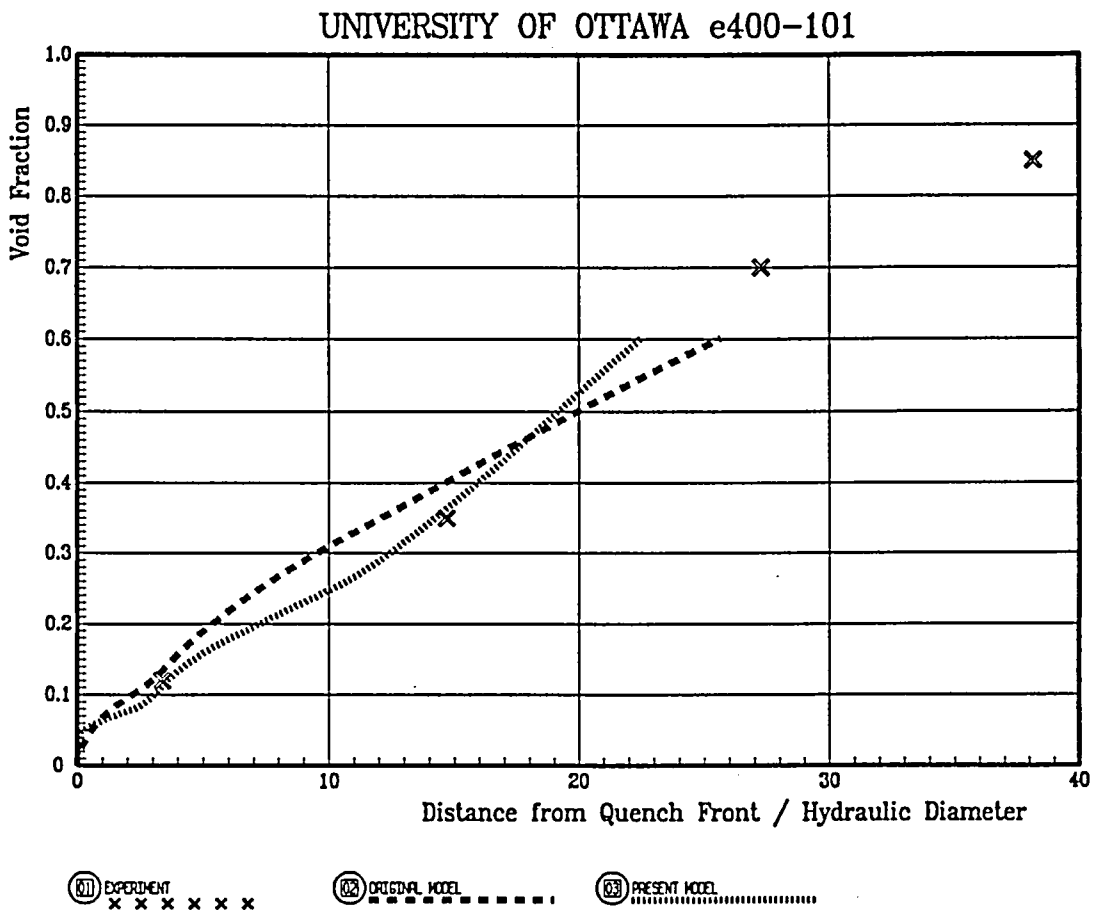
UNIVERSITY OF OTTAWA e400-101
Void Fraction
1.0
0.9
0.8
0.7
0.6
0.5
0.4
0.3
0.2
0.1
0
0
10
20
30
40
Distance from Quench Front / Hydraulic Diameter
01 EXPERIMENT
02 ORIGINAL MODEL
03 PRESENT MODEL

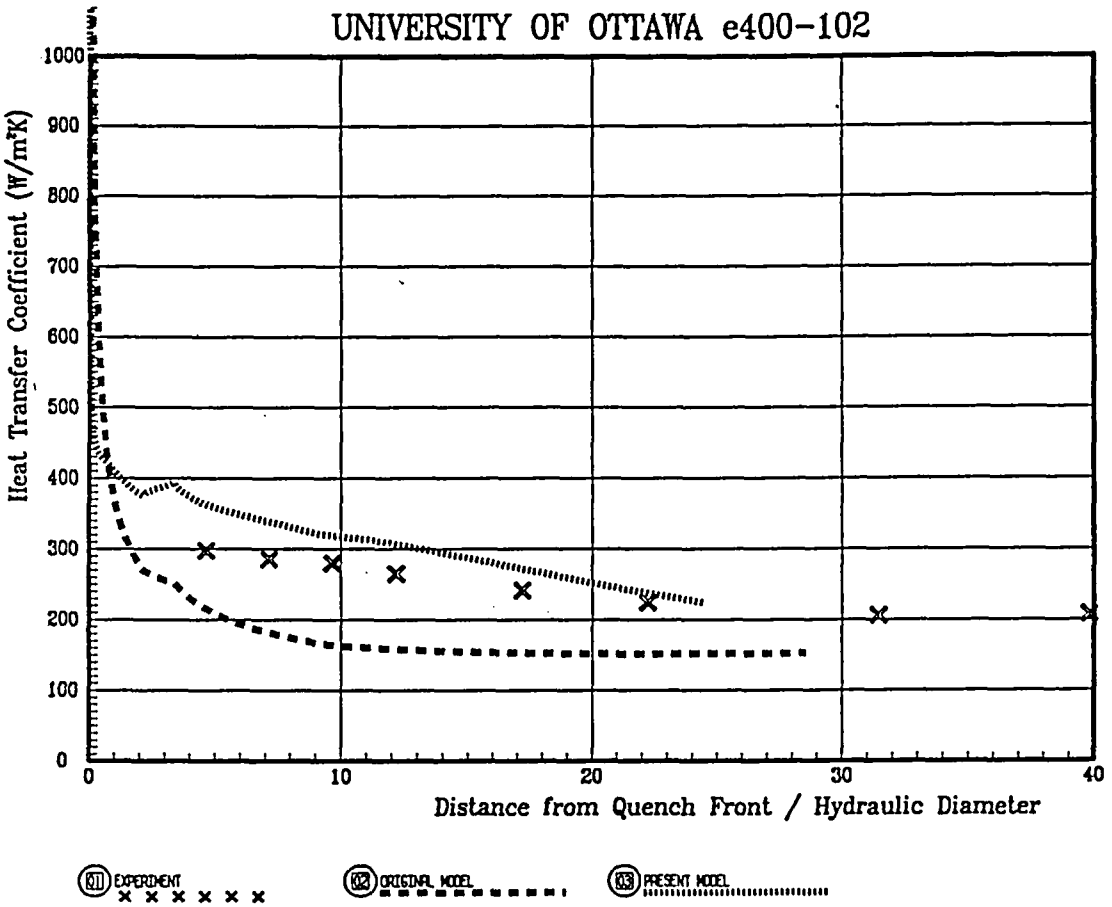
UNIVERSITY OF OTTAWA e400-102
Heat Transfer Coefficient (W/m²K)
1000
900
800
700
600
500
400
300
200
100
0
0
10
20
30
40
Distance from Quench Front / Hydraulic Diameter
01 EXPERIMENT
02 ORIGINAL MODEL
03 PRESENT MODEL

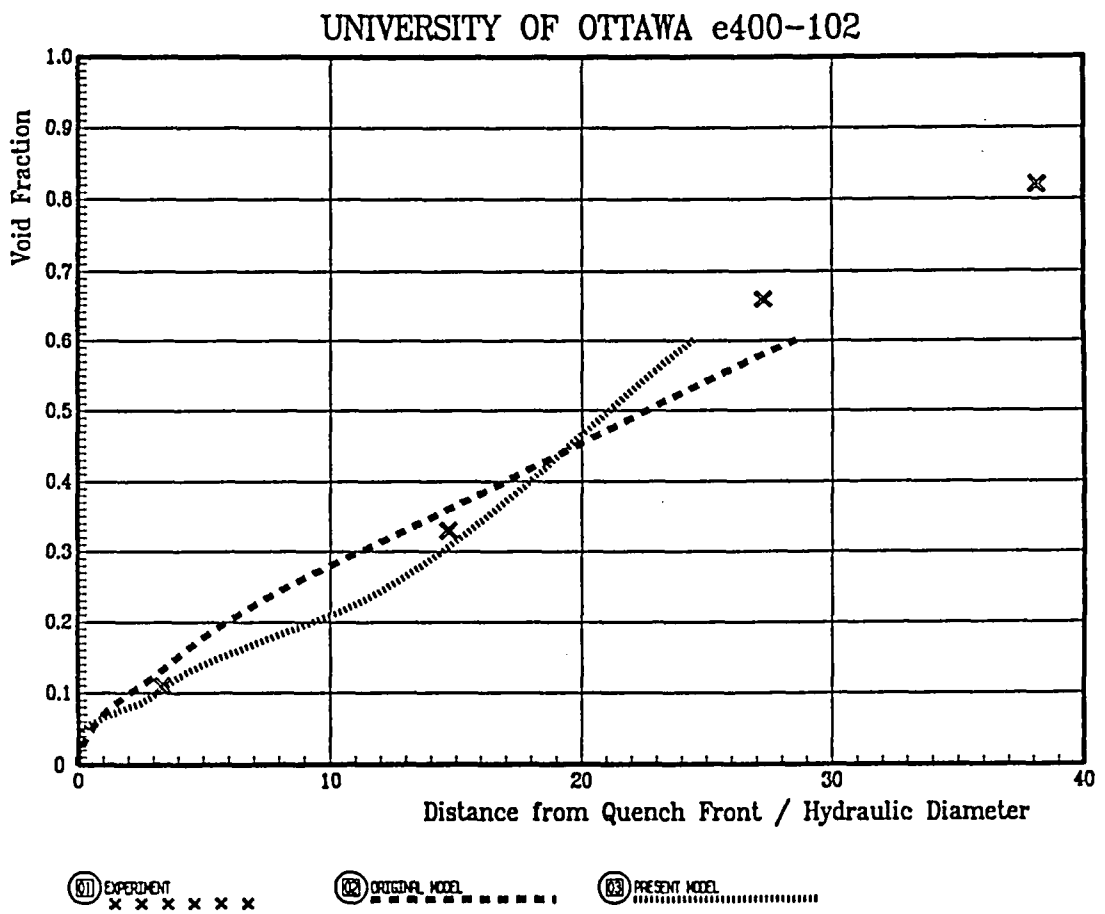
UNIVERSITY OF OTTAWA e400-102
Void Fraction
1.0
0.9
0.8
0.7
0.6
0.5
0.4
0.3
0.2
0.1
0
0
10
20
30
40
Distance from Quench Front / Hydraulic Diameter
01 EXPERIMENT
02 ORIGINAL MODEL
03 PRESENT MODEL

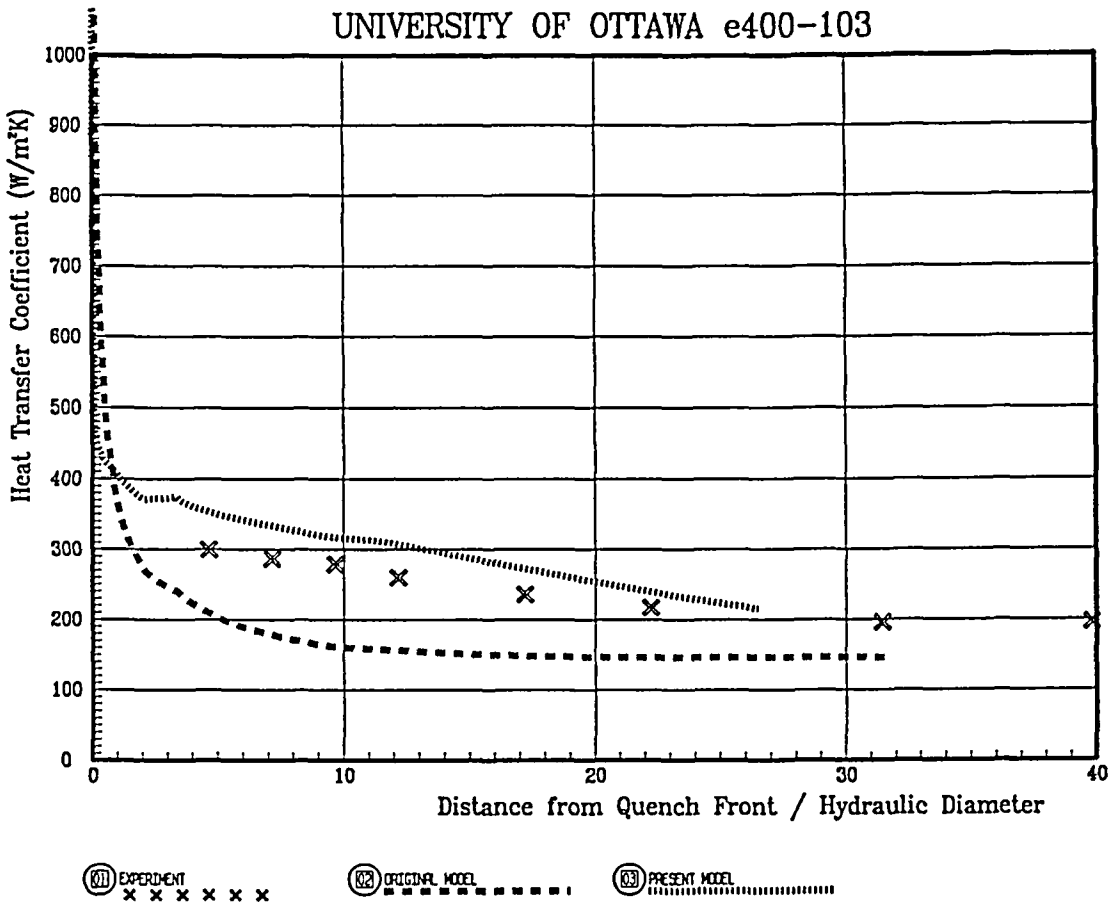
UNIVERSITY OF OTTAWA e400-103
Heat Transfer Coefficient (W/m²K)
1000
900
800
700
600
500
400
300
200
100
0
0
10
20
30
40
Distance from Quench Front / Hydraulic Diameter
01 EXPERIMENT
02 ORIGINAL MODEL
03 PRESENT MODEL

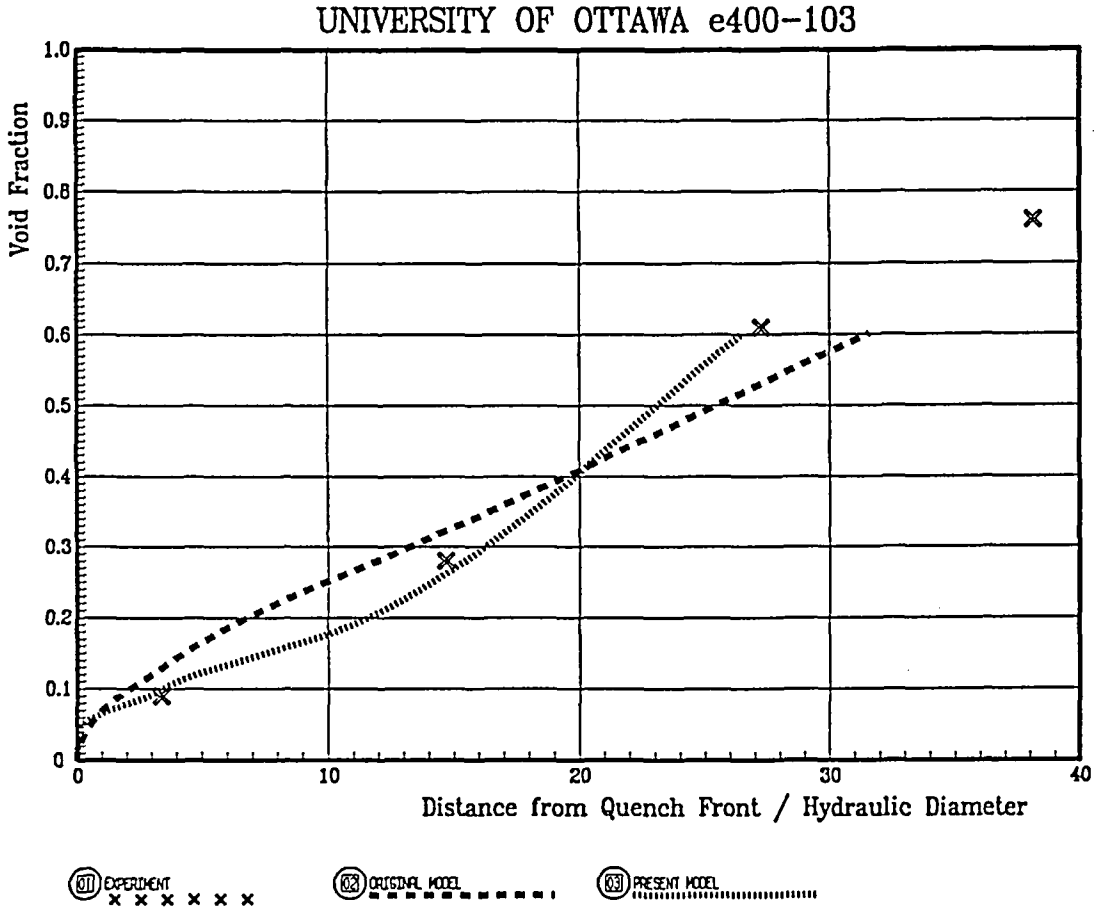
UNIVERSITY OF OTTAWA e400-103
Void Fraction
1.0
0.9
0.8
0.7
0.6
0.5
0.4
0.3
0.2
0.1
0
0
10
20
30
40
Distance from Quench Front / Hydraulic Diameter
01 EXPERIMENT
02 ORIGINAL MODEL
03 PRESENT MODEL

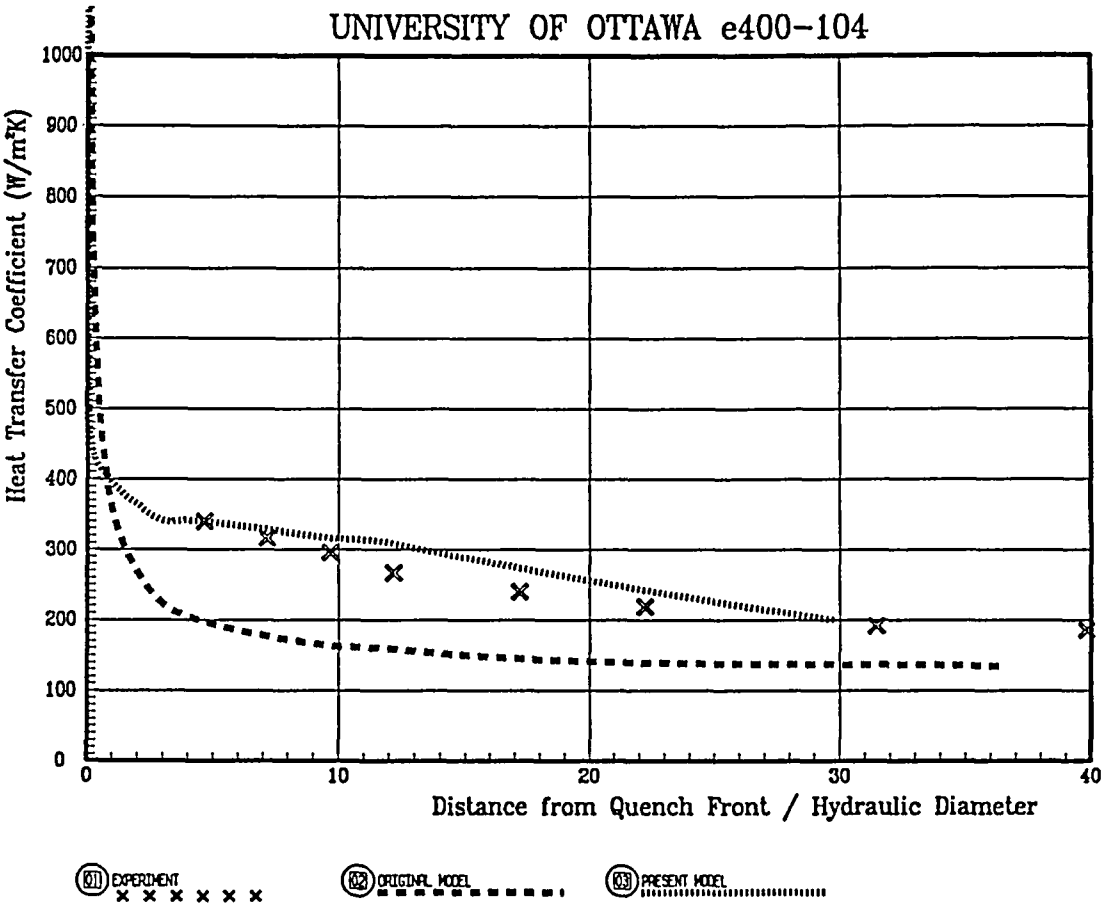
UNIVERSITY OF OTTAWA e400-104
Heat Transfer Coefficient (W/m²K)
1000
900
800
700
600
500
400
300
200
100
0
0
10
20
30
40
Distance from Quench Front / Hydraulic Diameter
01 EXPERIMENT
02 ORIGINAL MODEL
03 PRESENT MODEL

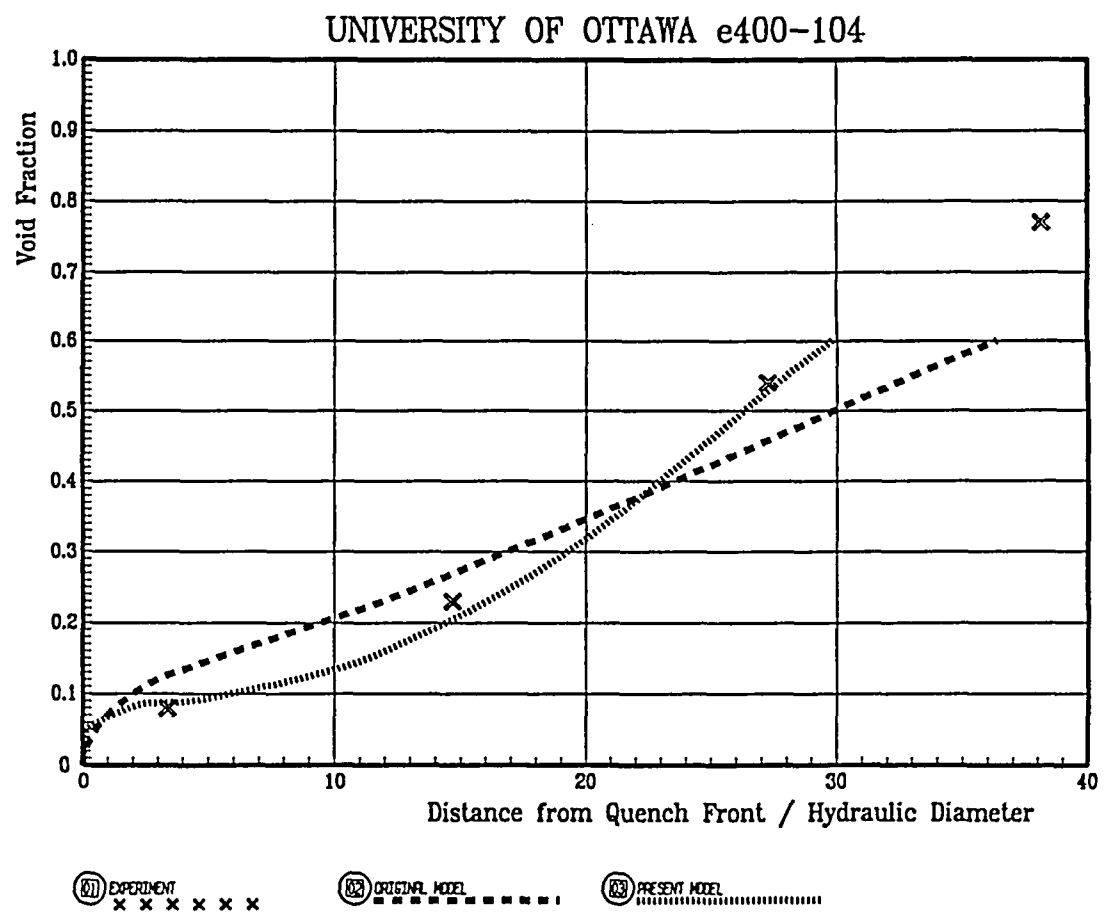
UNIVERSITY OF OTTAWA e400-104
Void Fraction
1.0
0.9
0.8
0.7
0.6
0.5
0.4
0.3
0.2
0.1
0
0
10
20
30
40
Distance from Quench Front / Hydraulic Diameter
01 EXPERIMENT
02 ORIGINAL MODEL
03 PRESENT MODEL

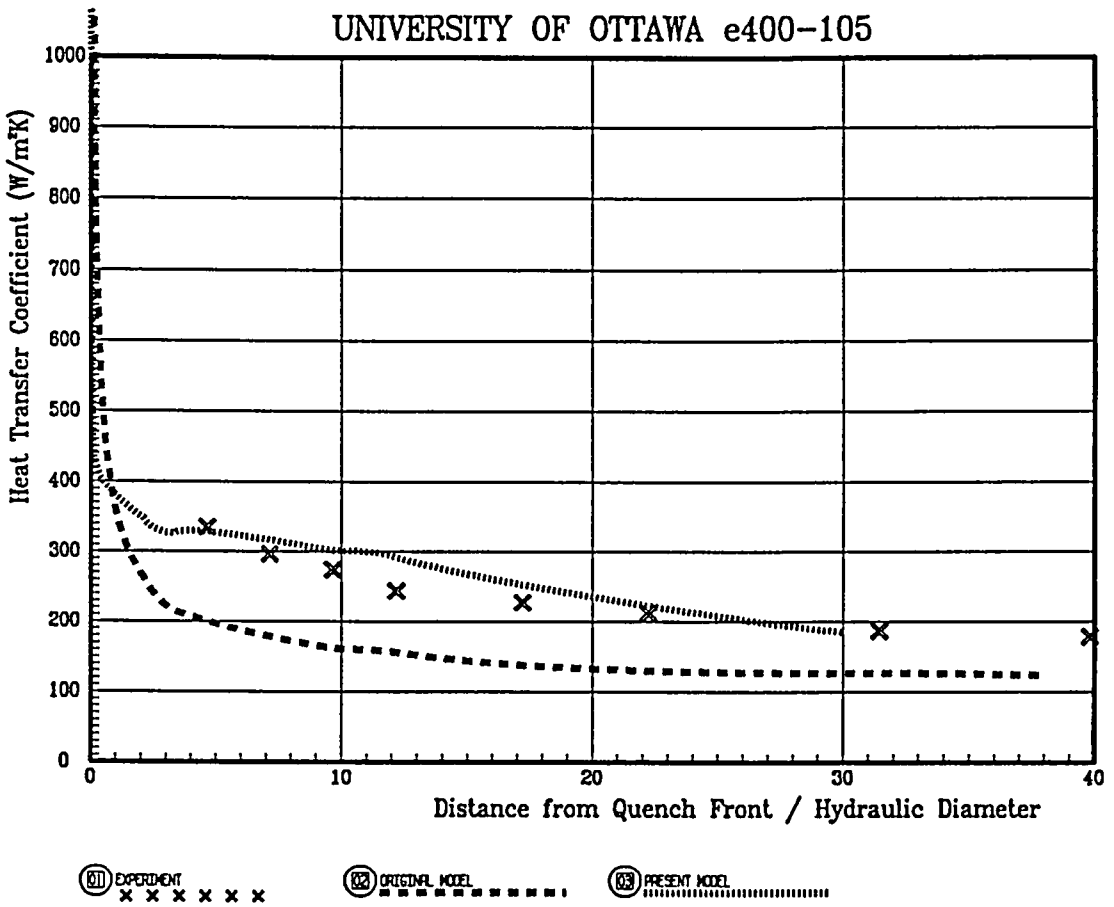
UNIVERSITY OF OTTAWA e400-105
Heat Transfer Coefficient (W/m²K)
1000
900
800
700
600
500
400
300
200
100
0
0
10
20
30
40
Distance from Quench Front / Hydraulic Diameter
01 EXPERIMENT
02 ORIGINAL MODEL
03 PRESENT MODEL

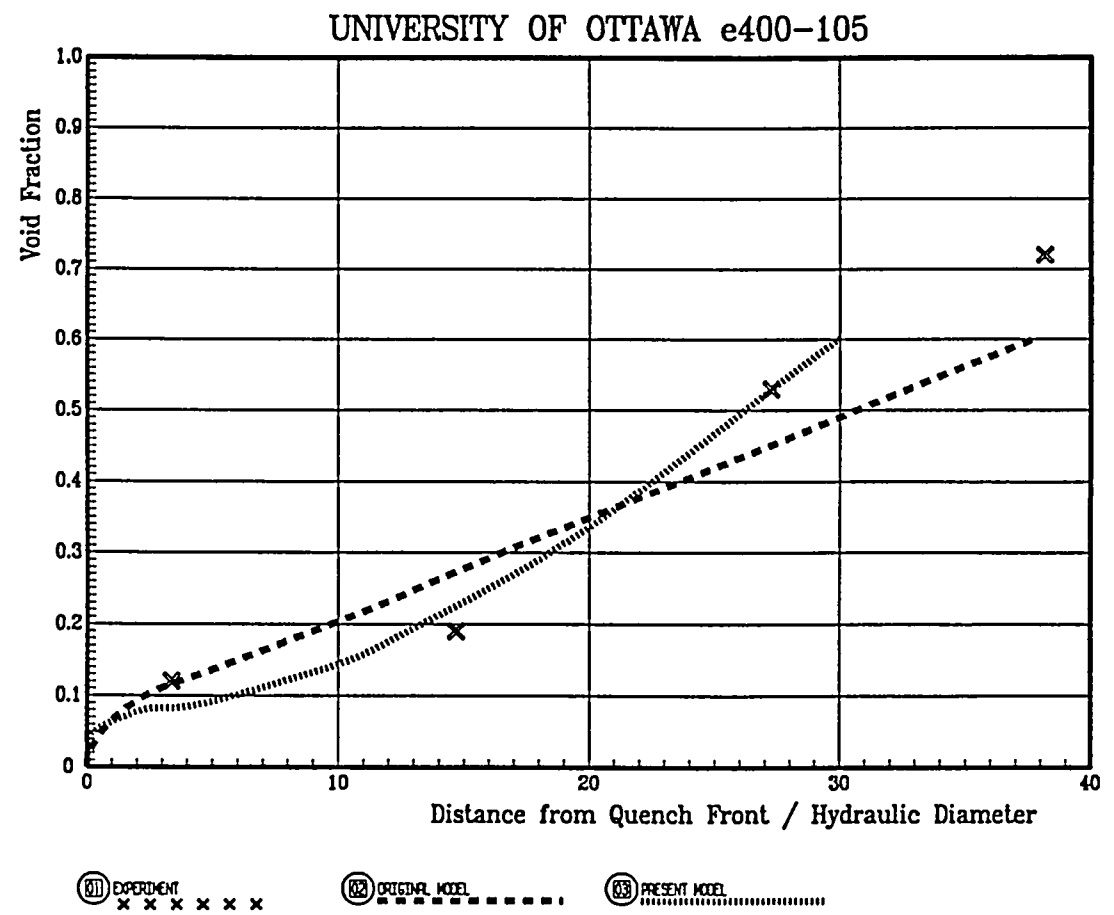
UNIVERSITY OF OTTAWA e400-105
Void Fraction
1.0
0.9
0.8
0.7
0.6
0.5
0.4
0.3
0.2
0.1
0
0
10
20
30
40
Distance from Quench Front / Hydraulic Diameter
01 EXPERIMENT
02 ORIGINAL MODEL
03 PRESENT MODEL

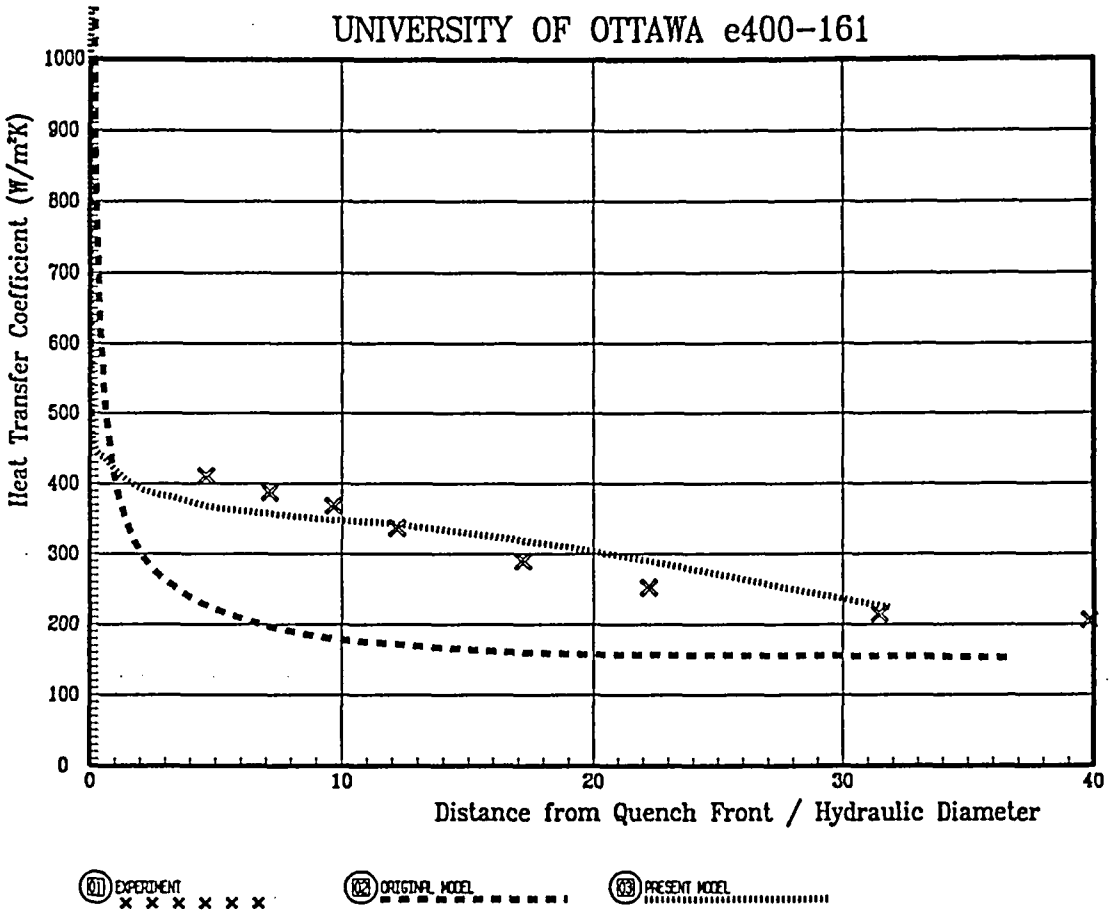
UNIVERSITY OF OTTAWA e400-161
Heat Transfer Coefficient (W/m²K)
1000
900
800
700
600
500
400
300
200
100
0
0
10
20
30
40
Distance from Quench Front / Hydraulic Diameter
001 EXPERIMENT
002 ORIGINAL MODEL
003 PRESENT MODEL

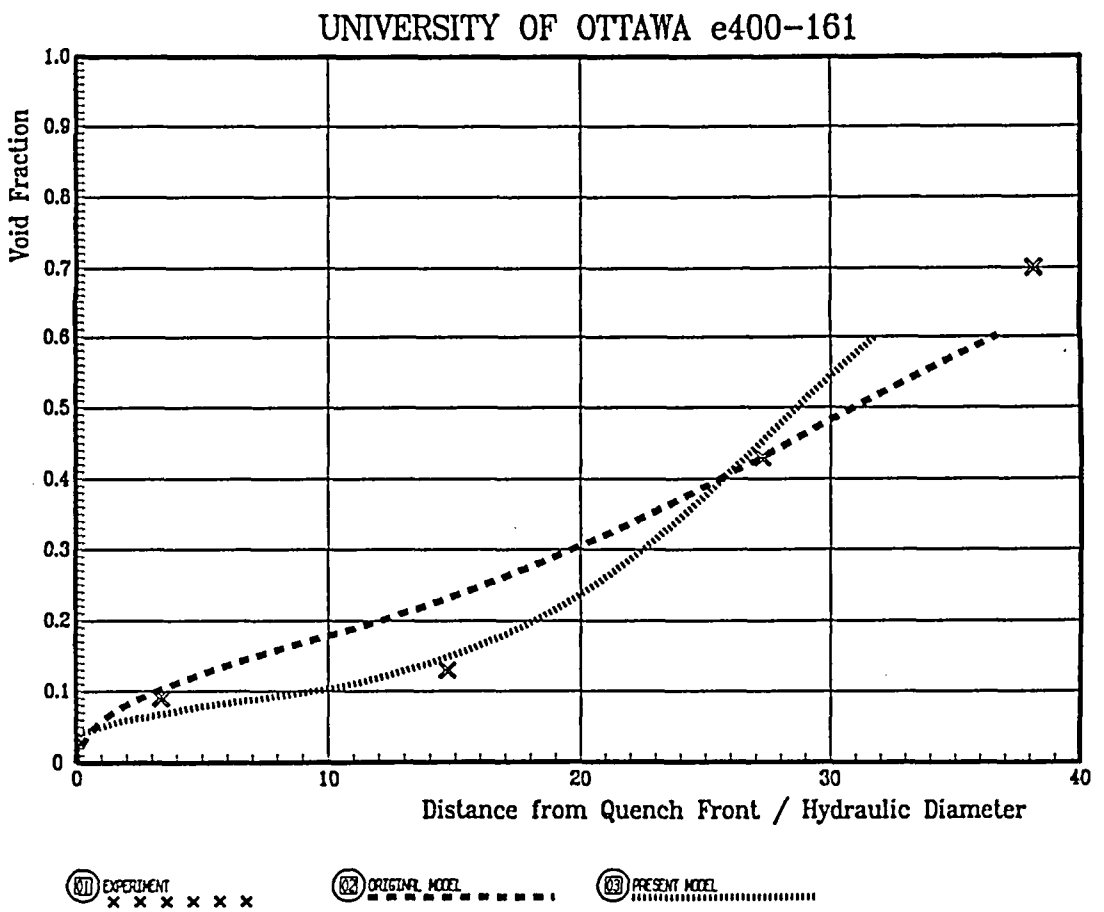
UNIVERSITY OF OTTAWA e400-161
Void Fraction
1.0
0.9
0.8
0.7
0.6
0.5
0.4
0.3
0.2
0.1
0
0
10
20
30
40
Distance from Quench Front / Hydraulic Diameter
001 EXPERIMENT
002 ORIGINAL MODEL
003 PRESENT MODEL

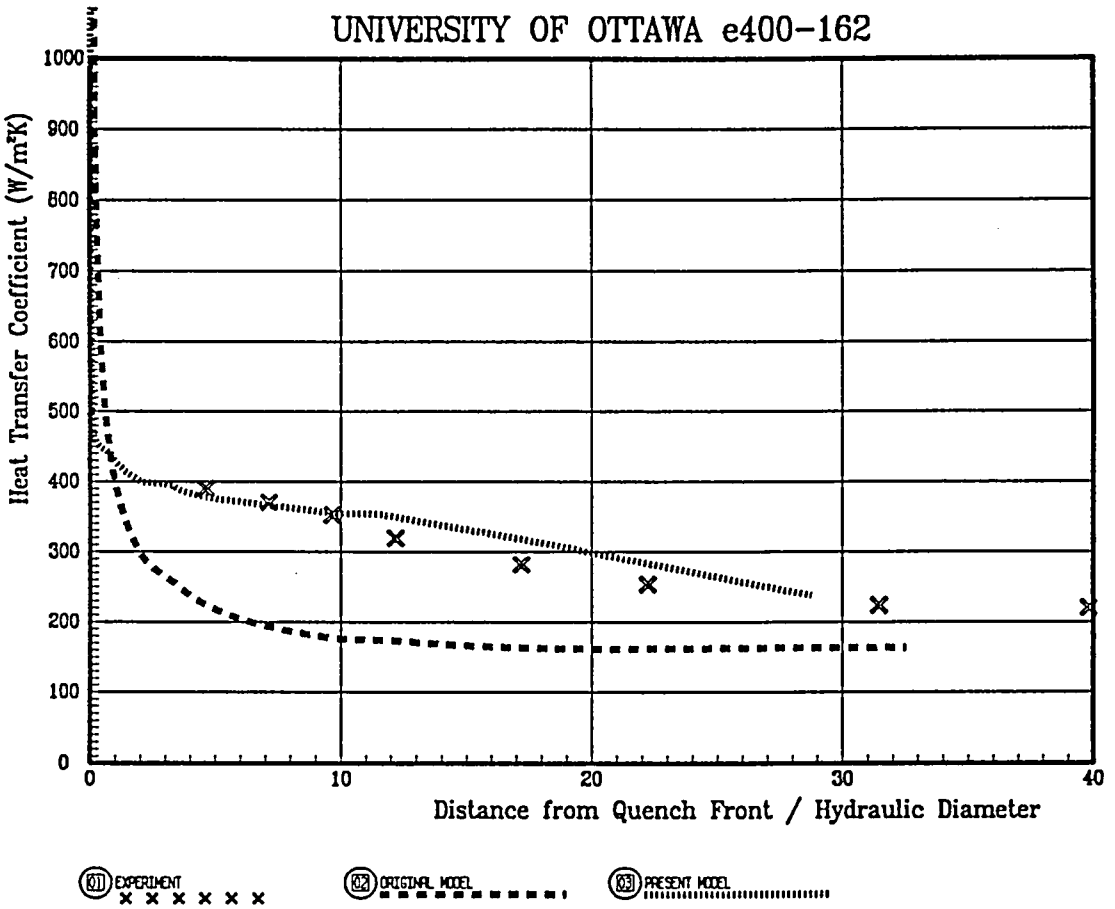
UNIVERSITY OF OTTAWA e400-162
Heat Transfer Coefficient (W/m²K)
1000
900
800
700
600
500
400
300
200
100
0
0
10
20
30
40
Distance from Quench Front / Hydraulic Diameter
01 EXPERIMENT
02 ORIGINAL MODEL
03 PRESENT MODEL

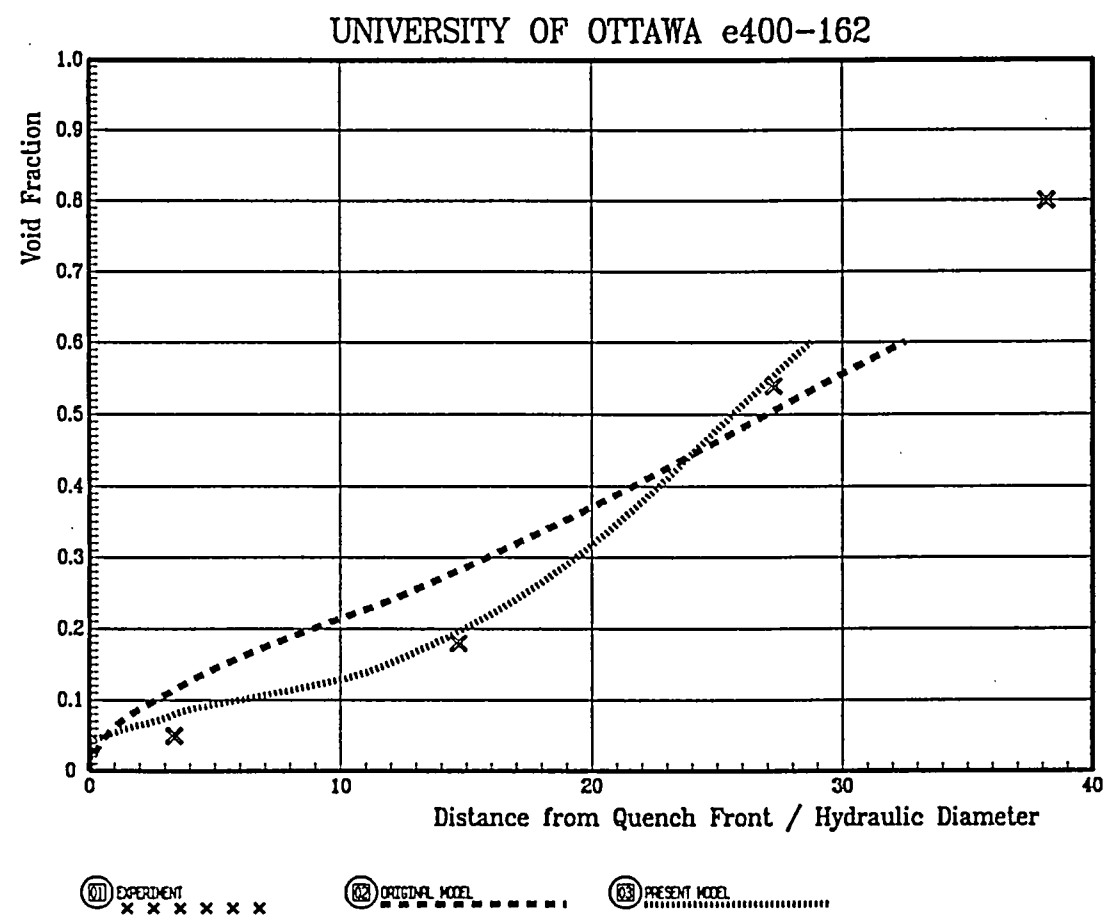
UNIVERSITY OF OTTAWA e400-162
Void Fraction
1.0
0.9
0.8
0.7
0.6
0.5
0.4
0.3
0.2
0.1
0
0
10
20
30
40
Distance from Quench Front / Hydraulic Diameter
01 EXPERIMENT
02 ORIGINAL MODEL
03 PRESENT MODEL

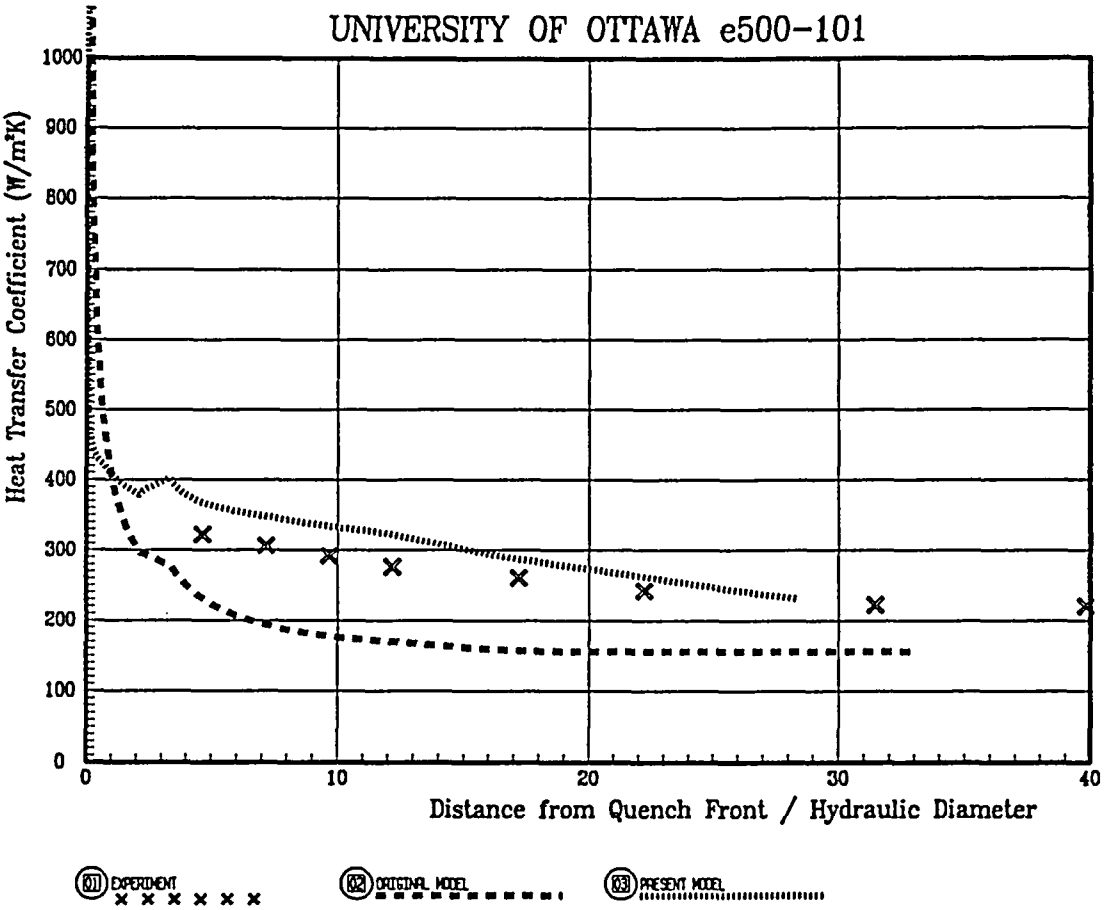
UNIVERSITY OF OTTAWA e500-101
Heat Transfer Coefficient (W/m²K)
1000
900
800
700
600
500
400
300
200
100
0
0
10
20
30
40
Distance from Quench Front / Hydraulic Diameter
01 EXPERIMENT
02 ORIGINAL MODEL
03 PRESENT MODEL

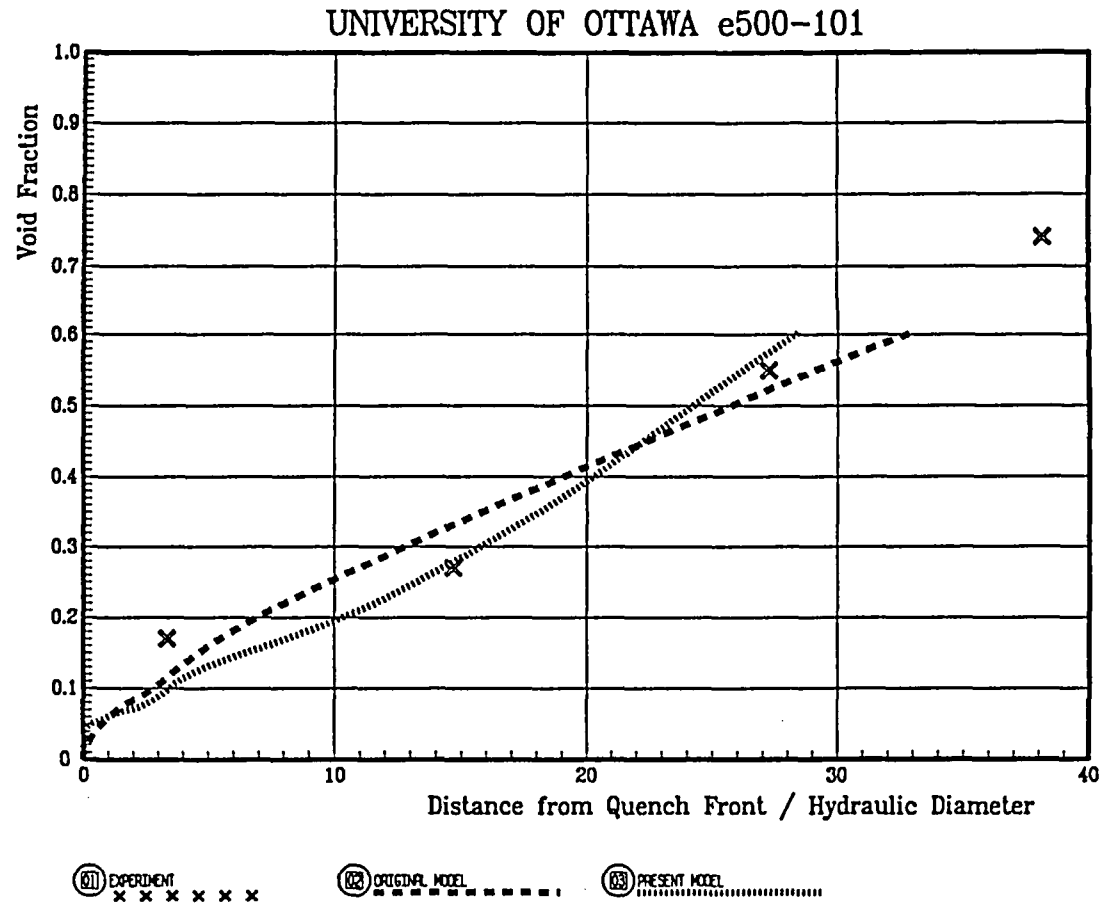
UNIVERSITY OF OTTAWA e500-101
Void Fraction
1.0
0.9
0.8
0.7
0.6
0.5
0.4
0.3
0.2
0.1
0
0
10
20
30
40
Distance from Quench Front / Hydraulic Diameter
01 EXPERIMENT
02 ORIGINAL MODEL
03 PRESENT MODEL

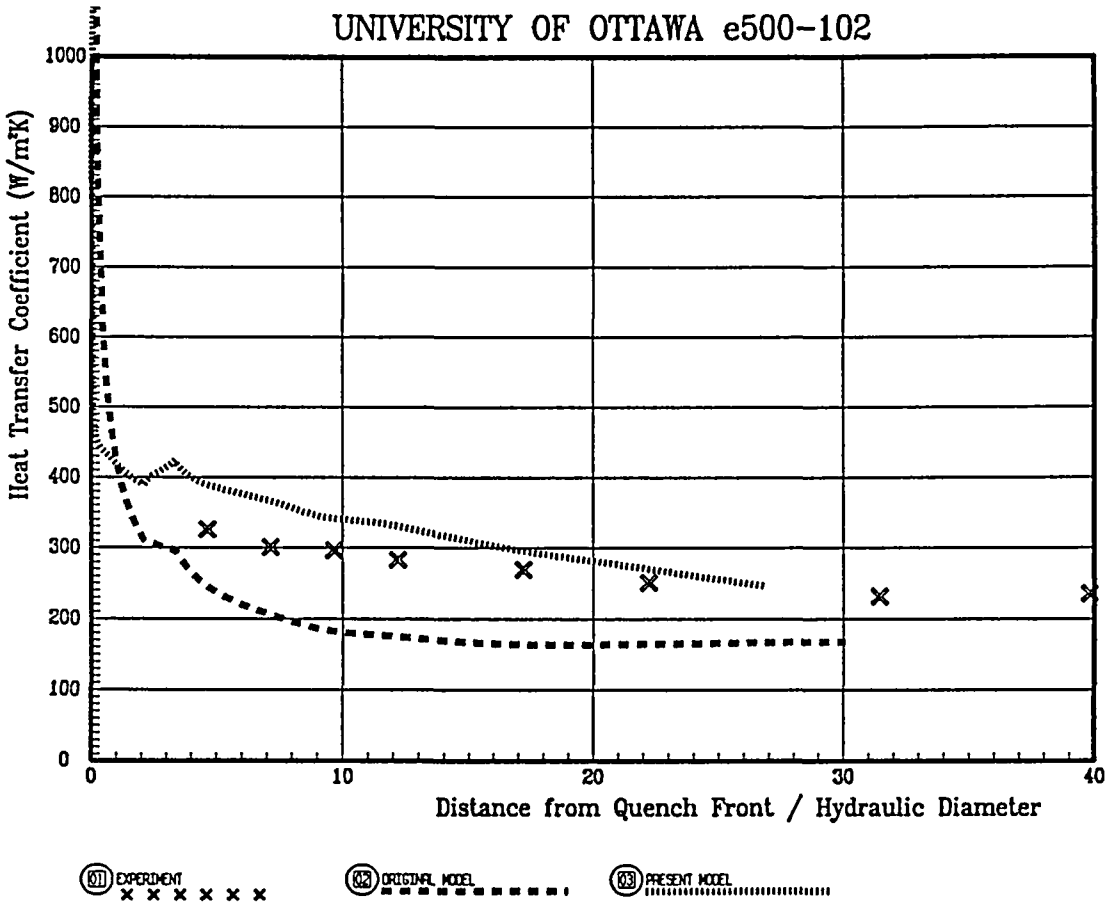
UNIVERSITY OF OTTAWA e500-102
Heat Transfer Coefficient (W/m²K)
1000
900
800
700
600
500
400
300
200
100
0
0
10
20
30
40
Distance from Quench Front / Hydraulic Diameter
01 EXPERIMENT
02 ORIGINAL MODEL
03 PRESENT MODEL

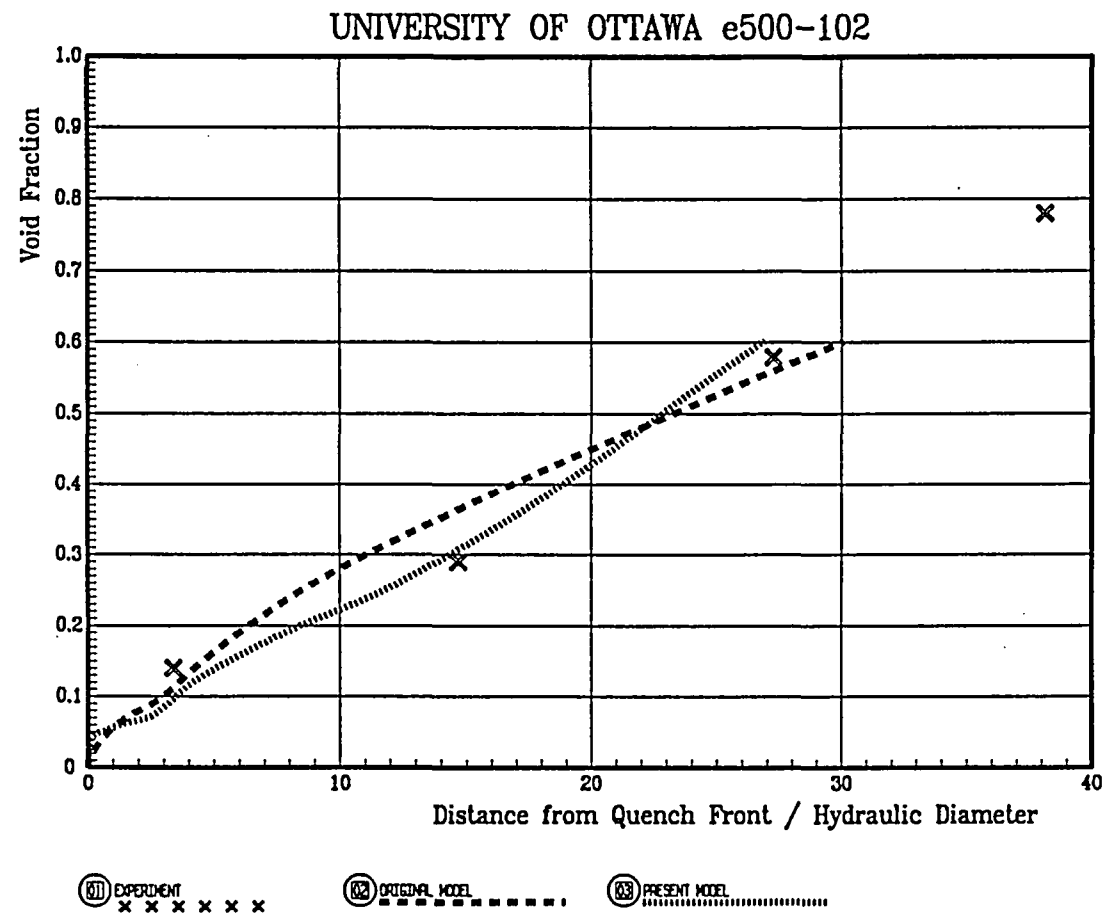
UNIVERSITY OF OTTAWA e500-102
Void Fraction
1.0
0.9
0.8
0.7
0.6
0.5
0.4
0.3
0.2
0.1
0
0
10
20
30
40
Distance from Quench Front / Hydraulic Diameter
01 EXPERIMENT
02 ORIGINAL MODEL
03 PRESENT MODEL

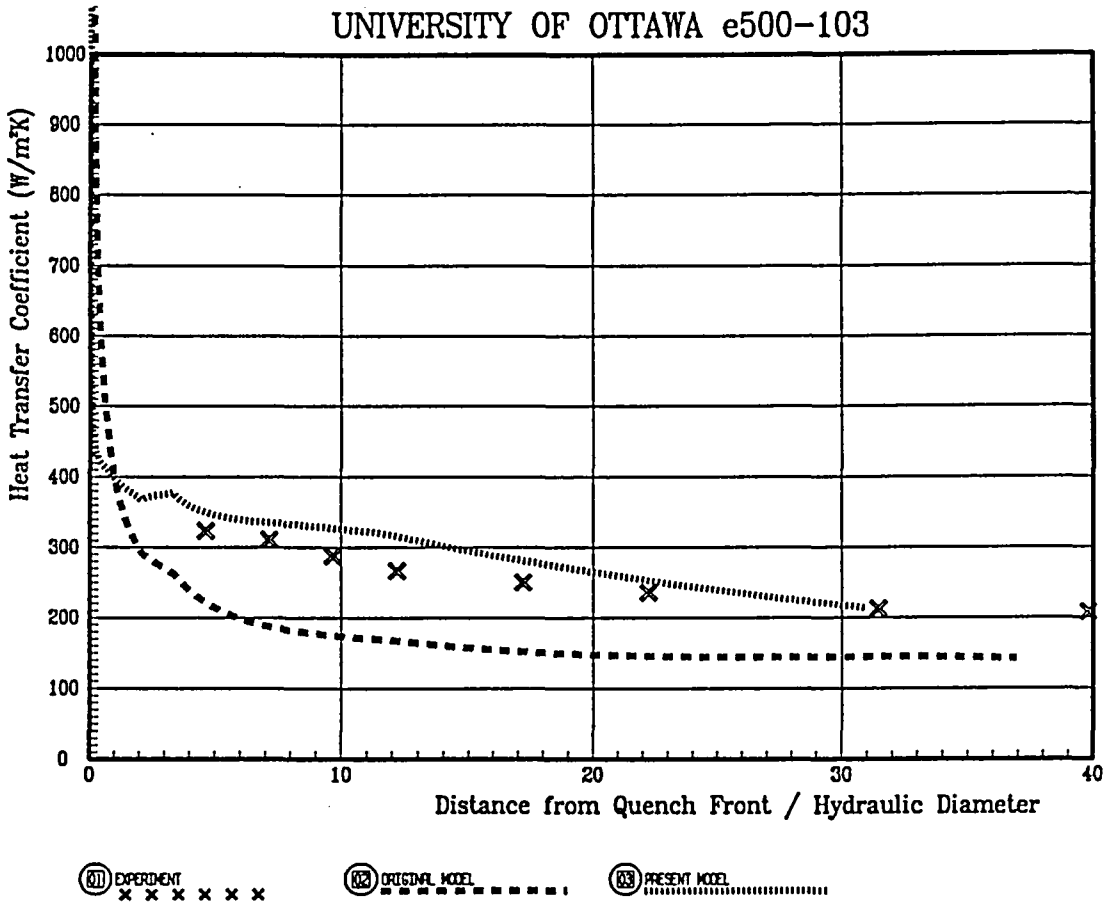
UNIVERSITY OF OTTAWA e500-103
Heat Transfer Coefficient (W/m²K)
1000
900
800
700
600
500
400
300
200
100
0
0
10
20
30
40
Distance from Quench Front / Hydraulic Diameter
01 EXPERIMENT
02 ORIGINAL MODEL
03 PRESENT MODEL

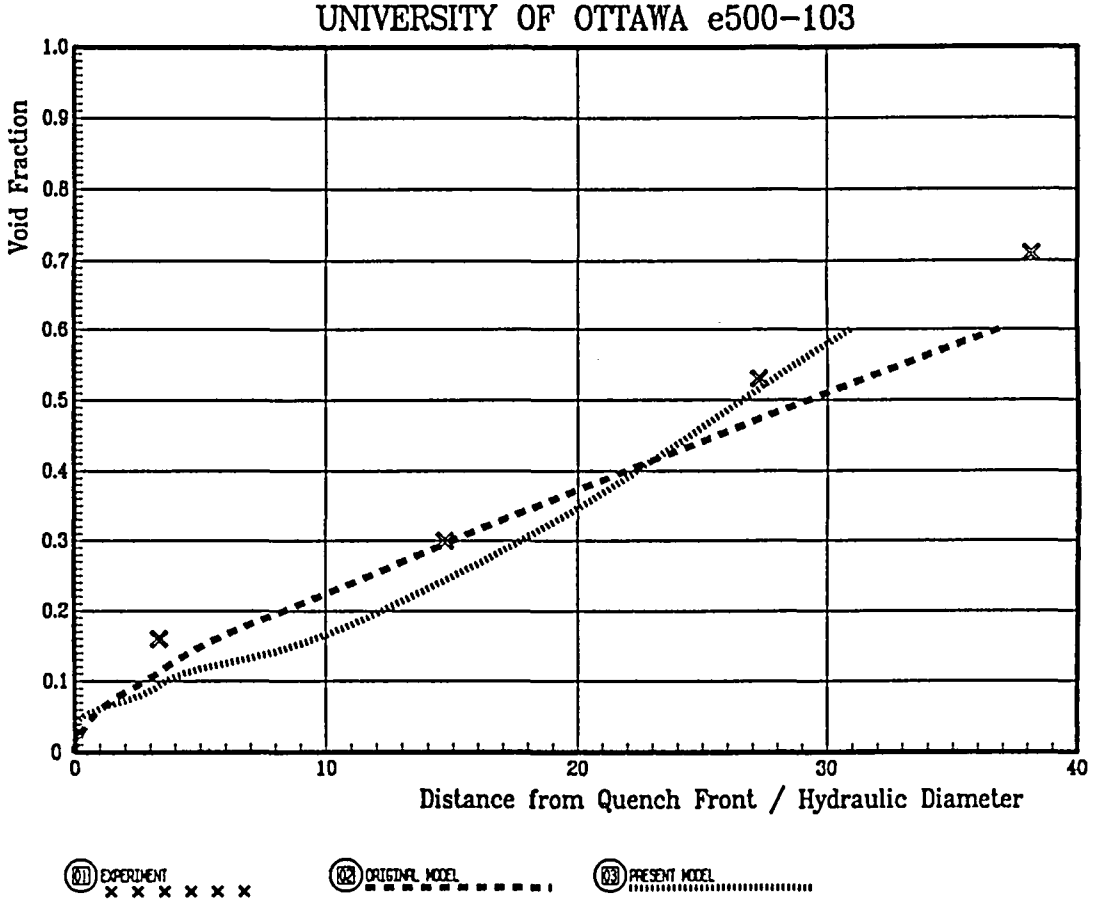
UNIVERSITY OF OTTAWA e500-103
Void Fraction
1.0
0.9
0.8
0.7
0.6
0.5
0.4
0.3
0.2
0.1
0
0
10
20
30
40
Distance from Quench Front / Hydraulic Diameter
01 EXPERIMENT
02 ORIGINAL MODEL
03 PRESENT MODEL

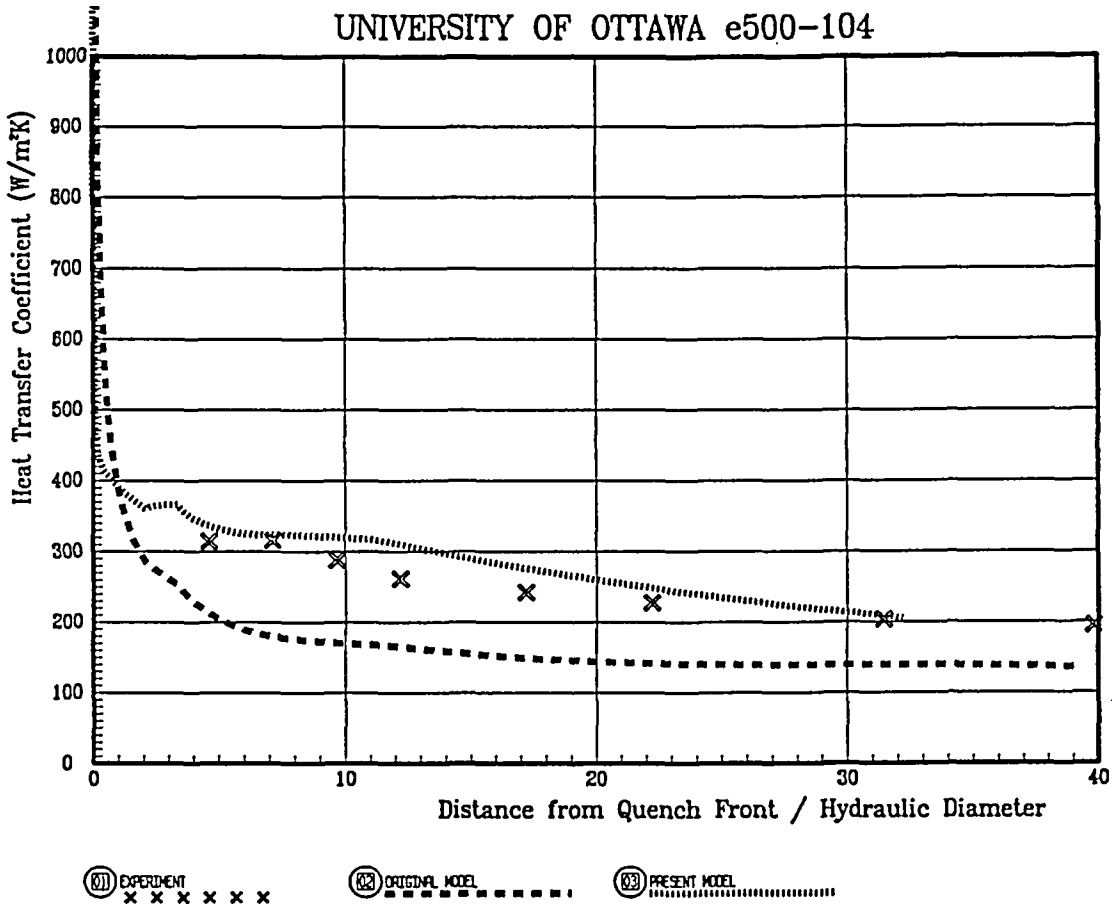
UNIVERSITY OF OTTAWA e500-104
Heat Transfer Coefficient (W/m²K)
1000
900
800
700
600
500
400
300
200
100
0
0
10
20
30
40
Distance from Quench Front / Hydraulic Diameter
01 EXPERIMENT
02 ORIGINAL MODEL
03 PRESENT MODEL

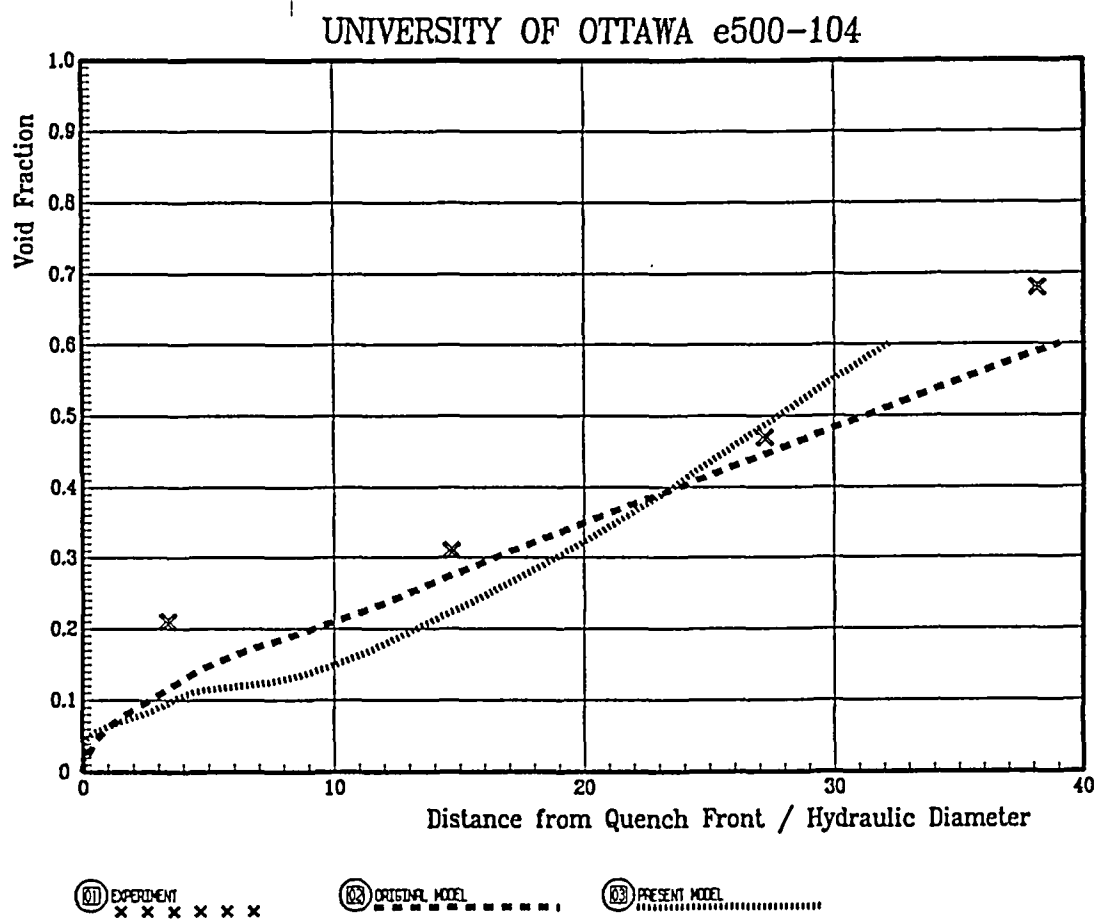
UNIVERSITY OF OTTAWA e500-104
Void Fraction
1.0
0.9
0.8
0.7
0.6
0.5
0.4
0.3
0.2
0.1
0
0
10
20
30
40
Distance from Quench Front / Hydraulic Diameter
01 EXPERIMENT
02 ORIGINAL MODEL
03 PRESENT MODEL

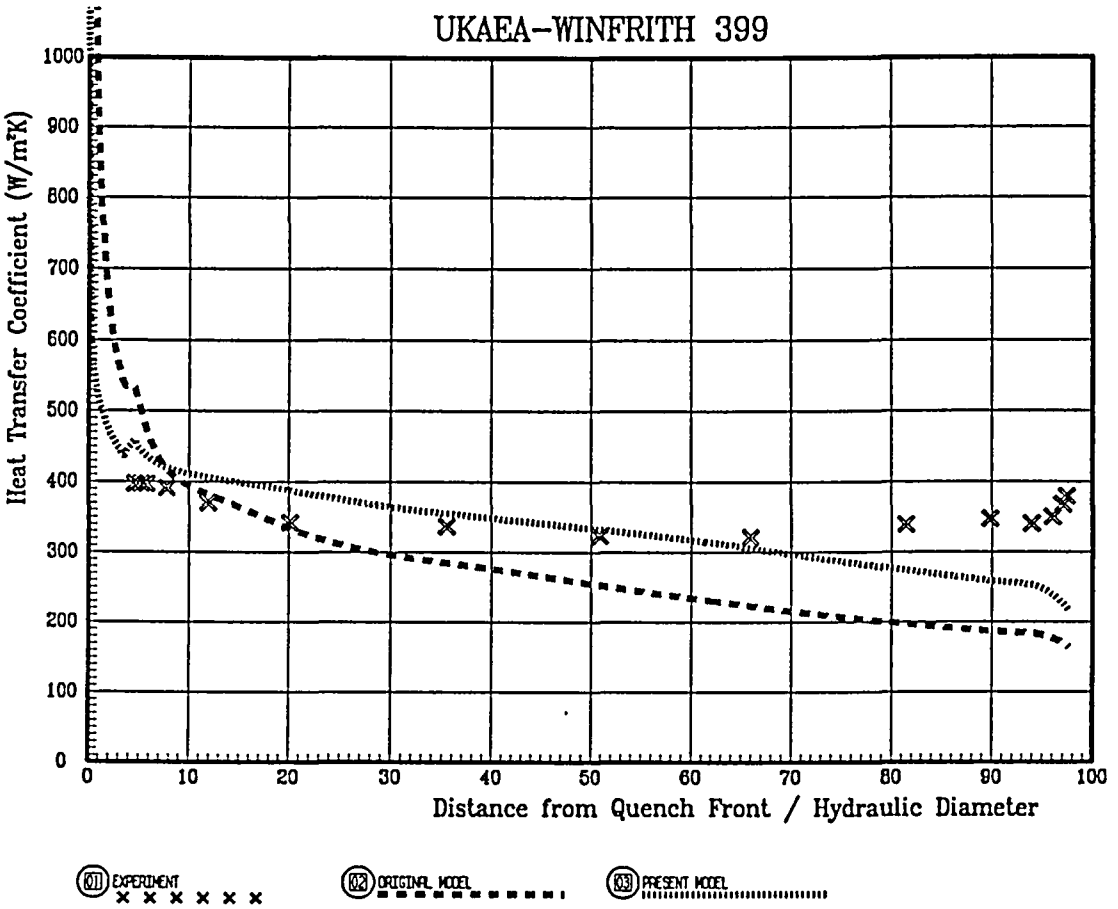
UKAEA-WINFRITH 399
Heat Transfer Coefficient (W/m²K)
1000
900
800
700
600
500
400
300
200
100
0
0
10
20
30
40
50
60
70
80
90
100
Distance from Quench Front / Hydraulic Diameter
01 EXPERIMENT
02 ORIGINAL MODEL
03 PRESENT MODEL

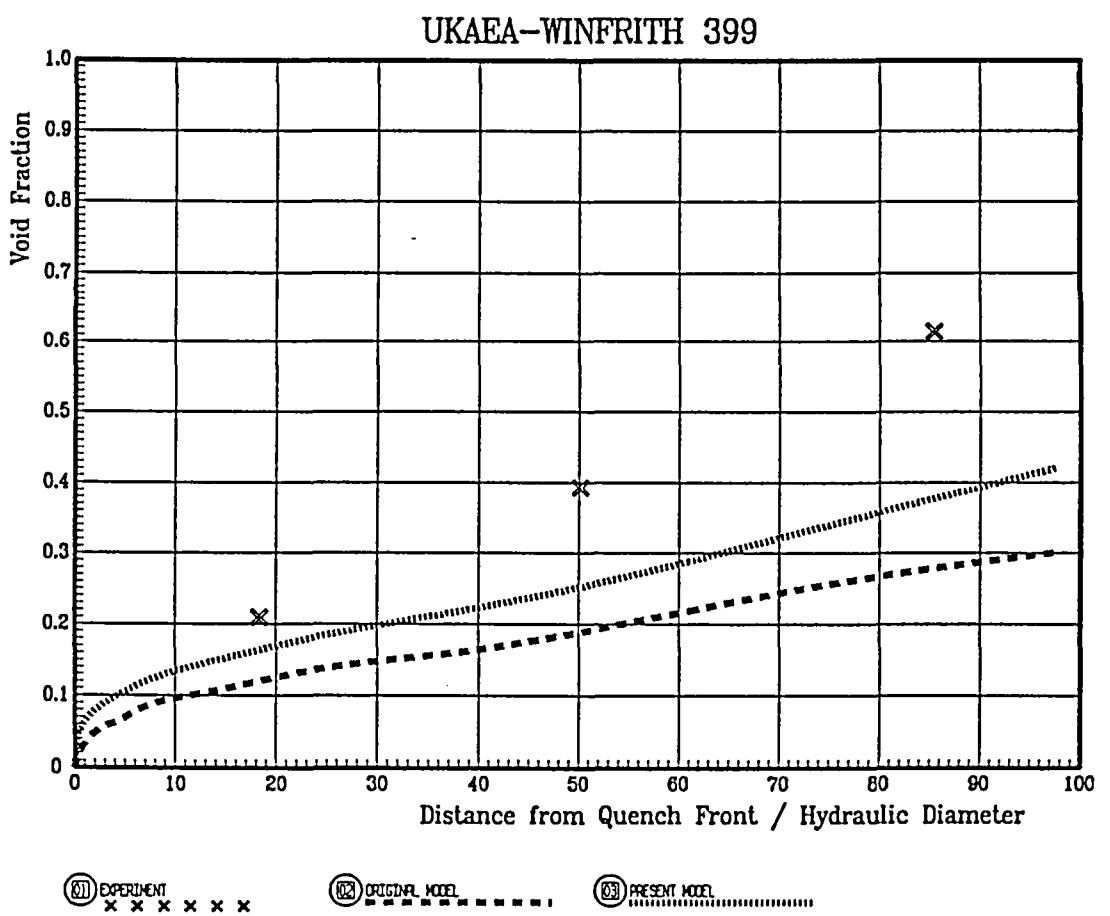
UKAEA-WINFRITH 399
Void Fraction
1.0
0.9
0.8
0.7
0.6
0.5
0.4
0.3
0.2
0.1
0
0
10
20
30
40
50
60
70
80
90
100
Distance from Quench Front / Hydraulic Diameter
01 EXPERIMENT
02 ORIGINAL MODEL
03 PRESENT MODEL

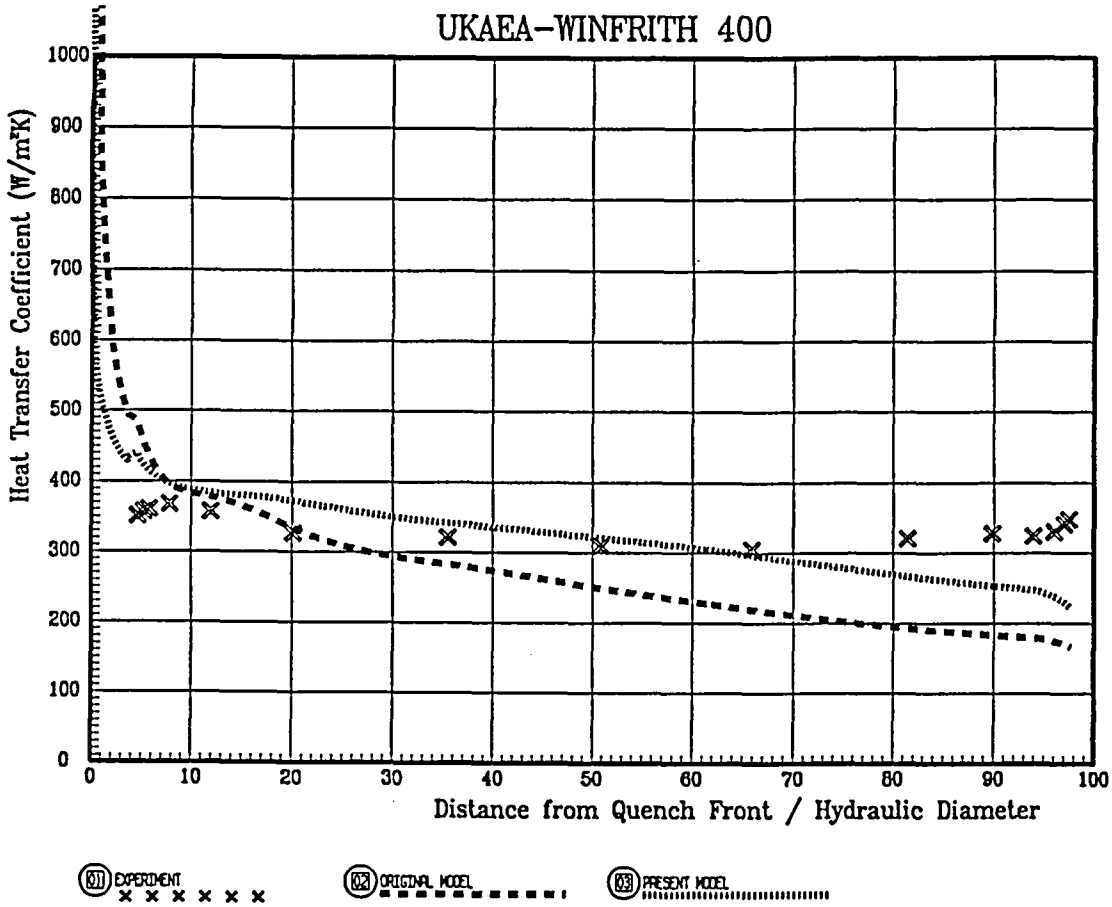
UKAEA-WINFRITH 400
Heat Transfer Coefficient (W/m²K)
1000
900
800
700
600
500
400
300
200
100
0
0
10
20
30
40
50
60
70
80
90
100
Distance from Quench Front / Hydraulic Diameter
01 EXPERIMENT
02 ORIGINAL MODEL
03 PRESENT MODEL

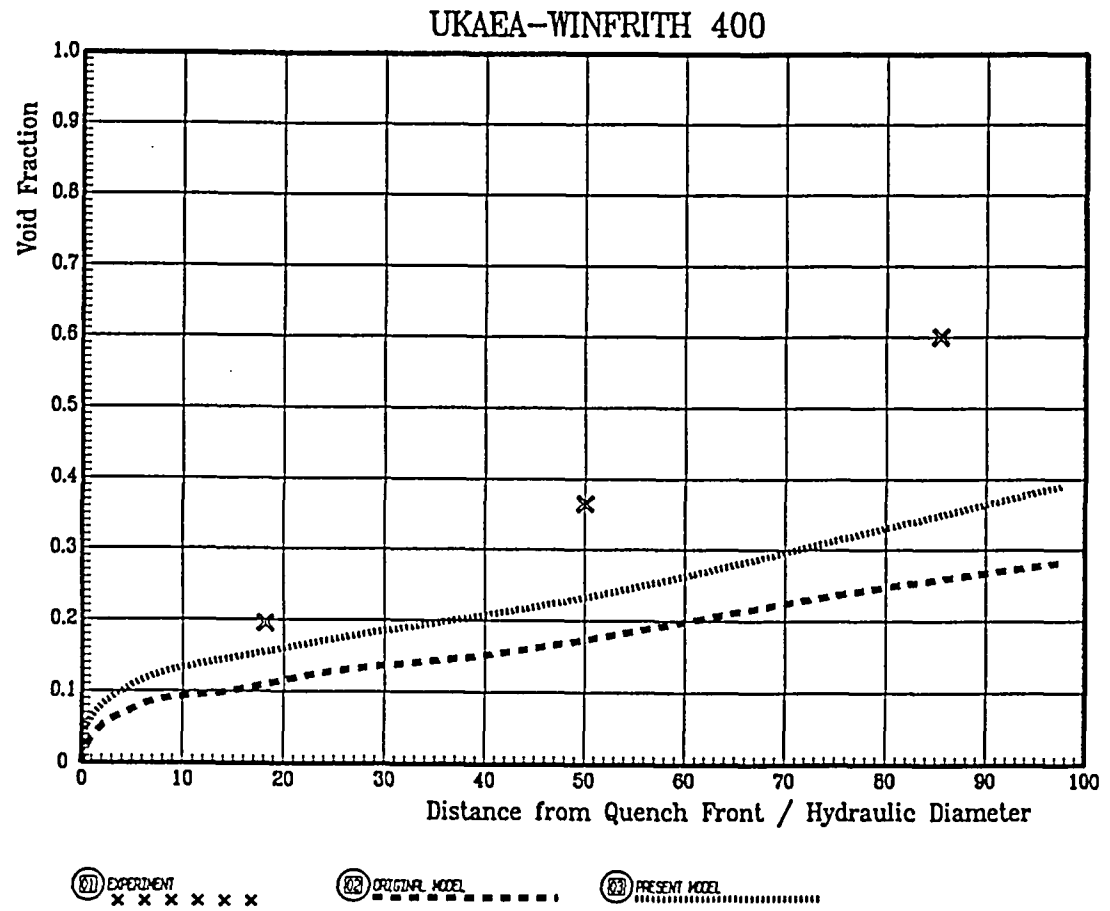
UKAEA-WINFRITH 400
Void Fraction
1.0
0.9
0.8
0.7
0.6
0.5
0.4
0.3
0.2
0.1
0
0
10
20
30
40
50
60
70
80
90
100
Distance from Quench Front / Hydraulic Diameter
01 EXPERIMENT
02 ORIGINAL MODEL
03 PRESENT MODEL

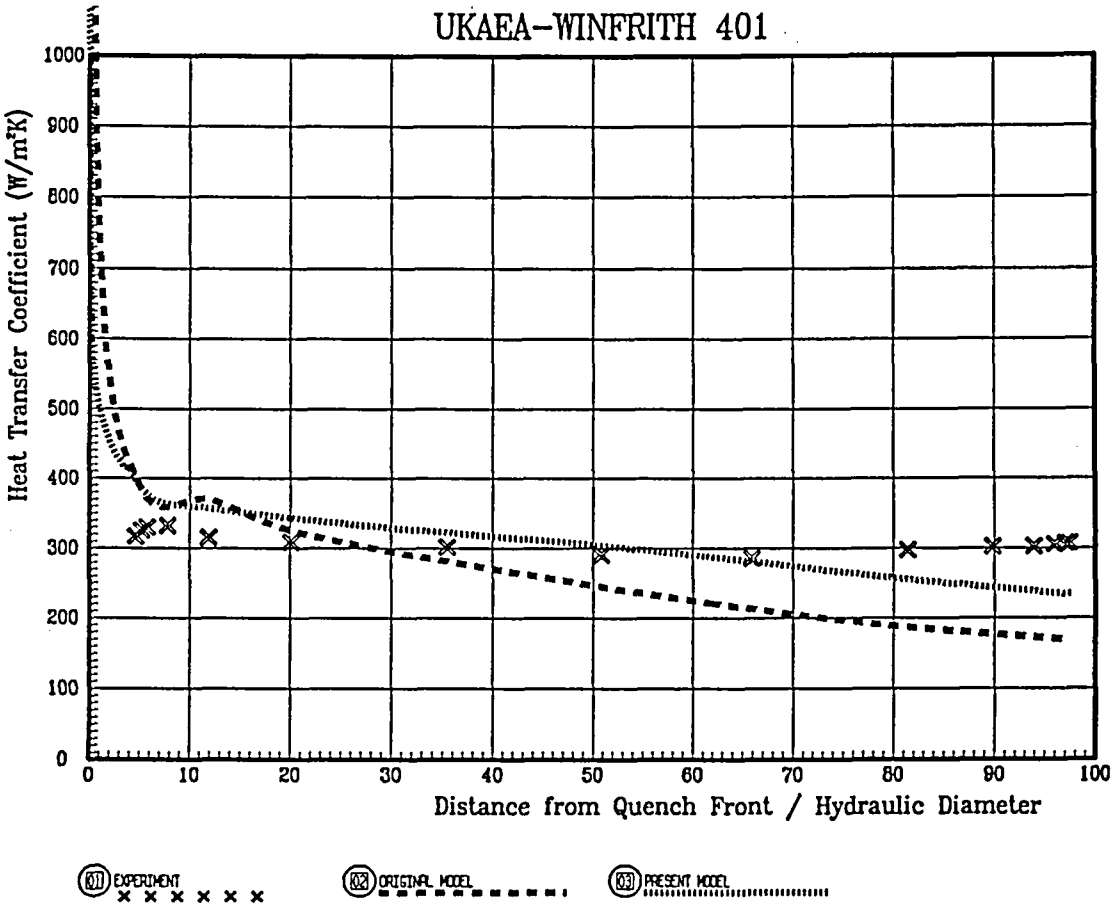
UKAEA-WINFRITH 401
Heat Transfer Coefficient (W/m²K)
1000
900
800
700
600
500
400
300
200
100
0
0
10
20
30
40
50
60
70
80
90
100
Distance from Quench Front / Hydraulic Diameter
001 EXPERIMENT
002 ORIGINAL MODEL
003 PRESENT MODEL

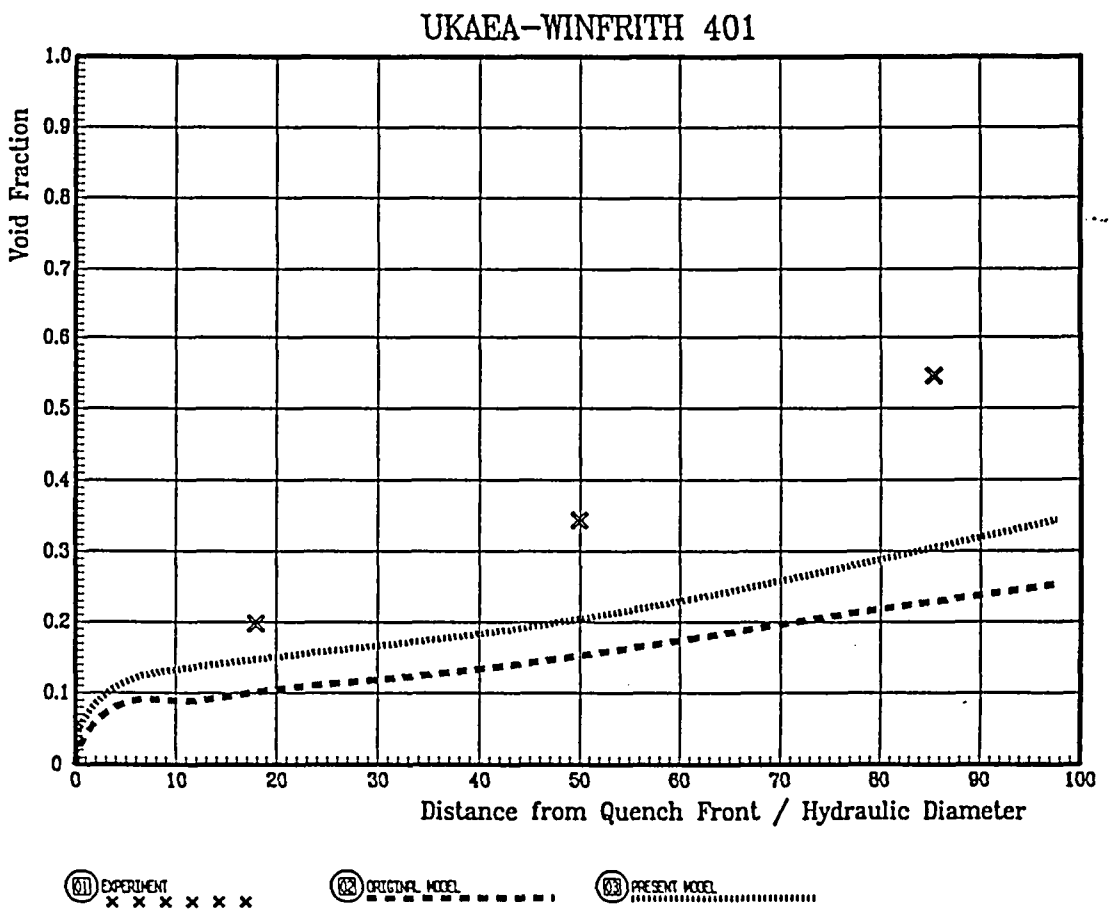
UKAEA-WINFRITH 401
Void Fraction
1.0
0.9
0.8
0.7
0.6
0.5
0.4
0.3
0.2
0.1
0
0
10
20
30
40
50
60
70
80
90
100
Distance from Quench Front / Hydraulic Diameter
001 EXPERIMENT
002 ORIGINAL MODEL
003 PRESENT MODEL

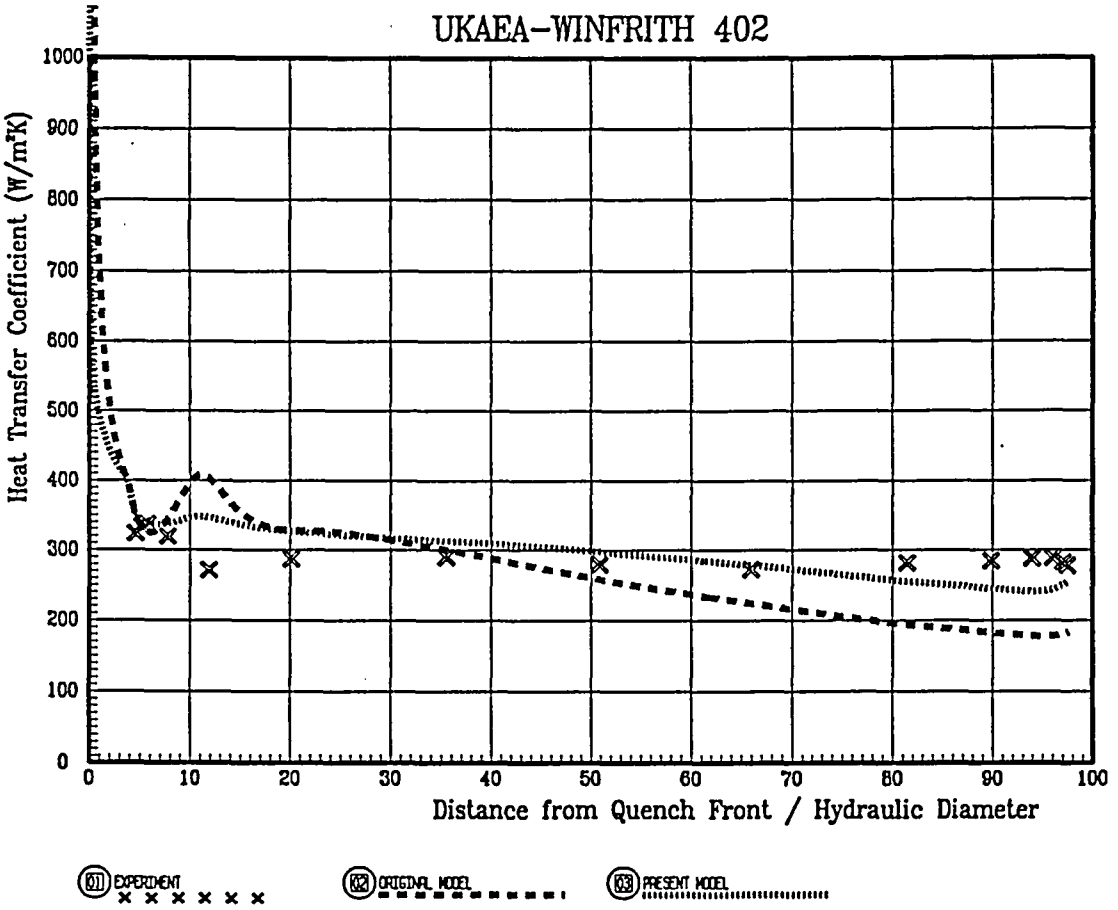
UKAEA-WINFRITH 402
Heat Transfer Coefficient (W/m²K)
1000
900
800
700
600
500
400
300
200
100
0
0
10
20
30
40
50
60
70
80
90
100
Distance from Quench Front / Hydraulic Diameter
01 EXPERIMENT
02 ORIGINAL MODEL
03 PRESENT MODEL

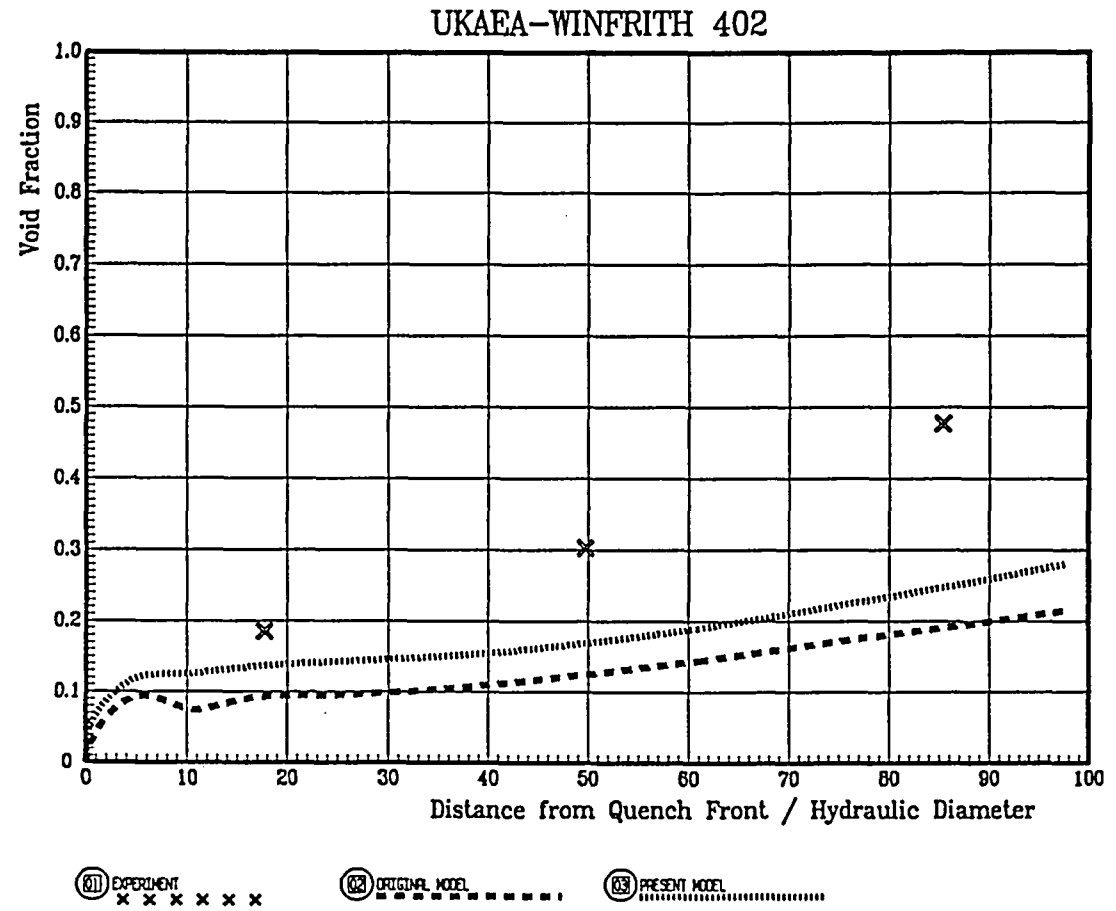
UKAEA-WINFRITH 402
Void Fraction
1.0
0.9
0.8
0.7
0.6
0.5
0.4
0.3
0.2
0.1
0
0
10
20
30
40
50
60
70
80
90
100
Distance from Quench Front / Hydraulic Diameter
01 EXPERIMENT
02 ORIGINAL MODEL
03 PRESENT MODEL

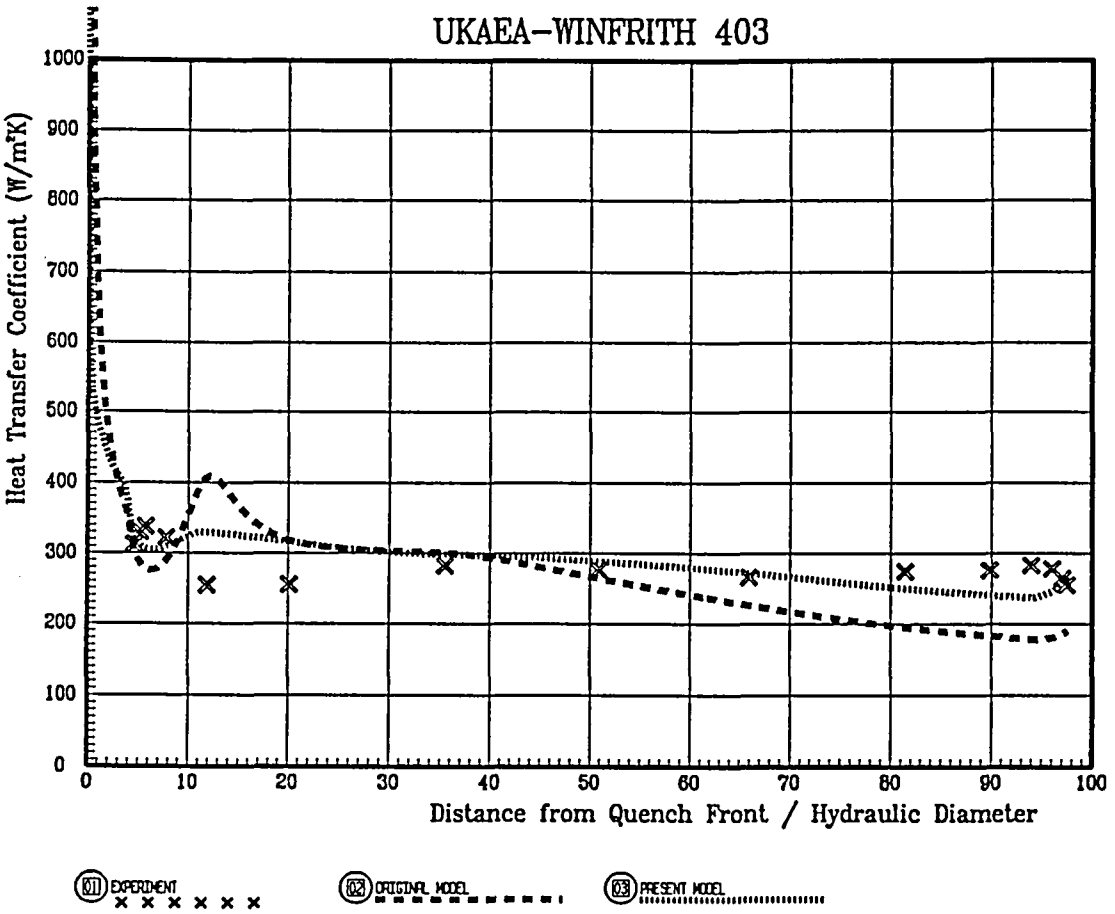
UKAEA-WINFRITH 403
Heat Transfer Coefficient (W/m²K)
1000
900
800
700
600
500
400
300
200
100
0
0
10
20
30
40
50
60
70
80
90
100
Distance from Quench Front / Hydraulic Diameter
01 EXPERIMENT
02 ORIGINAL MODEL
03 PRESENT MODEL

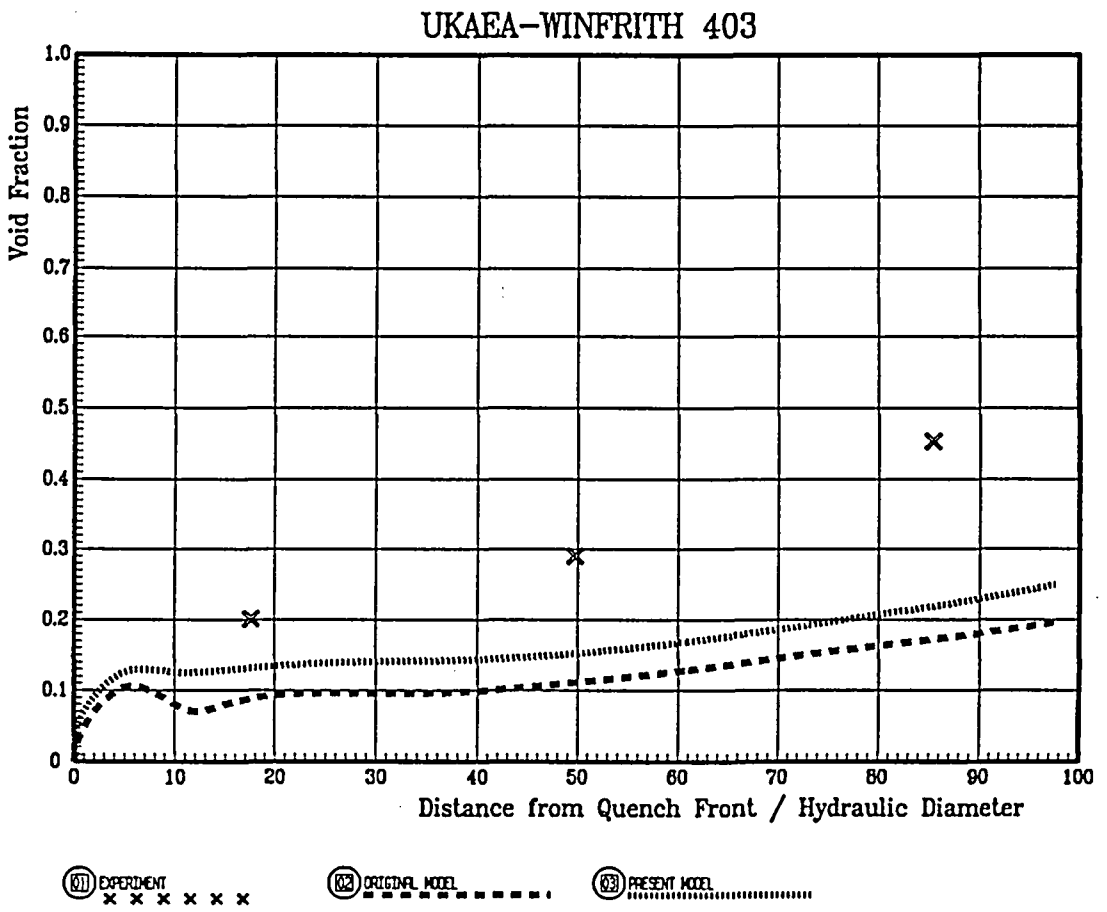
UKAEA-WINFRITH 403
Void Fraction
1.0
0.9
0.8
0.7
0.6
0.5
0.4
0.3
0.2
0.1
0
0
10
20
30
40
50
60
70
80
90
100
Distance from Quench Front / Hydraulic Diameter
01 EXPERIMENT
02 ORIGINAL MODEL
03 PRESENT MODEL

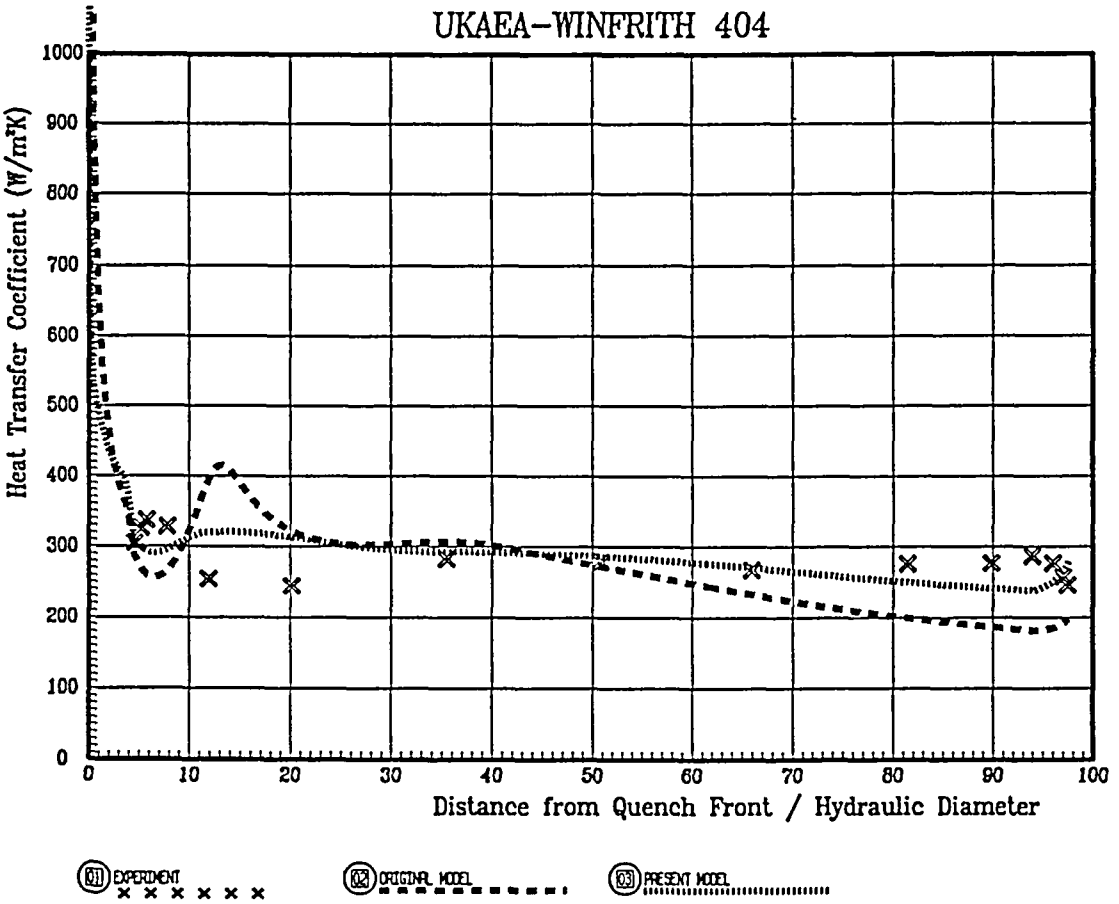
UKAEA-WINFRITH 404
Heat Transfer Coefficient (W/m²K)
1000
900
800
700
600
500
400
300
200
100
0
0
10
20
30
40
50
60
70
80
90
100
Distance from Quench Front / Hydraulic Diameter
01 EXPERIMENT
02 ORIGINAL MODEL
03 PRESENT MODEL

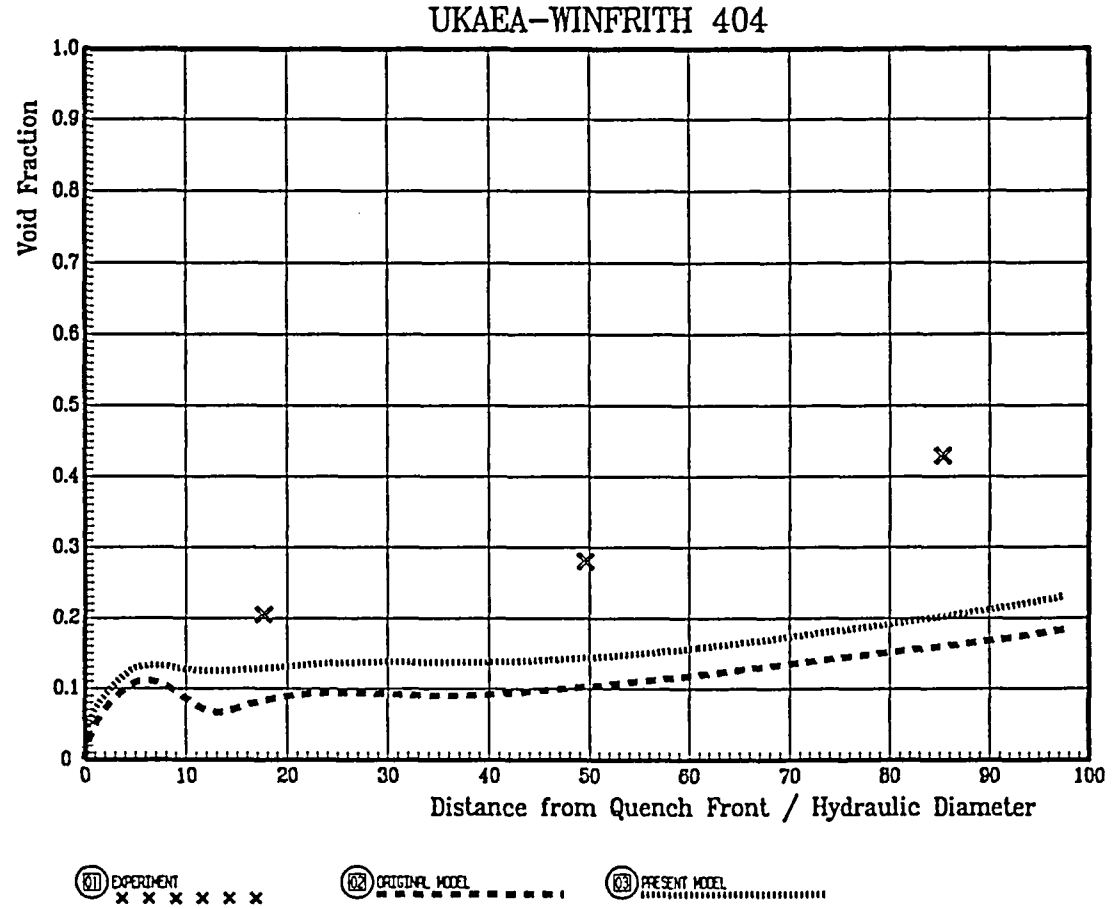
UKAEA-WINFRITH 404
Void Fraction
1.0
0.9
0.8
0.7
0.6
0.5
0.4
0.3
0.2
0.1
0
0
10
20
30
40
50
60
70
80
90
100
Distance from Quench Front / Hydraulic Diameter
01 EXPERIMENT
02 ORIGINAL MODEL
03 PRESENT MODEL

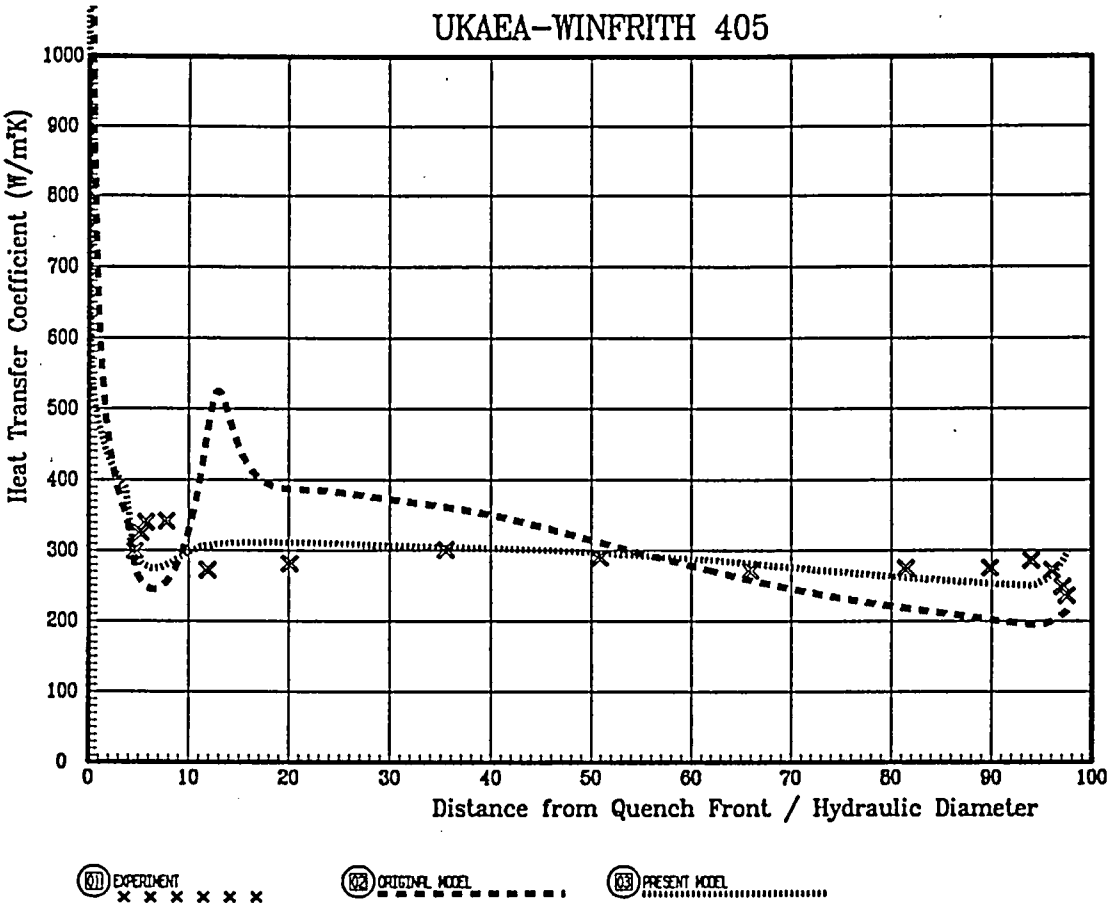
UKAEA-WINFRITH 405
Heat Transfer Coefficient (W/m²K)
1000
900
800
700
600
500
400
300
200
100
0
0
10
20
30
40
50
60
70
80
90
100
Distance from Quench Front / Hydraulic Diameter
001 EXPERIMENT
002 ORIGINAL MODEL
003 PRESENT MODEL

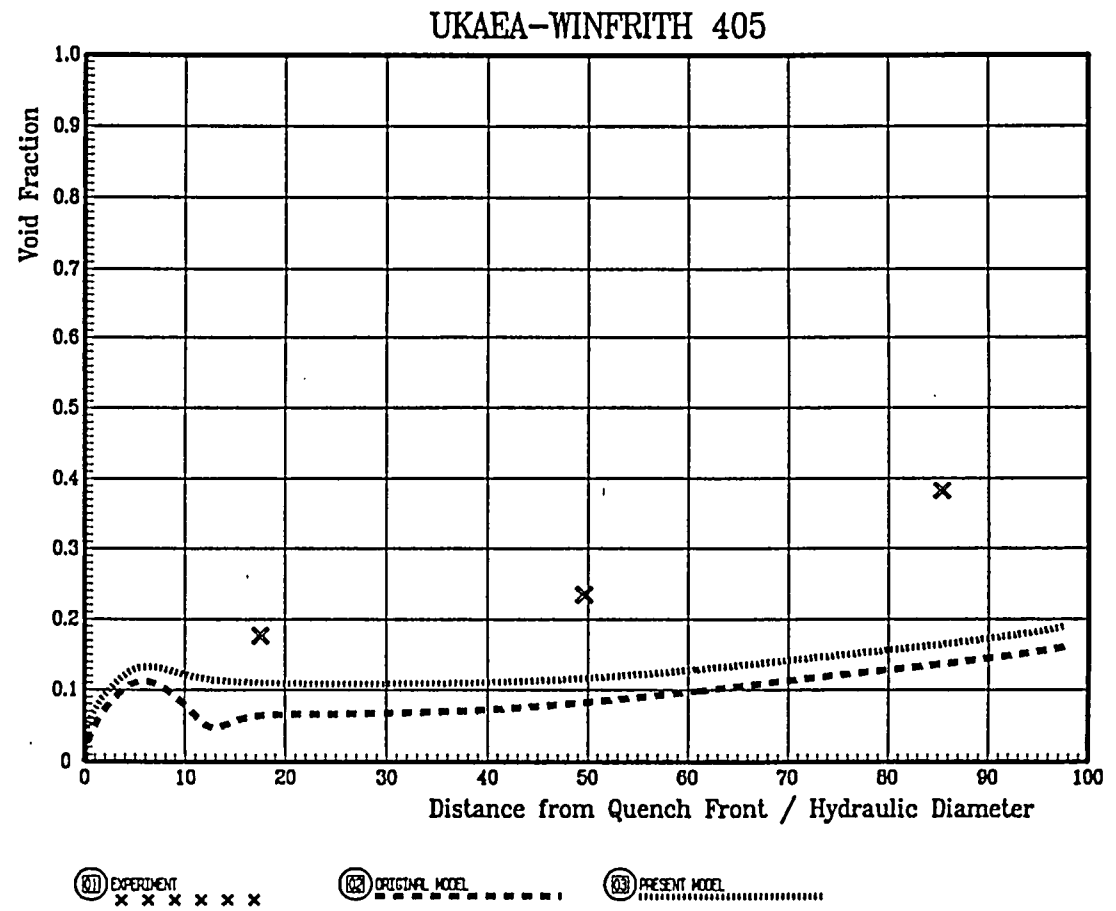
UKAEA-WINFRITH 405
Void Fraction
1.0
0.9
0.8
0.7
0.6
0.5
0.4
0.3
0.2
0.1
0
0
10
20
30
40
50
60
70
80
90
100
Distance from Quench Front / Hydraulic Diameter
001 EXPERIMENT
002 ORIGINAL MODEL
003 PRESENT MODEL

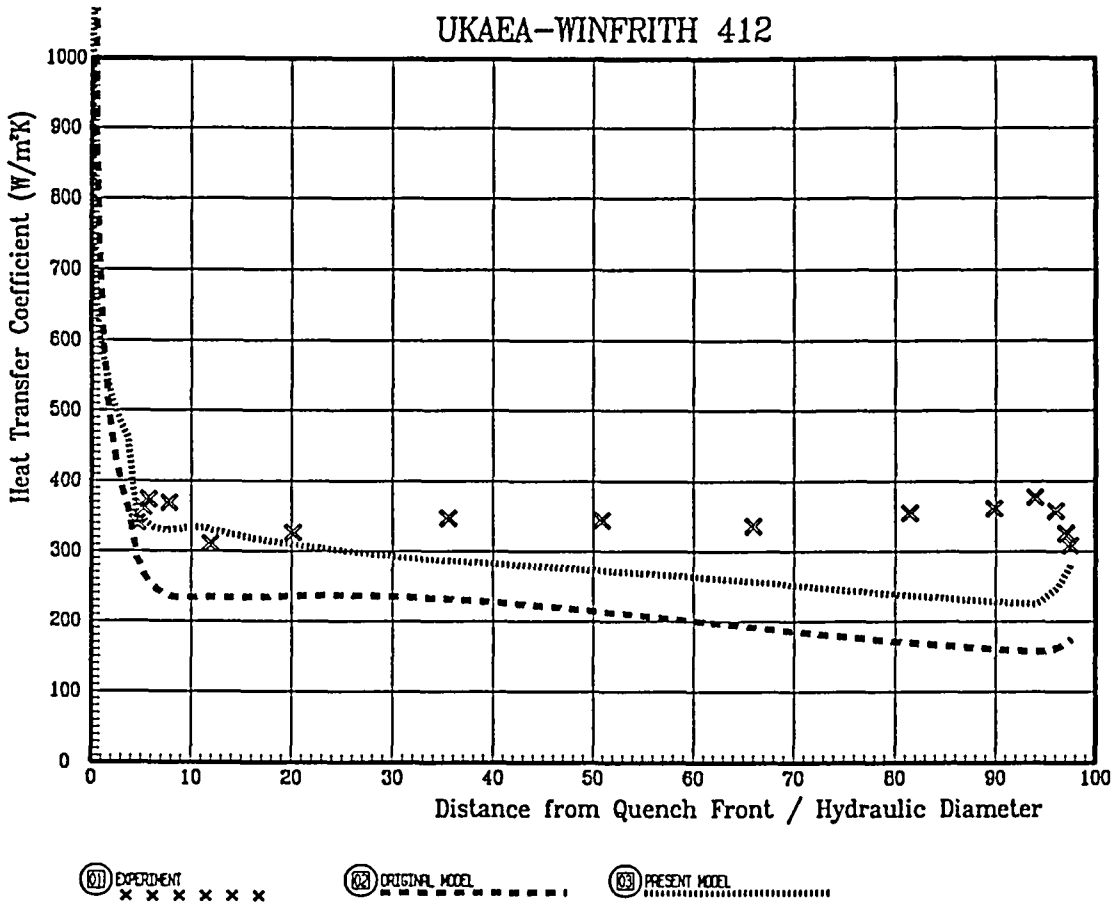
UKAEA-WINFRITH 412
Heat Transfer Coefficient (W/m²K)
1000
900
800
700
600
500
400
300
200
100
0
0
10
20
30
40
50
60
70
80
90
100
Distance from Quench Front / Hydraulic Diameter
01 EXPERIMENT
02 ORIGINAL MODEL
03 PRESENT MODEL

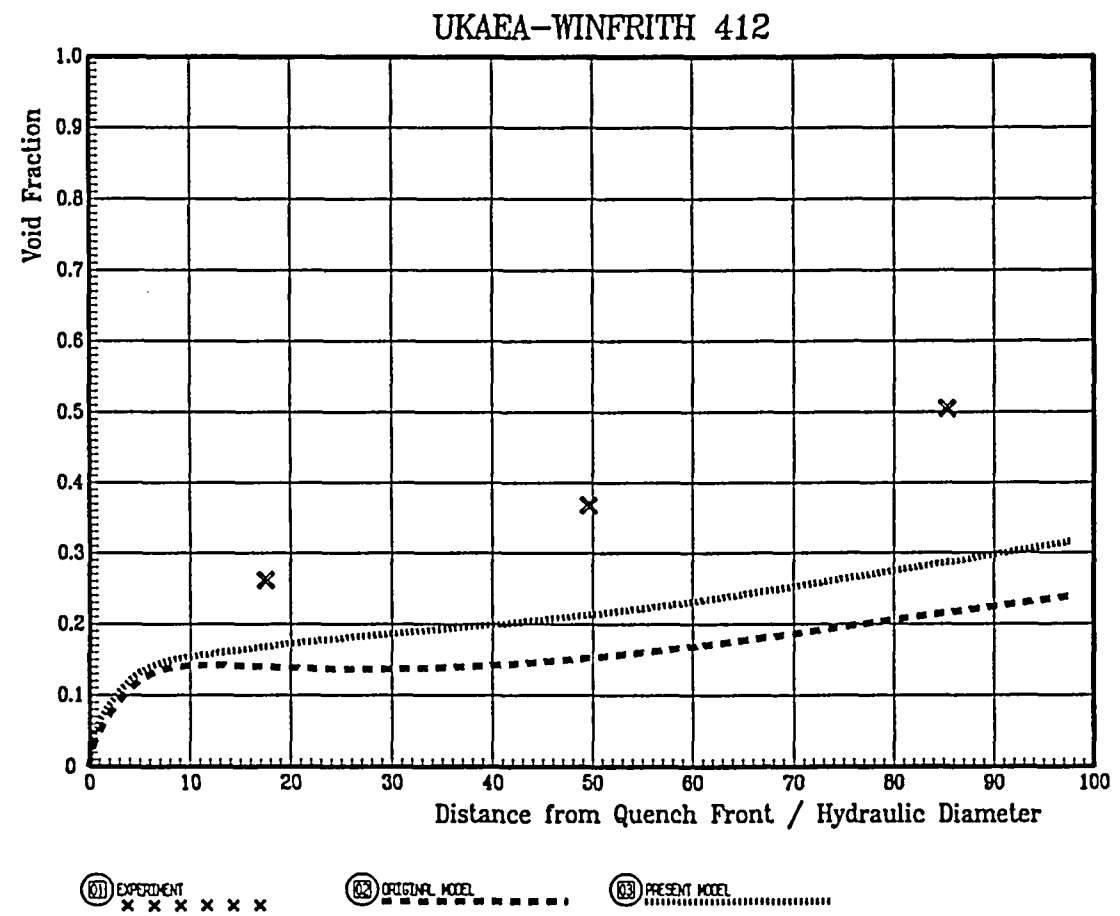
UKAEA-WINFRITH 412
Void Fraction
1.0
0.9
0.8
0.7
0.6
0.5
0.4
0.3
0.2
0.1
0
0
10
20
30
40
50
60
70
80
90
100
Distance from Quench Front / Hydraulic Diameter
01 EXPERIMENT
02 ORIGINAL MODEL
03 PRESENT MODEL

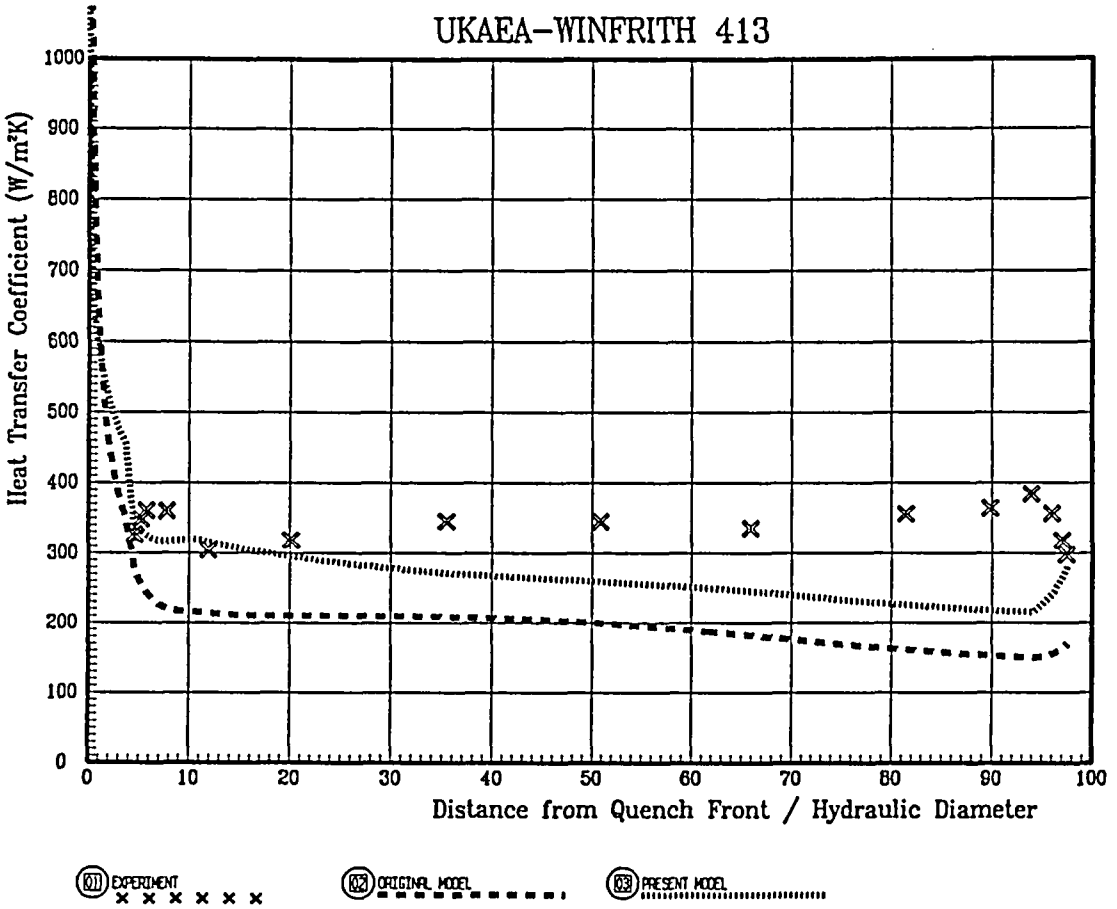
UKAEA-WINFRITH 413
Heat Transfer Coefficient (W/m²K)
1000
900
800
700
600
500
400
300
200
100
0
0
10
20
30
40
50
60
70
80
90
100
Distance from Quench Front / Hydraulic Diameter
001 EXPERIMENT
002 ORIGINAL MODEL
003 PRESENT MODEL

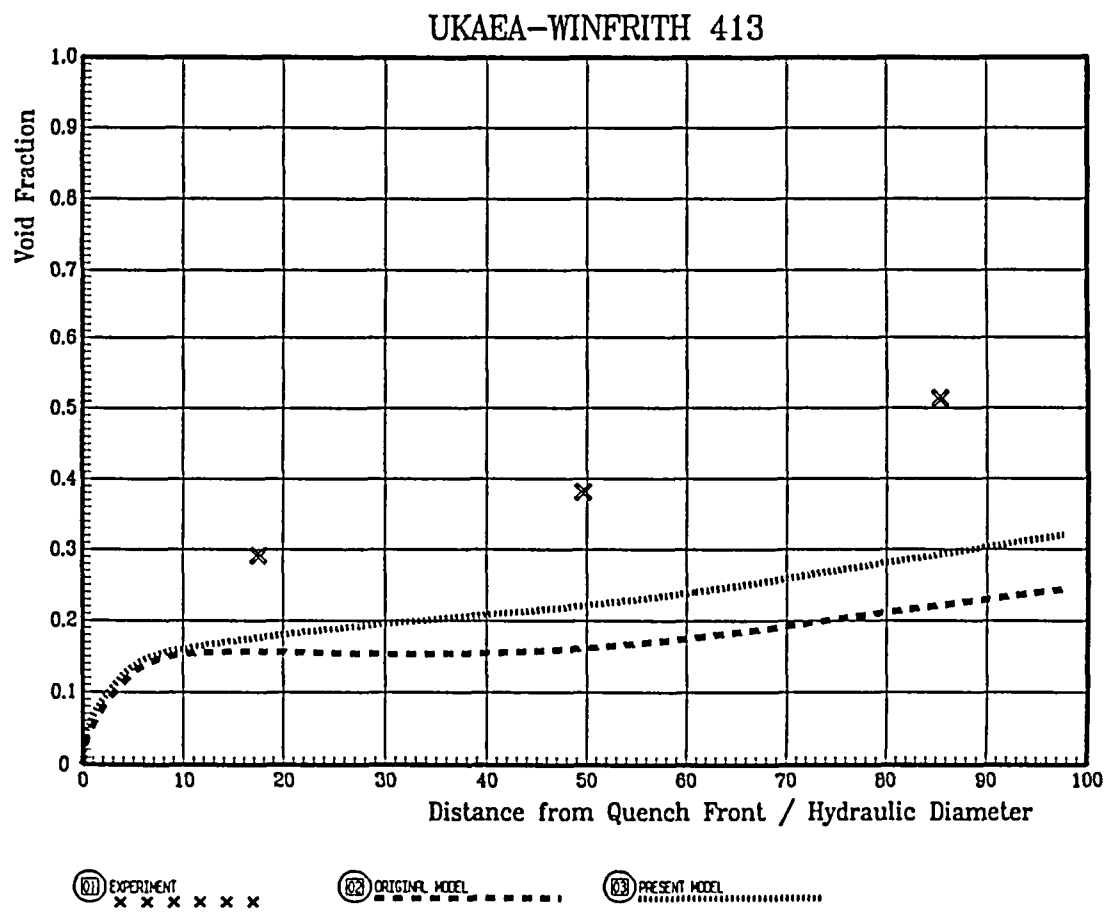
UKAEA-WINFRITH 413
Void Fraction
1.0
0.9
0.8
0.7
0.6
0.5
0.4
0.3
0.2
0.1
0
0
10
20
30
40
50
60
70
80
90
100
Distance from Quench Front / Hydraulic Diameter
001 EXPERIMENT
002 ORIGINAL MODEL
003 PRESENT MODEL

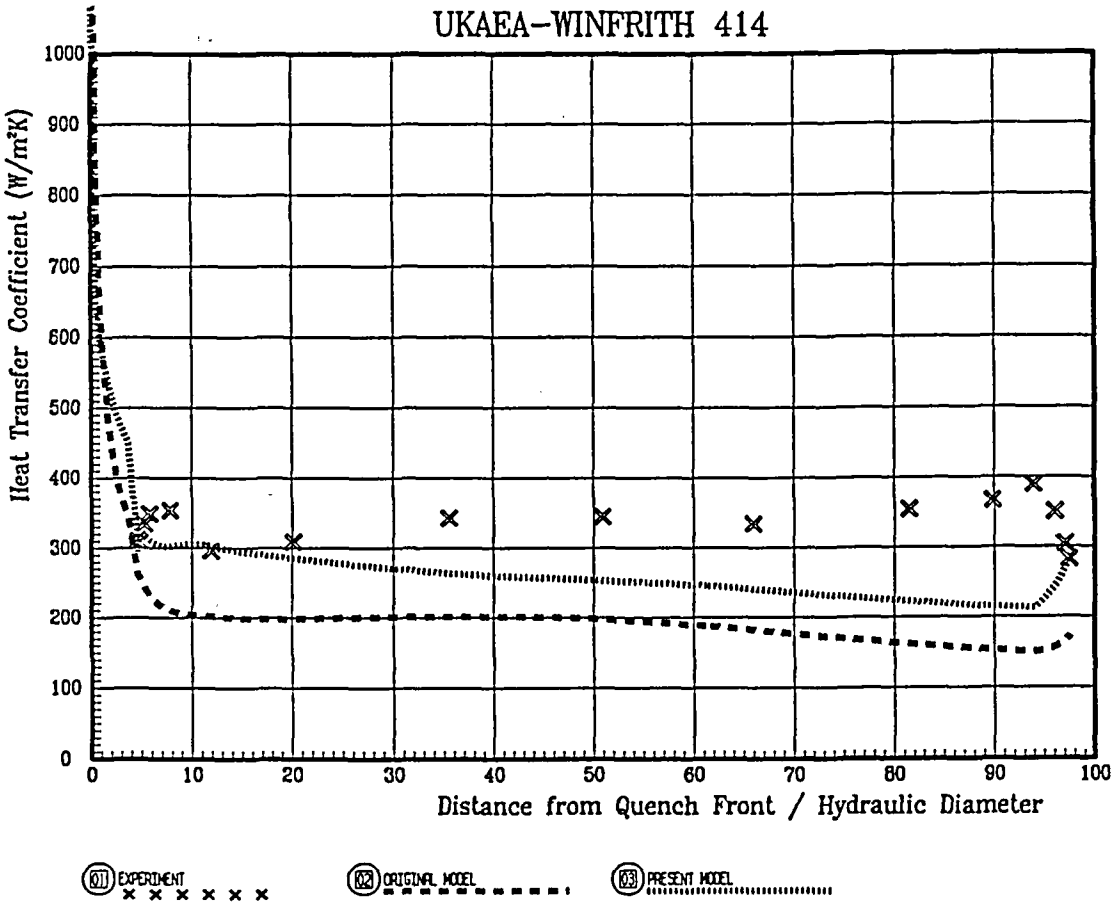
UKAEA-WINFRITH 414
Heat Transfer Coefficient (W/m²K)
1000
900
800
700
600
500
400
300
200
100
0
0
10
20
30
40
50
60
70
80
90
100
Distance from Quench Front / Hydraulic Diameter
01 EXPERIMENT
02 ORIGINAL MODEL
03 PRESENT MODEL

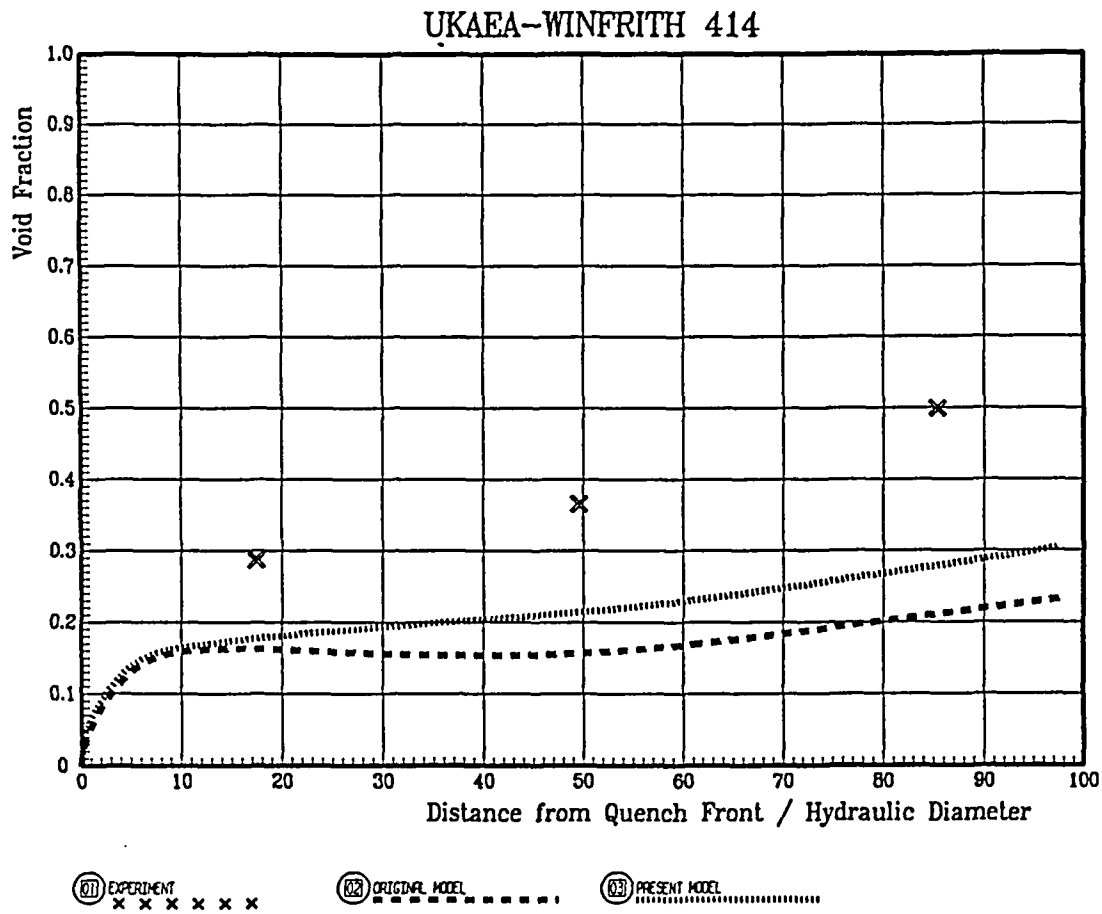
UKAEA-WINFRITH 414
Void Fraction
1.0
0.9
0.8
0.7
0.6
0.5
0.4
0.3
0.2
0.1
0
0
10
20
30
40
50
60
70
80
90
100
Distance from Quench Front / Hydraulic Diameter
01 EXPERIMENT
02 ORIGINAL MODEL
03 PRESENT MODEL

NRC FORM 335 (2-89) NRCM 1102, 3201, 3202

U.S. NUCLEAR REGULATORY COMMISSION

BIBLIOGRAPHIC DATA SHEET

(See instructions on the reverse)

1. REPORT NUMBER (Assigned by NRC, Add Vol., Supp., Rev., and Addendum Numbers, if any.)

NUREG/IA-0133
CAMP004

2. TITLE AND SUBTITLE

Development, Implementation, and Assessment of Specific Closure Laws for Inverted-Annular Film-Boiling in a Two-Fluid Model

3. DATE REPORT PUBLISHED

MONTH	YEAR
October	1996

4. FIN OR GRANT NUMBER

W6238

5. AUTHOR(S)

Francois de Cachard

6. TYPE OF REPORT

Technical

7. PERIOD COVERED *(Inclusive Dates)*

8. PERFORMING ORGANIZATION - NAME AND ADDRESS *(If NRC, provide Division, Office or Region, U.S. Nuclear Regulatory Commission, and mailing address; if contractor, provide name and mailing address.)*

Thermal-Hydarulics Laboratory
Paul Scherrer Institute
CH-5232 Villigen PSI
Switzerland

9. SPONSORING ORGANIZATION - NAME AND ADDRESS *(If NRC, type "Same as above"; if contractor, provide NRC Division, Office or Region, U.S. Nuclear Regulatory Commission, and mailing address.)*

Office of Nuclear Regulatory Research
U.S. Nuclear Regulatory Commission
Washington, DC 20555-0001

10. SUPPLEMENTARY NOTES

S. Smith, NRC Project Manager

11. ABSTRACT *(200 words or less)*

Inverted-Annular Film-Boiling (IAFB) is one of the post-burnout heat transfer modes taking place during the reflooding phase of the loss-of-coolant accident, when the liquids at the quench front is subcooled. Under IAFB conditions, a continuous liquid core is separated from the wall by a superheated vapour film. A key issue in IAFB modeling is to predict how the heat flux reaching the vapour-liquid interface is split into a liquid heating term and a vaporization term. In the model proposed, convective liquid heating is related to the liquid velocity relative to the interface and not the absolute liquid velocity, as in previous models.

12. KEY WORDS/DESCRIPTORS *(List words or phrases that will assist researchers in locating the report.)*

CAMP
RELAP5/MOD3

13. AVAILABILITY STATEMENT

unlimited

14. SECURITY CLASSIFICATION

(This Page) unclassified

(This Report) unclassified

15. NUMBER OF PAGES

16. PRICE

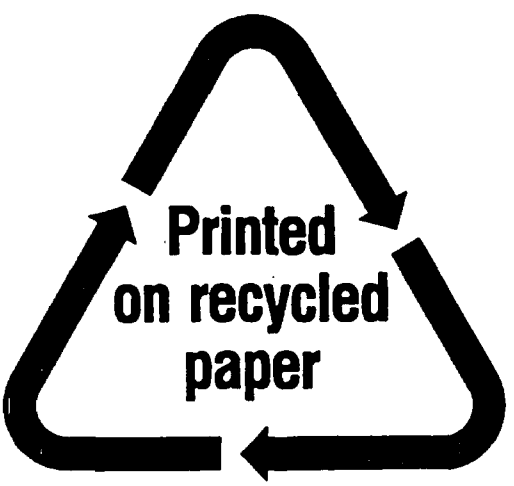

Federal Recycling Program

UNITED STATES
NUCLEAR REGULATORY COMMISSION
WASHINGTON, DC 20555-0001

OFFICIAL BUSINESS
PENALTY FOR PRIVATE USE, $300

SPECIAL STANDARD MAIL
POSTAGE AND FEES PAID
USNRC
PERMIT NO. G-67